Alma Mater Studiorum – Università di Bologna

DOTTORATO DI RICERCA IN
SCIENZE DELLA TERRA

Ciclo XXVII

Settore Concorsuale di afferenza: 04/A2
Settore Scientifico disciplinare: GEO/02

# Low-temperature thermochronological evolution of the Menderes and Alanya massifs (Turkey)

Presentata da: Dott. Francesco Mittiga

Coordinatore Dottorato
Prof. Jo De Waele

Relatore
Prof. William Cavazza

Co-relatori
Prof. Massimiliano Zattin
(Univerisità di Padova)
Prof. Aral I. Okay
(İstanbul Teknık Ünıversıtesı)

Esame finale anno 2015

*Wind in the east, mist coming in.*

*Like something is brewing, about to begin.*

*Can't put my finger on what lies in store*

*But I hope what's to happen, never happened before!*

*(For you Mrs. G.)*

## ACKNOWLEDGMENTS

Many people have contributed to the realization of this work. First of all, I would like to express my gratitude to my advisor Prof. William Cavazza for the helpful support of my PhD study and research. His guidance during all the time of research and writing, his constant motivations and discussions made me a more complete scientist. Without him this thesis would never be possible. Prof. Massimiliano Zattin taught me AFT counting and analysis and I am very grateful for his detailed comments and the support during the drawing up of this thesis. Prof. Aral Okay was a perfect mentor both during the collection of the samples and for the writing of this thesis. I also want to thank Dr. Claudio Dal Monte who advised me in the sample processing. Thanks to Prof. Marco Malusà from the University of Milan – Bicocca, for his useful comments on an earlier version of this dissertation. Special thanks to Dr. Maria Giuditta Fellin who taught me how to perform AHe and ZHe: her kindness and competence were a light during the darkest moments of this work (and not only).

During my Ph.D. I make acquaintance, between Bologna and Padua, of several special fellows –including (in strictly alphabetical order) Benedetta, Davide, Francesco, Irene, Veronica– and I want to thank you all for your hospitality and friendship. A special mention goes to my Ph.D. research partner Irene Albino: we shared travels, suffering, soups for breakfast, nights in the lab and other strange stuffs; thanks for all the support and the funniest moments.

Thanks to my Neapolitan brothers Antonio, Claudio and Giorgio: you know why.

Last but not least: my family! Deepest thanks for every time you believed in me and in my abilities, and for support every time i needed!

Thank you all, I have learned a lot from you and I will never forget you, even those who have lost during this wonderful journey!

Francesco

## Ringraziamenti

Molte persone hanno contribuito alla realizzazione di questo lavoro. Prima di tutto vorrei esprimere la mia gratitudine al mio relatore Prof. William Cavazza per il suo utile sostegno nel corso del percorso del mio dottorato. La sua guida durante sia il periodo di ricerca sia della stesura della tesi, la sua motivazione costante e le discussioni mi hanno reso uno scienziato più completo. Senza di lui questo lavoro non sarebbe stato possibile. Il Prof. Massimiliano Zattin mi ha insegnato la metodologia delle AFT ed io gli sono davvero grato per i commenti dettagliati e per il supporto durante la correzione di questa tesi. Il Prof. Aral Okay è stato una guida perfetta sia durante le campagne di campionamento in Turchia sia durante le fasi di stesura di questa tesi. Voglio inoltre ringraziare il Dott. Claudio Dal Monte che mi ha guidato nell'apprendimento delle procedure della preparazione dei campioni. Grazie al Prof. Marco Malusà dell'Università di Milano – Bicocca, che ha revisionato una versione preliminare di questo lavoro. Un ringraziamento speciale va alla Dott.ssa Maria Giuditta Fellin che mi insegnato come effettuare analisi AHe e ZHe: la sua gentilezza e competenza sono state una luce durante i momenti più bui di questo lavoro (e non solo).

Durante il mio dottorato ho conosciuto, tra Bologna e Padova, tanti compagni speciali – tra cui (in rigoroso ordine alfabetico) Benedetta, Davide, Francesco, Irene, Veronica- e perciò vorrei ringraziarvi tutti per la vostra ospitalità e per l'amicizia. Un ringraziamento speciale va alla mia compagna di squadra di ricerca Irene Albino: abbiamo condiviso viaggi, sofferenze, zuppe per colazione, nottate in laboratorio e altre cose strane; grazie per tutto l'aiuto e per tutti i momenti divertenti.

Grazie ai miei fratelli napoletani Antonio, Claudio e Giorgio: voi sapete per cosa.

Ultima ma non meno importanti: la mia famiglia! I miei più sentiti ringraziamenti per ogni volta che avete creduto in me e nelle mie capacità e per il supporto ogni volta che ne avevo bisogno.

Grazie a tutti, ho imparato molto da ciascuno di voi e non vi dimenticherò mai, soprattutto anche coloro ho perso nel corso di questo viaggio meraviglioso!

Francesco

## TABLE OF CONTENTS

## ABSTRACT

In this dissertation, the application of two low-temperature thermochronometers [fission-track analysis and (U-Th)/He analyses, both on apatite] to various tectonostratigraphic units of the Menderes and Alanya Massifs of Turkey has provided significant new constraints to the understanding of their structural evolution. Such constraints can be applied to more general interpretative models of post-collisional extensional processes in the eastern Mediterranean and elsewhere.

The Menderes Massif of western Anatolia is one of the largest metamorphic core complexes on Earth. Recent research on the Menderes is providing compelling results on the post-collisional tectonic evolution of the Aegean and peri-Aegean domain. The integration of the geochronometric dataset presented in this dissertation with preexisting ones from the literature delineates three groups of samples within the Menderes Massif. Such groups are chronologically and geographically defined: (i) samples from the northern and southern sectors of the massif –i.e. respectively north and south of the Gediz and Buyük Menderes detachment faults- yielded apatite fission-track ages ranging between the Late Oligocene and the Early Miocene, whereas (ii) samples from the central sector are younger, with most ages falling within the Middle-Late Miocene. The results of this study are consistent with the interpretation for a symmetric exhumation of the Menderes Massif.

The Alanya Massif of SW Anatolia has been interpreted as the southern margin of an 'Alanya ocean' originally located to the south of the Tauride carbonate platform. Northward subduction of this ocean led to Late Cretaceous thrusting and HP/LT metamorphism, followed by exhumation. Collision-related, northward backthrusting during the Paleocene-Early Eocene –likely resulting from the final closure of the İzmir–Ankara–Erzincan ocean to the north- created the present stacking order, thus implying that most exhumation had ended by Late Eocene time. Apatite fission-track ages from this study range from 31.8 to 26.8 Ma (Late Rupelian – Early Chattian) and point to a previously unrecognized mid-Oligocene cooling/exhumation episode, thus challenging the commonly held notion that the Alanya Massif did not suffer significant tectonic events after Eocene northward backthrusting. At this early stage in the structural understanding of the Alanya

Massif and the surrounding regions it is not possible to define whether the Oligocene cooling episode developed in an overall stress regime of syn-collisional compression or post-collisional extension. For the time being, we tentatively favour the interpretation of the mid-Oligocene fission-track ages from the Alanya Massif as the record of the structural inversion of the Alanya nappe stack, tectonic denudation, and cooling. This is in view of the overall transition from a compressional (Eocene) to an extensional (?Oligocene-Miocene) regime recognizable over the entire Aegean and peri-Aegean regions.

(U-Th)/He analysis on zircon crystals obtained from Late Cretaceous trondhjemites of the Troodos Massif igneous succession of Cyprus show that they cooled from emplacement temperature to 180° C in a relatively short time span, ranging approximately between 20 and 27 My. Such cooling could be either (i) an effect of the normal magmatic cooling of the plagiogranites or (ii) a result of exhumation. ZHe results from the Late Triassic turbiditic sandstones of the Vlambouros Formation indicate that the Mamonia mélange of southern Cyprus was never buried enough to reach the closure temperature of the ZHe radiometric system (ca. 200°C), thus retaining the Paleozoic signature of a previous sedimentary cycle.

## RIASSUNTO

L'applicazione di due metodi termocronologici delle basse temperature (analisi delle tracce di fissione e datazioni (U-Th)/He, entrambe su apatite) alle unità tettonostratigrafiche dei massicci del Menderes e di Alanya in Turchia meridionale ha permesso di ottenere nuovi risultati che vincolano meglio la loro evoluzione strutturale. Tali risultati possono essere applicati ai modelli interpretativi che ricostruiscono i processi di estensione post-orogenica che hanno interessato l'intera regione mediterranea ed altre aree simili.

Il Massiccio del Menderes, in Anatolia occidentale, è uno dei più grandi *metamorphic core complex* del pianeta. Lavori recenti hanno fornito risultati interessanti sull'evoluzione post-orogenica della regione egea e peri-egea. L'integrazione dei dati geocronologici ottenuti in questo lavoro con quelli presenti in bibliografia ha permesso di costituire un *dataset* che copre l'intero massiccio. I dati termocronologici sono suddivisibili in tre gruppi definiti cronologicamente e geograficamente: (i) i campioni provenienti dai settori settentrionali e meridionali del massiccio -rispettivamente a nord e a sud delle faglie a basso angolo di Gediz e Büyük Menderes- presentano delle età, ottenute mediante le tracce di fissione su apatite, che variano tra l'Oligocene superiore e il Miocene inferiore; (ii) i campioni provenienti dal settore centrale del massiccio hanno restituito delle età più recenti, concentrate perlopiù tra il Miocene medio e superiore. I risultati di questo lavoro confermano l'interpretazione di un'esumazione simmetrica per il Massiccio del Menderes.

Il Massiccio di Alanya, in Anatolia sudoccidentale, è stato da sempre interpretato come il margine meridionale del cosiddetto oceano di Alanya, un braccio di mare originariamente collocato a sud della piattaforma carbonatica dei Tauri. La subduzione verso nord di questo oceano, legata alla prima fase dell'orogenesi alpina, ebbe come conseguenza la strutturazione di una pila di falde nel Cretaceo superiore e l'instaurarsi di un regime metamorfico di alta pressione/bassa temperatura. Tali falde furono poi carreggiate verso nord in *backthrusting* durante una successiva fase compressiva avvenuta tra il Paleocene e l'Eocene inferiore. Tale fase tettonica determinò l'attuale geometria strutturale delle unità affioranti e fu verosimilmente l'effetto finale della collisione continentale lungo

la linea di sutura di İzmir-Ankara-Erzincan. Questa successione di eventi implicherebbe che l'esumazione sarebbe perlopiù terminata entro l'Eocene superiore. Viceversa le età ricavate dalle tracce di fissione su apatite in questo studio variano tra 31.8 e 26.8 Ma (Rupeliano superiore – Cattiano inferiore) e indicano perciò per la prima volta un episodio di raffreddamento/esumazione nell'Oligocene medio. Il livello delle conoscenze strutturali nel Massiccio di Alanya non è tale da poter definire se tale episodio si sviluppò in un contesto compressivo sin-collisionale o estensionale post-collisionale. Per il momento ipotizziamo preliminarmente che le età oligoceniche di raffreddamento/esumazione ottenute durante questo lavoro di tesi mediante l'analisi delle tracce di fissione su apatite indichino l'inversione strutturale, il denudamento tettonico e il conseguente raffreddamento delle falde del Massiccio di Alanya durante la transizione dal regime compressivo collisionale a quello estensionale post-collisionale nei Tauri centrali, per analogia con l'evoluzione generale del vicino dominio egeo e peri-egeo.

Le analisi (U-Th)/He sugli zirconi ottenuti dai plagiograniti tardo-cretacei della successione magmatica del Massiccio di Troodos a Cipro indicano che tali rocce si raffreddarono dalla temperatura di messa in posto a 180° C in un intervallo di tempo relativamente breve (27-20 Ma). Tale raffreddamento potrebbe essere il risultato del normale raffreddamento magmatico oppure derivare da processi esumativi. Analoghe analisi sulla Formazione di Vlambouros (Triassico superiore) indicano che, durante la sua tormentata evoluzione tettonico - strutturale, il mélange di Mamonia nella parte meridionale di Cipro non é mai stato sepolto abbastanza profondamente da raggiungere temperature superiori ai 200°C, la temperatura di chiusura del sistema radiometrico (U-Th)/He su zircone. Le torbiditi di Vlambouros hanno quindi conservato la firma isotopica relativa ad un precedente ciclo sedimentario del Paleozoico medio - superiore.

Chapter I

# INTRODUCTION

Over the last forty years metamorphic core complexes –in both oceanic and continental settings- have attracted much attention because they record fundamental thermomechanical processes in extending lithosphere (see Whitney et al., 2013, for a review). Metamorphic core complexes in continental settings commonly occur in orogenic belts and offer important opportunities to examine exposures of middle-to-lower continental crust in regions that have undergone large-scale post-orogenic extension.

The **Menderes Massif** of western Anatolia is one of the largest metamorphic core complexes on Earth. Despite much research progress in the past ten years, there are still substantial unresolved issues regarding the tectonic and metamorphic history of the Menderes Massif.

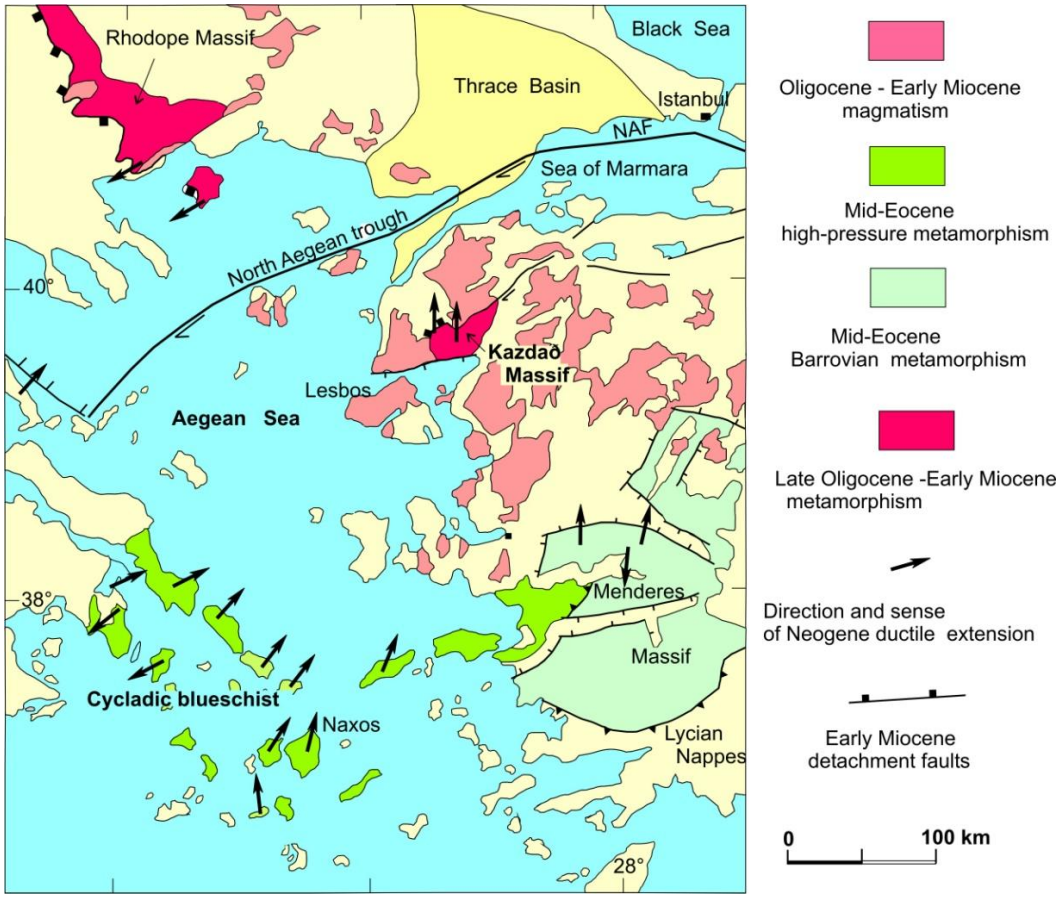


**Fig. 1.1 - The Menderes Massif of western Anatolia is a portion of a large extensional province comprising the Aegean and peri-Aegean regions. Extension followed crustal thickening in the Paleogene, a result of the closure of the northern branch of the Neotethys and the ensuing continental collision. Extension began in the Oligocene in the Rhodopes and shifted progressively to the south (Kazdağ, Menderes, Cyclades) mirroring the southward slab rollback of the Aegean subduction zone (drawing courtesy of A. I. Okay).**

The pre-Miocene tectonics of the Menderes Massif has been interpreted in terms of (i) a large-scale recumbent fold (Okay, 2001; Gessner et al., 2002), (ii) a series of nappes stacked during south-directed thrusting (Ring et al., 1999a; Gessner et al., 2001b), and (iii) a series of north-directed thrusts that subsequently collapsed either in a bivergent fashion (Hetzel et al., 1998) or through top-to-south extension (Bozkurt & Park, 1994; Bozkurt, 2007). The key controversies are focused on which structures are related to the kinematics of early Tertiary Alpine crustal shortening, which ones are related to late Tertiary crustal extension, and how this fits with the observed large-scale architecture of the massif.

This study is aimed at reconstructing the thermal history of the Menderes, in order to provide new constraints on the debated Paleogene-Neogene evolution of the western Anatolian region. This is achieved through the application of low-temperature thermochronometers such as apatite fission-track and (U-Th)/He on apatite on areas of the massif which previously had been studied only marginally. The obtained new geochronological data will be compared to the results available in the literature (e.g. Buscher et al., 2013; Gessner et al., 2001a; 2013; Ring et al., 2003; Thomson & Ring, 2006) to better constrain the evolution of the massif.

The same analytical approach was employed for the thermochronometric study of another major metamorphic salient of western Anatolia: the **Alanya Massif**
The Alanya Massif forms a large exposure of metamorphic rocks in a mountainous terrain north of the coastal town of Alanya in southwestern Turkey (Fig. 1.2) and it is dominated by three thrust sheets, of which the lower and upper ones are composed of high-temperature-low-pressure (HT-LP) rock types, whereas the middle one includes high-pressure-low-temperature (HP-LT) blueschists (Okay & Özgül, 1984). Blueschist metamorphism is thought to have occurred in pre-Maastrichtian times, consistent with initial thrusting taking place in the Late Cretaceous, and finally resulting in the assemblage of a north-verging nappe stack during Paleocene-Eocene time (e.g. Robertson, 2000). The high-grade metamorphic rocks of the Alanya Massif were exhumed prior to the Early Miocene, as shown by a widespread unconformable cover of transgressive Middle Miocene deposits (Geological Map of Turkey, 1:500000–Konya sheet). From a paleogeographic viewpoint, the protoliths of the Alanya Massif metamorphic rocks were interpreted as the deposits of a series of Neotethyan carbonate platforms and intervening basins (Robertson, 2000). The HP-LT rocks of the Alanya Massif could thus represent a

sutured small Neotethyan basin bordered by continental crust to the north and to the south. Such basin would have closed in the Late Cretaceous by northwest-directed subduction. In the Late Eocene the tectonic stack of the Alanya nappes was thrust over the Antalya Complex to reach the present-day structural configuration (Fig. 1.2). Thermochronological analyses of the Alanya Massif are nonexistent and this dissertation presents the first low-temperature thermochronometric data for this important geologic province.

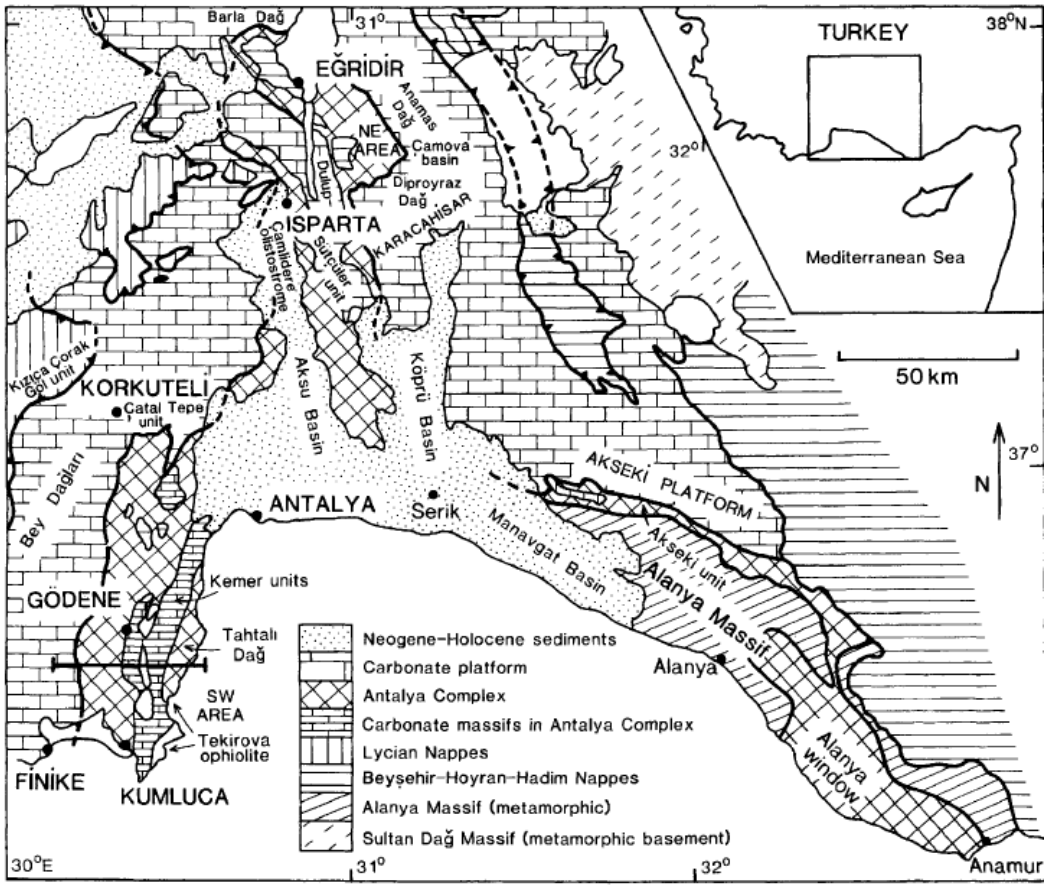


**Fig. 1.2 - Geological sketch map of the Bay of Antalya in southwestern Turkey (from Robertson, 2000).**

A third line of research comprised in this dissertation is represented by the attempt at determing the cooling history of selected rock units of the central and southern sectors of the island of Cyprus. The purpose of this line of research was twofold. Firstly, I attempted to apply apatite fission-track dating at the scarce granitoid rocks associated with the plutonic section of the Troodos Mountain ophiolitic suite. Small trondhjemite (plagiogranite) bodies occur either at the top of

the gabbro sequence or within the overlying sheeted dike complex of many ophiolites worldwide. As apatite is rather rare in rocks of basic composition such as those dominating ophiolitic suites, the occurrence of the plagiogranites might represent a unique opportunity to apply the apatite fission-tracks methods to ophiolitic successions. Secondly, the application of low-temperature thermochrometry to the rock unit of the Troodos and Mamonia accretionary complex might have shed light on the tectonic development of the entire southern Anatolia – Cyprus region, thus dovetailing nicely with our study of the Alanya Massif.

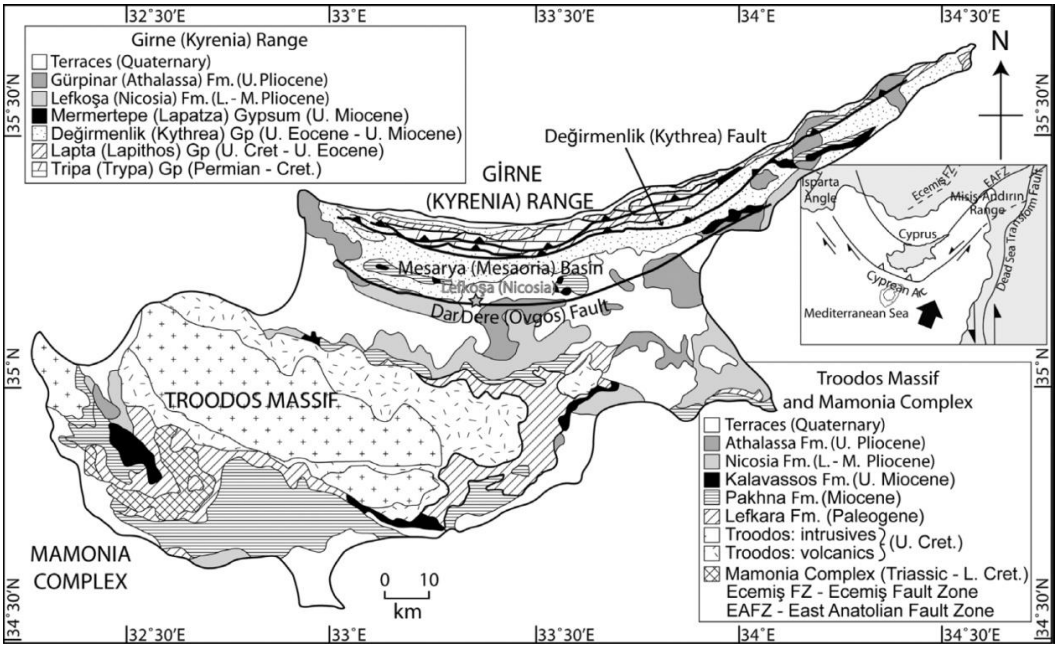


**Fig. 1.3 – Simplified geological map of Cyprus indicating the Kyrenia Range, the Troodos Massif and the Mamonia Complex. Inset: simplified tectonic sketch map of the Eastern Mediterranean region including regionally important lineaments, namely the Eastern Anatolian Fault Zone (EAFZ), the Dead Sea Transform Fault Zone and the Ecemiş Fault Zone (Ecemiş FZ) (from McCay et al., 2013).**

The present thesis is organized as follows:

- Chapter II provides a geological description of western Anatolia, with emphasis on the Menderes Massif, the Alanya Massif and southern Cyprus. The basic information on the Aegean region and the Tauride orogen is also provided, in order to better understand the descriptions of the Menderes Massif and the Alanya-Cyprus regions, respectively.

- Chapter III: in this chapter the location, lithology, coordinates, age of the 94 samples collected between Menderes Massif, Alanya Massif and Cyprus are shown.
- Chapter IV provides a synthesis of the fission-track and (U-Th)/He thermochronometric methods and describes the laboratory procedures for sample preparation and analysis.
- Chapter V presents the analytical results of this thesis referred to the Menderes Massif, the Alanya Massif and Cyprus.
- Chapter VI is a discussion of the dataset within the framework of the overall geology of the study area and compared to other similar areas. The new dataset presented in this dissertation is compared with pre-existing thermochronometric data from the literature.
- Chapter VII presents the main conclusions of this dissertation.

Chapter II

# GEOLOGICAL SETTING AND EVOLUTIONARY MODELS

The present-day setting of the Aegean and western Anatolian geological domains, in the Eastern Mediterranean (Fig. 2.1), is the result of the main tectonic processes that shaped the whole Mediterranean region: oceanic and continental subduction, mountain building, high-pressure and low-temperature metamorphism, back-arc extension, post-orogenic collapse and the ensuing development of metamorphic core complexes (see Cavazza et al. 2004, for a review). This chapter provides a review of the main geological features of the principal unit forming the Aegean and western Anatolian domains, including the Cycladic blueschists, the Menderes massif, the Lycian nappes, the Alanya massif, and Cyprus. This chapter provides essential introductory information for the Discussion section.

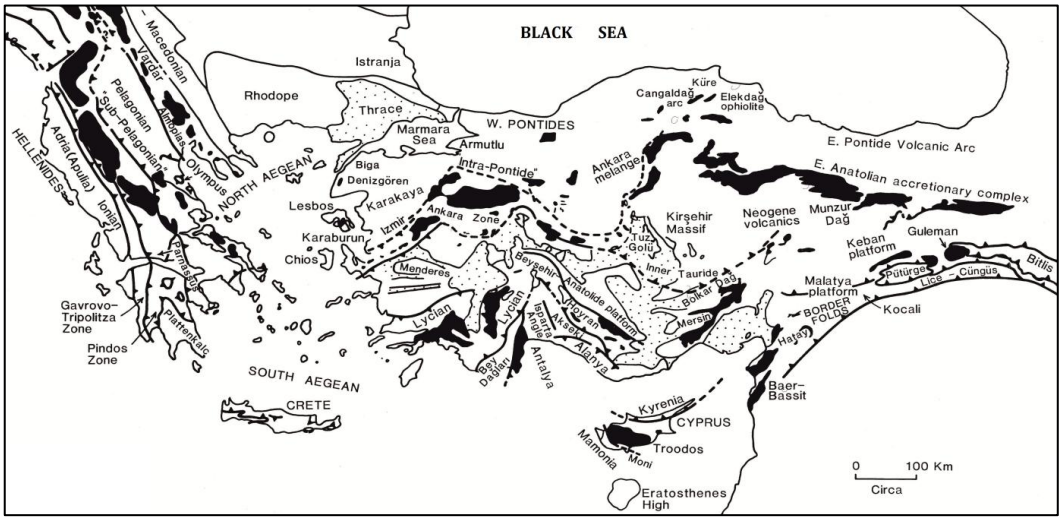


**Fig. 2.1 – Outline tectonic map of the easternmost Mediterranean showing the main tectonic units and features discussed (mod. after Robertson, 1998).**

## 2.1 THE RHODOPE MASSIF

The Alpine collisional system in the northern Aegean region exposes vast areas of crystalline basement in several internal metamorphic massifs including, from west to east, the Serbo-Macedonian massif, the Rhodope massif and the Strandja Massif (Figs. 2.1 and 2.2). These are pre-Alpine crustal domains that were actively involved during the Mesozoic-Cenozoic tectonic evolution along the southern margin of the Eurasian plate (e.g. Stampfli & Borel, 2004). Based on comparable lithology, metamorphic grade, and radiometric age constraints, they are considered elements of a more or less continuous belt of Variscan metamorphic and igneous basement

entities exposed also in the Sakarya Zone of western Turkey and the Pelagonian Zone of northern Greece (Okay et al., 1996a, 2001; Lips et al. 1998; Bonev et al., 2010).

The Rhodope massif (and its eastward continuation in the Strandja Mountains) is a large geological element cropping out in southern Bulgaria, northern Greece and northwestern (European) Turkey. It is dominated by high-grade basement metamorphic rocks intruded by unmetamorphosed Late Cretaceous to Miocene granitoids and covered by widespread Tertiary sedimentary, sedimentary-volcanic and volcanic rocks. This assemblage of Laurasian affinity suffered repeated phases of crustal thickening and exhumation during the Cretaceous and early Tertiary (e.g., Krohe & Mposkos, 2002).

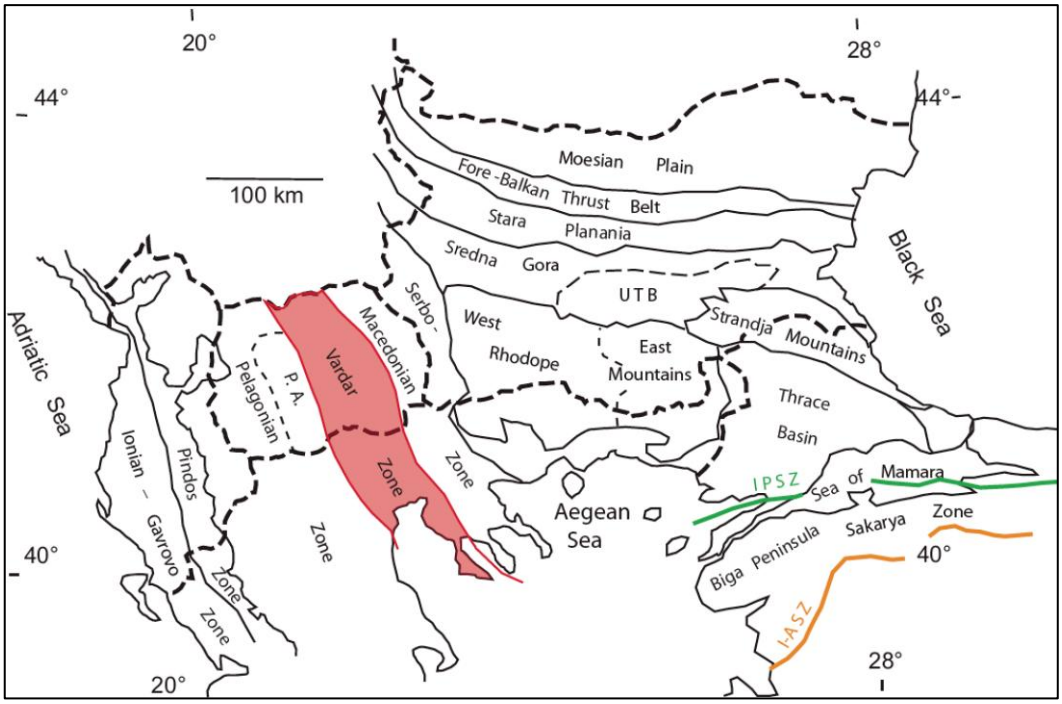


**Fig. 2.2 – Topographic and tectonic units mentioned in the text (from Burchfiel et al. 2008). The location of the Vardar suture zone (orange) and its eastward continuation in the Intra-Pontide suture zone (IPSZ—green) and Izmir-Ankara (I-A SZ—orange line) suture zones of northwestern Turkey are also shown. P. A.—Pelagonian antiform; UTB—Upper Thracian basin.**

The main phase of deformation occurred in the Maastrichtian-early Paleogene during the progressive closure of the Vardar ocean (e.g., Stampfli & Borel, 2004). It is interpreted as a south-verging nappe complex resulting from the ductile syn-metamorphic thrusting in the hanging wall of a north-dipping Cretaceous

subduction zone located in the Vardar suture zone (see next section) to the south (Ricou et al., 1998).

Ductile thrusting and the ensuing crustal thickening following the closure of the Vardar ocean created gravitational instability and crustal extension not only within the Rhodopes but throughout a vast region including southern Bulgaria, Macedonia, eastern Albania, northern Greece, and northwestern Turkey -the South Balkan extensional system of Burchfiel et al. (2008). Following diachronous closure across the suture zones, from the Middle Eocene to Late Oligocene, the transition from a regionally convergent to a regionally extensional tectonic setting occurred and was associated with abundant magmatism and formation of sedimentary basins. Extension was associated with lithospheric thinning probably related to changes in geometry of the subducted slab, dynamics of the mantle wedge, and beginning of slab rollback along the Hellenic subduction zone (see following sections).

## 2.2 THE VARDAR ZONE

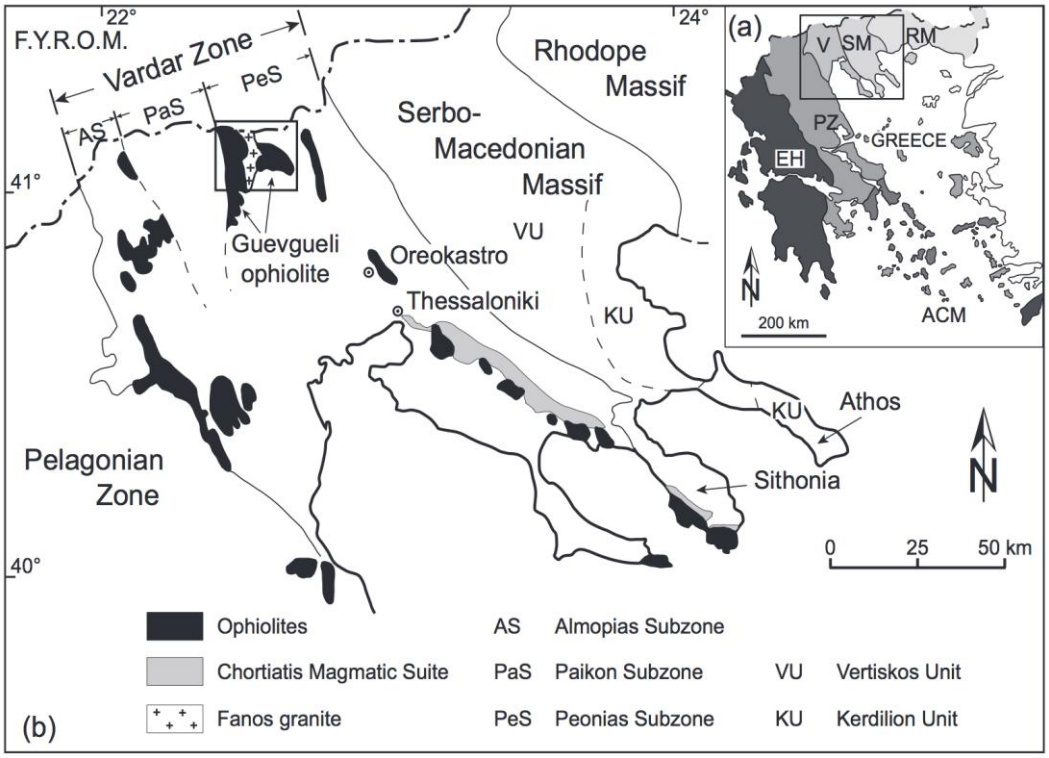


**Fig. 2.3 – (a) Simplified map of the tectono-stratigraphic zones of Greece modified after the IGME Geological Map of Greece (1983) scale1:500 000. RM: Rhodope Massif, SM: Serbo-Macedonian Massif, V: Vardar Zone, PZ: Pelagonian Zone, ACM: Attico-Cycladic Massif, EH: External Hellenides. (b) Simplified map of the Vardar Zone, modified after Mussallam & Jung (1986b). F.Y.R.O.M.: Former Yugoslav Republic of Macedonia.**

The Vardar zone is a prominent suture within the Alpine Mediterranean orogenic belt running parallel to the Hellenide-Dinaride chain in northern Greece and former Yugoslavia, respectively (Fig. 2.3). It is a commonly held notion that the Vardar suture continues across the extended northern Aegean domain into western Anatolia as the Izmir-Ankara suture. It is characterized by numerous ophiolitic bodies which originated from the Vardar Ocean *sensu lato*. The palaeotectonic evolution of the Vardar Ocean is a controversial topic as attested to by the large number of possible palinspastic alternatives (e.g., Ricou et al., 1998; Stampfli & Borel, 2004; Brown & Robertson, 2003, 2004, and references therein).

## 2.3 THE PONTIDES

Turkey is characterized by a very complex geology, whose main features are still poorly understood despite an increasing amount of geological data that have become available in the last twenty-five years. Geologically, it is divided into three main tectonic units: the Pontides, the Anatolide-Tauride terrane and the Arabian platform, from north to south (Fig. 2.4). These tectonic units, which were once surrounded by oceans, are now separated by sutures, which mark the tectonic lines or zones along which these oceans have disappeared (Okay, 2008).

The Pontides are an east-west trending orogenic belt stretching about 1,400 km, from SE Bulgaria to the Lesser Caucasus. They repeatedly underwent deformation during the Pan-African (Neoproterozoic), Variscan (Carboniferous), Cimmeride (Triassic - mid-Jurassic), and Alpide (Late Cretaceous - Paleogene) orogenies (Yılmaz et al. 1997; Tüysüz, 1999), with widespread reactivation of older structures and creation of complex tectonostratigraphic relationships.

Although presently constituting a discrete and continuous orographic element, the Pontides result from the amalgamation of three tectono-stratigraphic terranes: the Strandja Massif, the İstanbul terrane (İT), and the Sakarya terrane (ST).

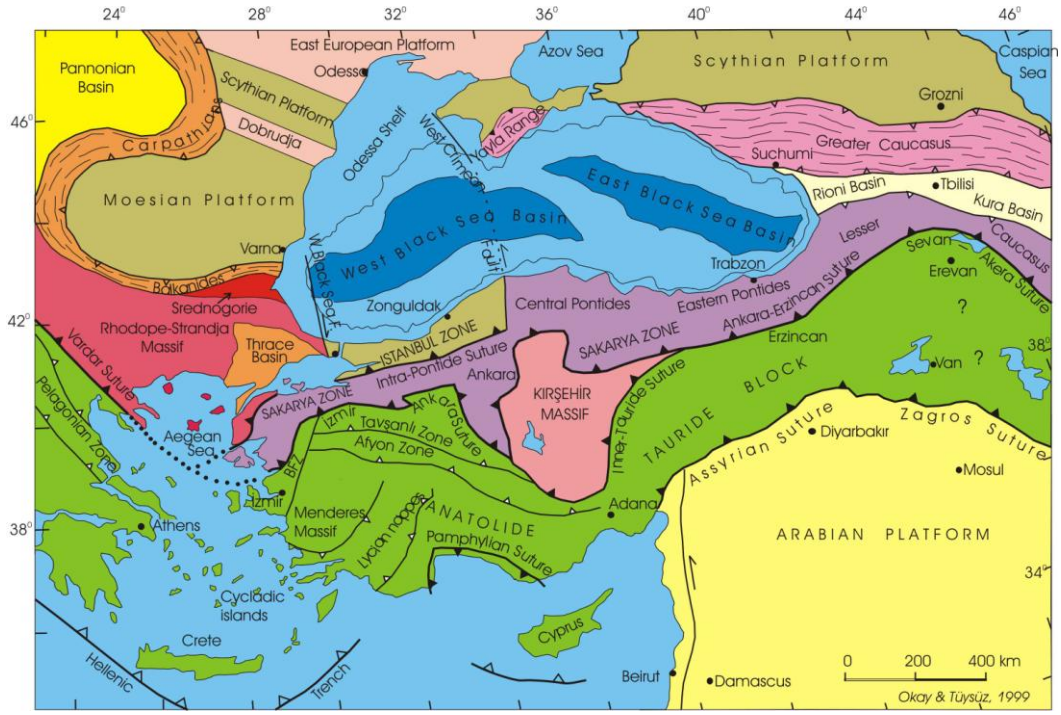


**Fig. 2.4 – Tectonic sketch of Anatolia and surrounding regions (from Okay & Tüysüz, 1999).**

There are various often conflicting views on the age and formation of the Intra-Pontide suture, the tectonic boundary between İT and ST (e.g., Şengör & Yılmaz, 1981; Yılmaz et al. 1994; Okay & Tüysüz, 1999; Yiğitbaş et al. 1999; Elmas & Yiğitbaş, 2001, 2005; Robertson & Ustaömer, 2004). It is considered by Okay & Tüysüz (1999) as the result of the progressive closure of an Intra-Pontide ocean during the Senonian. In contrast, according to Şengör & Yılmaz (1981) the Intra-Pontide suture formed in the Early Eocene after an orthogonal opening between İT and ST during the Liassic. Stampfli & Hochard (2009) support a Middle Jurassic collision between İT and ST. Akbayram et al. (2009) favor a Cenomanian collision. Based on thermochronometric data, Cavazza et al. (2012) concluded that İT and ST were mechanically coupled at least since the Paleocene.

The three distinct tectonostratigraphic terranes comprising the Pontides have markedly different geological characteristics. The Strandja Massif constitutes the easternmost part of the vast crystalline basement massif that includes the Rhodope and Serbo-Macedonian massifs. It consists of a Variscan crystalline basement no conformably overlain by a Triassic-Jurassic sedimentary succession (Aydın, 1974; Okay et al. 2006b; Sunal et al. 2006). Senonian andesites and associated granodiorites are widespread (Moore et al. 1980), and form a Late Cretaceous

magmatic belt that can be followed all along the Pontides. The İstanbul Terrane is a fragment of continental lithosphere about 400 km long (Fig. 2.4 & 2.5). It is made of a Late Precambrian basement complex overlain by a continuous Ordovician-to-Carboniferous sedimentary succession, which was deformed during the Variscan orogeny (Dean et al. 1997; Görür et al. 1997; Okay et al. 2008a). The late Paleozoic-Mesozoic stratigraphy is similar to that of the Moesian platform and -according to Okay et al. (1994) - prior to the Late Cretaceous opening of the western Black Sea the İT was situated south of the Odessa shelf. The Sakarya Terrane is an elongate lithospheric ribbon stretching >1,500 km from the Aegean sea to the Lesser Caucasus (Fig. 2.4 & 2.5). It is characterized by the absence of in situ Paleozoic sedimentary rocks and by the presence of a characteristic Permo-Triassic subduction-accretion complex (Karakaya-Küre Complex) unconformably overlain by ubiquitous Jurassic shallow-marine deposits (Okay & Göncüoğlu, 2004).

### 2.3.1 The Strandja Massif

The Strandja Massif forms part of a large crystalline terrane in the southern Balkans, which also includes the Rhodope. It consists of a Variscan crystalline basement overlain by a Triassic-Jurassic continental-to-shallow marine sedimentary sequence. The basement is made of predominantly quartzo-feldspathic gneisses intruded by Late Carboniferous - Early Permian granitoids (Okay et al., 2001; Sunal et al., 2006). The massif forms a belt about 200 km long and up to 50 km wide cropping out in a WNW-ESE direction along the Bulgaria-Turkish border (Fig. 2.5).

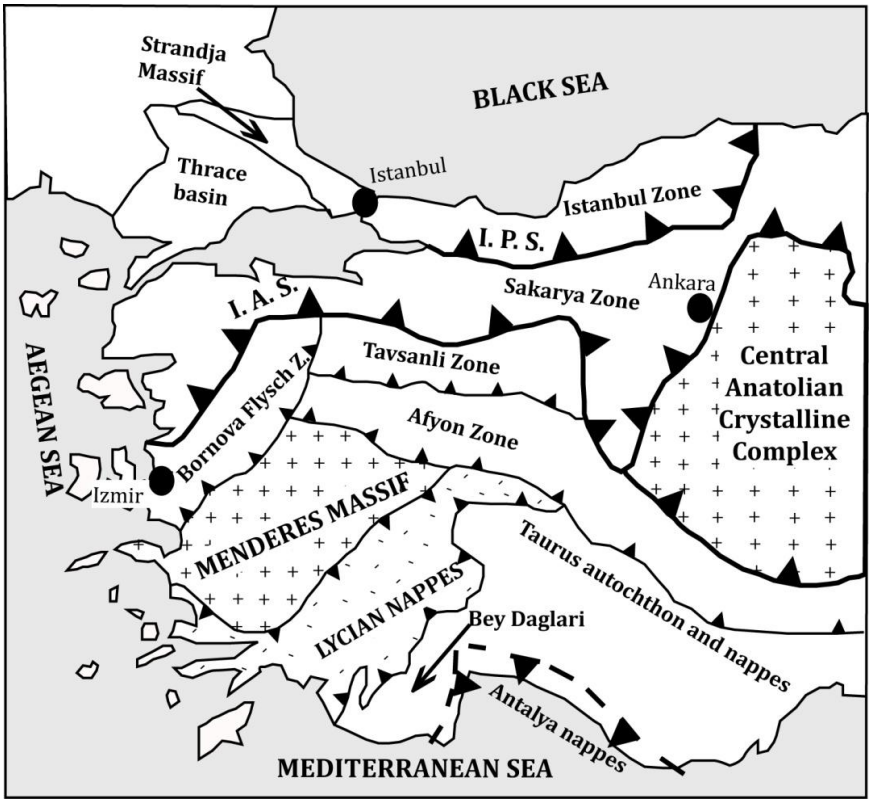


**Fig. 2.5 – Principal units of western Anatolia. I.P.S. Intra-Pontide suture; I.A.S. Izmir-Ankara-Erzincan suture.**

A sedimentary sequence of Triassic-Jurassic age lies unconformably on the Variscan basement (Chatalov, 1988). The Triassic series resemble the Germanic Triassic facies with a thick sequence of Lower Triassic continental clastic rocks overlain my Middle Triassic shallow marine carbonates (Hagdorn & Göncüoğlu, 2007). At around the Jurassic-Cretaceous boundary (150-155 My) the Strandja Massif underwent a second phase of deformation and metamorphism involving north- to northeast-vergent thrusting (Okay et al., 2001).

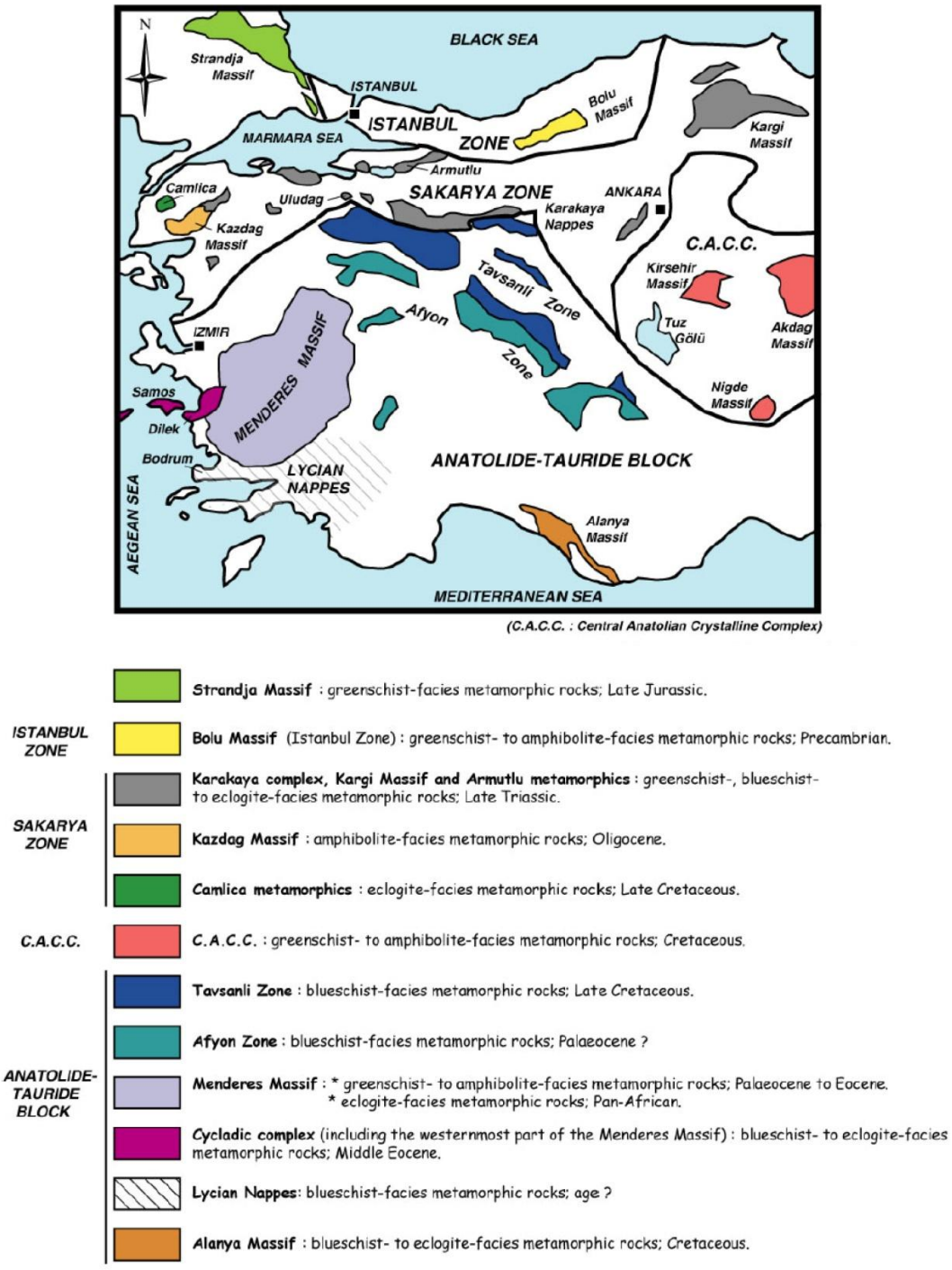


**Fig. 2.6 – Map showing the distribution of metamorphic rocks in western Turkey (from Rimmelé, 2003; mod. after Bozkurt & Oberhänsli, 2001).**

Following this mid-Mesozoic (Cimmerian) orogeny, the metamorphic rocks were unconformably overlain by Cenomanian shallow-marine sandstones. These sandstones pass up into a thick sequence of volcanic and volcanogenic rocks of Late

Cretaceous age, which extend into the Sredna-Gora zone in Bulgaria. This Late Cretaceous magmatic belt can be followed all along the Pontides along the Black Sea coast and represents a magmatic arc developed above the northward subducting Neotethyan ocean. In the Strandja Massif the Late Cretaceous magmatism also produced large number of andesitic dykes, sills, small intrusions and the Demirciköy pluton with an age of ca. 78 My (Moore et al., 1980).

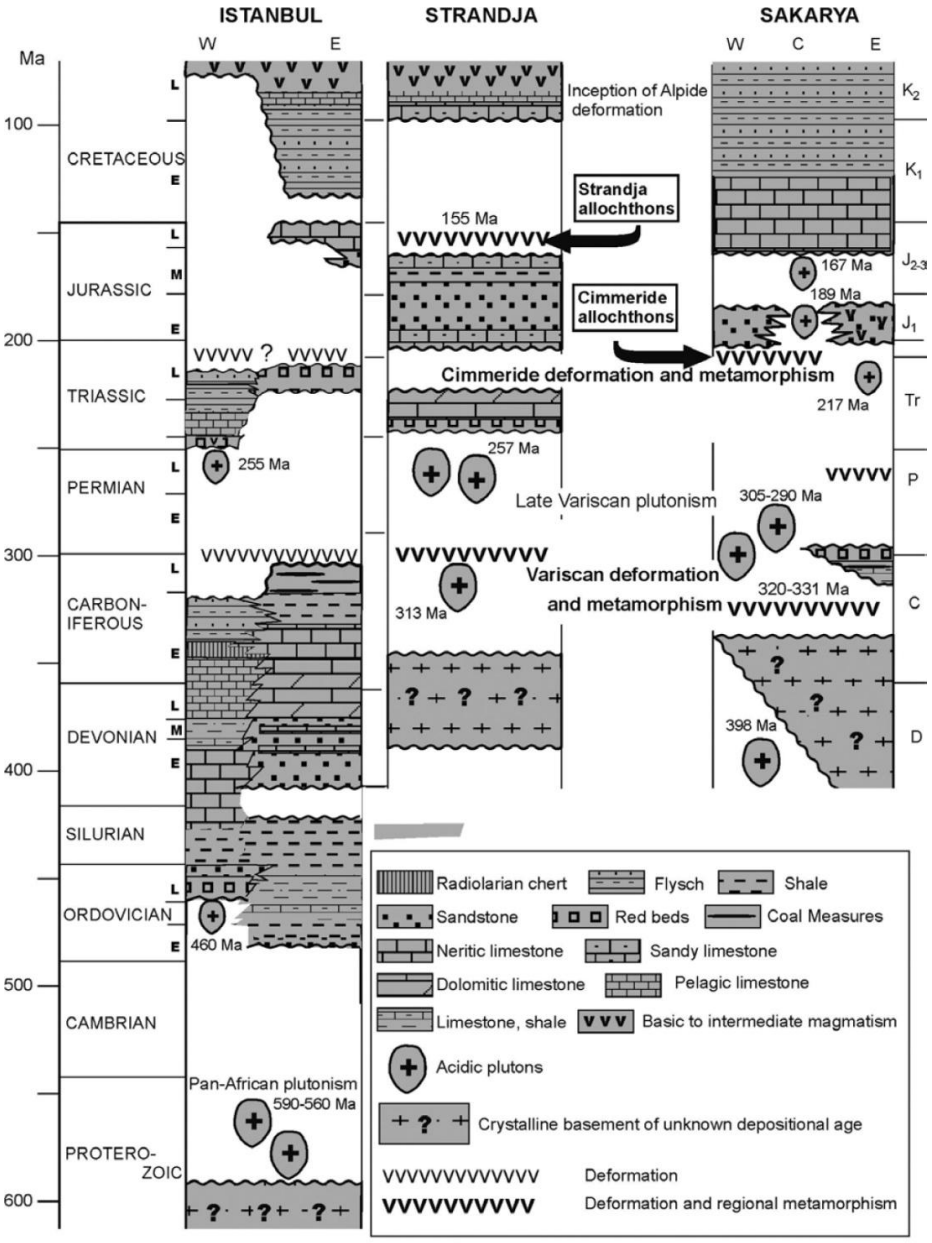


**Fig. 2.7 – Synthetic stratigraphic sections of the İstanbul, Strandja and Sakarya zone terrane (from Okay, 2008).**

### 2.3.2 The İstanbul Terrane

The İstanbul Terrane is a continental fragment, 400 km long and 55 km wide occurring along the southwestern margin of the Black Sea (Figs. 2.5 & 2.6). It has a Late Precambrian crystalline basement characterized by gneiss, amphibolite, meta-volcanic rocks, meta-ophiolite and voluminous Late Precambrian granitoids (Chen et al., 2002; Yiğitbaş et al., 2004; Ustaömer et al., 2005). The basement is mainly exposed in the Bolu Massif north of Bolu and is unconformably overlain by a continuous and well-developed sedimentary succession of Ordovician to Carboniferous in age (Fig. 2.6) (e.g., Görür et al., 1997; Dean et al., 2000).

The Paleozoic rocks were deformed by folding and thrusting during the Carboniferous during the Variscan orogeny and are overlain unconformably by a Triassic sedimentary sequence. The Triassic series is well developed east of İstanbul and shows a typical transgressive development starting with red sandstones with basaltic lava flows, passing up into shallow-marine and then deep-marine limestones, and ending with Upper Triassic deep-sea sandstones and shales. In the western part of the İstanbul Zone, the Jurassic and Lower Cretaceous sequence is absent, and the Paleozoic and Triassic rocks are unconformably overlain by Upper Cretaceous-Paleocene siliciclastic, carbonate and andesitic volcanic rocks. In contrast, in the eastern part of the İstanbul Zone there is a thick Middle Jurassic to Eocene succession marked by small unconformities.

The İstanbul Zone shows a Paleozoic-Mesozoic stratigraphy similar to that of Moesian Platform, and prior to the Late Cretaceous opening of the western Black Sea basin it was situated south of the Odessa shelf (Okay et al., 1994). Together with similar Paleozoic sequences farther west, including the Carnic Alps in Austria and Krajstides in Bulgaria, the İstanbul Zone and its continuation in the Scythian platform formed part of the passive continental margin of Laurasia. With the inception of back-arc spreading in the Late Cretaceous, the İstanbul Zone was rifted off from the Odessa shelf and was translated southward, opening the West Black Sea basin in its wake (Okay et al., 1994).

The İstanbul Terrane is separated from the Sakarya terrane by the Intra-Pontide suture marking the trace of the Intra-Pontide ocean (Şengör & Yılmaz, 1981). During the Carboniferous the Intra-Pontide ocean probably formed the eastern extension of the Rheic ocean (Okay et al. 2006a; 2008); it closed following the collision of the İstanbul and Sakarya terranes in the mid-Carboniferous. The

different Mesozoic stratigraphies of the İstanbul and Sakarya terranes suggest that the Intra-Pontide ocean reopened during the Triassic only to close again in the mid-Cretaceous (Okay, 2008).

### 2.3.3 The Sakarya Terrane

The Sakarya terrane forms an elongate crustal ribbon extending from the Aegean in the west to the Eastern Pontides in the east (Figs 2.5 & 2.6). In contrast to the İstanbul terrane, the sedimentary sequence starts with Lower Jurassic sandstones, which rest on a complex basement (Fig. 2.7). The crystalline basement of the Sakarya terrane can be broadly divided into three types:

(1) A high-grade Variscan metamorphic sequence of gneiss, amphibolite, marble and scarce meta-peridotite; the high-grade metamorphism is dated to the Carboniferous (330-310 My) by zircon and monazite ages from the Pulur, Kazdağ and Gümüşhane massifs (Topuz et al., 2004; 2007; Okay et al., 2006a). This Variscan basement was probably overlain by Upper Carboniferous molasse, which is only preserved in the Pulur region in the easternmost part of the Sakarya Zone (Okay & Leven, 1996).

(2) Paleozoic granitoids with Devonian, Carboniferous or Permian crystallization ages (Delaloye & Bingöl 2000; Okay et al. 2002; 2006a; Topuz et al. 2007). Small outcrops of these Paleozoic granitoids are scattered throughout the Sakarya terrane, and are unconformable overlain by Jurassic and younger sediments.

(3) A low-grade metamorphic complex (the lower Karakaya Complex) dominated by Permo-Triassic metabasite with lesser amounts of marble and phyllite. The Lower Karakaya Complex represents the Permo-Triassic subduction- accretion complex of the Paleo-Tethys with Late Triassic blueschists and eclogites (Okay & Monié, 1997; Okay et al., 2002), accreted to the margin of Laurussia during the Late Permian to Triassic.

The lower Karakaya complex is overlain by a thick series of strongly deformed clastic and volcanic rocks with exotic blocks of Carboniferous and Permian limestone and radiolarian chert. Several subunits are differentiated within this upper Karakaya complex, which are interpreted as trench turbidites or accreted oceanic islands (Federici et al., 2010). The age of these units ranges from Permian to

the Late Triassic. This complex basement was overlain unconformably in the Early Jurassic by a sedimentary and volcanic succession. The Early Jurassic is represented by fluvial to shallow marine sandstone, shale and conglomerate in the western part of the Sakarya Zone; in the eastern part volcanoclastic rocks are typically intercalated with the sandstones (Fig. 2.7). In the central Pontides granitic rocks were intruded into the basement during the Early to Mid Jurassic (Yılmaz & Boztuğ, 1986). The Lower Jurassic clastic and volcanoclastic series are overlain by an Upper Jurassic-Lower Cretaceous limestone sequence, which can be followed throughout the Sakarya Zone (Altıner et al., 1991). In the Eastern Pontides the Upper Jurassic–Lower Cretaceous limestones show an increasingly deeper marine character as they are traced south indicating the presence of a passive margin overlooking an ocean in the south. The limestones are overlain in the mid-Cretaceous by deep sea sandstones and shales marking the onset of the Alpide orogeny. In the Eastern Pontides an ophiolitic mélange was emplaced northward during this period leading to a local phase of contractional deformation (Okay & Şahintürk, 1997).

## 2.4 THE CYCLADES

Geologically, the Cycladic archipelago is characterized by a series of outcrops of HP/LT rocks: the Cycladic Blueschists. They crop out not only in the Cyclades but also in continental Greece (Olympus, Ossa and Pelion tectonic windows (e.g. Schermer, 1993) and Evia Island (Fig. 2.8) (e.g. Bonneau & Kienast, 1982). One major characteristic of this unit is the high-grade metamorphism and associated severe deformation preventing to easily establish its lithostratigraphy.

The Cycladic Blueschists belt comprises an alternation of metapelites, metabasites and marble. The metabasites are ancient flows, tuffs or basic clocks in a mélange as described in Syros Island (Bonneau et al., 1980). The vertical succession differs from one island to another one. This is mainly due to strong isoclinal folding. However, a general picture can be given as following (Bonneau et al., 1978; 1980).

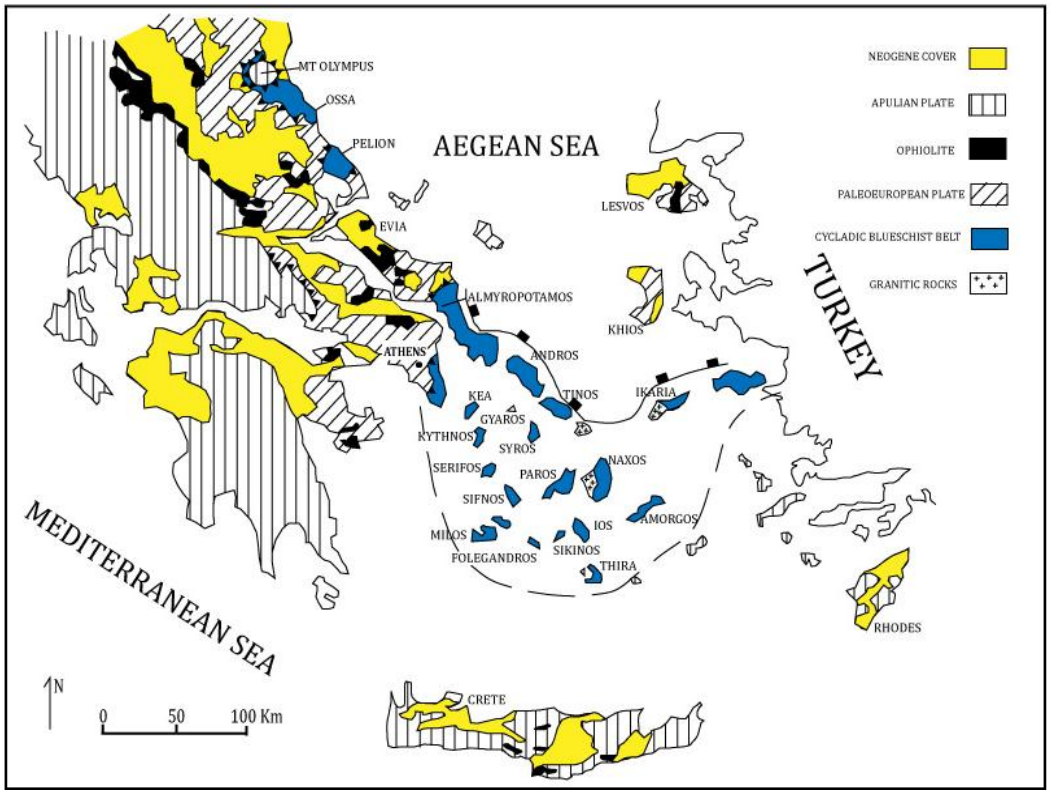


**Fig. 2.8 – Simplified tectonic map of the Cyclades (from Blake et al. 1981, mod.)**

(1) The deepest unit probably corresponds to the anatectic basement of Ios, Naxos and Paros and the associated post-Variscan sedimentary cover that comprise marbles and chloritoid-kyanite schists, intruded by Triassic granitoids (Engel & Reischmann, 1997; Reischmann, 1997). The marbles contain emery in Naxos and the geochemistry of the metabauxites closely matches that of Jurassic bauxites found elsewhere in the Hellenides and Dinarides (Feenstra, 1985).

(2) The blueschist and eclogite series of alternating marbles, metapelites and metabasites, cropping out in Tinos for instance, probably overlie this basal unit.

(3) An ophiolitic mélange, which is well exposed in the western part of Syros, is the upper metamorphic unit.

The Cycladic blueschists were exhumed in two stages corresponding to two metamorphic episodes (Jolivet & Brun, 2010). The first stage occurred during Eocene Hellenic subduction, during the final stage of the Alpine compressional event, when all units underwent HP-LT metamorphism under blueschist to eclogite facies conditions ($P_{max}$ = 20 kbar, $T_{max}$ = 600°C). The age of the HP metamorphism

event range from 78 to 35 My, with a mean Early Eocene (50-45 My) age (e.g. Trotet et al., 2001a&b; Parra et al., 2002; Ring & Layer, 2003). During subsequent tectonism in the Oligocene and Miocene, the extension associated with the rollback of the Aegean subduction zone determined the collapse of the Hellenic chain and the subsequent exhumation of the blueschists as Cordilleran-type metamorphic core complexes (Lister et al., 1984) with mainly NE-dipping low-angle normal faults (detachments) showing a dominant top-to-the-N or -NE sense of shear (Buick, 1991; Gautier et al., 1993; Vanderhaeghe, 2004). This was associated to a severe HT-LP overprint, coeval with the Aegean post-orogenic extension (Andriessen et al., 1979; Altherr et al., 1982; Wijbrans & McDougall, 1988; Keay et al., 2001). The degree of preservation of the HP-LT assemblages is variable from one island to the other.

## 2.5 ANATOLIDE-TAURIDE DOMAIN

The Anatolide-Tauride terrane (AT) is a large geological domain in southern Anatolia (Fig. 2.4). It shows Gondwana affinity but is separated from the Arabian platform by the Assyrian (Bitlis-Zagros) suture. To the north, the AT is bounded by the Izmir-Ankara-Erzincan suture, marking the closure of an oceanic domain originally present between the Pontides (Sakarya terrane) and the AT (e.g. Stampfli & Borel, 2004). The Izmir-Ankara-Erzincan suture is the major geological discontinuity in Anatolia as all terranes to the north of it have European (Laurasian) affinity whereas those to the south of it have African (Gondwanian) affinity. The AT forms the bulk of southern Turkey and, in contrast to the Pontides, shows a Palaeozoic stratigraphy similar to the Arabian Platform (Okay, 2008). During the obduction, subduction and continental collision episodes due to the progressive closure of the Izmir-Ankara-Erzincan ocean in the Late Cretaceous and Paleocene, the AT was in the footwall position and therefore underwent much stronger Alpide deformation and regional metamorphism than that observed in the Pontides (i.e. the upper plate). During the mid-Cretaceous a very large body of ophiolite and underlying tectonic slices of ophiolitic mélange were emplaced southward over the AT (Okay, 2008). The northern margin of the AT underwent HP/LT (high pressure/low temperature) metamorphism at depths of over 70 km under this oceanic thrust sheet. Erosional remnants of this thrust sheet of ophiolite and ophiolitic mélange occur throughout the AT. Although widely called a mélange, it

generally lacks an all-encompassing matrix, and represents rather a highly sheared Cretaceous accretionary complex. With the inception of continental collision in the Paleocene, the Anatolide-Tauride terrane was internally sliced and formed a south- to southeast-vergent thrust pile. Contraction continued until the Early to Middle Miocene in western Turkey and is still continuing in eastern Anatolia. The last significant episode of mechanical coupling along the Bitlis-Zagros suture zone occurred in the Middle Miocene, as shown by the thermochronological dataset of Okay et al. (2010).

In western Anatolia the different types and ages of Alpide metamorphism leads to the subdivision of the Anatolide-Tauride terrane into zones with different metamorphic features, in a similar manner to the subdivision of the Western Alps into Helvetics and Penninic zones (Okay, 2008). From north to south, there are three main regional metamorphic zones in the Anatolide-Taurides of western Anatolia: (i) a Cretaceous blueschist belt (the Tavşanlı Zone), (ii) a lower grade high-pressure metamorphic belt (the Afyon Zone), and (iii) a Barrovian-type Eocene metamorphic belt (the Menderes Massif) (Fig. 2.4). To the northwest of the Menderes Massif there is a belt of chaotically deformed uppermost Cretaceous-Paleocene flysch with Triassic to Cretaceous limestone blocks. This Bornova Flysch Zone has an anomalous position between the Izmir-Ankara suture and the Menderes Massif. The Taurides, which lie south of the metamorphic regions, consist of a stack of thrust sheets of Paleozoic and Mesozoic sedimentary rocks (e.g. Gutnic et al., 1979; Özgül, 1984). The Central Anatolian Crystalline Complex north of the Taurides is a region of metamorphic and plutonic rocks with Cretaceous isotopic ages. The question of the affinity of the Central Anatolian Crystalline Complex, whether part of the Anatolide-Tauride terrane, or a single terrane on its own, is not yet solved (Okay, 2008).

Following is a synthetic description of the principal unit of the Anatolide-Tauride domain.

### 2.5.1 Bornova Flysch Zone

The Bornova Flysch Zone is a 50 to 90 km wide and ~230 km long tectonic zone between the Menderes Massif and the İzmir-Ankara suture (Fig. 2.4). It consists of chaotically deformed Upper Maastrichtian-Lower Paleocene greywacke and shale with blocks of Mesozoic limestone, mafic volcanic rock, radiolarian chert and serpentinite (Erdoğan, 1990; Okay et al., 1996). Many of the blocks must have been

initially olistoliths but were subsequently tectonized. The size of the Mesozoic limestone blocks can be as large as 10 km or more, although some of the large "blocks" may consist of tectonically juxtaposed smaller blocks. The proportion of the ophiolitic clasts in the sheared clastic matrix increases eastward and the Bornova flysch passes laterally to an ophiolitic mélange. In the east the Bornova Flysch Zone is in contact with the Menderes Massif along post-Eocene normal faults.

The Bornova Flysch zone has formed by the rapid foundering and destruction of the Anatolide-Tauride carbonate platform during the Maastrichtian-early Paleocene. Large sections of relatively intact carbonate platform are exposed on the island of Chios and on the adjacent Karaburun Peninsula, where the stratigraphy is also most complete (Erdoğan et al., 1990). The blocks in the Bornova Flysch Zone generally consist of Triassic, Jurassic and Cretaceous marine limestones. Late Cretaceous is represented by deep marine red limestones, which lie unconformably over the older carbonates. The stratigraphy of some of the blocks in the Bornova Flysch Zone is similar to those described from the Lycian nappes, 300 km to the southeast (Okay & Altıner, 2007). This biostratigraphic similarity lends strong support for a northerly origin of the Lycian nappes. The flysch and the blocks are unconformably overlain by undeformed late Early Eocene neritic limestones. This constrains the age of the deformation in the Bornova Flysch Zone to Late Paleocene.

### 2.5.2 The Tavşanlı Zone

The Tavşanlı Zone is a regional blueschist belt in northwest Turkey, ~250 km long and ~50 km wide, immediately south of the main Neo-Tethyan suture (Figs. 2.4 & 2.5). The blueschist sequence in the Tavşanlı Zone consists of Permo-Triassic metapelitic schists at the base, Mesozoic marbles in the middle and a series of metabasite, metachert and phyllite at the top (Okay, 1984). The blueschists represent the subducted and subsequently exhumed passive continental margin of the Anatolide-Tauride terrane. Phengite Rb-Sr and Ar-Ar data from the blueschists indicate a Late Cretaceous (80 ± 5 My) age for the HP/LT metamorphism (Sherlock et al., 1999). The coherent blueschist sequence is tectonically overlain by a Cretaceous accretionary complex of basalt, radiolarian chert and pelagic shale. The accretionary complex exhibits generally a low-grade incipient blueschist metamorphism. Large tectonic slabs of ophiolite, predominantly peridotite, lie over the coherent blueschists or over the accretionary complex. The whole

tectonostratigraphic pile is intruded by calc-alkaline Eocene plutons, which form an elongate belt, 400 km long and 60 km wide, extending from the Sivrihisar region in the central Anatolia to the Marmara Sea (e.g. Harris et al., 1994; Okay & Satır, 2006; Altunkaynak, 2007). This Eocene magmatic belt constitutes either a magmatic arc or has formed as a result of slab break-off. Locally a low pressure - high temperature metamorphism has accompanied the intrusion of granodiorites.

### 2.5.3 The Afyon Zone

The Afyon Zone occupies the region between the Menderes Massif and the Tavşanlı Zone (Figs. 2.4 & 2.5). It exhibits the typical Tauride stratigraphy with a mixed carbonate clastic Paleozoic series overlain by Mesozoic marbles but shows a low-grade medium to high pressure metamorphism characterized by extensive occurrences carpholite and local sodic amphibole (Candan et al., 2005). The metamorphic rocks are tectonically overlain by an ophiolitic mélange and by ophiolites. The age of regional metamorphism is not analytically determined but is stratigraphically constrained as latest Cretaceous to Paleocene.

### 2.5.4 Central Anatolian Crystalline Complex

The Central Anatolian Crystalline Complex is a large region of metamorphic and granitic rocks with Cretaceous isotopic ages. An extensive Neogene sedimentary and volcanic cover leads to the subdivision of the Central Anatolian Crystalline complex into several submassifs; the important ones include Kırşehir, Akdağ and Niğde massifs (Fig. 2.9). The Central Anatolian Crystalline complex is regarded either as the metamorphosed northern margin of the Anatolide-Tauride terrane (e.g. Poisson et al., 1996; Yalınız et al., 2000) or a distinct terrane separated from the Anatolide-Taurides by the Inner Tauride Suture (Şengör et al., 1982; Görür & Tüysüz, 2001; Whitney & Hamilton, 2004). The metamorphic rocks of the Central Anatolian Crystalline Complex constitute a coherent metasedimentary sequence of gneiss, micaschist, metaquarzite, marble and calc-silicate rock, which are isoclinally folded and multiply deformed (Seymen, 1983).

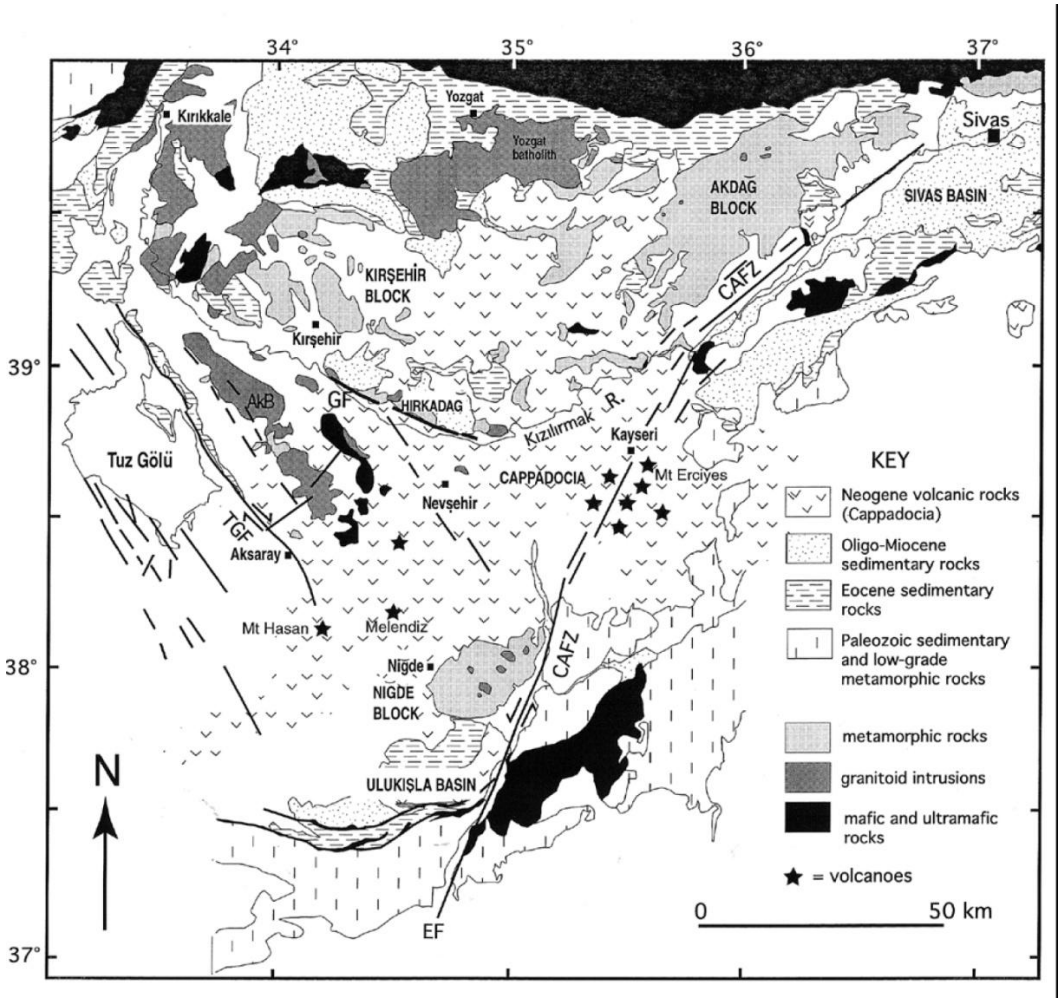


**Fig. 2.9 – Geological map of the Central Anatolian Crystalline complex (from Okay, 2008; mod. after Whitney & Dilek 2001).**

The regional metamorphism varies from greenschist to granulite facies and is of high temperature-medium/low pressure type. The maximum pressure attained during the metamorphism is ca. 6 kbar corresponding to depths of ca. 20 km (Whitney et al., 2003). This low- to medium-pressure metamorphism was overprinted in several submassifs by a lower pressure metamorphism associated with the emplacement of granitic intrusions. The age of regional metamorphism is Late Cretaceous (91-85 My) based on monazite and zircon U-Pb dating (Whitney et al., 2003; Whitney & Hamilton, 2004). The metamorphic rocks are tectonically overlain by an unmetamorphosed Late Cretaceous accretionary complex of basalt, radiolarian chert, pelagic limestone, sandstone and serpentinite. The accretionary complex as well as the metamorphic rocks is intruded by granitic rocks, which cover large areas in the Central Anatolian Crystalline Complex. The plutonic rocks are

mainly quartz-monzonites, quartz-monzodiorites, monzonites and monzodiorites with a calc-alkaline character, and their trace element geochemistry is compatible with a syn- to post-collisional tectonic setting (Akıman et al., 1993; Erler & Göncüoğlu, 1996; İlbeyli et al., 2004). There are also minor crustally derived peraluminous plutons. The K/Ar biotite and hornblende, titanite and zircon ages from the granitic rocks generally range from 95 to 70 My (Whitney et al., 2003; Köksal et al., 2004; Boztuğ et al., 2007). An upper age limit on the granitic magmatism as well as on regional metamorphism is provided by the Upper Maastrichtian terrigenous to shallow marine clastic and carbonate rocks, which lie unconformably on the metamorphic as well as on the granitic rocks (Seymen, 1983).

### 2.5.5 The Menderes Massif

#### *2.5.5.1 General description and definition*

The Menderes Massif of western Anatolia is exposed in a tectonic window of approximately 200×100 km exposing metamorphic rocks belonging to the basement complex of the Anatolide-Tauride terrane (Figs. 2.4, 2.5 & 2.6). Topographically, the central west coast of the Anatolian Peninsula is characterized by the transition from the Anatolian Plateau to the Aegean sea. The landforms of the area are mainly controlled by a series of E-W and ESE-WNW–oriented horsts and grabens that delimit mountain ranges and highlands. This Basin and Range-type topography is a consequence of Neogene-to-Recent normal and strike-slip faulting.

The Menderes Massif is tectonically overlain by nappes of the İzmir-Ankara Suture Zone (Şengör & Yilmaz, 1981) on its northern flank (including the Bornova Flysch zone), the Afyon zone on its eastern border (Şengör et al., 1984), and the Lycian nappes (Brunn et al., 1970; de Graciansky, 1972; Poisson, 1977) on its southern flank (Fig. 2.3, 2.4 & 2.5). The massif is described as the assemblage of a Precambrian core of micaschists, augen gneiss and minor granulite and eclogite intruded by voluminous metagranites with latest Precambrian (550 My) intrusion ages (e.g. Schuiling, 1962; de Graciansky, 1966; Dürr, 1975; Şengör et al., 1984). This Precambrian crystalline basement is overlain by Paleozoic to Lower Tertiary metasedimentary rocks constituting the 'cover' series. The oldest fossiliferous series in the cover sequence are the Permo-Carboniferous marble, quartzite and phyllite of the so-called Göktepe Formation. Through a clastic interval the Göktepe Formation

is overlain by a thick sequence of Mesozoic marbles. The top part of the marbles sequence contains an Eocene flysch sequence with serpentinite olistostrome.

In the Menderes Massif, pronounced magmatic activity occurred at the Proterozoic-Cambrian boundary (Hetzel & Reischmann, 1996; Dannat & Reischmann, 1999; Gessner et al., 2001a; Reischmann & Loos, 2001), in the mid-Triassic (Dannat, 1997; Koralay et al., 2001), and in the Miocene (Hetzel et al., 1995a; Collins et al., 2002). In the Cycladic zone, the granitic basement is of Carboniferous age (Reischmann, 1997; Engel & Reischmann, 1997). In addition, there were very limited Triassic intrusions (Reischmann, 1997; Ring et al., 1999b) and other prominent Miocene to Holocene magmatic activity in the Cycladic zone (Altherr et al., 1982).

***Menderes Nappes***

According to some authors (e.g. Ring et al., 1999b; Gessner et al., 2001a, 2001c) the geological structure of the Menderes Massif consists into a series of nappes. Although these nappes were never effectively found in field, these consist, from top to bottom, of the (1) Selimiye Nappe, an upper metasedimentary succession of intercalated marble and calc-schist; (2) Çine Nappe, a Proterozoic-Cambrian basement succession; (3) Bozdağ Nappe, a metapelitic succession with abundant amphibolite and a few marble lenses and (4) Bayındır Nappe, a lower metasedimentary succession (Ring et al., 1999b; Gessner et al., 2001a, 2001c). The structurally lowest unit exposed in the Menderes nappes, the Bayındır Nappe, is affected only by one major Alpine tectonometamorphic event, whereas in the overlying Bozdağ, Çine, and Selimiye Nappes, pre-Alpine and Alpine events are documented (Fig. 2.10) (Ring et al., 1999b; Gessner et al., 2001a, 2001c).

***Selimiye Nappe***

The Selimiye Nappe contains a metasedimentary sequence the basal part of which is of Precambrian age (Hetzel & Reischmann, 1996; Loos & Reischmann, 1999). The top of the nappe pile is made of Paleozoic metapelite, metabasite, and marble (Schuiling, 1962; Çağlayan et al., 1980; Loos & Reischmann, 1999; Régnier et al., 2003; Gessner et al., 2004).

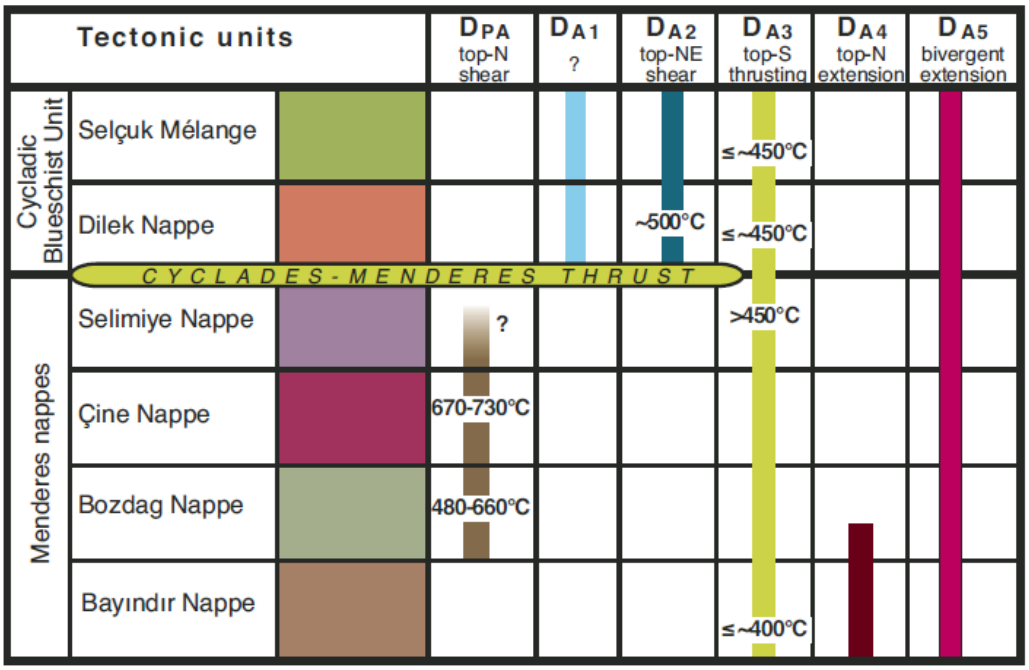


**Fig. 2.10 – Pre-Alpine and Alpine events DPA and DA1 to DA5 in the tectonic units of the Anatolide Belt in western Turkey. Temperature estimates after Gessner et al. (2001c), except for Çine and Bozdağ Nappes (Ring et al., 2001b) and Dilek Nappe (Will et al., 1998). Diagram indicates that the Anatolide Belt was assembled during DA3; subscripts PA and A denote pre-Alpine and Alpine deformation ages, respectively. After Gessner et al. (2001c).**

The tectonometamorphic history of the Selimiye Nappe remains controversial. Interpretations of the greenschist-facies Selimiye Shear Zone include (1) Alpine shortening (Gessner et al., 2001a, 2004); (2) Precambrian and Alpine polymetamorphic deformation (Régnier et al., 2003); (3) post-Precambrian, pre-Alpine monometamorphic deformation (Régnier et al., 2006); (4) folding during Alpine shortening (Erdoğan & Güngör, 2004); and (5) late Alpine extension (Bozkurt & Park, 1994). Bozkurt & Park (1994) have interpreted this shear zone as an extensional feature, but there is inconsistent evidence for a telescoped metamorphic field gradient or for a change in cooling history across it.

Another contentious issue is that a number of authors claim that the granitic rocks intrude lithologies that can be correlated with Mesozoic sediments and are therefore “Alpine” in age (Şengör et al., 1984; Erdoğan & Güngör, 1992; 2004; Bozkurt et al., 1993; 2001), whereas radiometric ages of the intrusions give late Proterozoic to Cambrian ages (Reischmann et al., 1991; Hetzel & Reischmann, 1996; Gessner et al., 2001a; 2004); thus lithological correlations in highly deformed metapelites can be problematic. Recently Candan et al. (2011) concluded, by

radiometric and petrographic analysis, that the meta-conglomerates of the cover series are relate to the Precambrian basement: this indicate that the basement originates the conglomerates and so exclude the 'Alpine' origin.

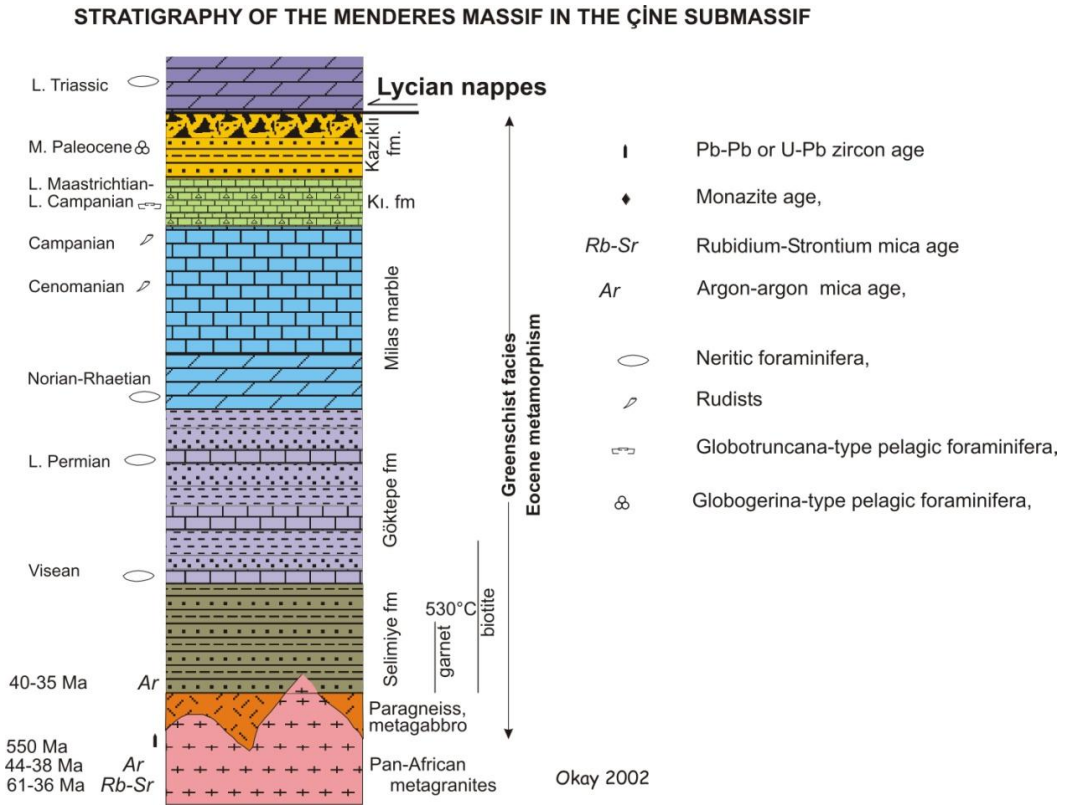


**Fig. 2.11 – Synthetic stratigraphic sections of the Menderes Massif (from Okay et al., 2008).**

In the Central Menderes Massif, top-NE shear-sense indicators dominate. At the northwestern margin of the Çine submassif, symmetric fabric elements such as strain shadows around feldspar and foliation boudinage occur together with minor top-NE kinematic indicators. In the central Çine submassif, both top-NE and top-SW kinematic indicators have been mapped. There is no evidence that the top-NE and top-SW kinematic indicators are of different generations, and no evidence that they developed during different metamorphic conditions. However, locally the top-SW indicators are inverted top-NE kinematic indicators owing to later recumbent tight to isoclinal folding about axes parallel to the NE-trending $D_{PA}$ stretching lineation. Mapping of the Çine Massif has revealed five generations of granitic intrusions, two of which are not affected by amphibolite-grade shearing. U-Pb dating has produced

Proterozoic to Cambrian ages for these rocks (Gessner et al., 2004), similar to the Birgi metagranite east of Ödemiş (Hetzel et al., 1998).

A further problem is that the Selimiye Shear Zone appears to be wrapped around the granites and orthogneisses toward the western outcrop limit of these lithologies, which has led to contradicting interpretations (Gessner et al., 2001b; Régnier et al., 2003, 2006; Gemici, 2004). There is little doubt, however, that the schists and marbles overlying the Selimiye Nappe can be correlated with Cycladic blueschists, and that these and the Lycian nappes preserve high-pressure metamorphic relicts for which there is no evidence in the Menderes nappes (Oberhänsli et al.,1998a; 1998b; 2001; Ring et al., 1999a; Rimmelé et al., 2001).

***Çine and Bozdağ Nappes***

Çine Nappe consists of deformed orthogneisses, largely undeformed metagranites, and minor pelitic gneisses, eclogites, and amphibolites. Protoliths of much of the orthogneiss-metagranite intruded at ca. 560–530 My (Loos & Reischmann, 1999; Gessner et al., 2001a; 2004). The underlying Bozdağ Nappe is made up of metapelite with intercalated amphibolite, eclogite, and marble lenses. Protolith ages of all rock types of the Bozdağ Nappe are unknown, but geologic constraints (Candan et al., 2001; Gessner et al., 2001a) suggest a Precambrian age for at least parts of these rocks. The Bozdağ Nappe was intruded by granitoids at 240–230 My (Dannat & Reischmann, 1999; Koralay et al., 2001).

***Bayındır Nappe***

The Bayındır nappe, at the base of this succession, contains sericitic to phyllitic mica schists, quartzites, and marbles of inferred Permo-Carboniferous (Candan, 1998, personal commun.) to Mesozoic (Özer & Sözbilir, 2003) age. These rocks were metamorphosed under lower greenschist-facies conditions at ca. 37 My (Lips et al., 2001). The absence of biotite in rocks of suitable bulk composition suggests temperatures below ca. 400 °C.

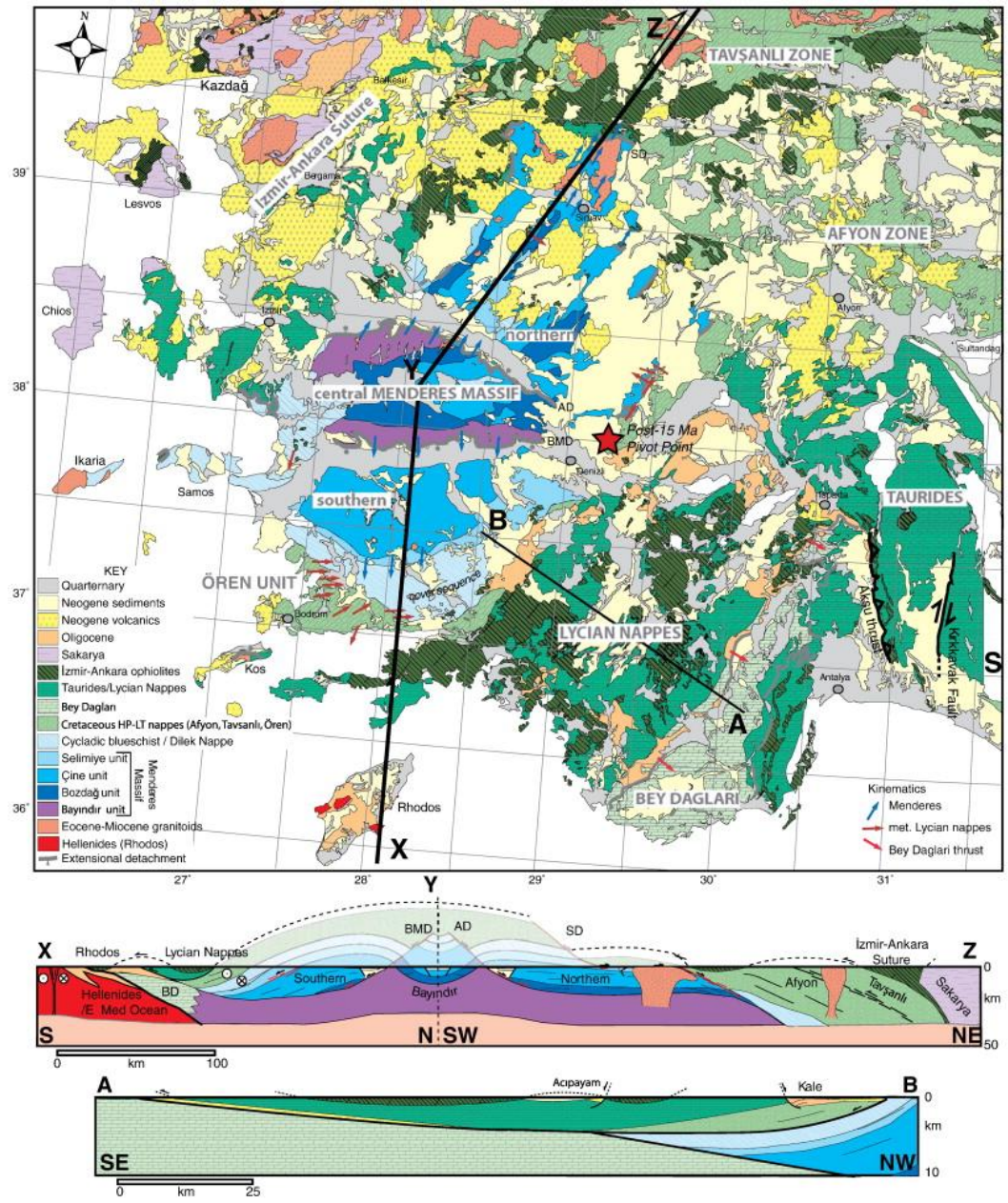


**Fig. 2.12 – Geological map of western Turkey, with schematic cross sections, based on the geological map of Turkey (MTA, 2002), with nappe subdivision in the Menderes Massif following Gessner et al. (2001b) and Régnier et al. (2007). The Dilek nappe in the southern Menderes Massif is based on the presence or absence of magnesiocarpholite and metabauxite, taken from the compilation of Rimmelé et al. (2003b). Arrows indicate shear sense with arrowhead pointing the direction of the tectonic top. AD = Alaşehir Detachment; BMD = Büyük Menderes Detachment; SD = Simav Detachment (from van Hinsbergen, 2010).**

### *2.5.5.2 Tectonostratigraphic description*

Studies based on fossil after Dürr (1975) suggest the Menderes Massif as the stratigraphic sequence as shown in Fig. 2.11, a product of Alpine compressional tectonics. In the period following this compression, the massif was exhumed along shear zones and low-angle normal faults that were products of Early Miocene extensional tectonics, and thus the massif took on much of its present-day form. Late Miocene – Pliocene E-W-trending graben systems separate the Menderes Massif into – from north to south – (i) the Eğrigöz, (ii) Gördes, (iii) Central Menderes Metamorphic Core Complex (CMCC) and (iv) Çine submassifs (Fig. 2.13)

- Eğrigöz: In this area the 'core' and 'cover' sequence (Dürr, 1975; Okay 2008) are separated by the Simav detachment fault (SDF). The hanging wall of the SDF consists of highly disrupted schist, marble, and ophiolitic flysch of the Cyclades blueschist unit and the İzmir-Ankara suture zone (Işık & Tekeli, 2001; Ring et al. 2003). The footwall comprises Precambrian gneisses of the Menderes nappe, and is locally intruded by two synkinematic Early Miocene (~21My) granitoids, the Eğrigöz and Koyunoba granites, elongates N–S. These synkinematics granites cover an area of about 400 $km^2$. The total extensional displacement along the SDF cannot be reliably determined from offset geologic markers, as rocks either side of the detachment represent units formerly juxtaposed by the earlier out-of-sequence Cyclades-Menderes thrust. The timing of cessation of movement along the SDF is constrained by 15.8–15.3 My volcano-sedimentary rocks deposited on the Simav detachment surface. This suggests that exhumation of the core rocks and the granitoids in this area must have occurred between 21-15 My. Thomson & Ring (2006) provide AFT, ZFT and AHe ages for the hanging wall and the footwall, concentrating between ~25 and ~19 My.
- Gördes: The rock units exposed in this area are grouped into four categories: (1) metamorphic rocks, including orthogneisses and metasediments comprising the northern Menderes Massif, (2) pegmatoids, (3) Neogene sedimentary rocks, and (4) Quaternary alluvial sediments. The orthogneisses, traditionally known as augen gneisses, occur in an about 1 to 4 km wide. They are interpreted as deformed and dynamo-thermally metamorphosed granitoid in the southern and central parts of the Menderes Massif. The augen gneiss contains zircon, present as short prismatic crystals

and apatite, as the commonest accessory mineral. Pegmatites form one of the most important and common lithologic association in the submassif area: they occur as a large dome intrusive into other metamorphic lithologies. The Neogene sedimentary rocks can be grouped into two as fluvial clastic rocks and the rocks with lacustrine origin. The Quaternary alluvial sediments being deposited presently within the submassif area and include poorly sorted sediments (block, cobble, boulder, pebble, sand, silt, clay) deposited along the alluvial fans, stream and river plains and valleys (Buğfaycioğlu, 2004).

- Central Menderes Metamorphic Core Complex (CMCC): the typical successions in this submassif outcrops in the Bozdağ region and in the Derbent region. Since the Early or Middle Miocene, NNE–SSW directed bivergent extension of the Menderes Massif nappe pile led to the formation of two detachments with opposite dips, the Gediz and Büyük Menderes detachments (Hetzel et al. 1995a; Gessner et al. 2001b, 2013; Ring et al. 2003) that border this whole region. In particular the Gediz detachment is spectacularly exposed on the northern flank of the Bozdağ block and dips ~ 15° to the NNE (Buscher et al. 2013); this have been pointed out by analysis on the abundant kinematic indicators that indicate a consistent top-to-the-NNE shear sense (Işık et al. 2003).

In the Bozdağ region the 'cover' series (Okay, 2008; Şengör et al., 1984) outcrops in northern part and are separated from the 'core' series (Okay, 2008; Şengör et al., 1984), which dominates in the southern part, by a major south-dipping thrust fault that has been reactivated by ductile and brittle normal faulting (Hetzel et al. 1998).

In the Derbent region the lithologies are the same. The gneiss complex (the 'core' series according to Okay, 2008; Şengör et al., 1984) structurally underlies all other rock-types in the Derbent area, and its base is not seen (Akkök, 1983). Its commonest rock types are porphyroblastic gneiss and augen gneiss with subordinate amounts of banded gneiss and massive granitic gneiss. The schist complex ('cover' series according to Okay, 2008; Şengör et al., 1984) overlies the gneiss complex structurally. The contact between the gneiss and schist complexes is sharp and most probably tectonic in nature.

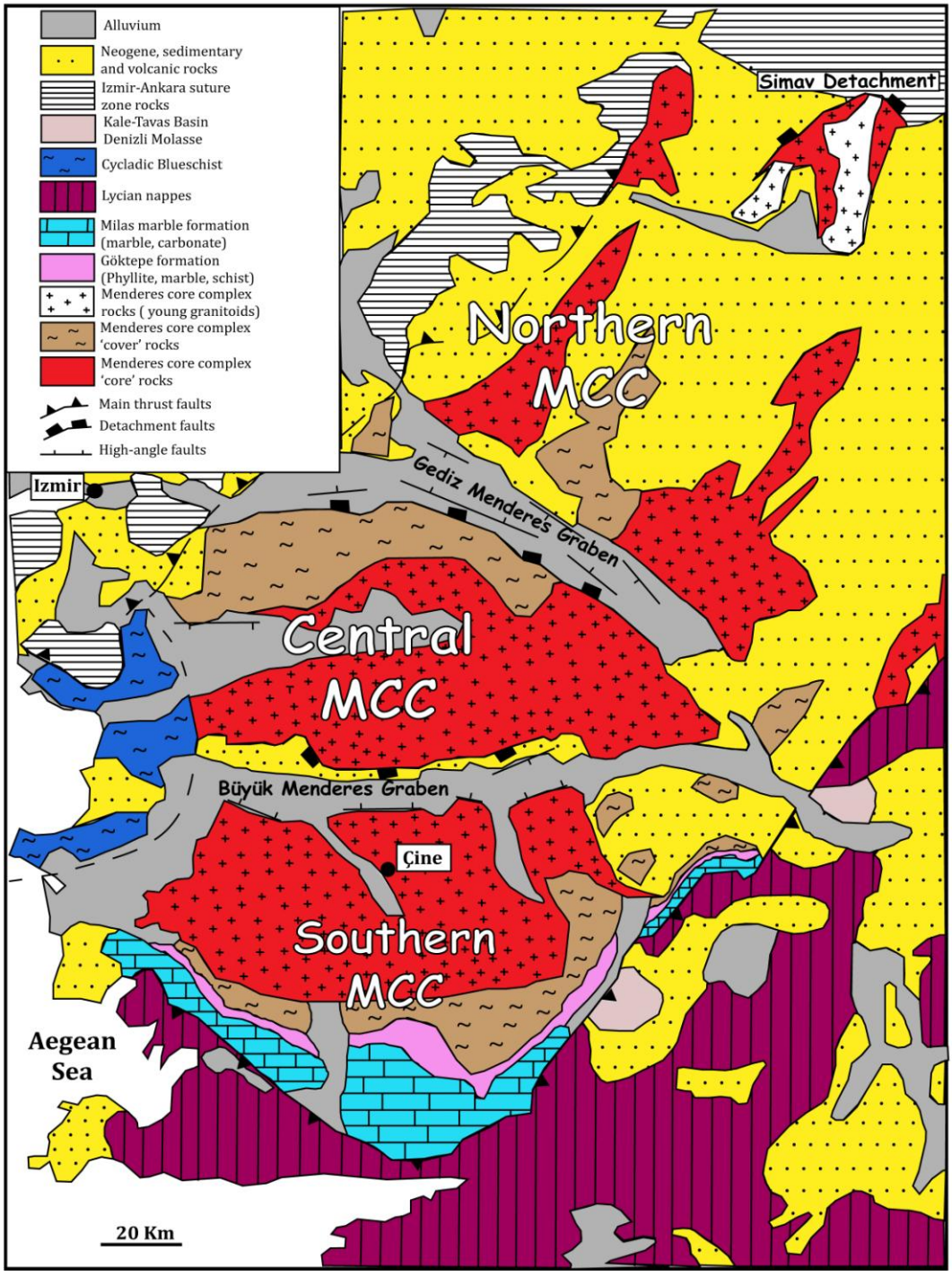


**Fig. 2.13 – Simplified geological map, with subdivision, of the Menderes Massif (base map from Işık et al., 2003, mod).**

The marbles ('cover' series according to Okay, 2008; Şengör et al., 1984) are underlain by the schist complex. Studies of contacts between the marbles and the schist complex have so far revealed no indications of an original unconformity between them. The marbles are commonly layered, layering

being defined by color, and probably representing relict bedding. (Akkök, 1983).

The ductile deformation in the CMCC was accompanied by the intrusion of a syntectonic granodiorites, SE of Salihli (in the Bozdağ region) into the 'cover' series. U–Pb dating of the granodiorites yielded intrusion ages of 15.0 ± 0.3 My (Salihli granodiorite) (Glodny & Hetzel 2007).

- Çine: the Menderes Massif sequence is simplest and best known here.

The 'core' sequence, especially in the region between the Bafa lake and Muğla, crops out made of Precambrian gneisses, and the 'cover' sequence of lower Paleozoic micaschists; Permo-Carboniferous metaquarzite, black phyllite and dark recrystallized limestone; Mesozoic, thickly bedded, recrystallized neritic limestones with bauxite horizons; recrystallized pelagic limestone and flysch of Paleocene to Early Eocene in age.

South of Çine it is possible to observe the Lycian nappes that overlie tectonically the Eocene flysch.

In this region can be recognized a Barrovian-type regional metamorphism of Eocene age that has affected the Menderes Massif; the metamorphic grade shows a gradual decrease upwards in the sequence (Ashworth & Evirgen, 1984; Okay, 1985; Satır & Friedrichsen, 1986). This regional metamorphism was related to the emplacement of the Lycian nappes over the Menderes Massif (Şengör et al., 1984), and has also affected the lower parts of the Lycian nappes, such that there is no metamorphic discontinuity between the Menderes Massif and the overlying nappes (Okay, 1989a).

Apart from the Eocene metamorphism, traces of an older Pan-African metamorphism have been documented in the Precambrian gneisses (Satir & Friedrichsen, 1986).

#### *2.5.5.3 Metamorphic evolution of the Menderes Massif*

The Menderes Massif had a complex, polymetamorphic history, although the number and timing of the different metamorphic phases are still controversial. The first event (M1) affected only the gneissic core and was an intense deformation and amphibolite-facies metamorphism associated with widespread migmatization and local anatexis (Şengör et al., 1984; Satir & Friedrichsen, 1986; Dora et al., 1995). Rb-Sr whole-rock ages of 502 ± 10 My (Satir & Friedrichsen, 1986) are the only

evidence for the amphibolite-facies metamorphism since the subsequent Tertiary events have almost erased all other evidence. It has been argued that highly deformed tonalitic and granitic intrusions dated at 471 ± 9 My (Rb-Sr whole rock analysis; Satir & Friedrichsen, 1986) mark the end of this episode (Şengör et al., 1984; Satir & Friedrichsen, 1986).

Although Candan (1995) considered the discovery of metagabbros with eclogite relics in the core as representing early high-pressure (HP) metamorphism prior to the M1 event, Oberhänsli et al. (1997) have pointed out that the age of (HP) metamorphism in the core gneisses still awaits clarification.

Akkök (1983) and Dora et al. (1995) speculated for a Triassic metamorphic event but did not present any geochronological or geological data; evidence for post-tectonic magmatism dated at 250-227 My (Dannat & Reischmann, 1998; Koralay et al., 1998) are only reported from the central and northern submassifs.

The Menderes Massif has suffered an HP-LT stage of metamorphism in the Early Eocene. This hypothesis is supported by the presence of blueschists and eclogites in the central submassif and into the Dilek mélange above the western part of the Menderes Massif, where the eclogites were found in an olistostromal unit on the top of the 'cover' series of Menderes Massif (Fig. 2.4) (Candan et al., 1997; 1998; Oberhänsli et al. 1997; 1998a). For these reasons the Menderes Massif has traditionally been interpreted as the eastern lateral continuation of the Cycladic zone or Cycladic massif (Dürr et al., 1978), where an old crystalline core is overlain by Paleozoic and Mesozoic cover series with metamorphic grade decreasing up section. This longstanding view was challenged by geochronological studies which show marked differences in the age of the basement of the Anatolide Belt and the Cycladic zone, respectively, indicating that the basement of the Cycladic zone and the Anatolide cannot be correlated. Candan et al. (1997) correlated the Dilek olistostromal eclogites with a similarly metamorphosed olistostromal unit on Syros Island. In the same region, this eclogite-bearing olistostrome tectonically overlies Mesozoic marble series intercalated with mafic metapelites and metavolcanites containing well-preserved blue amphiboles (Candan et al., 1997; Oberhänsli et al., 1998a). This blueschist-facies metamorphism (10 kbar min/470°C; Candan et al., 1997) dated Middle Eocene (40My, Ar/Ar on phengite, Oberhänsli et al., 1998a) was overprinted by a Barrovian-type metamorphism under greenschist-facies conditions during the Late Eocene-Early Oligocene (Candan et al., 1997). A correlation with the

blueschists of Samos island belonging to the Cycladic complex has been proposed (Candan et al., 1997; Oberhänsli et al., 1998a). Because of similar eclogite and blueschist metamorphic imprints described in the Aegean domain, many authors have argued that the Dilek region forms the eastward lateral continuation of the Cycladic complex, and have excluded it from the geological definition of the Menderes Massif. So two different units, the Cycladic Blueschist Unit and the underlying Menderes nappes, make up the Anatolide Belt (Ring et al., 1999a; Gessner et al., 2001a; b; c; Okay, 2001; Régnier et al., 2003).

Rimmelé et al. (2003) discovered Fe-Mg carpholite in the basal Permo-Triassic conglomerate of the 'cover' series of the Menderes Massif. These rare occurrences could show that the Menderes Massif has recorded HP-LT metamorphic conditions (10-12 Kbar, 440° C) after the Early Eocene in the Mesozoic part of the cover series.

A major event affecting the whole massif is the so-called Main Menderes Metamorphism (MMM), which is associated with an intense deformation. It corresponds to HT-LP conditions in the lower parts of the massif and only to greenschist facies conditions in the upper parts of the cover rocks. It is commonly believed that the MMM affected the whole massif. The maximum P-T estimates are around 9 kbar and 500-550°C (Okay, 2001). This regional metamorphism and deformation of the Menderes Massif is considered to be a direct consequence of the southward propagation of the Paleocene collisional front between the Sakarya zone in the north and the Anatolide-Tauride terrane in the south, with the consequent southward advance of the Lycian nappes (Şengör et al., 1984).

The last metamorphic event in the massif corresponds to greenschist retrogression associated the final exhumation of metamorphic rocks below flat-lying extensional shear zones (Lips et al., 2001). This last stage is coeval with the Aegean extension (Jolivet et al., 2004) and is associated with synkinematic Miocene granitoid intrusions (Bozkurt & Oberhänsli, 2001).

### 2.5.6 The Lycian Nappes

In the region between Bafa Lake and Denizli a rootless tectonic unit of Mesozoic continental margin deposits overlies tectonically the Lower Eocene flysch of Menderes Massif (Okay, 1989a). Such allochthonous units are collectively known as the Lycian nappes (Fig. 2.4).

### *2.5.6.1 General stratigraphy*

The Lycian nappes complex as being made of three main units: the 'Lycian Thrust Sheets' composed of upper Paleozoic to Tertiary sediments; a thick chaotic mélange unit (the 'Lycian Mélange'), tectonically overlain by the 'Lycian Ophiolites' which consist of sepentinized peridotites with a metamorphic sole (Fig. 2.14) (Rimmelé, 2003).

At the south of the Menderes Massif, the basal 'Lycian Thrust Sheets' widely crop out on the Bodrum peninsula. They are composed of Upper Permian-Lower Triassic reddish to greenish metapelites (the Karaova formation of Phillippson, 1910-1915) overlain by a thick succession of Middle Triassic-Middle Jurassic massive limestones and dolomites, grading upward to Upper Jurassic-Upper Cretaceous cherty limestone. This thick limestone succession is overlain by the Campanian to Maastrichtian Karaböğürtlen wildflysch (de Granciansky, 1972; Bernoulli et al., 1974; Okay, 1989a). This sequence records a continuous sedimentation from Late Paleozoic to Late Cretaceous. Recent investigations in this area revealed the occurrence of a widespread HP metamorphism documented by Fe-Mg-carpholite in the metasediments of the basal Karaova formation, which involves pressure of about 8 kbar and maximum temperature of 400° (Oberhänsli et al., 2001). HP-LT relics have also been found in klippen of Lycian nappes located at the top of the Menderes Massif. Up to this discovery of HP paragenesis in the Karaova formation, the base of the Lycian nappes was thought to have recorded only a weak low-grade metamorphism under greenschist-facies conditions (Ashworth & Evirgen, 1984).

### *2.5.6.2 Origins*

The origin of the Lycian Nappes has been the subject of much controversy. While some authors argued that the tectonic slices originated from north of the Menderes Massif (de Granciansky, 1972; Dürr, 1975; Dürr et al., 1978; Gutnic et al., 1979; Şengör & Yilmaz, 1981; Okay, 1989a; Collins & Robertson, 1997, 1998, 1999, 2003; Güngör & Erdoğan, 2001), others considered a "dual" origin (Poisson, 1977; Poisson, 1985; Özkaya, 1990; Ersoy, 1993). For example, de Graciansky (1972) restored the Lycian thrust slices to a root zone north of the Menderes Massif, while Poisson (1977) considered the sedimentary units associated with the peridotitic nappe as derived from the north and the other sedimentary thrust sheets as derived from an

intra-continental rift basin located between the Bey Dağlari platform (in the south, Fig. 2.5) and the Menderes Massif (the 'intra-Tauric trough' of Poisson, 1985). Ersoy (1993) also advocated this same dual origin concept but supported the idea that the units which derived from areas to the north of the Menderes Massif were only the ophiolitic slices which were transported southward by Late Cretaceous-Middle Miocene thrusts. The other units consist mainly of carbonate nappes originated from a trough located south of the Menderes Massif as described before by Poisson (1985). Based on the observation of distinct stratigraphic sequence in the Lycian allochthonous, Özkaya (1990) also claimed that the Lycian allochthonous units were derived from two distinct tectonic terrains. At the same time, Okay (1989a) confirmed the difference in the age deposition within the Lycian allochthonous units observed by Özkaya (1990) but contradicted the hypothesis of Özkaya (1990) affirming that all the thrust sheets were transported only from northwest to southeast. Other studies have suggested that the Lycian nappes originally formed the northern margin of the Menderes Massif and were tectonically transported southward (Dürr, 1975; Dürr et al., 1978; Gutnic et al., 1979; Şengör & Yilmaz, 1981; Collins & Robertson, 1997; 1998; 1999; 2003). Şengör & Yilmaz (1981) suggested that the Lycian Allochthonous belonged to the southern margin of the Neotethyan oceanic basin, located north of the Menderes platform. On the basis of a tectono-stratigraphic analysis, Collins & Robertson (1997; 1998; 1999; 2003) concluded that the Lycian Taurides consist of an allochthonous Mesozoic passive margin succession that was detached from its autochthon with a complex thrusts system and translated southeastward to its present position between Late Cretaceous and Late Miocene.

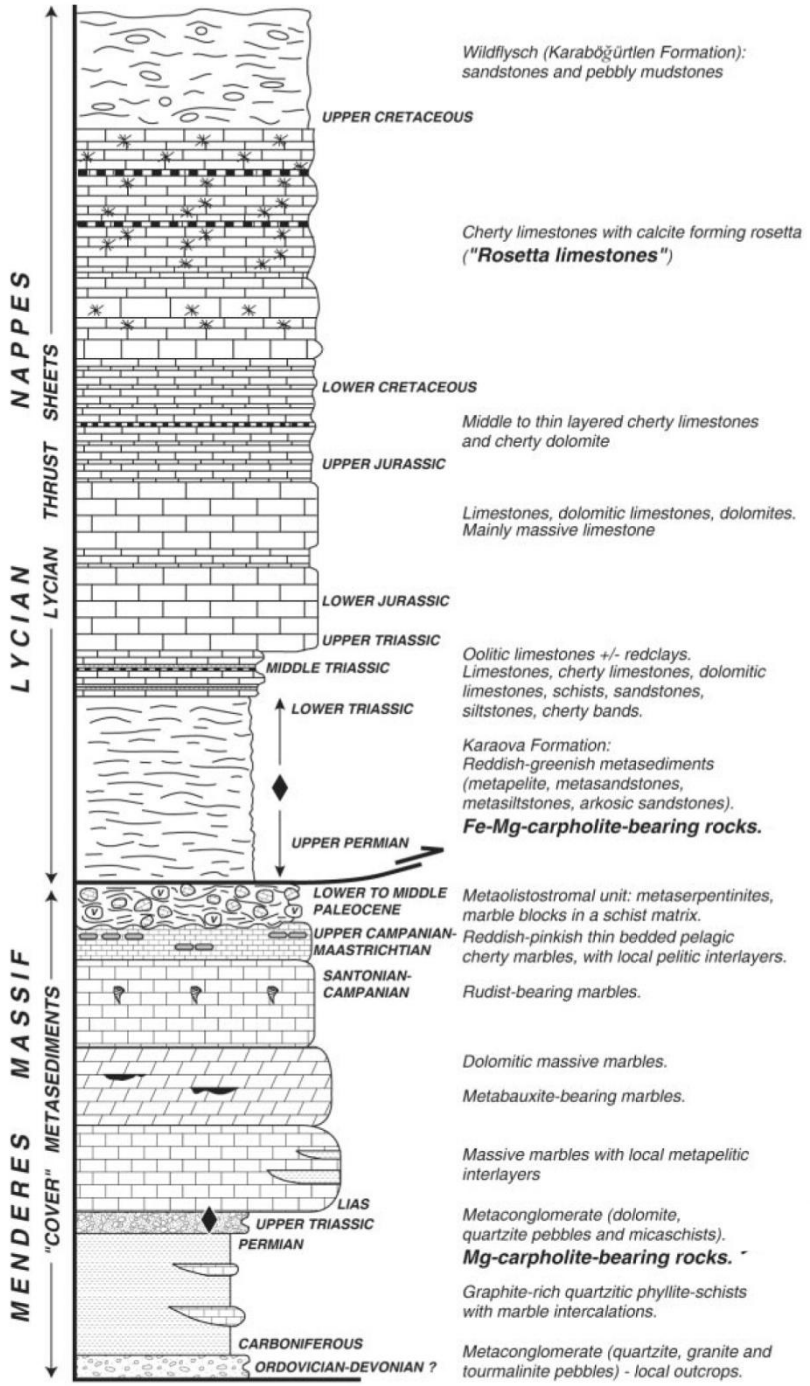


**Fig. 2.14 - Synthetic stratigraphic sections of the Menderes metasedimentary 'cover' and the overlying Lycian nappes (from Rimmelé et al. 2005).**

### 2.5.7 Sedimentary basins of the southern Menderes Massif

The sedimentary basins in the southern Menderes Massif crop out along the southwest Anatolian Shear Zone (Fig. 2.15) (Çemen et al., 2006), a theoretical

composite shear zone separating the highly extended Western Anatolia terrane to the north and the northwest from the Lycian nappes and the Tauride units to the south and the southeast, but not yet found in field. Several sedimentary basins are associated with the southwest Anatolian shear zone. From southwest to northeast, these basins are the Ören, Yatağan, Kale-Tavas, and Denizli basins.

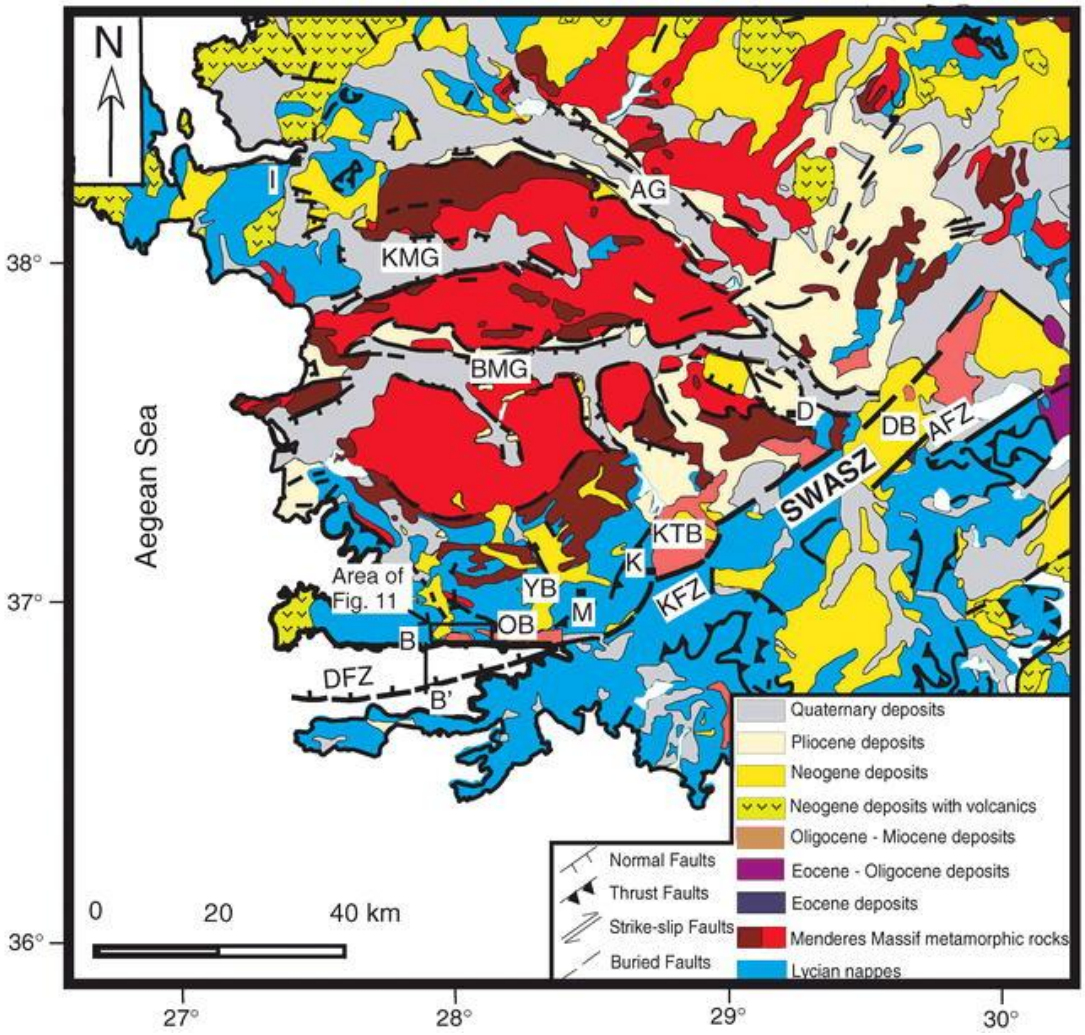


**Fig. 2.15 – Simplified geologic map showing the sedimentary basins adjacent to the Southwest Anatolian shear zone (SWASZ). Abbreviations: Towns: D—Denizli; I—İzmir; K—Kale; M—Muğla. Structural elements: AFZ—Acigol fault zone; AG—Alaşehir graben; BMG—Büyük Menderes graben; DB—Denizli basin; DFZ—Datça fault; KFZ—Kale fault zone; KMG—Kucuk Menderes graben; KTB—Kale-Tavas basin; OB—Ören basin; SWASZ—Southwest Anatolian shear zone; YB—Yatağan basin (from Çemen et al., 2006).**

#### *2.5.7.1 The Ören and Yatağan basins*

In the Ören and Yatağan basins, the basinal sediments unconformably overlie slightly metamorphosed successions of the dominantly carbonate rocks of the western Taurides. The basin fill in the two basins is similar and consists of a lower unit composed predominantly of coarse conglomerates grading upward to sandstones and an upper unit of shale-marl-dominated fine clastics (Yılmaz et al., 2000). The conglomerate unconformably overlies the Lycian nappes along the northern margin of the Gulf of Gökova. This discontinuously exposed conglomerate unit is termed the Gokceoren formation and is assigned a Late Oligocene age by Gürer & Yılmaz (2002). The conglomerate has been interpreted as a submarine alluvial fan deposit (Ozerdem et al., 2002). The northern boundary of the conglomerate is a down to the south normal fault system that may have been responsible for the unit's deposition. According to Çemen et al. (2006) this fault probably provided the highland for the formation of the conglomerate. A seismic reflection profile across the Gökova basin (Kurt et al., 1999) shows the presence of a major down-to-the-north fault along the southern margin of the Gulf of Gökova. The fault was named the Datça fault by Seyitoğlu et al. (2004). It has a large rollover anticline and associated antithetic faults that control the deposition in the Gulf of Gökova. However this fault activity started in the Late Miocene (Kurt et al., 1999) and so appears difficult that can be related to the basin formation. Recent study by Gürer et al. (2013) interpreted the Yatağan basin as an intermountain basin that developed, without any important tectonic control, between the Middle Miocene and Pliocene. The important event recorded during this period was the erosion of the uplifted cover units of the Menderes Massif, which caused the denudation of its gneissic core. The irregular topography created during this period caused the formation of an approximately NW-SE-trending fluviatile-lacustrine intermountain basin (Gürer et al., 2013).

#### *2.5.7.2 The Kale-Tavas basin*

The Kale-Tavas basin -a depression having SW–NE orientation (Fig. 2.15) - is the largest of the Cenozoic basins adjacent to the Southwest Anatolian shear zone. The basal sedimentary units of the Kale-Tavas basin are time equivalents of those of the Ören and Yatağan basins. The basin fill starts with Oligo-Miocene debris flows and fluvial deposits containing clasts derived from fault-controlled structural highs to

the south (Akgün & Sözbilir, 2001). According to Yılmaz et al. (2000) the Oligocene conglomerates of the Kale-Tavas basin contain predominantly ophiolitic material derived from the uppermost tectonic slice in the Lycian nappe pile, which was overlying the Menderes Massif in the Eocene (Şengör et al., 1984). The basin fill continues with lagoonal and shallow marine clastics and limestone lenses. The marine units are unconformably overlain by the Middle–Late Miocene continental clastics, which are capped by the Pliocene lacustrine limestones (Yılmaz et al., 2000).

The southeastern side of the basin is bounded by a northeast-southwest-trending normal fault that is part of the southwest Anatolian shear zone (Fig. 2.15). The fault controlled the accumulation of the basin fill and formed along the northern side of a southward-thrusting (Lycian nappe front) tectonic wedge (Yılmaz et al., 2000). So the Kale–Tavas basin is a syn-tectonic sedimentary basin that developed simultaneously with the thrust activity during Oligocene–Early Miocene. Tectonic control of the sedimentary processes, recorded in the rapid deepening and consecutive infilling of the Kale–Tavas basin, is a strong argument for interpreting it as a typical piggyback basin developed above the low-dipping normal fault plane (Gürer et al., 2013).

#### *2.5.7.3 The Denizli Molasse*

The Denizli molasse crops out NE of the city of Denizli. Its stratigraphy was studied in detail by Sözbilir (1997). The succession commences with Late Oligocene alluvial fan deposits and grades upward into fan delta - shallow marine deposits, including lenses of coal and carbonate deposition as patch reefs. Then the sequence continues with massive and cross-bedded conglomerates, planar cross-bedded and wave-rippled sandstones, bioturbated and fossiliferous mudstones, coal-bearing shales, lenses of reef limestones and sandstone-mudstone alternations that can be correlated with the Oligocene conglomerates in the Kale-Tavas basin (Akgün & Sözbilir, 2001).

#### *2.5.7.4 Tectonic significance of the basins*

Variations of the petrologic composition of the clastic units within the Ören, Yatağan, Kale-Tavas, and Denizli basins elucidate the structural evolution of both the southwest Anatolian Shear Zone and the adjacent Menderes Massif. The conglomerate series at the base of these basins clearly show a provenance from the

Lycian nappes (Sözbilir, 2002.). Metamorphic-derived detritus appears in the basin fill in the Early Miocene, when the sedimentary succession of the Ören, Yatağan, Kale-Tavas and Denizli basins show high-grade metamorphic rock fragments of the present-day Menderes Massif (Fig. 2.16) (Sözbilir et al., 2000). The rocks in the upper structural levels of the nappe pile (i.e., ophiolitic, recrystallized carbonate and low-grade phyllitic metamorphic rocks) provided clasts in the Oligocene; the high-grade metamorphic rocks were unroofed in the Miocene and provided clasts for the conglomerates in sedimentary basins (Fig. 2.16). This sedimentary record thus indicates that significant extension in western Anatolia started in the Oligocene, when the Lycian nappes were still covering the Menderes Massif. Seyitoğlu & Scott (1996) suggested that the Late Oligocene extension may have been initiated by an orogenic collapse of thermally weakened crust of the İzmir-Ankara suture zone.

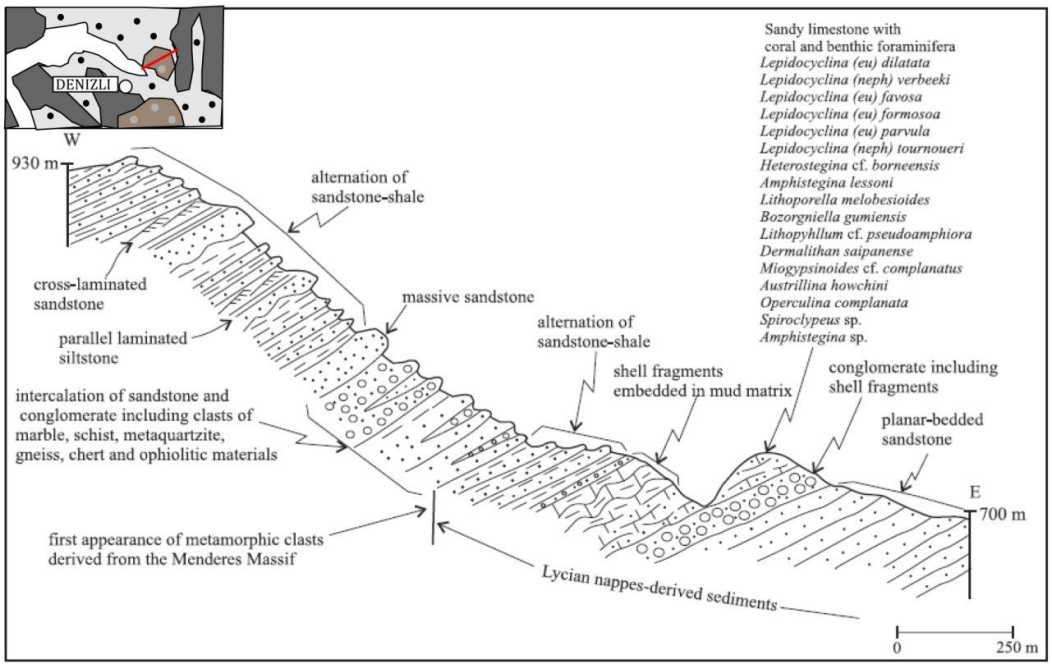


**Fig. 2.16 – Stratigraphic section of the Denizli Molasse showing the first appearance of metamorphic clasts in the upper part of the molasse sediments (after Sözbilir, 2002).**

### 2.5.8 The Taurides

The Taurides, one of the major units of the Alpine-Himalayan orogenic belt, extend for approximately 2,000 km parallel to Mediterranean coast of southern Anatolia (Fig, 2.17). The Taurides consist of a number of allochthonous and autochthonous sequences with distinct stratigraphical, structural and metamorphic features. A comprehensive tectonic classification of these sequences was proposed by Özgül (1976) regarding their paleogeographical origins. Özgül (1984) suggested the

presence of a central 'autochthonous' belt (Geyik Dağı Unit / Bey Dağlari platform), overthrust by northerly (Bozkir, Bolkar, and Aladağ Units) and southerly (Alanya and Antalya Units) derived tectono-stratigraphic units.

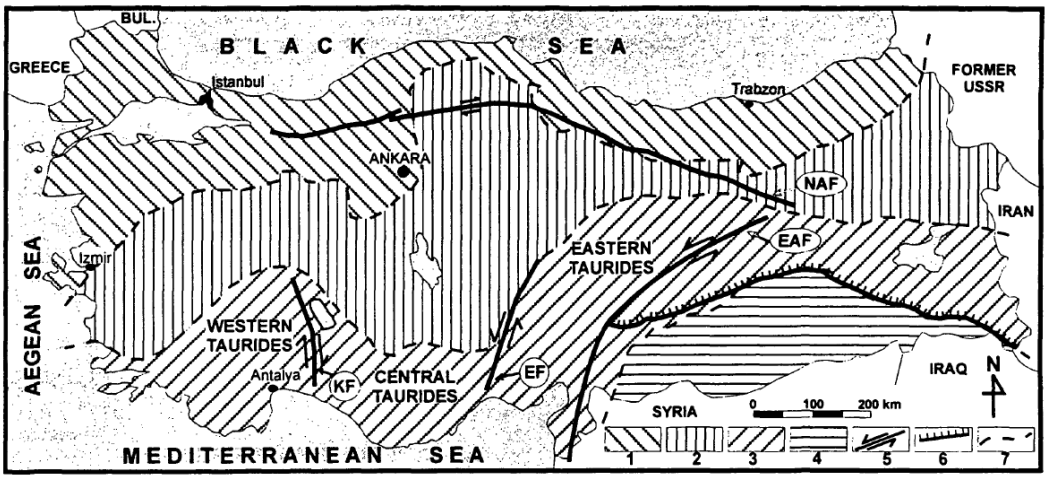


**Fig. 2.17 – Major tectonic units of Turkey and geographical-subdivision of the Taurides (simplified after Ketin, 1966 and Özgül, 1984). 1. Pontides, 2. Anatolides, 3. Taurides, 4. Border Folds, 5. Strike-slip faults, 6. Overthrust, 7. Border of the tectonic units. EAF: East Anatolian Fault, NAF: North Anatolian Fault, KF: Kirkkavak Fault, EF: Ecemiş Fault (from Tekin, 1999).**

South of the Lycian nappes (Fig. 2.18) crops out the Bey Dağlari platform. This platform is very important for this dissertation because it is autochthonous with respect to the Menderes and the Lycian units. The Bey Dağlari is composed of Lower Jurassic to Lower Miocene shallow-water limestones, overlain by Miocene arenites and shales (Bernoulli et al., 1974; Poisson, 1977; Gutnic et al., 1979; Hayward, 1984). On the eastern flank of the Bey Dağlari platform crop the Antalya nappes (Fig. 2.18), also known as Antalya unit (Lefèvre, 1967; Özgül, 1976), crop out. They are made of a succession of (i) Cambrian to Early Triassic platform-type carbonates and clastics; (ii) Middle Triassic debris-flow deposits, shale, radiolarite, pelagic limestone and submarine volcanic rocks, and (iii) Late Triassic turbiditic sandstones.

The Taurides consist of a stack of thrust sheets generally made of Paleozoic to Early Tertiary sedimentary rocks (Okay, 2008). The topmost thrust sheet is instead made of ophiolite and/or ophiolitic mélange, which form large isolated *klippen* through the Taurides (e.g. Gutnic et al. 1979; Özgül, 1984). Thrusting occurred repeatedly in the Late Cretaceous, in the Eocene and in the Early Miocene, and

shows southward younging. The earliest contractional event was the obduction of the ophiolite over the Anatolide-Tauride terrane during the mid-Cretaceous. The obduction event was associated with deep subduction and high-pressure metamorphism of the northern margin of the Anatolide-Tauride terrane and the generation of the Tavşanlı Zone. The more distal portions of the obducted ophiolite were emplaced over the Cretaceous sedimentary rocks of the Taurides. (Okay, 2008)

The continental collision during the Late Paleocene-Early Eocene between the Anatolide-Tauride and the Sakarya terranes led to a second phase of contraction by folding and thrusting in the Taurides. Major events during this Eocene phase include the thrusting of the Lycian nappes over the Menderes Massif and the consequent regional metamorphism of the Menderes Massif. (Okay, 2008) Most of the present nappe structure in the Central and Eastern Taurides was formed during the Eocene. In the Early Miocene the Lycian nappes were thrust southeastward over the Bey Dağlari autochthon. The thrust sheets are generally thought to have been emplaced from north to south with the possible exception of the Antalya Nappes around the bay of Antalya, which are widely regarded to have been thrust northward. The Antalya nappes are generally regarded as representing the southern passive continental margin of the Anatolide-Tauride terrane. West of Antalya Bay they are tectonically overlain by the Tekirova ophiolite, regarded as a fragment of the southern branch of the Neo-Tethys. East of the Antalya Bay, the metamorphic Alanya nappes with blueschists and eclogites lie tectonically over the Antalya nappes. (Okay, 2008)

Strictly speaking, the Alanya Massif is part of the Taurides but it will be described separately in the following section because of its importance for this dissertation.

### 2.5.9 The Alanya Massif

The Alanya Massif (Blumenthal, 1951) forms a high topographic dome in the Taurides north of Cyprus (Fig. 2.18). This massif, which tectonically overlies the Antalya unit, shows many of the key features of the Alpide blueschist units, such as the passive continental margin-type protoliths, juxtaposition of metamorphic units with differing metamorphic grades, and complex metamorphic histories.

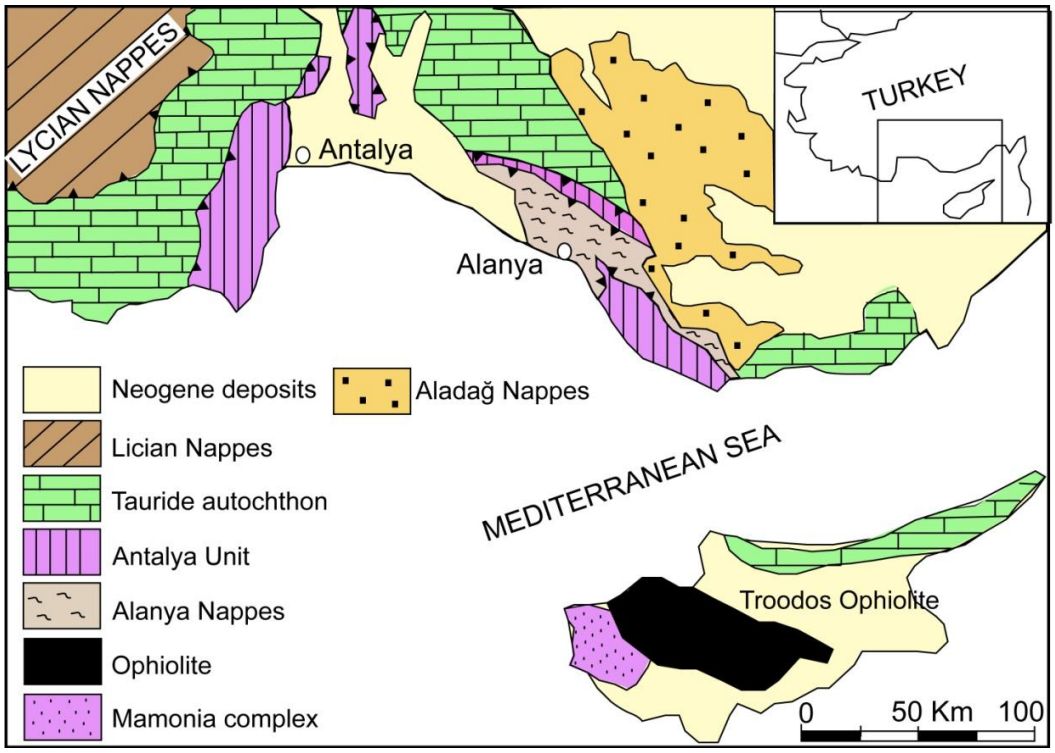


**Fig. 2.18 – Geological map of the Alanya region (mod. after Okay, 1989a).**

The Alanya metamorphic complex comprises three superimposed flat-lying nappes of platform-type shallow-water lithologies that tectonically overlie the largely unmetamorphosed Mesozoic continental margin sediments of the Antalya complex (Şengör & Yilmaz, 1981; Okay, 1989c; Okay & Özgül, 1984).

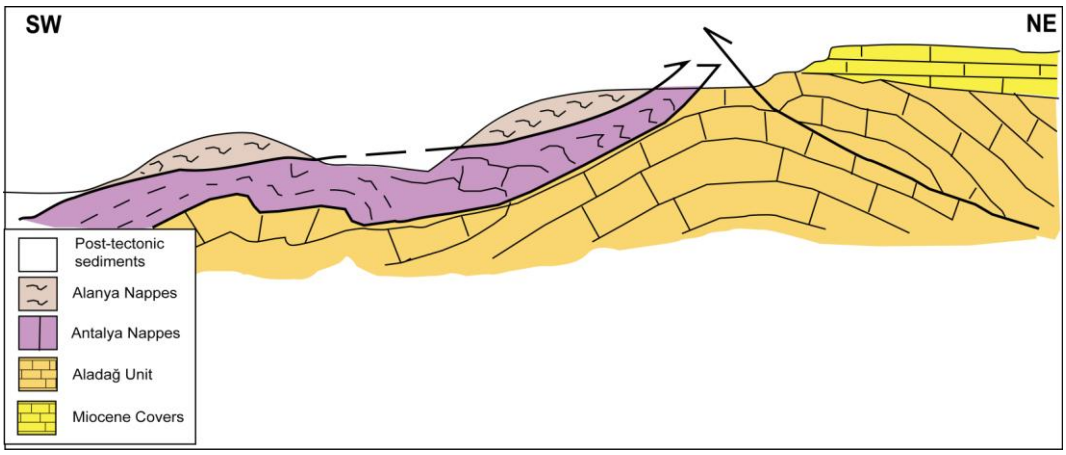


**Fig. 2.19 – Geological section of the Alanya Massif. Alanya and Antalya nappes are impiled on the relative autochthon Tauride platform (Aladağ unit); note the position of the Alanya nappes thrusted over the Antalya nappes which crop out in the region in a tectonic window; in the NE position an angular unconformity marks the Miocene transgression of the carbonate on the Aladağ unit.**

### *2.5.9.1 Alanya metamorphic nappes*

The metamorphic rocks of the Alanya Massif consist of the Mahmutlar and Yumrudağ nappe complexes (at lower and upper structural positions, respectively), which have experienced Barrovian-type MP / LT, and the intermediate Sugözü nappe, which was affected by blueschist- to eclogite-facies conditions (fig. 2.20).

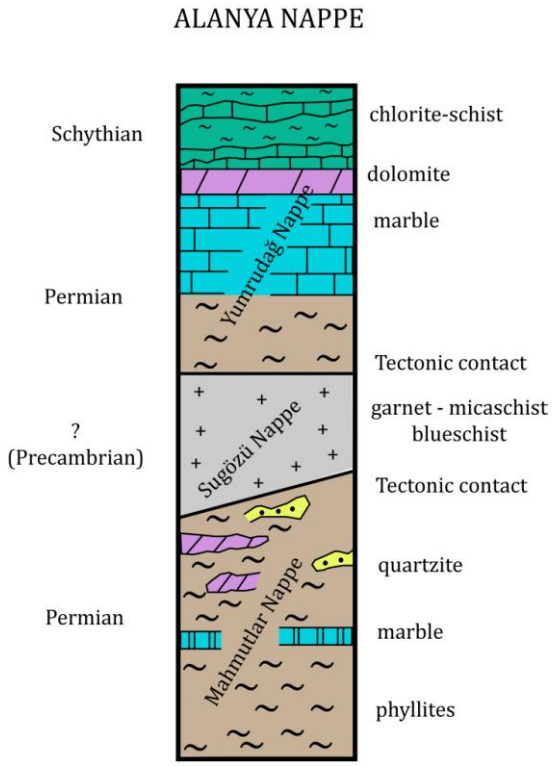


**Fig. 2.20 – Synthetic stratigraphic sections of the Alanya Nappes**

The *Mahmutlar nappe* is the structurally lowest nappe and consists of metapelites, metadolomites, recrystallized limestones and quartzites, with minor amounts of metadolerites and recrystallized radiolarian cherts (Okay, 1989b; Bozkurt & Oberhänsli, 2001). The thickness of the Mahmutlar nappe is difficult to estimate as its lower contact is below sea level. The metamorphic grade in the Mahmutlar nappe continuously increases from northeast to southwest. In the northeast clastic quartz and feldspar grains in coarse sandstones are still recognizable, whereas near the coast pelites contain biotite and newly formed small garnets along with oligoclase, quartz, phengite and chlorite (Okay & Özgül, 1984). Fossil assemblages

preserved within the recrystallized limestone suggest that part of the sequence is of Permian age (Özgül, 1985).

The intermediate unit, the *Sugözü nappe*, is mainly composed of well-foliated mica-garnet schists, with thin intercalations and boudinaged lenses of eclogites and blueschist metabasites (with garnet, glaucophane, paragonite and barroisite). The eclogites grade into blueschists. The garnet-mica schists were probably originally siliceous shales (Okay & Özgül, 1984). The apparent thickness of the Sugözü nappe ranges from 100 to 800 metres; despite its relative thinness this nappe shows a remarkable lateral continuity as it is traceable for over 40 kilometres along the coast. The presence of sodic amphibole inclusions in garnet porphyroblasts in garnet-mica schists suggests that the HP/LT metamorphism was overprinted by Barrovian-type greenschist-facies metamorphism (Okay, 1989b). Along all the contact with the other nappes the foliation in the garnet-mica schists is parallel to the foliation in the overlying schists. The demarcation of the Sugözü nappe is made in the field solely on the presence of garnet, as garnet-bearing units are lacking in both the Yumrudağ and Mahmutlar nappes (Okay & Özgül, 1984).

The *Yumrudağ nappe* is the structurally highest and constitutes the bulk of the Alanya Massif. It consists of schists overlain by a thick sequence of recrystallized limestone. The passage from the schists to the overlying carbonates is gradational. Pelites, psammites, calc-schists, meta-dolomites and thin recrystallized limestone bands are the major lithologies of the schist unit. The thickness of the schist unit is very variable: in some areas it is completely cut out and the carbonates rest directly on the garnet micaschists of the Sugözü nappe (Okay & Özgül, 1984). Permian algae and gastropods are relatively abundant in the recrystallized limestone intercalations (Blumenthal, 1951).

#### *2.5.9.2 Geochronology*

Çetinkaplan et al., (2014) have perform mica $^{40}Ar/^{39}Ar$ and zircon U/Pb dating on eclogite-blueschist facies metamorphism with epidote-amphibolite overprint in Sugözü nappe and Barrovian-type greenschist facies metamorphism in the other nappe units of the Alanya Massif in order to verify the age of the metamorphism. U-Pb zircon dating yields 84 My, Santonian, for eclogite facies metamorphism. Phengitic white micas from the host rock of eclogites gives identical ages of about 84 My, Santonian. Comparing blueschist (450-500 $^{o}C$/10-13 kbar) metamorphism and

the peak P/T conditions of the eclogite (550-560 °C/14-19 kbar) for the Alanya Massif and the closure temperature of white mica (550-600 °C, Villa, 1998; Di Vincenzo et al., 2004), these ages may be close to the crystallization age, as the cooling ages following eclogite and blueschist facies metamorphism.

### *2.5.9.3 Alanya tectonic window*

Sedimentary and low-grade metasedimentary rocks belonging to the Antalya unit crop out in a large tectonic window within the Alanya Massif extending for 75 km along the coast (Fig. 2.21). The southwestern margin of the Alanya nappes is below sea level whereas its northeastern flank tectonically overlies the Antalya Unit. In the northwestern part of the window a 150 m thick succession of Upper Cambrian - Lower Ordovician sandstones and siltstones with rare, red nodular limestone intercalations is overlain by Upper Permian neritic carbonates. An orthoquartzite horizon between the Lower Paleozoic sandstones and Permian carbonates is interpreted as the transgressive base of the Permian. A distinctive feature of these sandstones is the presence, especially in the upper levels, of olistoliths –up to several kilometers in size- made mostly of Permian limestone, Ordovician sandstone and Cambrian red nodular limestone.

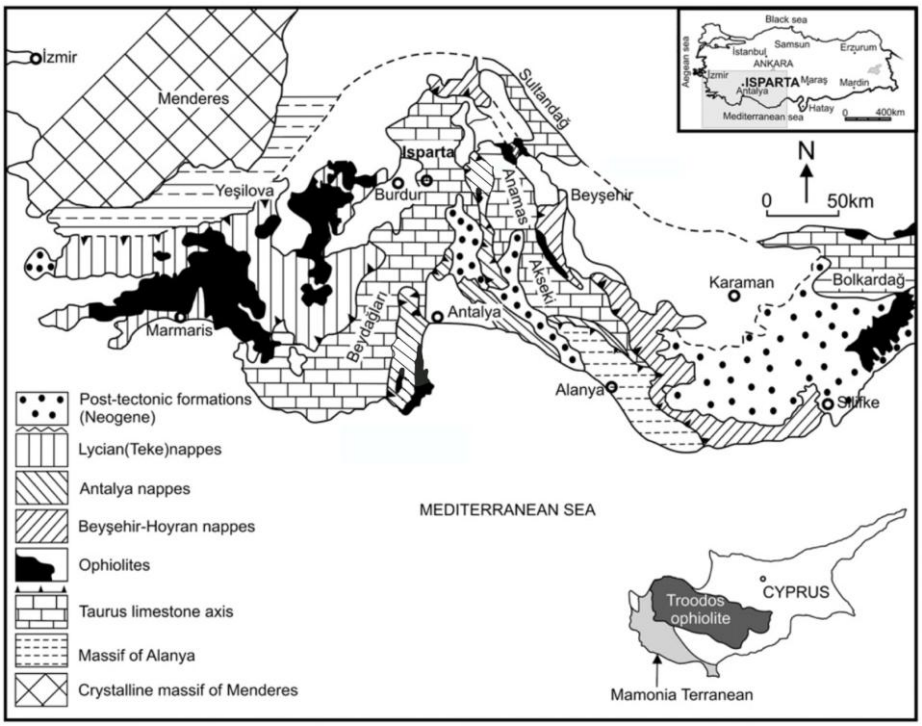


**Fig. 2.21 - Geological map of the Alanya region (Elitok, 2012 mod.).**

Jurassic and Cretaceous rocks occur in only few areas in the Alanya tectonic window. They are faulted against the much more abundant Triassic rocks and comprise a 150 m sequence of multicolored radiolarian cherts and pelagic limestones. At the top of the sequence there is a Maastrichtian shale unit with olistoliths ranging in age from Cambrian to Cretaceous (Okay & Özgül, 1984).

The Antalya unit within the window is affected by thrusting so that the stratigraphic sequences are repeated several times. The thrusts tips trend in a north-south direction and are truncated by the overlying Alanya Nappes. On a smaller scale, the Triassic sandstones and shales are strongly and complexly deformed. Metamorphic recrystallization and penetrative cleavage are lacking in the northeastern part of the window and develops gradually towards the coast. Along the coast the shales are converted into quartz-chlorite-sericite schists with an irregular penetrative cleavage. However, the grade of metamorphism in the window is less than in the surrounding schists of the Alanya Nappes (Okay & Özgül, 1984).

## 2.6 ARABIAN PLATFORM

The northern margin of the Arabian platform is represented by southeast Anatolia, south of the Assyrian (Bitlis-Zagros) suture (Fig. 2.1) (Okay, 2008). During the Mesozoic and the Paleogene the Arabian Platform was separated from the Anatolide-Tauride terrane by the southern branch of the Neo-Tethys, which today is represented by the Assyrian suture (Şengör & Yılmaz, 1981). The Arabian Platform has a Pan-African crystalline basement overlain by a thick Paleozoic-to-Tertiary sedimentary succession. In most areas of southeast Anatolia only the Cretaceous and younger deposits crop out (Okay, 2008).

## 2.7 CYPRUS

The geology of Cyprus has played an important role in the development of plate tectonics theory, especially concerning the formation of ophiolites, i.e. fragments of oceanic crust and mantle exposed on land. Cyprus geology also provides insights into the paleogeography of the Tethys ocean that once separated the Eurasian and African continents.

The island is divided into three geological terranes, from north to the south: Kyrenia Range, Troodos Massif and Mamonia Complex (Fig. 2.22).

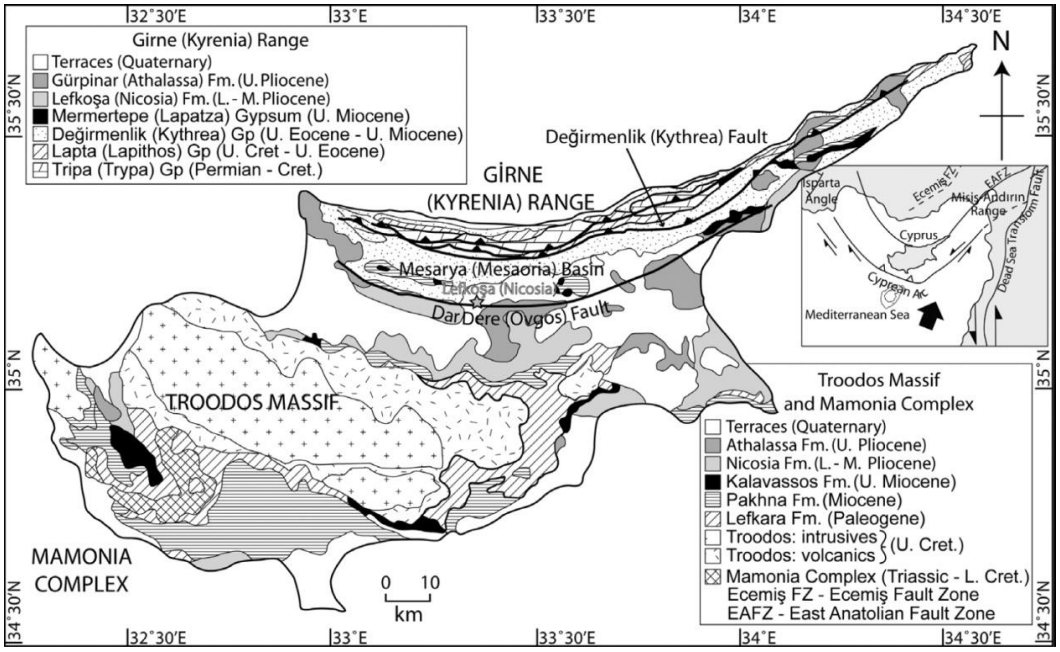


**Fig. 2.22 – Simplified geological map of Cyprus indicating the Kyrenia Range, the Troodos Massif and the Mamonia Complex. Inset: simplified tectonic sketch map of the Eastern Mediterranean region including regionally important lineaments, namely the Eastern Anatolian Fault Zone (EAFZ), the Dead Sea Transform Fault Zone and the Ecemiş Fault Zone (Ecemiş FZ) (from McCay et al., 2013).**

### 2.7.1 The Kyrenia Range

The Kyrenia Range is the northernmost geological zone of Cyprus and is considered to be a southern portion of the Taurides. It forms a narrow, steep-sided mountain chain rising abruptly from the surrounding lowlands. The crest of the range for most of its length varies in altitude between 800 and 1,000 m. To the north this very rugged range is separated from the sea by a narrow terraced coastal plain less than 5 km wide. In contrast, it is flanked to the south by the broad lowlands of the Mesaoria Plain (Fig 2.22).

The axis of the western and central segments of the Kyrenia Range is dominated by Triassic to Cretaceous platform carbonates whereas the eastern range crest is characterized by Palaeogene pelagic carbonates and volcanic rocks, in turn overlain by Middle Eocene sedimentary melange ('olistostromes'; Fig. 2.23) (Robertson et al., 2012). The flanks of the range are largely made of Neogene and

Plio-Quaternary sedimentary deposits (e.g. Robertson & Woodcock, 1986; Kelling et al. 1987; Zitter et al., 2003; Harrison et al. 2004).

The Kyrenia Range developed in several main phases. A Late Cretaceous phase remains poorly known, with both large-scale thrusting and strike-slip faulting (Baroz, 1979; Robertson & Woodcock, 1986). Collision in the Taurides to the north became more pervasive and by mid-Eocene time the Kyrenia Range came under a general N-S compression, culminating in major southward thrusting (Baroz, 1979; Robertson & Woodcock, 1986). Continued convergence of Africa and Eurasia was accommodated by subduction, possibly in a trench located off southern Cyprus, and the range was thus located broadly in a fore-arc setting during Oligocene and Miocene time. The area subsided rapidly and was enveloped in thick Miocene flysch, fed into the eastern Mediterranean from the Tauride Mountains through a huge submarine fan complex located to the northeast (Robertson & Woodcock, 1986). Differential vertical movements south of the range were coupled with general uplift, isolating the area from the surrounding east Mediterranean sea floor in the Late Miocene (Robertson & Woodcock, 1986). Renewed compressional deformation from Late Miocene-Early Pliocene time saw large-scale thrusting and northward tilting of the eastern and central range areas and large-scale, more open, folding further east (Robertson & Woodcock, 1986). Uplift of the Kyrenia Range mainly took place during Late Pliocene–Quaternary time. The main controls of uplift were subduction beneath Cyprus, collision of the Eratosthenes Seamount with the Cyprus trench and the westward tectonic escape of Anatolia towards the Aegean region (Robertson, 1998; Kempler & Garfunkel, 1994; Kempler, 1998; Harrison et al., 2004).

In the western and central Kyrenia Range Robertson et al. (2012b) individuate an unconformity between metamorphosed and recrystallized Triassic–Cretaceous platform carbonates and unmetamorphosed Upper Cretaceous–Paleogene pelagic carbonates and volcanic rocks (Fig. 2.23). The unconformity surface is highly irregular, with angular protrusions and declivities surrounded and filled by pink pelagic limestone belonging to the unmetamorphosed sequence; this mark a regional structural and metamorphic break (Robertson et al., 2012b).

The Mesozoic carbonate platform, estimated as at least several kilometers thick (Baroz, 1979; Robertson & Woodcock, 1986), was deeply buried, metamorphosed, exhumed and then covered by pelagic carbonate and talus derived from the metamorphosed carbonate platform beneath. Taking into account the

occurrence of pelitic rocks throughout the Kyrenia Range and the persistence of chlorite and stilpnomelane, Baroz (1979), estimated the burial temperature as up to 450° C (greenschist facies). The peak metamorphic pressure remains unconstrained in the absence of a diagnostic mineral assemblage.

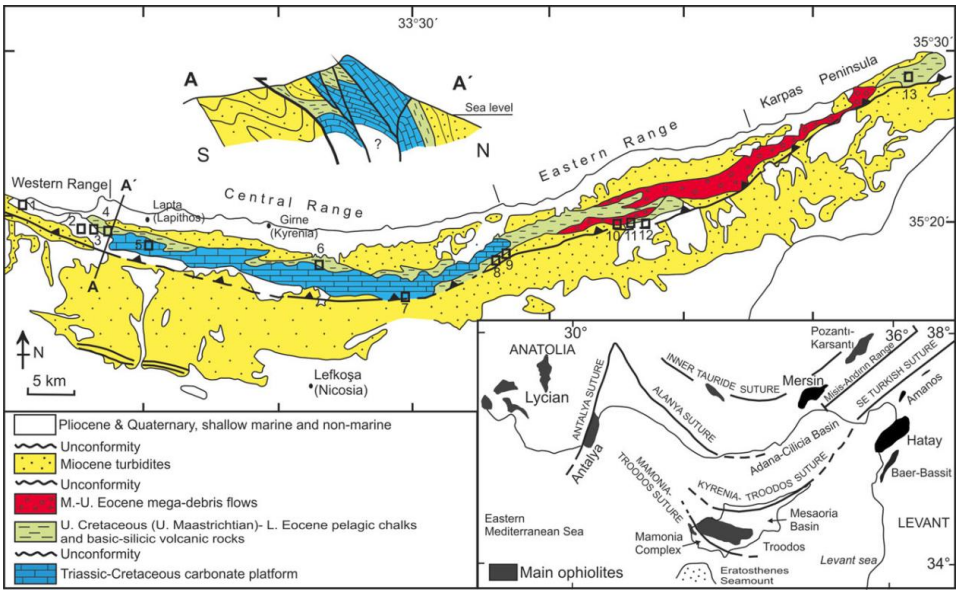


**Fig. 2.23 – Regional geological setting of the Kyrenia Range in the northern part of Cyprus. Outline map based on Baroz (1979) and Robertson & Woodcock (1986). Upper left: Simplified cross-section of the Kyrenia Range, modified from Baroz (1979) and Robertson & Woodcock (1986). Below right: Setting in the Eastern Mediterranean, showing the main sutures and the Upper Cretaceous ophiolites. Locations for which new microfossil data are given here are numbered on the map, with small boxes. 1 – Kayalar (Orga), 2 – Geçiköy (Panagra), 3 – Selvilitepe (Fourkovouno), 4 – Karşıyaka (Vassilea), 5 – Alevkaya Tepe (Kiparisso Vouno), 6 – Beylerbey (Bellapais), 7 – Değirmenlik (Kithrea), 8 – Ergenekon (Ayios Chariton), 9 – Tirmen (Trypimeni), 10 – Mallıdağ(Melounda), 11 – Çınarlı (Platani), 12 – Ağıllar (Mandes), 13 – Balalan (Platanisso) (from Robertson et al., 2012b).**

In principle the unconformity could be explained by either erosion or tectonic exhumation of the carbonate platform. The second option is preferred because (1) the greenschist-facies metamorphism implies at least several kilometers of burial of the carbonate platform but there is little erosional detritus above the unconformity; (2) the basal overlying sediments are pelagic carbonates with no evidence of subaerial exposure; (3) tectonic breccias below the unconformity were reworked as texturally immature (angular) material directly above the unconformity.

The Kyrenia Range carbonate platform rocks were therefore exhumed and exposed on the seafloor in a submarine, pelagic-depositing setting by Late Maastrichtian time. The talus above the unconformity mainly accumulated by debris-flow and rock fall processes indicating the existence of a rugged seafloor

topography. The timing of the deformation and metamorphism are only loosely constrained because the metacarbonate platform has so far yielded only Triassic and Late Jurassic ages (Ducloz, 1972; Baroz, 1979; Robertson & Woodcock, 1986; Hakyemez et al., 2000).

Further north, parts of the Tauride carbonate platform were deformed by thrusting and folding during Late Cretaceous time but remained regionally unmetamorphosed (e.g. Robertson, 1998) in contrast to the Kyrenia Range.

### 2.7.2 The Troodos complex

The Troodos is arguably the best documented ophiolite in the world (e.g. Moores & Vine, 1971; Varga & Moores, 1985; Robinson & Malpas, 1990; Robertson & Xenophontos, 1993; Robertson & Xenophontos, 1997). Initially considered as an example of the typical oceanic lithospheric section, geochemical evidence shows that the Troodos differs from the composition of most oceanic crust at mid-ocean spreading ridges (Robertson & Xenophontos, 1997). Mapping, combined with the results of scientific drilling, revealed the stratigraphy shown in Fig. 2.24.

The lowest units of the Troodos complex are harzburgites, with a penetrative tectonic fabric. These are interpreted as deformed upper mantle remaining after extraction of the melts that constructed the overlying crustal units. The harzburgites are overlain first by layered cumulates, then by non-cumulate rocks (e.g. massive gabbro). Dunite bodies within the harzburgites are interpreted as mantle diapirs produced by partial melting of the underlying upper mantle. Plagioclase lherzolites are interpreted as fertile mantle, rather than refractory residues. Podiform chromites are of cumulate origin, unlike some in other ophiolites. High-level plagiogranites below the sheeted dikes and small trondhjemite bodies within the gabbros are interpreted as siliceous residues from fractional crystallization.

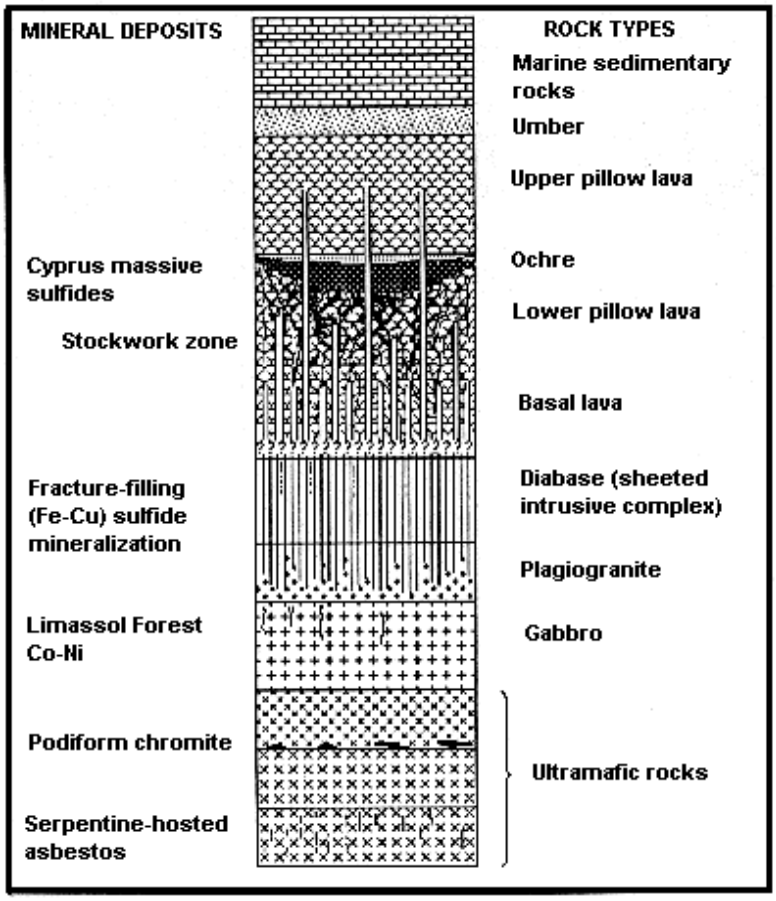


**Fig. 2.24 – Generalized lithological column of the Troodos ophiolite showing the relationship between sulphide mineralization and the Upper and Lower Pillow Lavas (mod. after Constantinou, 1980).**

Detailed mapping shows that the sheeted dikes were tapped off magmas from near the top of gabbros. The evidence of small-scale intrusive relationship supports a multiple, rather than a single, magma chamber model for the lower crustal units (Fig. 2.25) (Robertson & Xenophontos, 1997). The non-cumulate gabbros are mapped as small high-level intrusions. The gabbros are separated from the overlying sheeted complex by zones of intense shearing, interpreted as important extensional detachment faults. The sheeted complexes comprise dikes without host rock, and are thus unambiguous evidence of formation by a spreading process. The dikes mainly trend N-S, vary from vertical to locally subhorizontal and range in metamorphic grade from zeolite to greenschist facies (Robertson & Xenophontos, 1997). The dikes were deformed by extensional faulting. Such fault took place before, during and after magma injection. Traced upwards, screens of pillow lavas appear between the sheeted dikes.

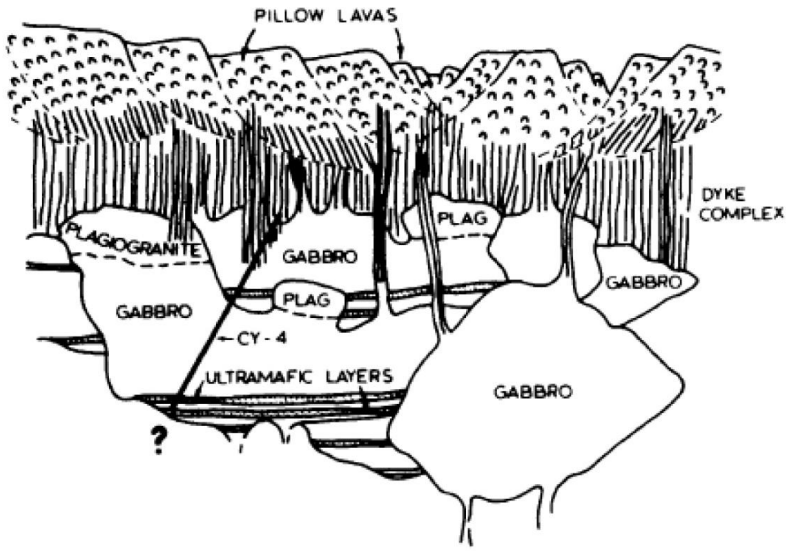


**Fig. 2.25 – Geometric arrangement of the Troodos crustal sequence. A multiple, rather than single, magma chamber model is preferred, as proposed by Moores & Vine (1971) (from Robinson & Malpas, 1990).**

Traditionally, the extrusives were divided into Basal Group (lava screens within dikes), lower Pillow Lavas and upper Pillow Lavas. The extrusives include important sulphide mineralization, mostly located beneath the higher extrusives. The main primary minerals are pyrite, chalcopyrite and numerous minor mineral (Robertson & Xenophontos, 1997).

The Troodos Massif is bounded to S by an E-W-trending tectonic lineament, the South Troodos (or 'Arakapas') Transform Fault Zone that is interpreted as an inactive oceanic transform fault. This comprises distinctive basement and cover units. The basement is dominated by highly tectonized harzburgites, locally cut by high level gabbroic intrusion (trondhjemite) and multiple dikes. The overlying cover succession is made up of alternations of volcanic and sediments. The volcanic include much depleted lavas that are exposed in the higher lavas of the Troodos Massif. The interbedded sediments are mainly volcaniclastic debris flows, rock-fall deposits, turbidites and hemipelagic mudstone; these were produced by submarine erosion of active fault scarps within the transform zone (Robertson & Xenophontos, 1997).

### 2.7.3 The Mamonia Complex

The Mamonia Complex is a complex and varied mélange of sedimentary, igneous and volumetrically minor metamorphic rocks cropping out in southwestern Cyprus (Fig. 2.22). It comprises two main litho-tectonic components: (i) Mesozoic sediments and volcanics that predate the genesis of the Troodos Massif; (ii) ophiolitic rocks of Late Cretaceous age (Robertson & Xenophontos, 1997).

The volcanic-sedimentary unit is itself subdivided into a mainly volcanic unit (Dhiarizos Group) and a wholly sedimentary unit (Ayios Photios Group). The Dhiarizos Group is mainly subaqueous, basic extrusives, locally interbedded with ribbon radiolarites and fine-grained limestones, dated as Late Triassic. The lavas are locally depositionally overlain, first by Upper Triassic ammonite-bearing red pelagic limestones and then by mudstone and distal turbidites. Trace-element studies of the extrusive indicate within-plate- and mid-ocean ridge-type tectonic settings (Robertson & Xenophontos, 1997). The Ayios Photios Group comprises Upper Triassic quartzose turbidites, locally mixed with redeposited shallow-water carbonates (Vlambouros Fm.; Fig. 2.26), and rare Late Triassic fine-grained deepwater limestones. Overlying Jurassic-Early Cretaceous successions are non-calcareous ribbon radiolarites, interbedded with variable abundances of redeposited shallow-water carbonates and terrigenous turbidites.

The ophiolite slivers, representing the second lithotectonic component of the Mamonia Complex, are dated as Late Cretaceous, based on an upward depositional passage into volcaniclastic sediments. The ophiolitic slivers include harzburgites, gabbros, sheeted dikes and very depleted volcanic.

The Dhiarizos Group is interpreted as crust generated during opening of the Mesozoic Tethys ocean; the ophiolite slivers are interpreted as remnants of oceanic crust and mantle (Robertson & Xenophontos, 1997).

**Fig. 2.26 – Turbidites of the Vlambouros Formation, lower Mamonia Complex. Sandstone layers strongly bioturbated; in the zooming the detailed of the mixing in the turbidites with the intercalation of red cherts and biomicrite.**

## 2.8 GEODYNAMIC EVOLUTION OF THE AEGEAN-ANATOLIAN REGION

The present geodynamic context of the eastern Mediterranean involves four major tectonic plates: Eurasia, Africa, Arabia and Anatolia. It is dominated by two major phenomena: the subduction of the African plate under Eurasia and the fast southwestward escape of Anatolia guided by the motion of the Arabian block towards the north. Observing the high seismicity in the whole region, McKenzie (1972) established a model founded on rigid micro-plates (Fig. 2.27); this model is based on the existence and movement of the Anatolian microplate and the Aegean microplate between Africa and Eurasia. According to this interpretation, the northward motion of Arabia produced the westward extrusion of Anatolia, this escape being responsible for the southwestward motion of the Aegean microplate (e.g. Rimmelé, 2003).

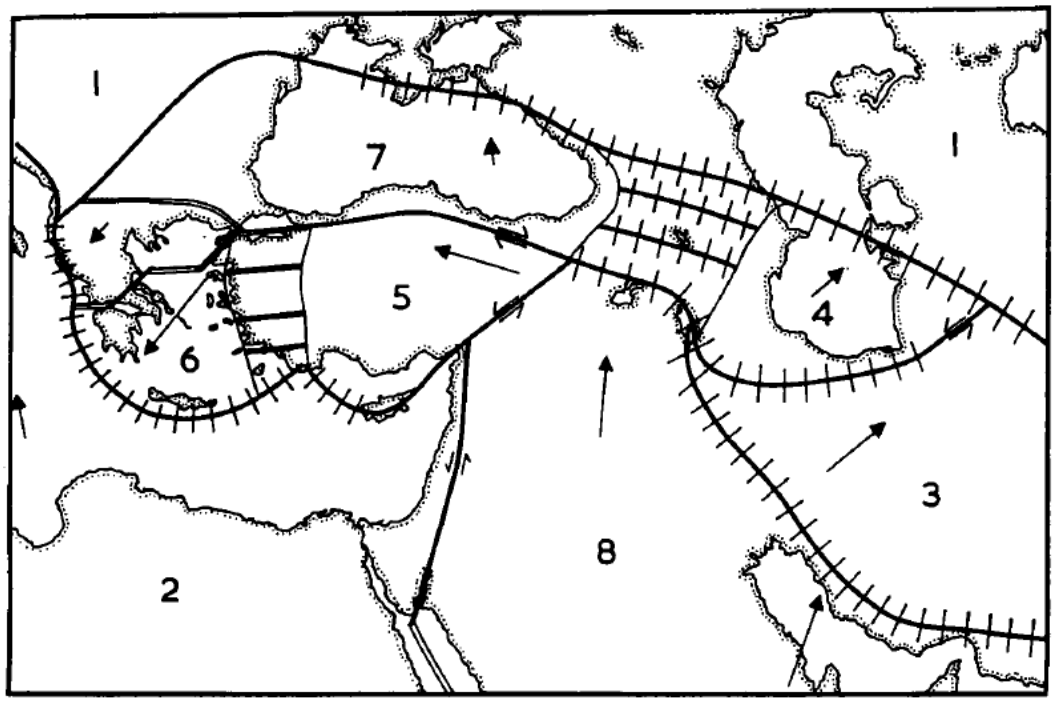


**Fig. 2.27 – Model involving Anatolian and Aegean rigid micro-plates. The arrows show the directions of motion relative to Eurasia and their lengths are approximately proportional to the magnitude of the relative velocity. Plate boundaries across which extension is occurring are shown by a double line, transform faults by a single heavy line and boundaries across which shortening is occurring by a solid line crossed by short lines at right angles. The activity in western Turkey and in the Caucasus is due to normal faulting and thrusting respectively, but the plate boundaries shown in the figure in these regions do not correspond to individual plates and their boundaries, but only represent the general nature of the deformation. The plates are assigned the following numbers: 1 Eurasian, 2 African, 3 Iranian, 4 South Caspian, *5* Turkish, 6 Aegean, 7 Black Sea and 8 Arabian (from McKenzie, 1972).**

### 2.8.1 The Hellenic orogen

The Hellenic orogen, which extends into the Aegean area and Turkey, is a composite of three orogenic belts (Fig. 2.28).

The *Cimmerian orogenic belt*, which includes the Rhodope, Serbomacedonian, Circum Rhodope, Axios, and Pelagonian zones in Greece and the Sakarya, Kirklareli, Sinop, and Bayburt zones in Turkey (Şengör et al., 1984; Okay et al., 2001), represents an internal orogenic belt created in pre-Late Jurassic times as a result of the collision of northward-drifted Cimmerian continental fragments with Eurasia. Ophiolites originated from small ocean basins were mainly emplaced onto the Cimmerian continental margins in the Middle Jurassic (Şengör et al., 1984; 1988; Mountrakis, 1986; Robertson et al., 1996).

The *Alpine orogenic belt* includes the External Hellenides as well as Pindos-Subpelagonian ophiolites and oceanic (Neo-Tethyan) sedimentary units (Smith et al., 1975; Robertson & Dixon, 1984; Dercourt et al., 1993; Dilek et al., 2005). This belt formed in two successive stages. The first stage, in Late Jurassic and Cretaceous times, began with the intraoceanic subduction in the Neo-Tethys and after that the subduction of the Neo-Tethyan oceanic crust beneath the composite Cimmeria-Eurasia plate and the obduction of the ophiolites onto the Cimmerian continental margin (Robertson et al., 1996). The second stage took place in the Tertiary as a result of the final collision of the Apulia plate with the composite Cimmeria-Eurasia plate, producing an intensive imbrication of the Hellenides zones. The two stages are clearly separated, for the Tertiary Pindos flysch deposited after the obduction of the ophiolites and was imbricated without the ophiolites (Mountrakis et al., 1993).

The *Mesogean orogenic belt* along the External Hellenic orogenic arc developed as a result of the subduction of the Mesogea-Africa plate beneath the composite Alpine-Cimmeria-Eurasia plate in the Miocene–Pliocene and the subsequent exhumation of the Cretan–southern Peloponnesus core complexes (Kilias et al., 1994). The Mesogean orogeny certainly can be considered the final stage of the Alpine orogenic process, but the term “Mesogean orogenic belt” is used in order to show that these core complexes represent the more recent geotectonic situation in the eastern Mediterranean region that is still in process.

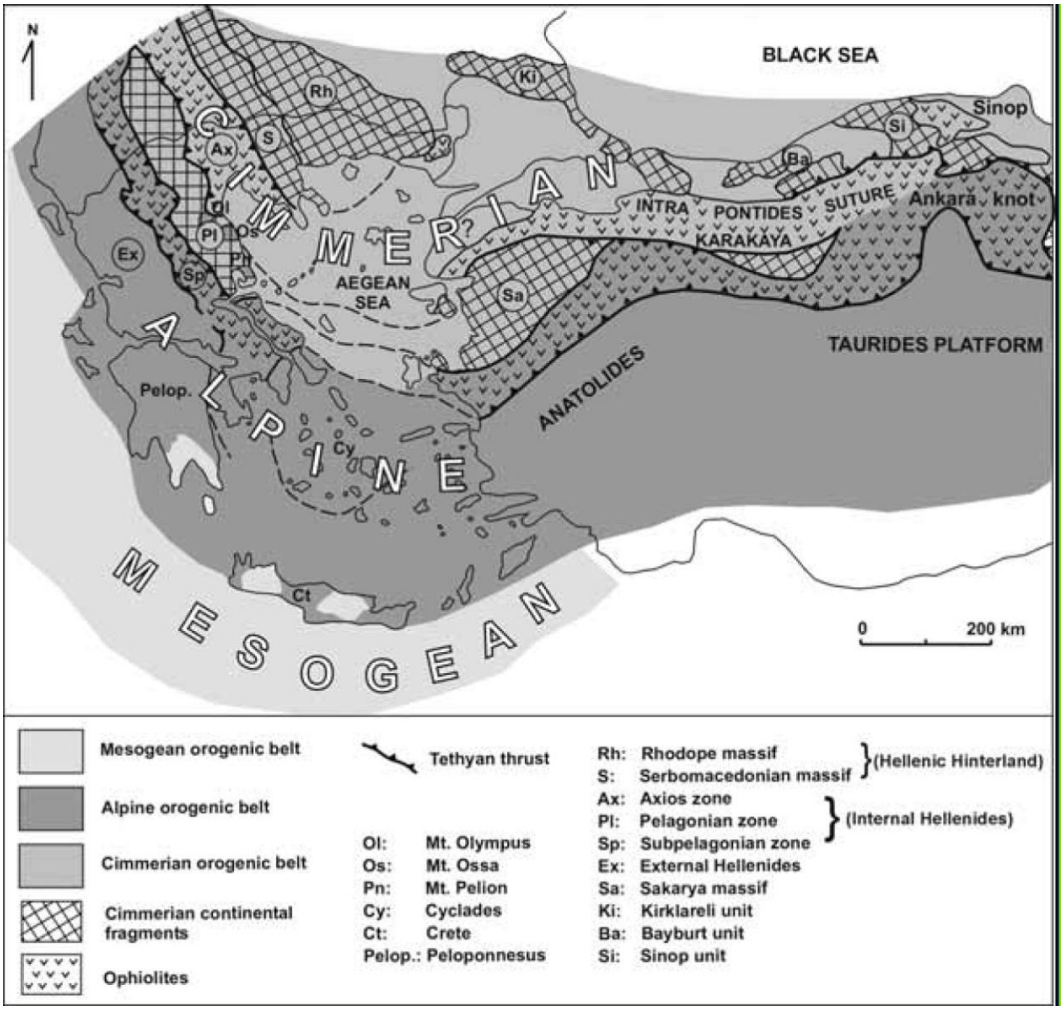


**Fig. 2.28 – Structural map showing three belts of the Hellenic orogen and their extension into Turkey. Cimmerian continental fragments: Kirklareli (Ki), Pelagonian (Pl), Rhodope (Rh), Sakarya (Sa), Serbomacedonian (S), Sinop (Si). Ophiolitic sutures: Ankara, Axios (Vardar) zone (Ax), Karakaya, Subpelagonian zone (Sp) (from Mountrakis, 2006).**

Detailed structural analyses have shown that deformational episodes associated with the evolution of these three orogenic belts have overlapped in space and time. The Alpine deformation affected the Cimmerian belt (Mountrakis, 1982; 1986; Kilias et al., 1999), and the Mesogean tectonics overprinted the Alpine belt (Fassoulas et al., 1994; Kilias et al., 1994).

Tertiary collisional tectonics was associated with the formation of two main high-pressure–low-temperature (HP-LT) metamorphic belts with blueschists and eclogites in two concentric internal and external zones. The internal one, formed in the Eocene (ca. 45 My), represents the suture zone between the Internal and the External Hellenides; the external zone was formed in the Late Oligocene–Early

Miocene (ca. 25 My) within the External Hellenides, i.e., the Ionian zone (Seidel et al., 1982).

The Alpine orogeny consists of two stages: the first began in the Late Jurassic and the Cretaceous with the subduction of the Neo-Tethys, and the second in the Tertiary (Eocene–Oligocene–Miocene) with the final continental collision of the Apulia microplate with the composite Cimmeria-Eurasia plate. The Mesogean orogeny took place in the Miocene–Pliocene after the collision of the Apulia microplate and was associated with the migration of the subduction process southward to the Mesogean Ridge. The new subduction of the Africa-Mesogea plate beneath the new Eurasian margin started in the Miocene–Pliocene along the Hellenic arc and now is developing along the Mesogean Ridge (Fig. 2.29).

The Tertiary collisional tectonics formed the nappe pile of the Hellenic orogen. A major late orogenic extensional phase followed the imbrication nappe stacking and lithospheric thickening during the Tertiary and produced in the nappe pile a strong orogenic collapse and crustal thinning. This extensional deformation was associated with exhumation of lower crustal units. As a result, several metamorphic core complexes were exposed on the island of Crete and in the south Peloponnesus along with a series of tectonic windows of platform carbonates of the External Hellenides in the Cyclades islands and continental Greece (Lister et al., 1984; Avigad & Garfunkel, 1991; Fassoulas et al., 1994; Vandenberg & Lister, 1996; Ring et al., 1999b).

It thus appears that during the Alpine and Mesogean orogenic events successive compressional and extensional deformation episodes migrated southwestward as a result of successive subductions. Hence, crustal thickening produced by compressional tectonics in each area was followed by an extensional exhumation of lower plate rocks.

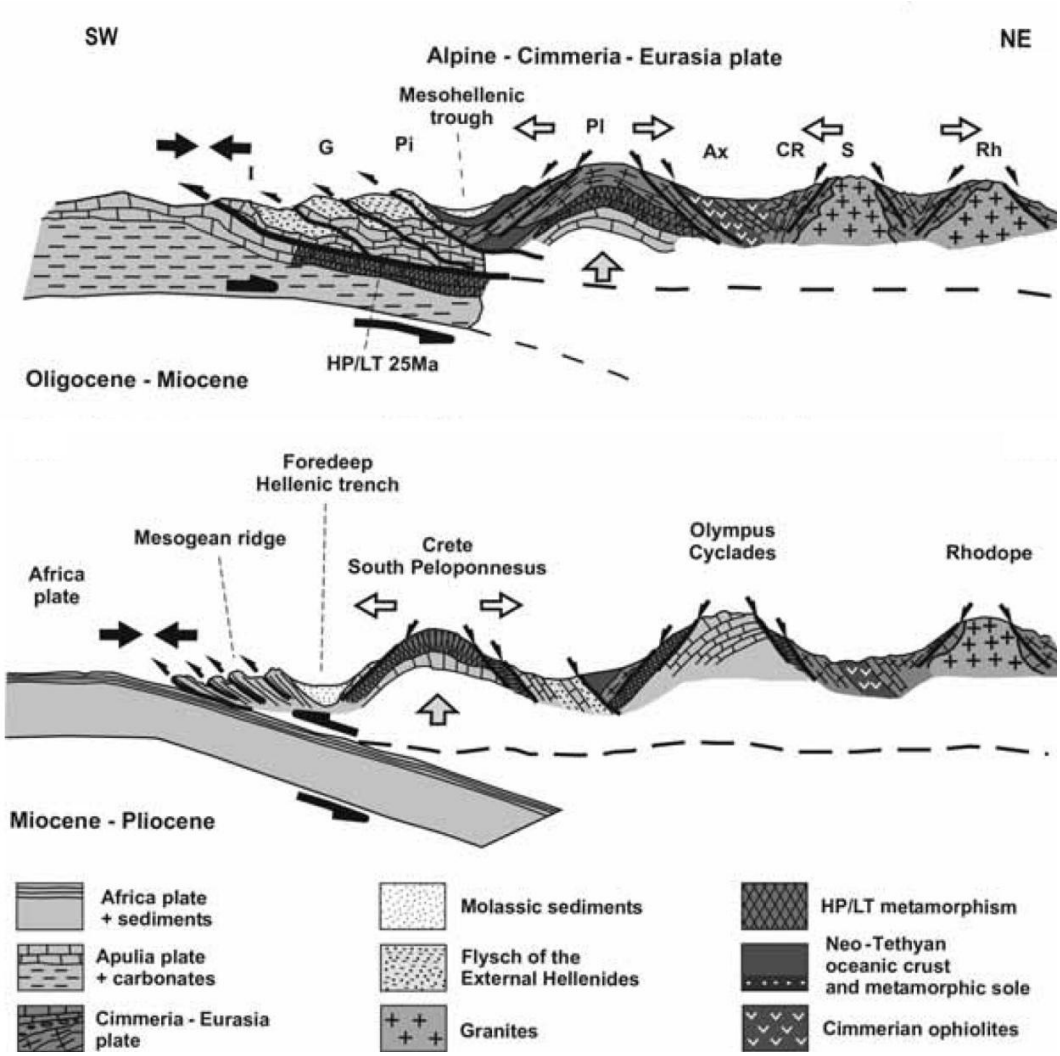


**Fig. 2.29 – Geodynamic reconstruction of the Hellenides. Above: after the subduction of the Neo-Tethyan oceanic crust beneath the Cimmerian continental margin, which produced compressional tectonics and so the nappe stacking and crustal thickening along the convergent margin and intraplate extensional tectonics in the back-arc area, the extension evolved resulting in crustal thinning, uplift and exhumation of the lower tectonic units and pluton emplacement in the Rhodope zone. Successive migration of the compressional and extensional tectonics in the Hellenic Hinterland and the Internal and External Hellenides and the formation of both the 45 My and 25 My H*P*-L*T* metamorphic belts are also shown. Below: geodynamic cross-section showing the Mesogean orogeny during the Miocene–Pliocene. Also shown are the migration of compressional deformation to the Mesogean Ridge, along with extensional tectonics in the Hellenides causing the uplift and exhumation of tectonic windows in the area of Crete, the South Peloponnesus, and Olympus (from Mountrakis, 2006).**

### 2.8.2 Extrusion of Anatolia

Westward extrusion of the Anatolia-Aegean block is related to the northward motion of Arabia with respect to Eurasia. Such motion, which began between 12 and 15 My (Dercourt et al., 1986), has a present-day velocity of about 6 mm/yr along the Dead Sea transform fault. The escape of Anatolia towards the west is guided by major active faults: the dextral North Anatolian Fault (NAF) and the sinistral East Anatolian Fault (EAF). The motion along the EAF is about 10 mm/yr (McClusky et al., 2000). The NAF constitutes the boundary between the Anatolian block and Eurasia. It was formed some 15 My ago and progressively propagated westward (Barka, 1992; Le Pichon et al., 1995; Armijio et al., 1999), reaching at present a length in excess of a 1,000 km. Le Pichon et al. (1995) described the motion of the Anatolian-Aegean block with respect to Eurasia as an anticlockwise quasi-rigid block rotation with a pole of rotation located around the Nile Cone. Successive geodetic work (Fig. 2.30) (McClusky et al., 2000; Relinger et al., 1997; 2006) has confirmed the first-order rigid behaviour of Anatolia.

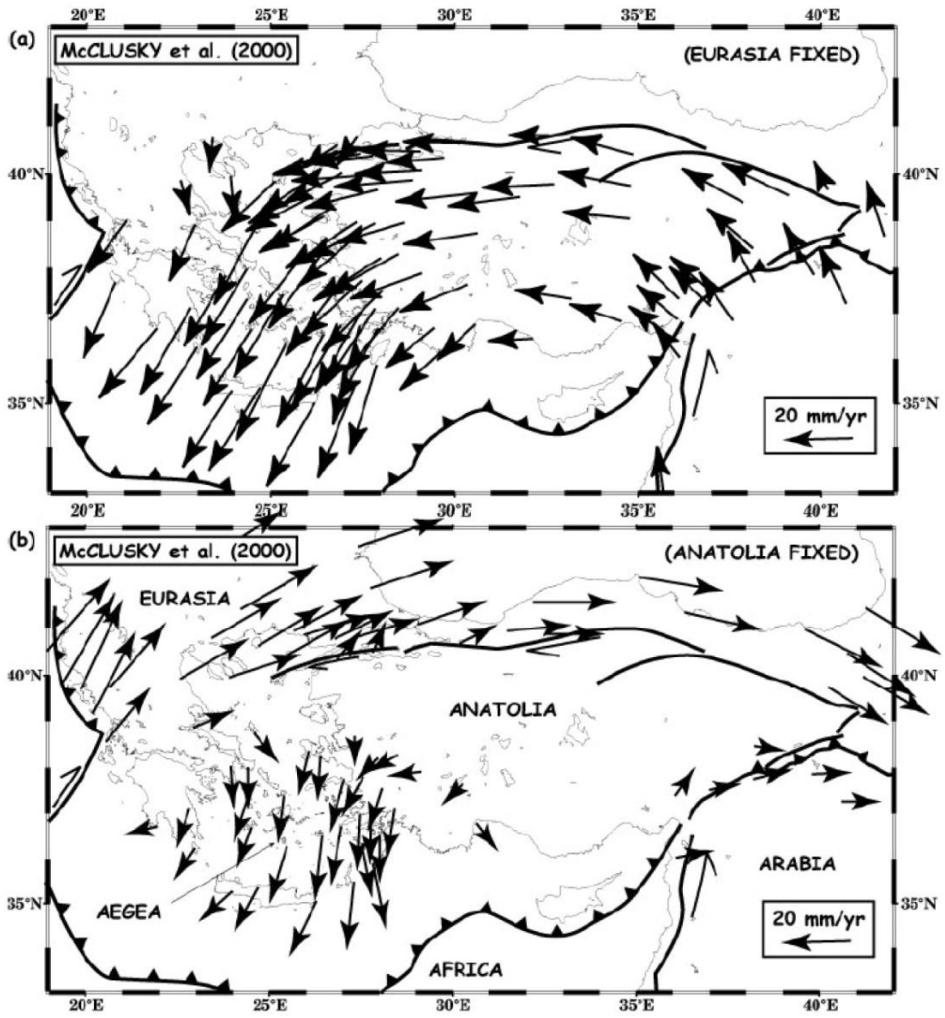


**Fig. 2.30 – GPS velocity field after McClusky et al. (2000): (a) GPS horizontal velocities with respect to Eurasia; (b) GPS horizontal velocities with respect to Anatolia (from Rimmelé, 2003; mod. after Jolivet, 2001).**

### 2.8.3 Aegean extension

The present-day extension in the Aegean domain is kinematically controlled by the extrusion of Anatolia along the NAF. However, as explained above, such escape tectonics did not start before the mid-Miocene, and the cumulative displacement along the NAF amounts to a maximum of 85 km (Barka, 1992; Armijio et al., 1999). In consequence, the fast westward migration of Anatolia cannot explain the major part of the Aegean extension which occurred much earlier (Seyitoğlu et al., 1992; Jolivet et al., 1994a; b; Jolivet & Faccenna, 2000; Gautier et al., 1999, Seyitoğlu et al., 2002). The Aegean sea formed in the back-arc region of the Hellenic trench from the Late Oligocene until present. Subduction of the African Plate beneath the Anatolian block proceeds at a fast rate (30-40 mm/yr, Le Pichon et al., 1995). Extension has

taken place on a previously thickened continental crust, the deep parts of which are now exhumed at the surface (Lister et al., 1984). Subduction of oceanic lithosphere began at least 40 My ago, as attested by seismic tomographic studies (Spakman, 1990). Extension has migrated southward continuously from Early Miocene to the Present (Jolivet et al., 1998). During the migration, arc volcanism has migrated at same rate, around 30 mm/yr (Fytikas et al, 1984: Jolivet et al., 1998). Radiochronological data of magmatic rocks, granitoids and volcanic rocks, along an N-S transect Rhodope-Cyclades-Crete, shows a sudden southward migration from 25 to 30 My, which is consistent with the inception of backarc extension at the same period. The thrust front has migrated with the slab retreat of the subduction zone. It was in Crete in the Early Miocene and is now south of the Mediterranean ridge. Extension is active today in the western part of the Aegean region and is concentrated in the Gulf of Corinth above the Hellenic subduction (Armijio et al., 1996; Jolivet & Faccenna, 2000).

### 2.8.4 From the Hellenic orogen to the Aegean sea

Although extension is presently localized in a few areas of the Aegean-Anatolian region, it was distributed over a wider zone during the Oligocene-Miocene time (Jolivet, 2001). Consequently to the Late Cretaceous closure of the Neo-Tethyan ocean in the northern part of the Aegean domain, continuing convergence led to shortening of the Apulian continental crust (Bonneau, 1982; Dercourt et al., 1986; Fig. 2.31).

This event is responsible for the formation and exhumation of high-pressure rocks, such as the Cycladic Blueschist (Bonneau & Kienast, 1982). Shortening and syn-orogenic exhumation occurred during the Late Cretaceous until the Eocene. High H pressure/low-temperature (HP-LT) metamorphic rocks, which underwent blueschist- to eclogite-facies conditions, were brought in the upper crust.

An acceleration of slab retreat changed the subduction regime and caused the collapse of the thickened Hellenic mountain belt and the formation and crustal thinning of the Aegean sea from Late Oligocene to the Present (Fig. 2.30) (Jolivet & Faccenna, 2000). Gautier et al. (1999) claimed that the initiation of Aegean extension did not result from the lateral escape of Anatolia. Instead, extension started owing to a process of gravity spreading of the continental lithosphere that had previously been thickened during Alpine collision.

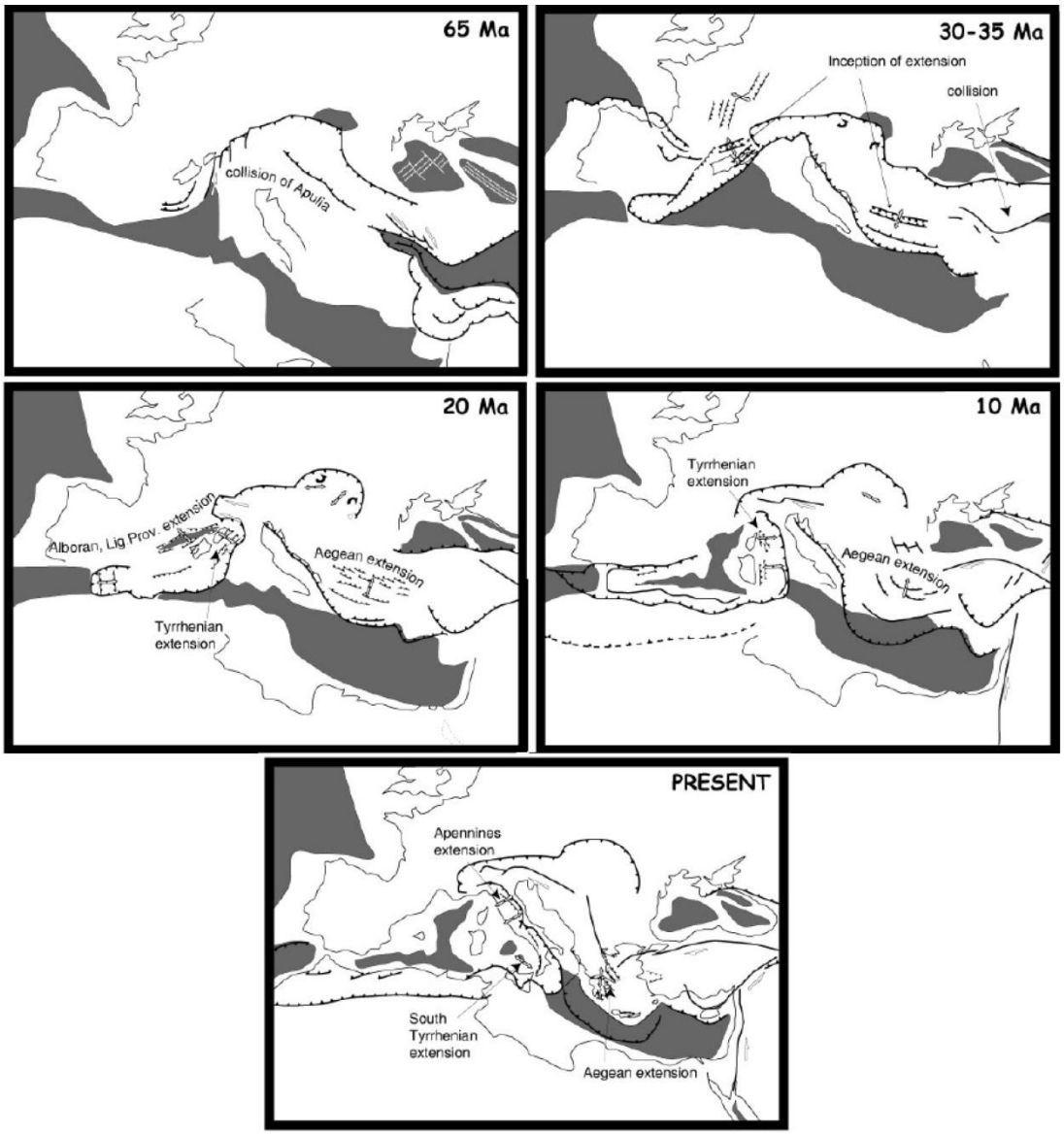


**Fig. 2.31 – Paleotectonic reconstruction of the Mediterranean region (from Rimmelé, 2003a; mod. after Dercourt et al., 1986; Jolivet & Faccenna, 2000).**

Extension is recorded in metamorphic core complexes which crop out in the Cyclades, in western Turkey (e.g. Cavazza et al., 2009), as well as in the Rhodope Massif (see Burchfiel et al., 2008, for a review). Post-orogenic extension is characterized by large-scale detachments which eventually led to the final exhumation of metamorphic core complexes (Lister et al., 1984; Avigad, 1990; Avigad & Garfunkel, 1991; Faure et al., 1991; Lister & Baldwin, 1993; Gautier & Brun, 1994; Jolivet et al., 1994b; Jolivet & Patriat, 1999). Detachments are found in almost all the Cycladic islands, in the Rhodope and, as we will see, in the Menderes

Massif (Hetzel et al., 1995a, b). This post-orogenic extensional event is associated with a high-temperature/low-pressure (HT-LP) metamorphic gradient (e.g. Main Menderes Metamorphism).

While the back-arc region was extending (Cyclades, Menderes Massif), the frontal part of the orogen was still experiencing syn-orogenic thickening and formation of HP-LT rocks and their exhumation (Crete and Peloponnese) (Fassoulas et al., 1994; Jolivet et al., 1994a; Doutsos et al., 2000; Ring et al., 2001a).

Exhumation of those more recent high-pressure units was mainly achieved by N-S extension along shallow north-dipping shear zones evolving into brittle detachments with a similar shallow dip at the top of the accretionary complex. Post-orogenic extension in the back-arc region is also N-S or NE-SW. Displacement of the hanging wall is consistently towards the north or northeast in the Cyclades, towards the southwest in the southern Rhodope massif and bivergent in the Menderes Massif (Rimmelé, 2003).

## 2.9 RELATIONSHIP BETWEEN SOUTHERN ANATOLIA AND CYPRUS

According to numerous authors there are sever affinities between the units crop out in the southwestern Anatolia and the units crop out in the island of Cyprus.

First can be individuate a correlation between the Alanya Massif and the Kyrenia Range of northern Cyprus. The western part of the range is dominated by a Mesozoic carbonate platform that was metamorphosed under greenschist facies conditions during the Late Cretaceous (Baroz, 1979; Robertson et al., 2012b). The platform was exhumed to the seafloor and covered by within plate-type (extension related) basalts and pelagic carbonates during the Maastrichtian (Robertson et al., 2012). The Kyrenia Range also includes large (up to hundreds of meter-sized) blocks of unmetamorphosed Middle Permian to Cretaceous neritic limestones that occur within Eocene thrust-related olistostromes (i.e. large-scale debris flows; Ducloz, 1972; Baroz, 1979; Robertson & Woodcock, 1986). The crust beneath the Cilicia Basin that separates Cyprus from mainland Turkey is assumed to be continental (e.g. see Makris et al., 1983; Calon et al., 2005a; b), but this does not preclude the possibility of a Paleogene or older suture zone there. Robertson et al. (2013) interpretation is that a narrow Mesozoic 'Alanya ocean' was separated from a wider

Southern Neotethys to the south by a relatively narrow strip of continental crust, which included the Precambrian high-grade metamorphic rocks (Sugözü nappe). The Late Cretaceous metamorphism of the Kyrenia Range Mesozoic platform is seen as the result of intra-continental shortening, although subduction of an additional oceanic strand between the Kyrenia platform and the Alanya continental rocks to the north cannot be ruled out (see Robertson et al., 2012b). The unmetamorphosed Middle Permian limestone blocks in the eastern part of the Kyrenia Range were emplaced from an original shallow-marine basin that was probably located to the north of the Mesozoic Kyrenia carbonate platform (Robertson et al., 2013).

Remnants of the rifted northern continental margin of the Southern Neotethys, comparable with the Antalya Complex, are preserved in the Mamonia Complex, western Cyprus (Ayios Photios and Dhiarizos Groups) (Robertson & Woodcock, 1979; Robertson, 2007; 2013).

The Troodos ophiolite in considered to have formed within the Southern Neotethys above a northward-dipping intra-oceanic subduction zone at around 90 My (Mukasa & Ludden 1987; Gass 1990). Remnants of oceanic crust of transform fault affinities are exposed in south and SW Cyprus (e.g. Malpas et al., 1992; 1993; Robertson & Xenophontos, 1993). The Southern Neotethys subducted northwards during the Late Cretaceous, giving rise to localized arc-type volcanism within the Kyrenia Range (Baroz, 1979; Robertson et al., 2012b). Tuffaceous sediments of the Campanian–Maastrichtian Kannaviou Formation that overlies the Troodos ophiolitic massif in western Cyprus are likely to have been derived from this arc (Robertson, 1979; Gilbert & Robertson, 2013).

Chapter III

# SAMPLING

The studied areas are located (i) in the central and southern Menderes Massif, (ii) in the Alanya Massif and (iii) Cyprus. We collected eighty samples distributed over a wide area in western Anatolia and fourteen samples from the island of Cyprus (Figs. 3.1 & 3.2). Samples from the Menderes Massif Menderes Massif are mostly magmatic and metamorphic rocks from both the 'core' (i.e. from the basement complex) and the 'cover'. Samples from the Alanya Massif are sandstone, meta-sandstone and other metamorphic rocks (see Chapter II). Samples from Cyprus include a variety of rock types coming both from the Troodos Massif and the Mamonia Complex (see Chapter II). Tables 3.1 & 3.2 list all samples taken during this research.

**Table 3.1 – List of samples taken in western Anatolia.**

| Sample | Rock type | Age | Source | Elevation | UTM Coordinates |
|---|---|---|---|---|---|
| **TU299** | Meta-granite | Neoproterozoic | Menderes | 6m | 36S 0547640 4150041 |
| **TU300** | Schist | Precambrian | Menderes | 10m | 35S 0547780 4148298 |
| **TU301** | Schist | Precambrian | Menderes | 15m | 35S 0548429 4146450 |
| **TU302** | Phyllite | Permian-Carboniferous | Menderes | 25m | 35S 0547797 4144898 |
| **TU303** | Phyllite | Permian-Carboniferous | Menderes | 137m | 35S 0549766 4142071 |
| **TU304** | Flysch | Eocene | Menderes | 209m | 35S 0557097 4128645 |
| **TU305** | Meta-sandstone | Cretaceous | Lycian | 8m | 35S 0558256 4121235 |
| **TU306** | Meta-sandstone | Cretaceous | Lycian | 591m | 35S 0632603 4107071 |
| **TU307** | Sandstone | Cretaceous | Lycian | 599m | 35S 0632825 4106316 |
| **TU308** | Sandstone | Cretaceous | Lycian | 455m | 35S 0633757 4104479 |
| **TU309** | Schist | Permian-Carboniferous | Menderes | 821m | 35S 0610909 4142356 |
| **TU310** | Quartz-schist | Paleozoic/Precambrian | Menderes | 826m | 35S 0679615 4153133 |
| **TU311** | Schist | Paleozoic/Precambrian | Menderes | 876m | 35S 0619332 4157664 |
| **TU312** | Schist | Paleozoic/Precambrian | Menderes | 438m | 35S 0602595 4140620 |
| **TU313** | Meta-granite | Neoproterozoic | Menderes | 306m | 35S 0600710 4142865 |
| **TU314** | Meta-granite | Neoproterozoic | Menderes | 398m | 35S 0599984 4147764 |
| **TU315** | Meta-granite | Neoproterozoic | Menderes | 227m | 35S 0596499 4152502 |
| **TU316** | Meta-granite | Neoproterozoic | Menderes | 68m | 35S 0589045 4171395 |
| **TU317** | Meta-granite | Neoproterozoic | Menderes | 163m | 35S 0581531 4174605 |
| **TU318** | Meta-granite | Neoproterozoic | Menderes | 51m | 35S 0574905 4179263 |
| **TU319** | Schist | Precambrian | Menderes | 941m | 35S 0662827 4184188 |
| **TU320** | Schist | Precambrian | Menderes | 934m | 35S 0659545 4184900 |
| **TU321** | Schist | Precambrian | Menderes | 1216m | 35S 0657810 4186009 |
| **TU322** | Schist | Precambrian | Menderes | 1362m | 35S 0655769 4185008 |
| **TU323** | Schist | Precambrian | Menderes | 597m | 35S 0655607 4174487 |
| **TU324** | Flysch | Cretaceous | Lycian | 1059m | 35S 0665211 4169049 |
| **TU325** | Sandstone | Eocene | Lycian | 1113m | 35S 0691067 4165310 |
| **TU326** | Sandstone | Eocene | Lycian | 1400m | 36S 0241171 4103185 |
| **TU327** | Schist | Precambrian | Alanya | 11m | 36S 0400852 4049300 |
| **TU328** | Meta-sandstone | Permian | Alanya | 22m | 36S 0422983 4032753 |
| **TU329** | Sandstone | Triassic | Antalya | 65m | 36S 0430896 4033713 |
| **TU330** | Sandstone | Triassic | Antalya | 159m | 36S 0435165 4038196 |
| **TU331** | Sandstone | Triassic | Antalya | 254m | 36S 0450336 4001208 |
| **TU332** | Sandstone | Triassic | Antalya | 432m | 36S 0466917 3994541 |
| **TU333** | Sandstone | Triassic | Antalya | 141m | 36S 0470095 3989508 |
| **TU334** | Schist | Precambrian | Alanya | 124m | 36S 0489594 4002748 |
| **TU335** | Schist | Precambrian | Alanya | 20m | 36S 0490798 40034225 |
| **TU336** | Schist | Precambrian | Alanya | 241m | 36S 0492149 4004204 |
| **TU337** | Sandstone | Triass | Aladağ | 1692m | 36S 0458621 4079380 |
| **TU338** | Sandstone | Ordovician | Geiykdag | 1422m | 36S 0452504 4094224 |
| **TU339** | Sandstone | Ordovician | Geiykdag | 1328m | 36S 0452400 4103074 |
| **TU340** | Porphyry | Precambrian | Menderes | 1110m | 36S 0240841 4254676 |
| **TU341** | Porphyry | Precambrian | Menderes | 1299m | 36S 0240668 4252768 |

| | | | | | |
|---|---|---|---|---|---|
| **TU342** | Porphyry | Precambrian | Menderes | 1039m | 36S 0257662 4273864 |
| **TU343** | Meta-flysch | Eocene | Lycian | 164m | 35S 0565776 4096588 |
| **TU357** | Metaconglomerate | Miocene | Yenidere | 510m | 35S 0649353 4149261 |
| **TU358** | Conglomerate | Miocene | Yenidere | 469m | 35S 0648917 4149984 |
| **TU359** | Quartzite | Miocene | Muğla | 884m | 35S 0651189 4154725 |
| **TU360** | Conglomerate | Oligo-Miocene | Denizli | 942m | 35S 0699641 4198555 |
| **TU361** | Sandstone | Oligo-Miocene | Denizli | 697m | 35S 0703090 4199345 |
| **TU362** | Quartzite | Permo-Carboniferous | Menderes | 288m | 35S 0670556 4214896 |
| **TU363** | Mica-schist | Permo-Carboniferous | Menderes | 233m | 35S 0677659 4220251 |
| **TU364** | Meta-granite | Precambrian | Menderes | 709m | 35S 0659423 4212433 |
| **TU365** | Mica-schist | Permo-Carboniferous | Menderes | 1151m | 35S 0650807 4215843 |
| **TU366** | Mica-schist | Precambrian | Menderes | 609m | 35S 0652961 4222806 |
| **TU367** | Mica-schist | Precambrian | Menderes | 345m | 35S 0645902 4232230 |
| **TU368** | Gneiss | Precambrian | Menderes | 625m | 35S 0656212 4238722 |
| **TU369** | Schist | Precambrian | Menderes | 475m | 35S 0653603 4239045 |
| **TU370** | Mica-schist | Precambrian | Menderes | 93m | 35S 0581871 4274832 |
| **TU371** | Schist | Precambrian | Menderes | 111m | 35S 0580534 4283847 |
| **TU372** | Gneiss | Precambrian | Menderes | 234m | 35S 0599673 4277118 |
| **TU373** | Para-gneiss | Precambrian | Menderes | 509m | 35S 0603908 4287463 |
| **TU374** | Quartzite | Permo-Carboniferous | Menderes | 526m | 35S 0569799 4253909 |
| **TU375** | Quartzite | Permo-Carboniferous | Menderes | 692m | 35S 0572883 4242646 |
| **TU376** | Gneiss | Precambrian | Menderes | 395m | 35S 0572771 4235109 |
| **TU399** | Metasandstone | Triassic | Alanya | 127m | 36S 0399313 4055116 |
| **TU400** | Sandstone | Late Triassic | Antalya | 1017m | 36S 0416480 4074723 |
| **TU401** | Sandstone | Late Triassic | Antalya | 611m | 36S 0419442 4071592 |
| **TU402** | Sandstone | Late Triassic | Antalya | 450m | 36S 0423640 4068997 |
| **TU403** | Metasandstone | ? | Alanya | 373m | 36S 0417001 4069269 |
| **TU404** | Qz-mica schist | ? | Alanya | 289m | 36S 0399177 4056394 |
| **TU405** | Quartzite | ? | Alanya | 521m | 36S 0424974 4039764 |
| **TU406** | Micaschist | ? | Alanya | 736m | 36S 0427421 4040234 |
| **TU407** | Metaquarzite | ? | Alanya | 995m | 36S 0436261 4044235 |
| **TU408** | Sandstone | Eocene | Up. Nappes | 1223m | 36S 0444908 4050584 |
| **TU409** | Sandstone | Eocene | Up. Nappes | 1250m | 36S 0451301 4060816 |
| **TU410** | Sandstone | Eocene | Up.Nappes | 1378m | 36S 0462999 4058235 |
| **TU411** | Sandstone | Ordovician | Up.Nappes | 1076m | 36S 0453624 4106807 |
| **TU412** | Sandstone | Permian | Up.Nappes | 1872m | 36S 0451993 4076787 |
| **TU413** | Sandstone | Permian | Up.Nappes | 1474m | 36S 0450593 4073171 |

**Table 3.2 – List of samples taken in Cyprus.**

| Sample | Lithology | Age | Source | Quote | Coordinates |
|---|---|---|---|---|---|
| **CY1** | Plagiogranite | Pre-Campanian | Troodos | 895m | 36S 0494902 3862756 |
| **CY2** | Plagiogranite | Pre-Campanian | Troodos | 1232m | 36S 0493351 3866408 |
| **CY3** | Plagiogranite | Pre-Campanian | Troodos | 1167m | 36S 0482943 3867830 |
| **CY4** | Plagiogranite | Pre-Campanian | Troodos | 905m | 36S 0484805 3861250 |
| **CY5** | Plagiogranite | Pre-Campanian | Troodos | 1087m | 36S 0486304 3861005 |
| **CY6** | Quart. Sandstone | Triass | Mamonia | 235m | 36S 0463239 3843684 |
| **CY7** | Quart. Sandstone | Triass | Mamonia | 173m | 36S 0467028 3847707 |
| **CY8** | Plagiogranite | Pre-Campanian | Troodos | 220m | 36S 0507764 3851235 |
| **CY9** | Plagiogranite | Pre-Campanian | Troodos | 455m | 36S 0513861 3852010 |
| **CY10** | Qz Mica Schist | ? | Mamonia | 3m | 36S 0440448 3879649 |
| **CY11** | Turb. Sandstone | Triass | Mamonia | 316m | 36S 0440561 3874319 |
| **CY12** | Sandstone | Triass | Mamonia | 208m | 36S 0442120 3877930 |
| **CY13** | Sandstone | Triass | Mamonia | 27m | 36S 0442120 3877930 |
| **CY14** | Quart. Sandstone | Early Cretaceous | Mamonia | 101m | 36S 0514704 3843639 |

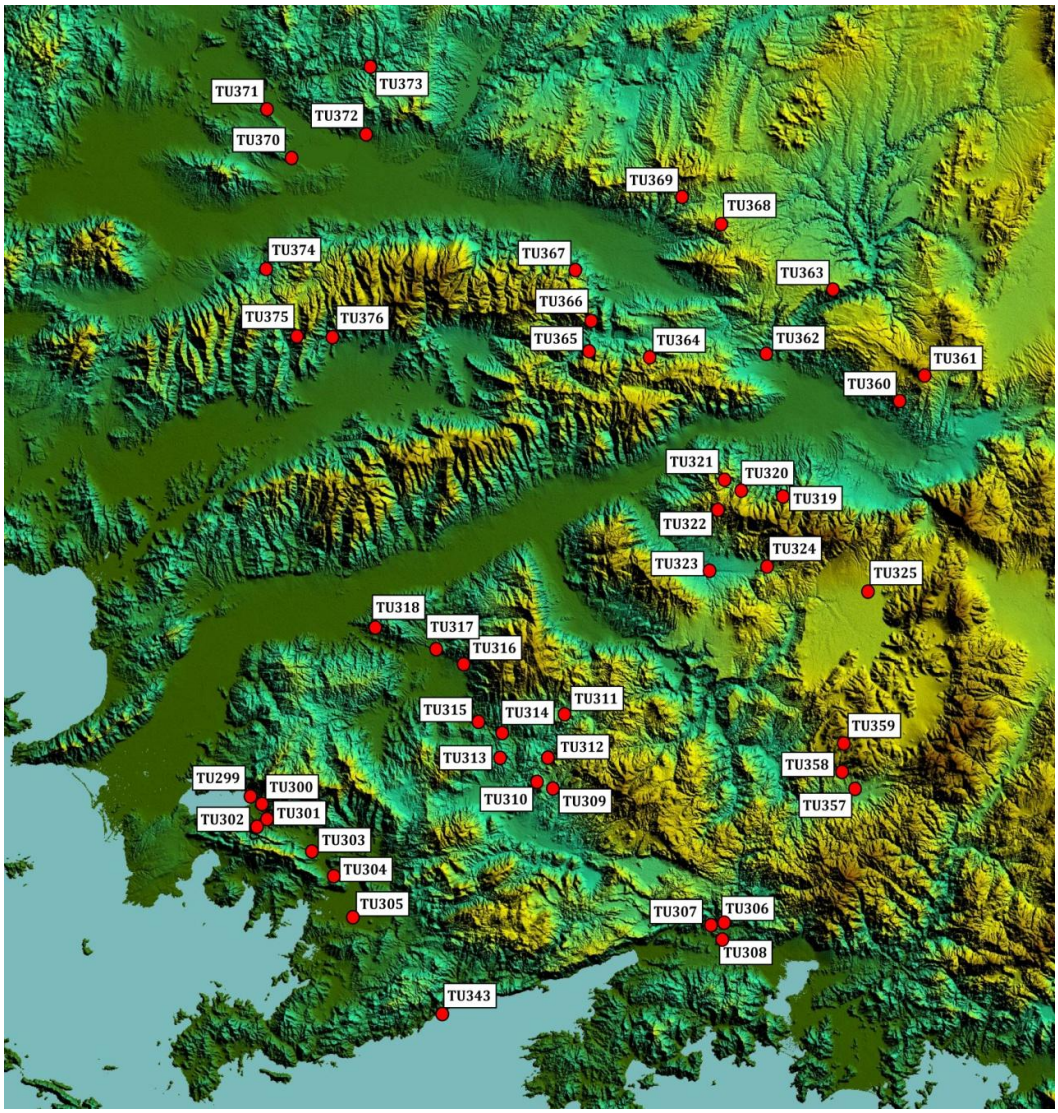


**Fig. 3.1 – DEM showing the location of the samples taken from the Menderes Massif.**

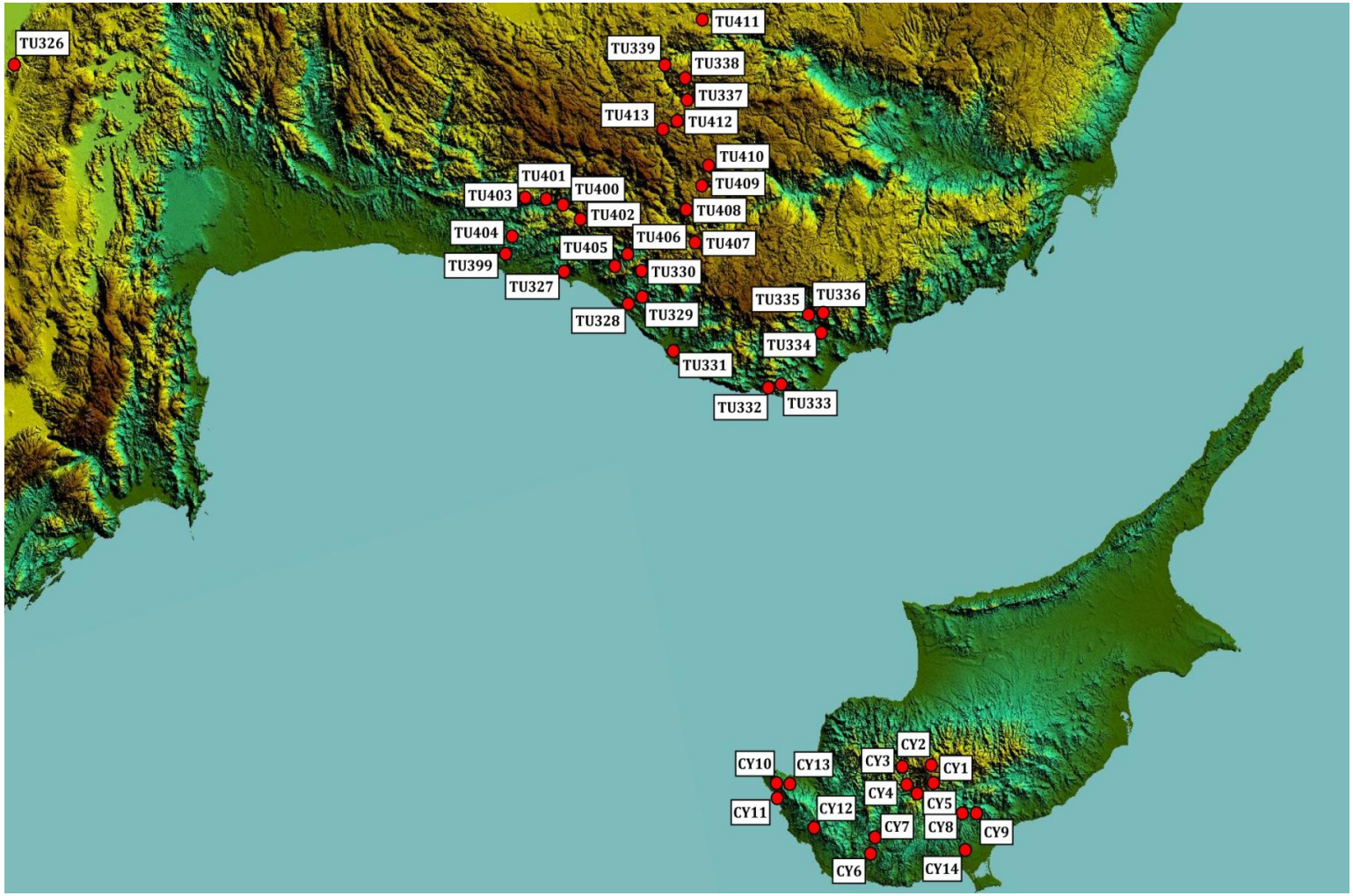


**Fig. 3.2 – DEM showing the locations for the samples taken in the southern Turkey and Cyprus.**

Sampling was carried out in two phases: first during the first year of PhD in July 2012, second during the second year of PhD in July 2013 in collaboration with Prof. Aral Okay from the İstanbul Teknık and Dr. Irene Albino from the University of Bologna.

The sampling phase was followed by an intense phase of work in laboratory. Each sample was prepared following the procedures illustrated in the next chapter to obtain the apatite grains for fission-track analysis.

A first phase of analysis took place from July to November 2012, during which were processed the samples ranging between TU299 and TU343. Despite our efforts we had to discard nineteen samples because they either did not contain enough apatite grains or the apatite grains did not contain enough fission tracks.

A second phase of analysis was performed from July to November 2013, during which were processed the samples ranging between TU357 and TU376. In this case from the twenty sample processed, we discarded six samples because apatite where absent.

A new sampling campaign in the Alanya Massif was undertaken during June 2014. Fifteen new samples from such massif are currently being processed.

Chapter IV

# METHODS

In this chapter the fundamentals of the thermochronometrical methods used in this study are briefly presented. Thermochronometry as a discipline is relatively recent (the first FT papers date back to the 1960s: e.g. Fleischer et al., 1965; Fleischer & Price, 1964; Naeser, 1967; Wagner, 1969), and therefore it is subject to a rapid evolution of techniques and its potentialities and fields of application are still being investigated; furthermore many complications both theoretical and technical are still unsolved.

Here, based on the plentiful literature available, the well consolidated and widely accepted principles and techniques of such discipline are presented, with the aim not to examine and discuss its details but to provide the reader with an adequate background to the comprehension of the main contents of the present study. The methods hereafter described, including sampling, analysis and interpretation, follow the same routine currently adopted in most of the centers where thermochronometry is performed. Main references for this and the following paragraph are the synthetic works provided by Reiners & Ehlers (2005) and Reiners & Brandon (2006).

## 4.1 PRINCIPLES OF THERMOCHRONOMETRY

The thermal sensitivity of radioactive systems depends on their tendency to turn from a closed to an open system condition with increasing temperatures. Thermochronometry plays on the sensitivity to a low temperature range (between ca. 30°C and 550°C) of some radioactive systems (thermochronometers) to understand thermal histories of rocks and minerals in that temperature range.

Three groups of thermochronometers are currently of common use: the (U-Th)/He and the fission tracks systems, based on the production of respectively He and lattice defects (fission tracks) by decay of U and Th in U-Th bearing minerals (primarily apatite and zircon) and the $^{40}Ar/^{39}Ar$ systems based on the production of $^{40}Ar$ by the decay of $^{40}K$ in K bearing minerals (feldspar, micas, hornblende). Thermal sensitivities of these thermochronometers can be quantitatively predicted, as the processes of removal of the daughter products of the radioactive decays (i.e. the opening of the system) can be well represented by thermally activated diffusion: this allows using them to constrain thermal histories of minerals and of host rocks.

In Fig. 4.1 the thermal sensitivities (represented by closure temperatures, see the text below for definition) of the most common thermochronometers are indicated.

Thermal history of a rock in such low temperature range results from the interaction between its movements relative to the earth's surface and the crustal thermal field and its variations in space and time. As a consequence, in some settings and under proper assumptions thermochronometry can be eventually used to infer burial and exhumation history of rocks. The low-temperature thermochronometers used in this study are the apatite and zircon (U-Th)/He systems (AHe and ZHe) and apatite fission track system (AFT).

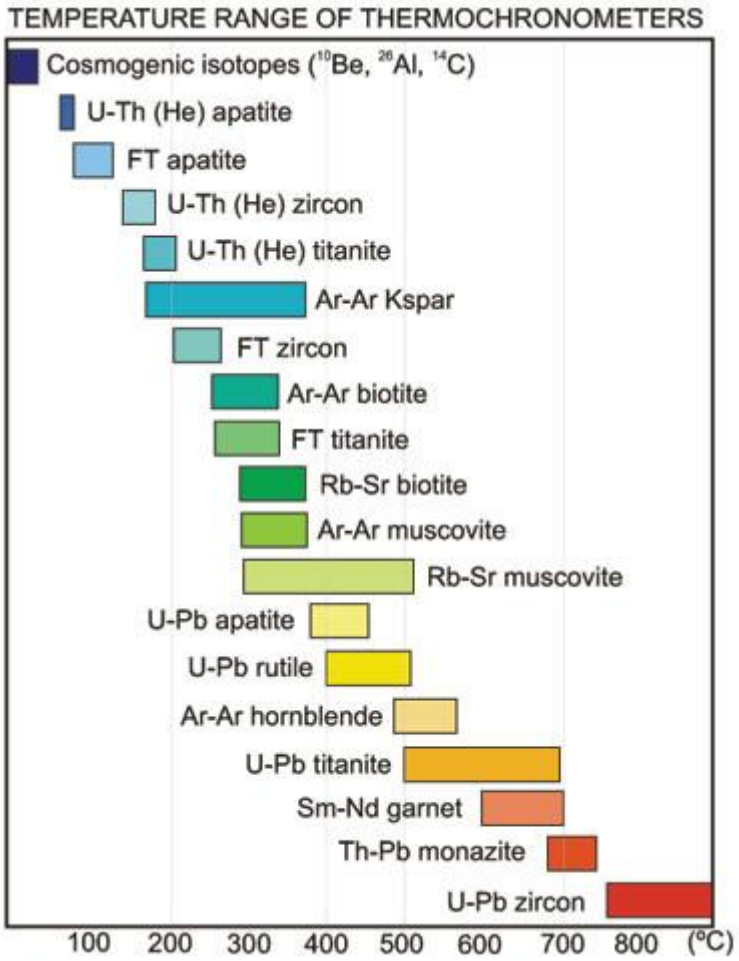


**Fig. 4.1 – Nominal closure temperatures of various geochronometers and thermochronometers. Systems are ordered by closure temperature on the Y-axis.**

The closure of a thermochronometer occurs through a range of decreasing temperatures for which the retention of products of the decay by the system

progressively increase from 0% at the base (maximum temperature) to 100% at the top (minimum temperature): this temperature interval is defined Partial Annealing Zone (PAZ) when referred to fission track thermochronometer or Partial Retention Zone (PRZ) when referred to (U-Th)/He thermochronometer. To give an estimate of thermal sensitivity of a thermochronometer the closure temperature ($T_c$) concept is often used in place of the PAZ or PRZ: this is defined as the temperature of a rock at its thermochronometric cooling age, assuming a steady monotonic cooling history. In Fig. 4.2 a schematic representation of the PAZ and $T_c$ concepts is presented.
The concept of reset is used to refer to rocks that, after having been hold for a certain time at low T, were heated up to temperatures high enough to re-open the system, before the final cooling to surface temperature.

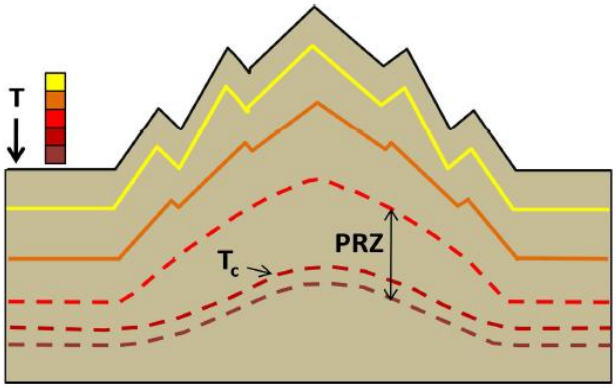


**Fig. 4.2 – Schematic representation of the PAZ and Tc concepts. (after Vernon, 2008). Colored lines indicate isotherms; dashed lines indicate PAZ bounding isotherms and the Tc isotherm.**

Another very important concept is the exhumation: this defines the movements of a rock with respect to the earth's surface (Reiners & Brandon, 2006). Exhumation can be either tectonic or erosional (or a combination of the two), as it always occur by denudation, understood as removal of rock or soil by tectonic (normal faulting or ductile thinning) and/or erosional processes (Reiners & Brandon, 2006). Rock uplift and surface uplift are used to describe the vertical motion of a rock or of a portion of the earth near or at the surface relative to a datum, such as sea level (England & Molnar, 1990; Reiners & Brandon, 2006). In Fig. 4.3 the concepts of denudation and uplift are schematically illustrated.

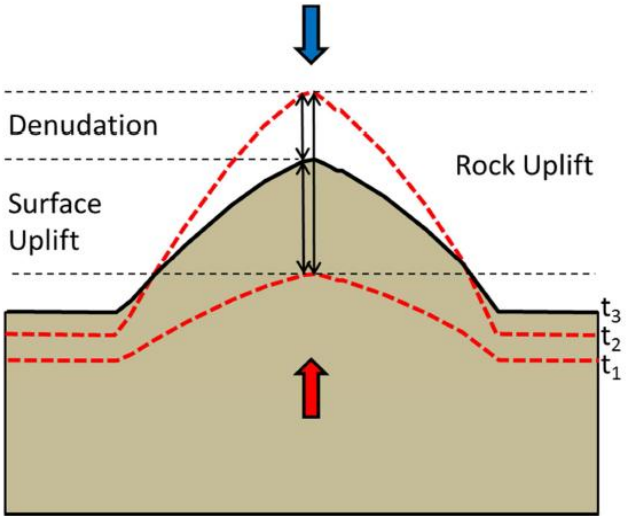


**Fig. 4.3 – Schematic representation of the denudation and uplift concepts. Dashed lines indicate paleosurface at times t1 and t2, whereas solid black line indicates the present day (t3) surface. The red arrow indicates the rock uplifting forces (tectonics, buoyancy) and the blue arrow indicates the denudational processes (tectonics, erosion) (after Andreucci, 2013).**

In order to use thermochronometric dates to constrain thermal histories, laboratory stepwise heating experiments are commonly used to calibrate the relationship between decay product retention and temperature and time. The results are compared with dates of boreholes samples, where present day thermal profile of the crust can be directly measured. Crustal sections exposed by normal faulting are also used to improve the understanding of the retention behaviour of thermochronometers as a function of temperature and depth (Reiners & Brandon, 2006). These studies give generally concordant results, suggesting that the relationship between daughter products retention and temperature is well understood.

The calibration of kinetic models for the retention of single thermochronometers allows one to define their PRZ and Tc for given cooling rates. The thermochronometric age has a true temporal meaning by itself only in case of monotonic cooling, when it corresponds to the cooling through the closure temperature. To reconstruct more complex thermal histories backward thermal modelling is used. For example in fission tracks analysis apatites all have the same initial length of about 16 microns but anneal at rates proportional to temperatures, starting from about 60 °C. Over geological time scales, partial annealing of fission tracks occurs at temperatures between about 60 and 125 °C (see section 4.2).

Because tracks shorten in relation to the degree and duration of heating, the measurement of fission track lengths gives information about the thermal evolution within the PAZ temperature range. A quantitative evaluation of the thermal history can be carried out through modeling procedures, which find a range of cooling paths compatible with the AFT data (Ketcham, 2005). In this dissertation, inverse modeling of track length data was performed using the HeFTy program (Ehlers et al., 2005), which generates the possible T–t paths by a Monte Carlo algorithm, assuming a starting time and temperature. In general, all time-temperature histories should begin at a sufficiently high temperature to ensure that there is total annealing as an initial condition. Thus, the earliest T-t constraint should have a minimum temperature above the total annealing temperature of the most resistant apatite being modeled. An exception to this principle might be the modeling of rapidly cooled volcanic rocks where it is known a priori that the initial condition is represented by zero tracks present at some temperature below the total annealing temperature. The gauge of the match between the modelled thermal history and the experimental data is given by the Goodness Of Fit parameter (GOF), which indicates the probability of failing the null hypothesis that the model and data are different. In general a value of 0.05 or higher is considered not to fail the null hypothesis, and thus reflects an acceptable fit between model and data. A modelled thermal history is considered good when it has GOF>0.5 (Ketcham, 2009).

## 4.2 FISSION TRACK THEMOCHRONOMETRY

Fission track thermochronometry is based on the production of narrow lattice damages by the spontaneous fission of U. Such dating method has been widely used in the last thirty years to constrain thermal histories in many geological settings. Early work by Naeser (1967) and Wagner (1968; 1969) first established the basic procedures that enabled FT dating to be routinely applied to geological problems. Fleischer et al. (1975) summarized the early studies of the broader discipline of nuclear track detection in solid state materials. More recent comprehensive overviews of fission track applications have been provided by Dumitru (2000), Gallagher et al. (1998), Gleadow et al. (2002), Naeser & McCulloh (1989), Wagner & Van den Haute (1992), Van den Haute & De Corte (1998). The synthetic works of

Braun et al. (2006), Donelick et al. (2005), Reiners & Brandon (2006), Tagami & O'Sullivan (2005), are used as main references for this paragraph, which presents an overview of the fission tracks (FT) dating method. Since in this PhD work apatite has been the only mineral phase dated by FT, this chapter deals in particular with the AFT dating method.

### 4.2.1 Formation of fission tracks

The FT analysis uses the radioactive system composed by $^{238}U$ and linear lattice damages (fission tracks) produced by its spontaneous fission in apatite and zircon (e.g. Price & Walker, 1963; Fleischer et al., 1975). The assumption that fission tracks are generated only by decay of $^{238}U$ is based on the low abundance/low decay constant of other isotopes decaying by spontaneous fission (Tab. 4.1). When a heavy unstable nucleus decays by spontaneous fission it splits into two nuclear fragments which are pushed away to each other by a combination of energy released by the nuclear fission and coulomb repulsion forces. The passage through the crystal lattice of the two positively charged nuclear fragments induces a change of electrostatic charge in the surrounding lattice region. Charge variation induces, in turn, widespread dislocation of atoms from their lattice positions, generating the high defect density which characterizes fission tracks (Fig. 4.4; Ion explosion spike theory, Fleischer et al., 1965; 1975). Fresh FT have lengths of ca. 11 μm in zircon and ca. 16 μm in apatite (Reiners & Brandon, 2006). The accumulation of fission tracks in time (t) is described by the decay equation properly modified to account for the fact that $^{238}U$ decays not only by spontaneous fission with a decay constant $\lambda f = 8.5\ 10^{-17} yr^{-1}$ but also by α decay, with a much higher decay constant $\lambda\alpha=1.5\ 10^{-10}\ yr^{-1}$ (Tagami & O'Sullivan, 2005):

$$N_{s=}\frac{\lambda_{f^{238}}}{\lambda_{\alpha}}N(e^{\lambda_{\alpha}t}-1)$$

**Table 4.1- Relative abundances of U isotopes, total half life and half life due to spontaneous fission decay process.**

| | Relative abundance (with respect to $^{238}U$) | Half Life (yr) | Half life – spont. fission (yr) |
|---|---|---|---|
| $^{232}Th$ | $4^{d}$ | $1.40x10^{10}$ | $1.0x10^{21}$ |
| $^{234}U$ | $5.44x10^{-5}$ | $2.46x10^{5}$ | $1.5x10^{16}$ |
| $^{235}U$ | $7.25x10^{-3}$ | $7.04x10^{8}$ | $1.0x10^{19}$ |
| $^{238}U$ | 1 | $4.47x10^{9}$ | $8.2x10^{15}$ |

**d-geochemical average**

**a)** **b)** **c)**

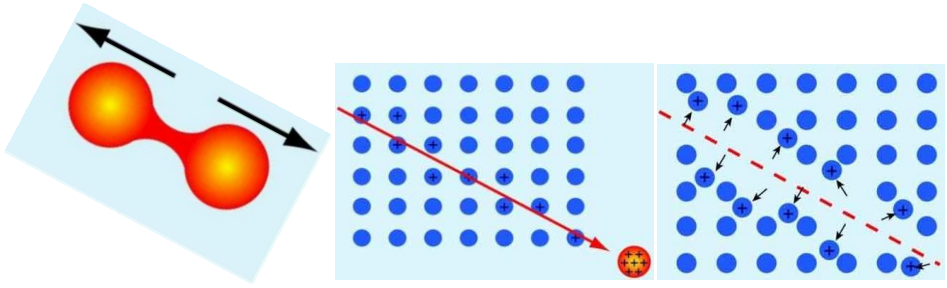

**Fig. 4.4 – The 'Ion Explosion Spike' model for FT formation (from Fleischer et al., 1975). The Heavy nucleus splits in two nuclear fragments (a); the two positively charged fragments are pushed away from each other and along their track they tear off electrons from the atoms of the lattice (b); the positively charged atoms along the track dislocate from their lattice position due to repulsive electrostatic forces (c).**

### 4.2.2 Analytical procedures and grain age calculation

To infer single crystal age the most commonly adopted technique is the External Detector Method (EDM), which main stages are schematically indicated in Fig. 4.5. The mineral grains to be dated are mounted in epoxy resin, polished and chemically etched. The tracks, and more in general the lattice defects, etch more rapidly than the intact crystalline lattice, and thus become visible for counting. After chemical etching the spontaneous tracks density of single mineral grain can be determined. In order to determine the $^{238}U$ initial concentration, the EDM plays on the constant natural $^{235}U/^{238}U$ ratio ($7.252x10^{-3}$). A sheet of U-free mica is placed over the polished mount. Neutron irradiation in a nuclear reactor induces fission of $^{235}U$. Nuclear fragments belonging to atoms placed close to the polished surfaces of the

grains are injected in the mica sheet forming fission tracks in its lattice. Induced fission track density can be then measured on the mica surface after proper chemical etching. From $^{235}U$ the $^{238}U$ content is then calculated. The induced tracks are present also in the grain mount, but they are not revealed since the chemical etching of the minerals is done before the neutron irradiation. The mica monitor and the mount are assembled in the same slide and analyzed with an optical microscope implemented with a sliding table and dedicated software. Before analyzing the sample three reference points in the mount and their correspondents in the mica are used to calibrate the system, so that the coordinates of the location on the external detector corresponding to the grains can be automatically calculated. The operator is then enabled to measure spontaneous and induced track density for the single mineral grains (Reiners & Brandon, 2006).

The AFT age of a single apatite grain determined using the EDM method is given by:

$$t_i = \frac{1}{\lambda_d} \ln\left(1 + \lambda_d \zeta g \rho_d \frac{\rho_{s,i}}{\rho_{i,i}}\right)$$

Where subscript i refers to grain i; $t_i$ is fission track age of grain i; $\lambda_d$ is the total decay constant of $^{238}U$; $\zeta$ is the calibration factor based on EDM of fission track age standards, depending on the microscope and operator; g is the geometry factor for spontaneous fission track registration, $\rho_d$ the induced fission track density for a uranium standard corresponding to the sample position during neutron irradiation, $\rho_{s,i}$ is the spontaneous fission track density for grain i; $\rho_{i,i}$ is the induced fission track density for the grain i (Donelick et al., 2005).

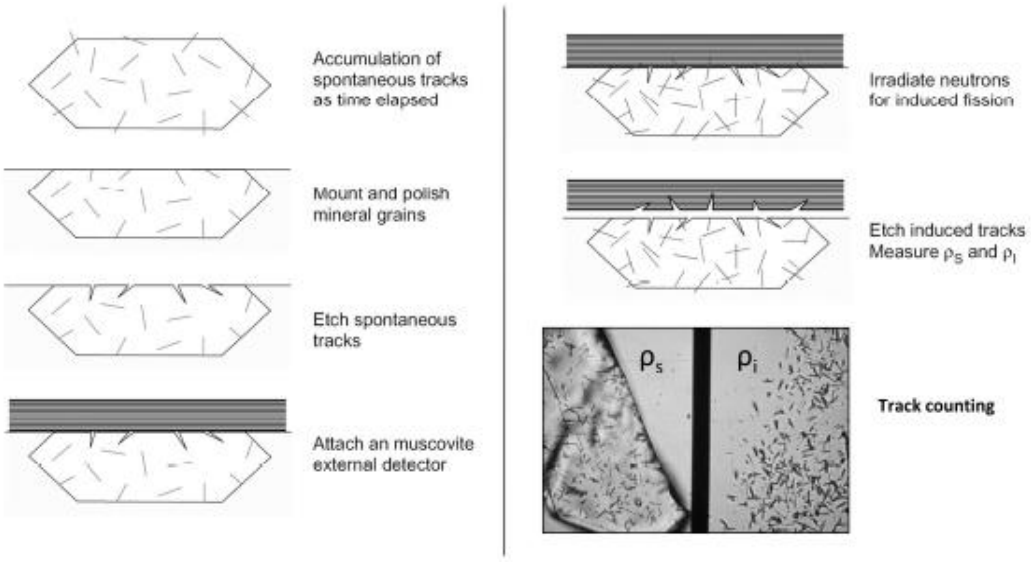


**Fig. 4.5 – Schematic procedure for FT analysis with the EDM method (from Tagami & O'Sullivan, 2005). Source for the picture of spontaneous and induced tracks is the www.geotrack.com.au website.**

### 4.2.3 Retention and annealing of FT

Fission track annealing is a temperature dependent diffusional process, to which the Arrhenius law can be applied. However, in contrast to the He diffusion models, there is no accepted physical model of fission track annealing processes at the atomic level, since the process of fission track annealing is much more complicated than the diffusion of a single atomic species out of a mineral lattice, and still poorly known (Braun et al., 2006). Fission tracks annealing models have thus been developed using a completely empirical approach, looking at what form of the annealing relationship best fit the data statistically (Braun et al., 2006).

Several kinetic models have been developed from different experiments: in the so-called fanning Arrhenius models, in a $T^{-1}$-ln(t) space, the annealing isopleths fan out from a single point (Crowley et al., 1991; Ketcham et al., 1999; Laslett et al., 1987); whereas in the curvilinear Arrhenius models (Ketcham et al., 1999; 2007) the annealing isopleths are slightly curved. The curvilinear Arrhenius models were obtained by imposing the model to fit both the experimental data and two benchmarks for annealing at geological timescales (Ketcham et al., 1999). FT annealing behaviour is independent on grain size, but it is demonstrated to vary with apatite chemistry, with retention increasing with increasing Cl/(F+Cl) ratio (Green et al., 1985), although other cations and anions substitutions also play a role

(Barbarand et al., 2003; Carlson et al., 1999; Donelick et al., 1999; Ketcham et al., 1999). Moreover the annealing behaviour also depends on the crystallographic orientation of the tracks with higher annealing rate for tracks orthogonal than tracks parallel to the C-axis of the crystal (Donelick et al., 1999; Green et al., 1986; Ketcham et al., 2007).

The $D_{par}$, i.e. the mean width of fission tracks etch pits, is a commonly used proxy for track retentivity of single crystals, first proposed by Ketcham et al. (1999). Other kinetic indicators alternative to $D_{par}$ are Cl and OH contents (Ketcham et al., 1999; 2007). The kinetic models proposed by Ketcham et al. (1999; 2007), are, in fact, multi compositional models, accounting for the different kinetic behaviours of crystals belonging to the same rock (this typically occurs for sedimentary rocks). The single grain annealing equations in the multi compositional models differ to each other by a parameter $r_{mr0}$, defined by Ketcham et al. (1999), which is calculated from the kinetic indicator ($D_{par}$, Cl, OH).

The effects of annealing can be quantified by measuring the lengths of horizontal confined tracks (Gleadow et al., 1986; Fig. 4.6).

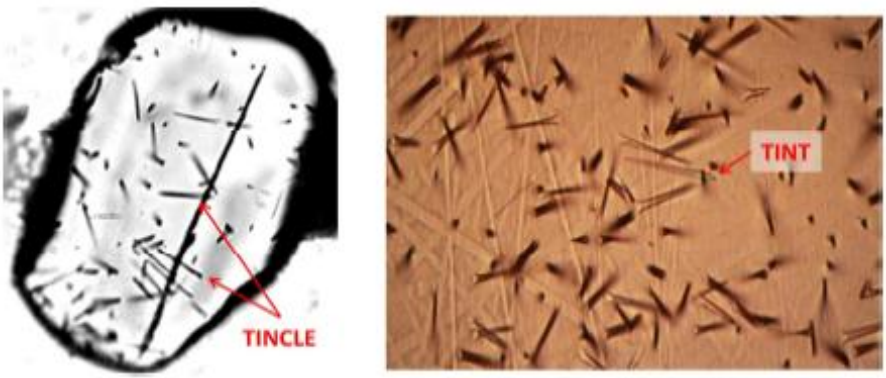


**Fig. 4.6 – Confined horizontal tracks: 'Track in cleavage' (TINCLE) and 'Track in track' (TINT). The first picture is from Paul & Fitzgerald (1992), and the second from the www.sciencelearn.org.nz website.**

This depends on the fact that tracks form continuously, and thus each track experiences a different portion of the integrated thermal history (Braun et al., 2006). Therefore the track lengths distribution, obtained by measuring a sufficient number of horizontal confined tracks (preferably ≥100) contains information on the thermal history experienced by the sample (Braun et al., 2006; Fig 4.7).

The AFT PAZ values are generally comprised between 30°C and 130°, but can be significantly different depending on cooling rate and apatite chemistry (Reiners & Brandon, 2006; Fig. 4.6).

AFT $T_{cs}$ generally vary between ca 80°C and 120°C, but still being largely affected by apatite composition. An apatite of "average" composition (Ketcham et al., 1999) has, for cooling rates of 10°C/My, Tc=116°C.

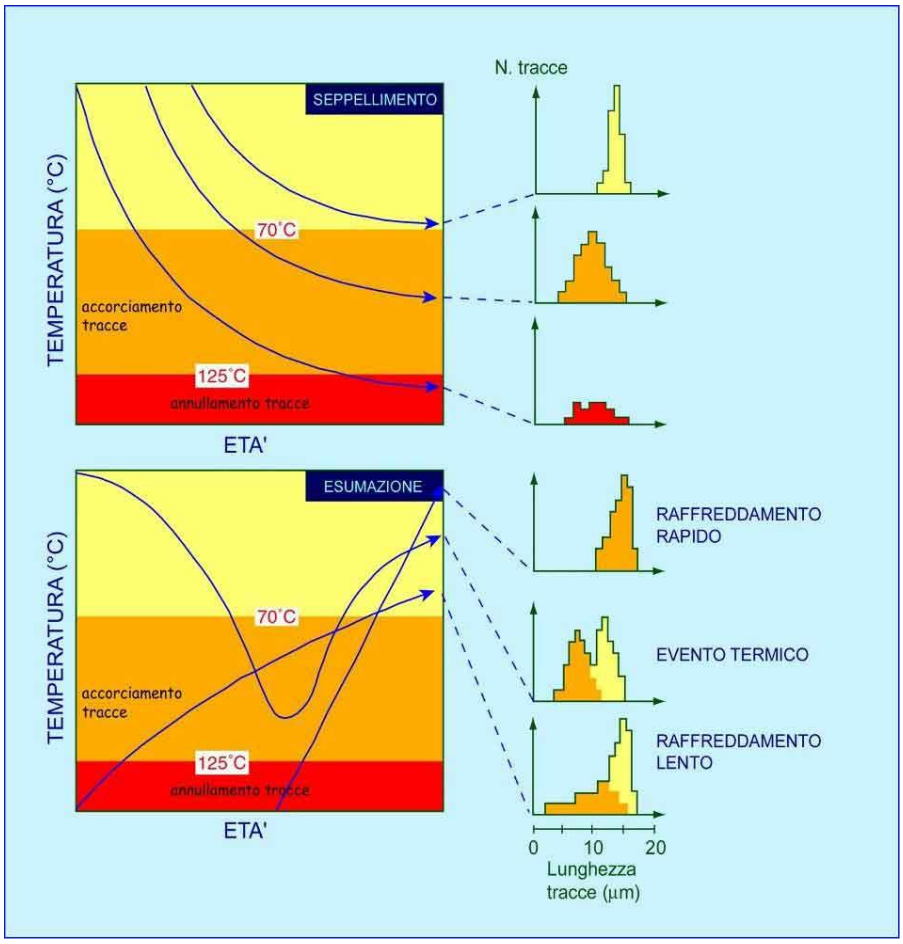


**Fig. 4.7 - Relationships between track length distribution and thermal history (modified after Wagner & Van Den Haute, 1992).**

### 4.2.4 Data analysis and interpretation

Usually track densities are measured on 20 to 40 grains of the same sample, whereas 40 to 100 lengths are measured per sample. The measured parameters are the numbers of spontaneous and induced tracks, the area, the mean $D_{par}$ of the grain for track density measurements, and the lengths, orientation with respect to C-axis and mean $D_{par}$ for track lengths measurements.

For this PhD thesis the program running on Matlab, Zetage (Brandon & Fellin, 2012) was used to value single grain ages, sample pooled and central ages, $\chi^2$ probability and age dispersion. The most common way to visualize AFT age data is with radial plots (Fig. 4.8). The Y axis represents the standard error $((a_g-a_c)/\sigma)$ of the single grain age (ag) with respect to the central age of the whole population ($a_c$) and the X axis represents the relative error ($1/\sigma$) decreasing toward the radial scale. Single grain ages are read on the intercept with the radial axis (plotted on a logarithmic scale) of the line drawn through the single grain point and the origin.

The statistical parameter which best describes the age of an FT age population is the central age (Galbraith, 1990), which takes into account the lognormal nature of the $\rho_s/\rho_i$ ratio (Vermeesch, 2008).

The $\chi^2$ statistical test (Galbraith, 1981) is used to define the probability that all the grains counted belong to a single population of ages. A probability ($P\chi^2$) of less than 5% is evidence of an asymmetric spread of single grain ages, and thus it indicates the presence of several age populations. An asymmetric spread in individual grain ages can result either from inheritance of detrital grains from mixed detrital source areas, or from differential annealing in grains of different compositions (Green et al., 1989).

A detrital sample is to be considered completely reset if all grain ages belong to the same population (high $P\chi^2$ value) and they are all younger than the depositional age. Partially reset samples are usually characterized by low $P\chi^2$ values (i.e. large dispersion) and have some grains younger and some older than the depositional age. Not reset samples are finally characterized by very low $P\chi^2$-square values and by thermochronometric ages all older than depositional ages.

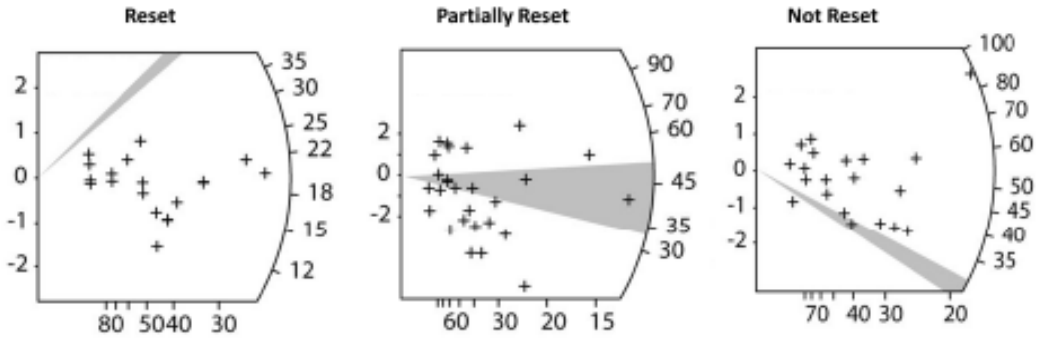


**Fig. 4.8 – Examples of radial plots referred to sedimentary rocks heated to different degree.**

## 4.3 HELIUM THERMOCHRONOMETRY

(U-Th)/He dating is based on the α-decay of Uranium and Thorium. U-He radioisotopic system was discovered by Ernest Rutherford in the first decade of the 20th century. After a first flowering of He dating in the scientific community of that time, the method was gradually abandoned in the next few decades. By about 1940, when U-Pb dating became widely available, it also became evident that He dating provided, in most cases, largely underestimated formation ages, and He loss was recognized to be responsible for such. Zeitler et al. (1987) first suggested that He ages could represent cooling rather than formation ages, opening the way to He thermochronometries.

In this section principles and applications of He thermochronometers are presented. The main references used, to which the reader is addressed for a more exhaustive description of methods are Braun et al. (2006), Ehlers & Farley (2003), Farley (2000), Reiners & Brandon (2006), Reiners et al. (2004).

### 4.3.1 He ingrowth

(U-Th)/He thermochronometry is based on the production of He nuclei (α particles) by the U and Th decay series and, to a minor extent, by α- decay of 147Sm. The equation for He ingrowth in time (t) is:

$$^{4}He = 8^{238}U(e^{\lambda_{238}t} - 1) + 7^{235}U(e^{\lambda_{235}t} - 1) + {}^{232}Th(e^{\lambda_{232}t} - 1) + {}^{147}Sm(e^{\lambda_{147}t} - 1)$$

where He, U, Th and Sm refer to present-day amounts, and λ is the decay constant ($\lambda^{238} = 1.551 \times 10^{-10}yr^{-1}$; $\lambda^{235} = 9.849 \times 10^{-10}yr^{-1}$; $\lambda^{232} = 4.948 \times 10^{-11}yr^{-1}$; $\lambda^{147} = 0.654 \times 10^{-11}\ yr^{-1}$).

The coefficients preceding the U and Th abundances account for the multiple α particles emitted within each of the decay series. This equation can be simplified, since the $^{238}U/^{235}U$ ratio has in the solar system a constant value of 137.88 (Steiger & Jager, 1977). $^{235}U$ can be then written as a function of $^{238}U$ and the ingrowth of helium with time can be written as a function of the elemental U, Th and He abundances or concentrations.

The He ingrowth equation assumes absence of $^4$He, both initial and produced by sources extraneous to the crystal, and secular equilibrium among all daughters in the decay chain. In case of zircons these assumptions are valid in most cases, whereas, due to the lower U and Th content typically yielded by apatites, for such mineral phase the presence of external sources of He can be represented by U-Th rich inclusions (zircons, monazite) or coating (oxides and oxhydroxide). In this case a most careful selection of the grains to be analyzed is required.

### 4.3.2 Analytical procedures

Grain selection and packing are made under optical stereoscope. Intact, prismatic, unabraded and inclusion free grains are preferably selected for analysis. Selected grains are then digitally photographed and geometrically characterized by measuring each grain for its prism length (parallel to the c axis) and prism width in at least two different orientations (perpendicular to the c axis). Grains are than packed in Nb or Pt tubes or foils (Fig. 4.9).

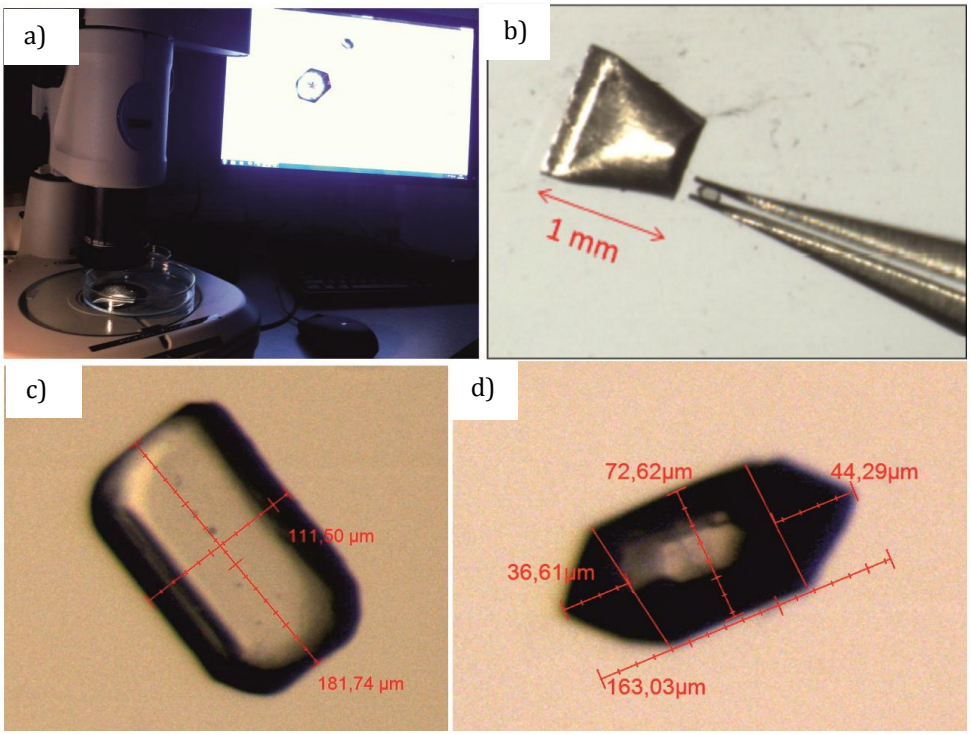


**Fig. 4.9 – Grain selection and picking: the grains are poured in a petri-dish for grain selection under optical microscope (a); the selected grains are photographed and measured, for apatite length and width are measured on two sides parallel to the c-**

**axis (c) , for zircons the tips heights are also measured (d). Grains are finally packed in Nb tubes (b).**

A two-stage analytical procedure is commonly used to measure $^{4}$He, U, Th and Sm. In the first stage the crystal is degassed by heating and $^{4}$He is measured by gas-source mass spectrometry. In the second stage, after chemical dissolution of the crystal, U, Th and Sm contents are measured by inductively coupled plasma mass spectrometry.

### 4.3.3 α – ejection correction

The measurements described above account for the bulk He, U, Th and Sm contents, however the resulting dates require a correction for He loss occurred by ejection of α particles outside the crystal domain. As a matter of facts, since the α particles emitted by U, Th and Sm travel a distance of ca. 20 μm, part of those emitted close to the crystal edges are ejected out of the crystal and injected in the surrounding phases (Fig. 4.10). The loss of α particles leads to an underestimation of the age of the crystal. The magnitude of α-ejection is controlled by surface to volume ratio and by spatial distribution of the parent atoms relative to the crystal surface. Assuming an idealized geometry of the crystal and an homogeneous distribution of U, Th and Sm in the crystal, the fraction of He retained can be calculated as a function of the crystal size, as described by Farley (2002). Therefore, to account for α-ejection it is a common practice to measure the physical dimensions of the crystal to be dated and to calculate an homogeneous α-ejection correction factor (HAC), to which the raw date has to be multiplied, to obtain the age corrected for ejection (Farley, 2002). The assumption of homogeneous distribution of parent nuclides is in some cases unsatisfied due to the frequent occurrence of internal zonation: since zonation is a random feature, it affects age reproducibility between different crystals of the same sample: poor age reproducibility can be therefore caused by the application of α-ejection correction to zoned crystals (e.g. Ehlers & Farley, 2003).

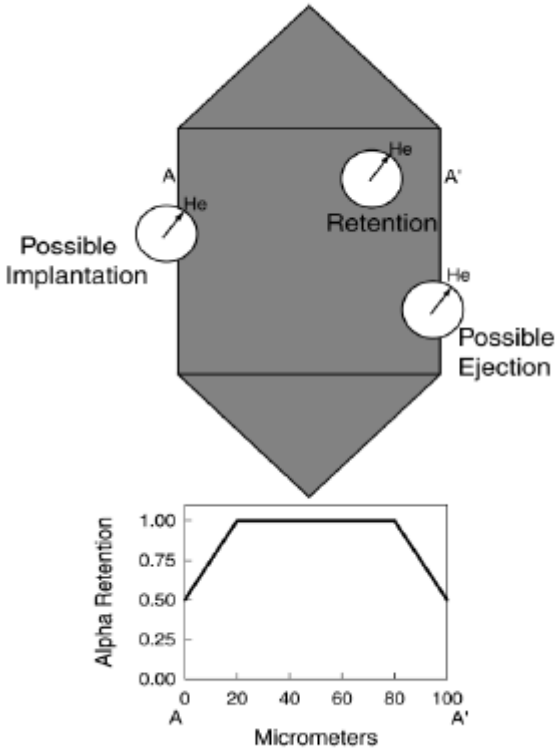


**Fig. 4.10 – The effects of long α–stopping distances on He retention (from Farley, 2002). The upper figure illustrates the three possibilities within a schematic crystal: retention, possible α ejection, and possible α implantation. The center of the circle denotes the site of the parent U or Th nuclide, and the edge of the white circle labelled He indicates the locus of points where the α particle may come to rest; the arrow indicates one possible trajectory. The lower plot shows schematically how α retention changes from rim to core to rim along the path A-A'; exact equations defining the shape of this curve as a function of grain size were given by Farley et al. (1996).**

### 4.3.4 Diffusion behaviour

In order to use He dates to constrain thermal histories, an accurate knowledge of He diffusivity in the dated phases is required. Laboratory stepwise heating experiments have commonly been used to calibrate the relationship between diffusivity and temperature (e.g. Farley, 2000; Fechtig & Kalbitzer, 1966; Shuster et al., 2006), that is demonstrated to be well described by the Arrhenius relationship formulated as follows (Fechtig & Kalbitzer, 1966):

$$\frac{D}{a^2} = \frac{D_0}{a^2} e^{\frac{-E_a}{RT}}$$

Where $D_0$ is the frequency factor, that is diffusion at infinite temperature ($m^2s^{-1}$), $E_a$ is the activation energy (J $mol^{-1}$), T is the temperature (K), R is the gas law constant (8.3145 J $mol^{-1}$ $K^{-1}$) and a is the radius of the spherical diffusion domain (m; Fechtig & Kalbitzer, 1966). The diffusion domain size (a) corresponds, in most cases, to the crystal size (Farley, 2000; Reiners & Brandon, 2006), implying a dependence of $T_c$ and PRZ on the grain size.

Kinetic models for He diffusion comprise the diffusion equation and the diffusion parameters ($E_a$, $D_0$).

The currently accepted and most used model for He diffusion in apatite is that proposed by Farley (2000) based on the previous equation, nevertheless subsequent models have been proposed to account for radiation damages effect on He diffusivity. Shuster et al. (2006) demonstrated that, in fact, diffusivity generally decreases with increasing He content.

This is interpreted to be due to the effects of He trapping by α-recoil lattice damages. Shuster et al. (2006) proposed then a kinetic model where diffusivity is a function of [He], and where the annealing of traps occurs with the same kinetics as He loss. Subsequent work by Shuster & Farley (2009) pointed out that trap annealing may correspond to fission track annealing. This implies that [He] is an inadequate proxy for traps as it diffuses out of the crystal earlier than trap annealing. Therefore Flowers et al. (2009) proposed a Radiation Damage Accumulation and Annealing Model (RDAAM) which uses the fission track annealing model of Ketcham et al. (2007) to characterize diffusivity-altering damage annealing.

As for He diffusion in Zircon the currently used diffusion model is that proposed by Reiners et al. (2004) also based on above equation. An effect of radiation damages on He diffusion in zircons has also been demonstrated (e.g. Damon & Kulp, 1957), nevertheless a kinetic model accounting for such effect has not been formulated so far.

The diffusion parameters obtained by calibration of the diffusion equation through step heating experiments are used to estimate the PRZ and the $T_c$ for He thermochronometers of given grain size and for given cooling rates.

PRZ for AHe varies between ca. 20°C and 60°C (Reiners & Brandon, 2006; Fig 4.14), whereas closure temperatures are in the range 40°C – 80°C (Fig. 2.6), for cooling rates of 10°C/My and diameter of the spherical domain of 60 μm, AHe

$T_c$=67°C (Reiners & Brandon, 2006). As for ZHe the PRZ ranges between ca. 90°C (for hold time higher than 250 My) and 185°C (for minimum hold time; Fig. 4.14); $T_c$s range between ca. 140°C and 200°C (Fig. 4.15); e.g. for a 60 μm grain diameter and a cooling rate of 10°/My, $T_c$=183°C.

### 4.3.5 The effect of slow cooling

The transition from retention to diffusion of radiogenic He can be slow or incomplete. This is particularly true for samples which underwent slow cooling or prolonged stay in the PRZ. For such samples the thermochronometric ages have no meaning in terms of temperature, representing instead a more complex thermal history. In fact, the magnitude of the effect on age of subtle factors controlling He diffusion (like zonation, crystal size, kinetic parameters) increases with decreasing cooling rates (Ehlers & Farley, 2003). Most of all, crystal size (of intact crystals) tends to correlate with age in case of slow cooling, since it affects both α-ejection and He diffusion kinetics. The correlation between crystal size and age may be then used to model thermal histories of samples that slowly cooled through the He PRZs.

### 4.3.6 Data analysis and interpretation

In most studies three to five replicates of the same rock sample are analyzed. The data are then processed to test their significance and their meaning.

Age reproducibility of crystals belonging to the same rock sample is first checked. In case of well reproducible samples the weighted mean of ages can be used for interpretation (as suggested by Fitzgerald et al., 2006) and the $T_c$ concept can generally be applied, whereas in case of high dispersion single grain ages are preferably shown. As described in previous paragraphs many sources of age dispersion may be present.

If age dispersion is only due to differences in grain size in crystals of a slowly cooled sample, then a correlation between grain age and radius will be observed. In this case age dispersion adds further information to the reconstruction of the thermal history of the sample.

In case age dispersion is due to radiation damages a correlation between grain age and eU should be observed. Also in this case dispersion do not preclude to use dates for reconstructing thermal histories, provided the RDAAM model of Flowes et al. (2009).

Age dispersion occurs in partially reset samples as well as in unreset detrital samples. Incomplete or null reset of detrital samples also implies that part or all of the LAG times are ≥0; in other words part or all of the depositional ages are younger than thermochronometric ages. In case the sample is completely unreset ages actually indicate the cooling of the source rocks prior to erosion, transport and deposition. Thus ages from detrital unreset samples can be used for detrital thermochronology, which statistics usually require a larger number of data. On the other hand, partially reset ages cannot be used to infer information on the cooling of neither the detrital sample nor the source rocks. In all the cases described above age dispersion can then be used to obtain information on the thermal history of the sample.

Nonetheless age dispersion can also be induced by crystal defects: in this case dispersion has no meaning in terms of thermal history, being due to the presence of biased ages.

- zonation, inclusions and coating may also tend to induce age dispersion, by leading to a violation of some of the fundamental assumptions for He dating and HAC, such as uniform U-Th distribution in the crystal and absence of external He sources. In this case a correlation between age and U-Th contents (often expressed as effective uranium, eU= [U] + 0.235×[Th]) could be observed;
- Features like abrasion and rounding may also induce incorrect application of the HAC.
- Dispersion may be finally arising from fractured and/or broken crystals to which the model for diffusion kinetics and possibly the HAC are improperly applied.

## 4.4 SAMPLE PREPARATION PROCEDURES

The apatite and zircon separation from the rock samples was performed at the Laboratory of Sedimentary Petrography of the Department of Biological, Geological and Environmental Sciences of the University of Bologna, following the procedures described in Donelick et al. (2005). Rock disaggregation was performed using a disk-mill and a jaw crusher. After disaggregation the crushed material was sieved using 250μm sieve-cloth and the >250 μm fraction was processed again in order to obtain material all of sand size. The material was then washed using a washing table with

riffles, in order to discard the fine grained fraction. The sand-sized material was then processed with a Frantz Isodynamic magnetic separator, in order to discard the magnetic fraction. Heavy-liquid separation was performed in two steps. The fraction with density higher than ρ=2.97 g/cm$^3$, obtained from the first separation with tetrabromoethane, contains both apatite (ρ=3.1-3.35 g/cm$^3$) and zircon (ρ=4-4.70 g/cm$^3$). Apatite are then concentrated through the second separation with diiodomethane (ρ=3.33 g/cm$^3$).

Preparation of grain mounts for neutron irradiation for the AFT analysis continued with the mounting: a mixture of resin and hardener (the proportions depending on the specific product used) was prepared. Each sample number was then engraved on microscope slides, previously cleaned with acetone. The slide (with the engraved number on the bottom of the glass) was put in a hot plane (also the temperature depended on the resin used) and some drops of the resin were put in the middle of the glass. The resin was carefully mixed to eliminate possible air bubbles. Apatite grains were then mixed with the resin on an area of about 1x1.5 cm. the resin was cured leaving the mounting on the hot plane for some minutes.

Grain mounts were then polished to expose inner crystal surfaces and to smooth them to eliminate defects that can obstruct track counting. After polishing the grain mounts are chemically etched with $HNO_3$ 5M for 20 seconds, in order to highlight the spontaneous tracks.

A mica sheet with low-U content was then placed over each grain mount to form a mount-mica couple fastened with adhesive tape. The mount-mica packages were then stacked in standard irradiation tubes (Fig. 4.11); at the two ends of each stack of samples two packages constituted by standard CN5 glass, of known U content and mica were placed in order to monitor neutron fluence during irradiation.

Sample irradiation with thermal neutrons was performed in the reactor at the Radiation Center of Oregon State University. Grains from forty-one samples were sent to irradiation, since in the other thirty-nine the number of apatite grains found was insignificant. Irradiation took place with a nominal neutron fluence of 9 x 1015 n cm$^{-2}$. After irradiation each mount-mica package was opened and the mica sheets were chemically etched with HF 40% for 40 minutes in order to highlight the fission tracks induced by neutron irradiation. Apatite fission track analysis could then be performed on mount-mica couples mounted on microscope slides.

Manual picking of apatite and zircon grains for He analysis was performed at the Institute of Geochemistry and Petrology of the Swiss Federal Institute of Technology (ETH-Zürich). In both cases an optical stereoscope with an integrated camera was used in order to take pictures of the selected crystals and to measure them for α-ejection correction. Crystals were then packed in Pt tubes of 1mm heights that worked as a micro-furnace for crystal heating and He extraction during analysis.

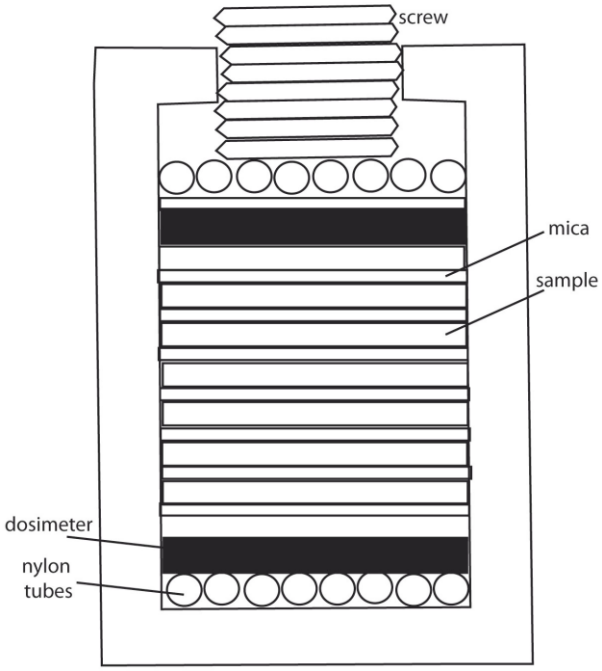


**Fig. 4.11 – Holder for irradiation and position of sample, mica and dosimeters.**

## 4.5 ANALYTICAL FACILITIES AND PROCEDURES

### 4.5.1 AFT analysis

FT ages were calculated using the external-detector and the zeta calibration methods (Hurford & Green, 1983) with IUGS age standards (Durango, Fish Canyon and Mount Dromedary apatites; Hurford, 1990) and a value of 0.5 for the $4\pi/2\pi$ geometry correction factor. Sixteen to twenty crystals per sample were used for fission-track counting. AFT ages are reported in Table 5.1.

AFT analysis was performed at the Institute of Geochemistry and Petrology of the ETH in Zürich. The basic equipment used for analysis is a ZEISS Axioscope,

equipped with motorized stage, connected to a computer and to the high resolution digital camera Invenio 5DII. In this way it is possible to proceed to counting spontaneous ($\rho_s$), induced ($\rho_i$) and measuring confined track just by the use of the PC screen. The tracks are counted on the same area of each crystal on the crystal itself and on the corresponding image in the mica sheet.

The software DeltaPix InSight is used for calibrate the sliding table before track counting, using reference points in the grain mount and in the mica sheet, so that the coordinates of the selected crystals can be registered and coordinates of the corresponding images in the mica can be automatically calculated. By this software it's enough possible measure track lengths.

### 4.5.2 AHe and ZHe analysis

Helium analysis was performed at the Institute of Geochemistry and Petrology of the ETH (Zürich). The packets containing the crystals to be analyzed, and the standard crystals are placed in a stainless steel planchet (Fig. 4.12 A) and heated with Nd-YAG and Diode laser to be analyzed for $^{4}He$ using a sector gas mass spectrometer (Fig. 4.15 B). Between 2 and 5 replicates of every sample were measured.

Helium blanks (0.1-0.05 fmol 4He) are determined by heating empty packets with the same procedure. Following He measurements, the crystals were spiked with $^{233}U$, $^{229}TH$ and $^{149}Sm$, dissolved in 30% $NO_3$ and analyzed by ICP-Quadrupole Mass spectrometer for $^{238}U$, $^{232}Th$, and $^{147}Sm$. The total analytical error was computed as the relative standard error of weighted uncertainties on U, Th, Sm and He measurements. α-ejection corrections were made following Farley (2002).

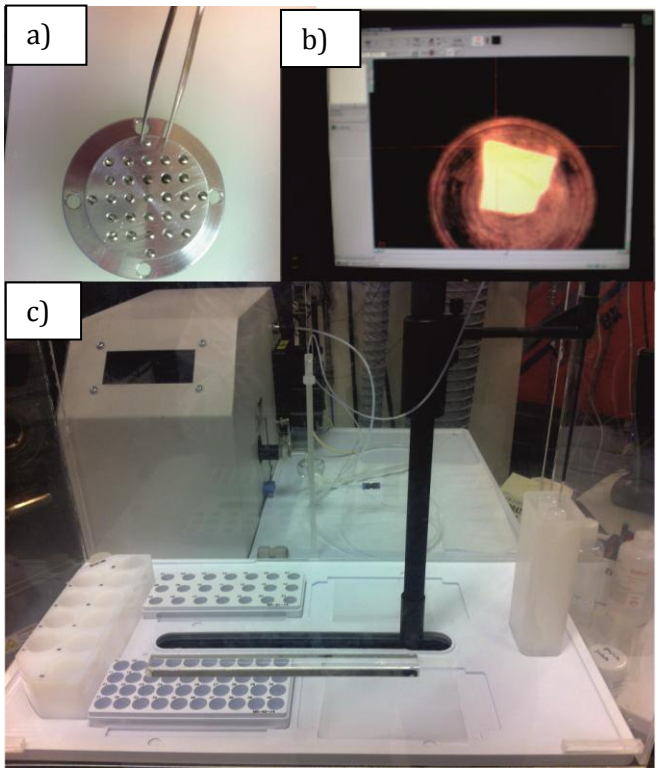


**Fig. 4.12 – AHe and ZHe analytical procedures: a) stainless steel planchet for He analysis in the quadrupole mass spectrometer; b) sample being hit and heated by laser beam; c) Inductively coupled plasma MS for U, Th, Sm analysis.**

## 4.6 FROM THERMOCHRONOMETRIC AGES TO EROSION RATES

In section 4.1 were given the definitions of the exhumation and denudation (Reiners & Brandon, 2006).

Thermochronometric data are related to thermal history, which is in turn related, in most cases, to burial and exhumation history. There are, however several complications in the relationships between the three, since erosion rates influence both the crustal thermal field and the thermal sensitivities of the thermochronometers. In other words changes in erosion rates induce both an increase of the temperatures to which the thermochronometers are sensitive and a thermal advection of the isotherms, resulting in much younger thermochronometric ages. In Fig. 4.13 an example of such effect is shown (from Reiners & Brandon, 2006), and in Fig. 4.14 and 4.15 the Partial annealing/retention zones and closure temperatures of the most common thermochronometers are shown (Reiners & Brandon, 2006).

Thus, given a certain crustal thermal model, thermochronometric ages can be uniquely related to erosion rate only if it was steady prior as well as after the closure of the system. Shallow isotherms are able to recover more rapidly from transients, therefore the lower the $T_c$ of the thermochronometer, the safer the assumption of steady state. Under the assumption of a certain thermal field and of steady state erosion rate closure temperature and closure depth can be estimated, and the range of possible erosion rates can be defined. Changes in erosion rates with time can be estimate from measurements of multiple cooling ages from the same rock, taking care in considering transient thermal effects. To this purpose vertical age transects are also of common use: the slope of age-elevation relationship constituting an estimate of erosion rate in the time interval of the cooling ages.

Willett & Brandon (2012) summarize all the previous assumptions into a simple Matlab file in which it is possible to insert the following input data to obtain an erosion rate estimate. Primary data are (i) a thermochronometric age with the kinetic information for calculating closure of the system and (ii) an estimate of the present-day geothermal gradient. Secondary information includes the surface topography in the vicinity of a measured age, surface temperature, and duration of erosion prior to the present. Although these latter quantities can often be estimated roughly, any estimate of erosion rate depends directly on the present-day geothermal gradient and the accuracy of the estimate is as sensitive to the geothermal gradient as it is to the measured age.

The largest limitation of the method is the requirement that the erosion rate must be constant from the time of closure to the present day. This is a stricter requirement than that of age-elevation plots that resolve erosion rate directly over the measured age range. Given that erosion rate should be constant until the present day, the expressions derived by Willet & Brandon (2012) are best applied to active tectonic environments where erosion is on-going.

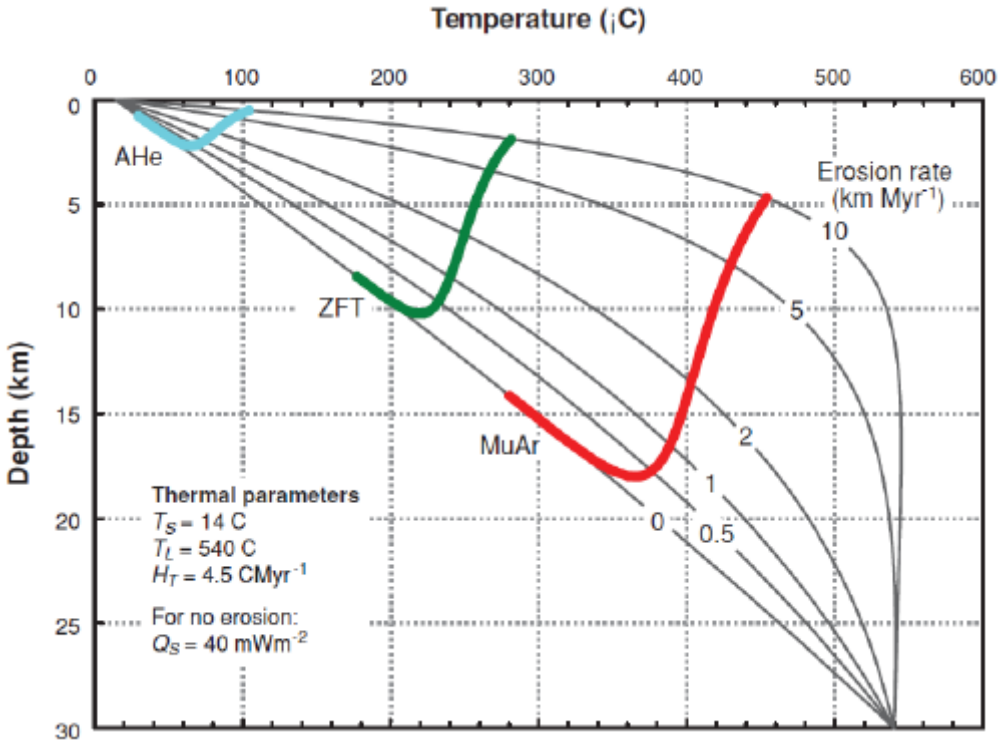


**Fig. 4.13 – Influence of erosion rate on the thermal profile and closure temperatures at steady state (Reiners & Brandon, 2006). The thermal profiles are steady-state solutions for a one-dimensional thermal field with a steady erosion rate. Temperature is held fixed at the top and bottom of a 30-km thick infinite layer. Erosion is represented by a steady velocity through the layer. The specific thermal parameters used for this model are based on the northern Apennines of Italy, which is a fairly typical convergent orogeny: TS= surface temperature; TL=temperature at the base of the layer; HT= internal heat production; Qs= heat flow at surface. The colour lines show the effective closure temperature for apatite He (AHe), zircon fission track (ZFT), and muscovite Ar (MuAr) as a function of increasing erosion rate.**

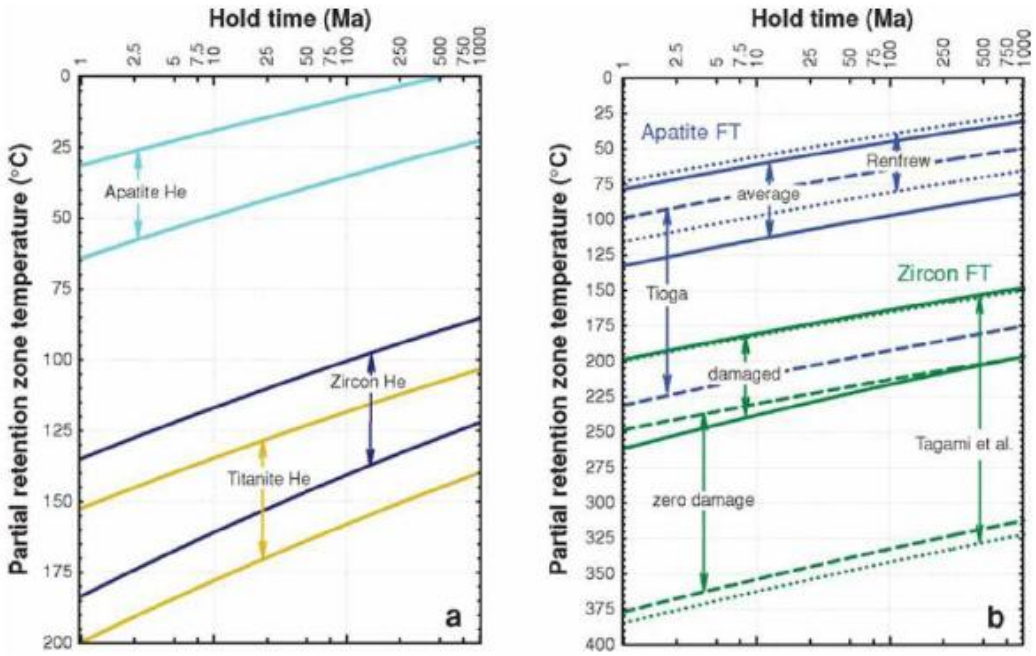


**Fig. 4.14 – Partial Retention Zones for He and FT thermochronometers as a function of hold time (from Reiners & Brandon, 2006). The upper and lower boundaries indicate respectively 90% and 10% retention; estimates were determined using the Closure program with parameters in Tab. 1 and 3 of Reiners & Brandon (2006).**

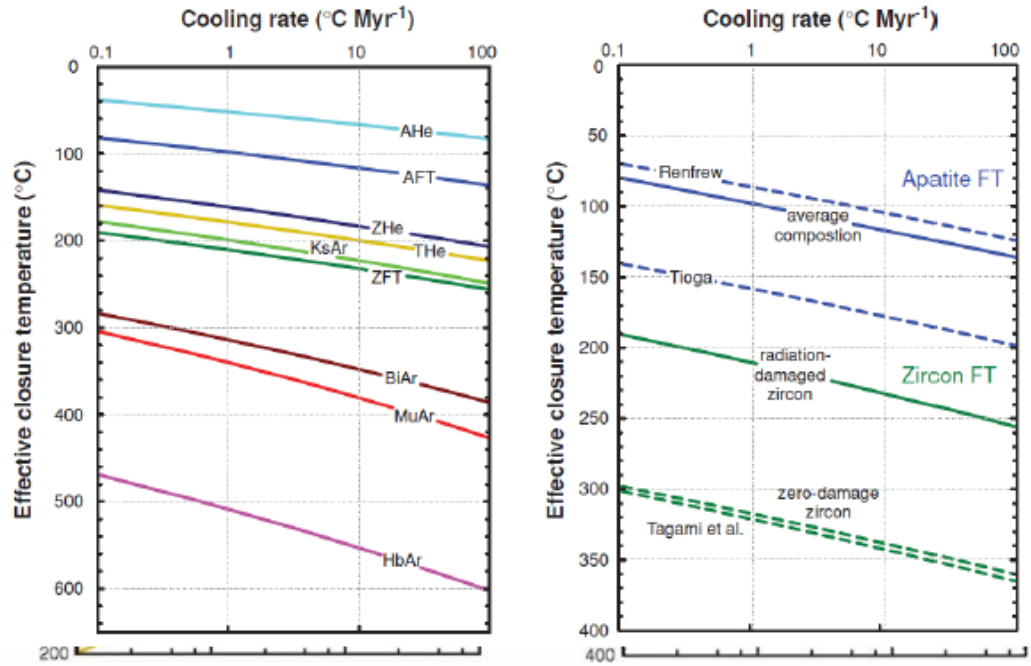


**Fig. 4.15– Effective closure temperature (Tc) as a function of cooling rate for common He, FT, and Ar thermochronometers (from Reiners & Brandon, 2006). Estimates shown here are based on Equation 7 and parameters in Tables 1–2 of Reiners & Brandon (2006). Results were calculated using the Closure program.**

Chapter V

# ANALYTICAL RESULTS

## 5.1 AFT RESULTS

AFT ages in the **Menderes Massif** range between ca. 26 and 18 My (Late Chattian-Burdigalian) (Table 5.1, Fig. 5.1). Most ages (nine out of a total of fourteen) are from the Çine sub-massif massif, i.e. the southern part of the massif. In this region, there is an evident northward younging of the FT ages. Considering the whole AFT dataset obtained from the Menderes Massif during this study, all older AFT ages (> 20 My) were yielded by the samples located along the margins of the massif. Such geographic trend in age distribution is consistent with the results of previous thermochronological studies, as it will discuss at length in the next chapter.

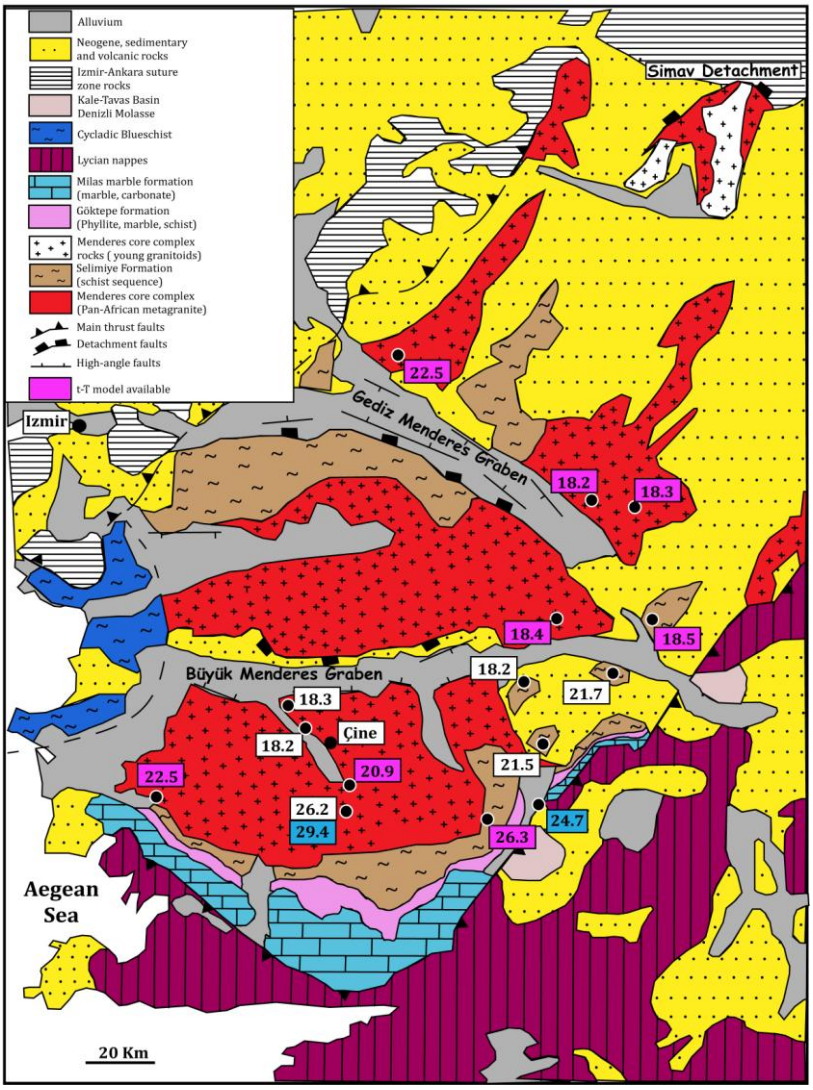


**Fig. 5.1– Geological map with AHe from Menderes Massif. White square indicate AFT ages, blue square indicate AHe ages (base map from Işık et al., 2003, mod.).**

AFT ages from the **Alanya Massif** range between ca. 31 and 26 My (Rupelian-Chattian) (Table 5.1, Fig. 5.2). Despite the relatively small dataset, these are the first low-temperature thermochronological ages ever obtained in the area. The two samples from the structurally highest Alanya nappes (TU328, a Permian semischist, and TU335, a Precambrian schist) yielded Rupelian (Early Oligocene) ages of 31.80 ± 3.7 and 28.88 ± 3.2 My, respectively. The one sample (TU333, a Triassic sandstone) taken from the underlying Antalya Unit has a slightly younger Chattian (Late Oligocene) age of 26.78 ± 2.7 My. These differences are at the limit of resolution of the analytical error; if confirmed by the analyses of the new samples being processed this would delineate a trend of progressively younger ages with increasing depth within the nappe stack of the Alanya region.

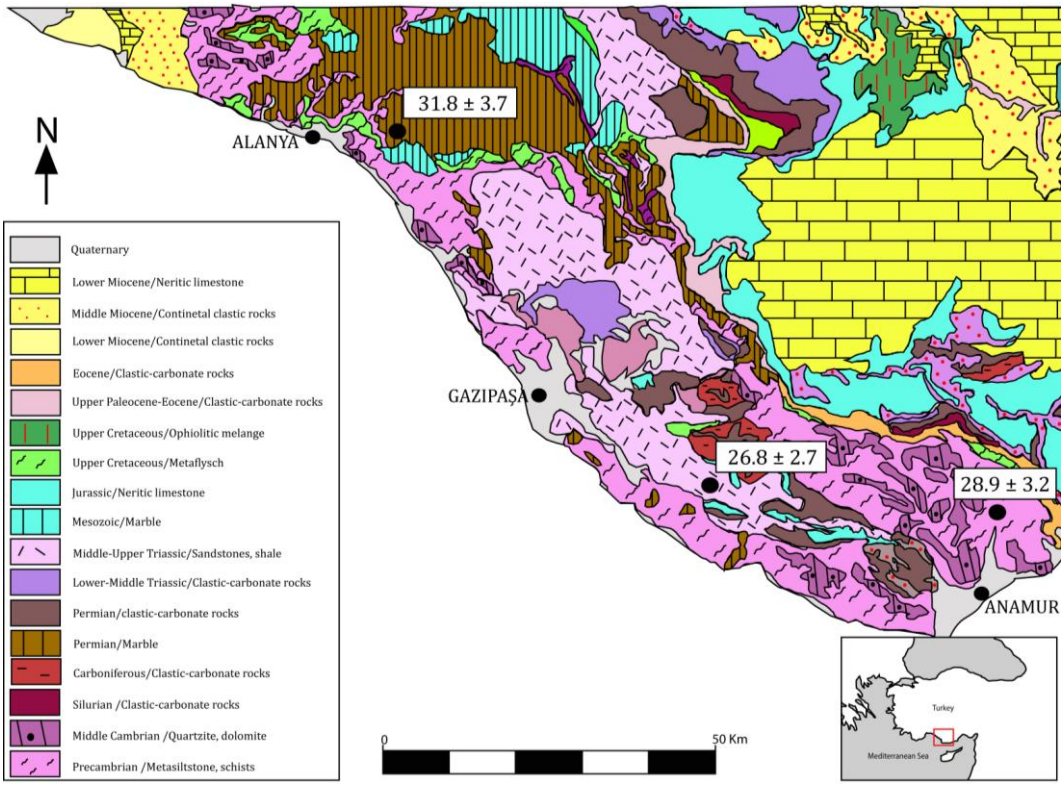


**Fig. 5.2 – Geological map with AFT from Alanya Massif (base map from the Geological Map of Turkey, 1:500000, Mineral Research & Exploration General Directorate, Ankara).**

**Table 5.1 – Apatite fission-track data from western Anatolia**

| Sample number | Lithology | No. of crystals | Spontaneous | | Induced | | $P(\chi)^2$ | Dosimeter | | Age | Mean U conc. | Mean confined track length | No. of tracks measured |
|---|---|---|---|---|---|---|---|---|---|---|---|---|---|
| | | | $\rho_s$ | $N_s$ | $\rho_i$ | $N_i$ | | $\rho_d$ | $N_d$ | (Ma) ± 1s | (ppm) | (μm) ± std. err. | |
| **MENDERES** | | | | | | | | | | | | | |
| TU299 | Meta-granite | 20 | 5.66 | 201 | 4.45 | 1570 | 50.99 | 1.05 | 4440 | 22.45 ± 1.7 | 50 ± 3 | 13.17 ± 1.00 | 10 |
| TU311 | Schist | 30 | 1.79 | 137 | 1.31 | 1104 | 31.71 | 1.26 | 6610 | 26.25 ± 2.4 | 13 ± 1 | 14.27 ± 0.80 | 24 |
| TU314 | Meta-granite | 20 | 4.68 | 173 | 3.38 | 1216 | 38.24 | 1.10 | 8573 | 26.18 ± 2.2 | 39 ± 2 | - | - |
| TU315 | Meta-granite | 20 | 11.4 | 228 | 11.3 | 2612 | 90.16 | 1.24 | 7561 | 20.92 ± 1.4 | 111 ± 5 | 13.72 ± 0.55 | 45 |
| TU317 | Meta-granite | 20 | 1.71 | 86 | 1.98 | 917 | 22.73 | 1.19 | 9246 | 18.67 ± 2.1 | 20 ± 1 | - | - |
| TU318 | Meta-granite | 20 | 4.3 | 168 | 4.58 | 1707 | 56.81 | 1.11 | 8900 | 18.27 ± 1.5 | 48 ± 3 | - | - |
| TU321 | Schist | 20 | 1.6 | 42 | 1.44 | 377 | 97.17 | 1.16 | 9803 | 21.66 ± 3.4 | 15 ± 2 | - | - |
| TU322 | Schist | 16 | 1.36 | 37 | 1.41 | 347 | 78.86 | 1.02 | 4959 | 18.28 ± 3.1 | 14 ± 2 | - | - |
| TU323 | Schist | 14 | 0.73 | 18 | 0.6 | 143 | 98.89 | 1.01 | 4565 | 21.48 ± 5.2 | 6 ± 1 | - | - |
| TU362 | Quartzite | 18 | 0.8 | 34 | 0.5 | 246 | 99.9 | 0.818 | 3893 | 18.50 ± 3.3 | 7 ± 1 | 12.26 ± 1.02 | 8 |
| TU364 | Meta-granite | 20 | 1.9 | 128 | 1.4 | 930 | 58.2 | 0.815 | 3879 | 18.36 ± 1.9 | 21 ± 2 | 12.34 ± 1.89 | 9 |
| TU368 | Gneiss | 20 | 9.5 | 355 | 6.93 | 2549 | 4.5 | 0.804 | 3824 | 18.32 ± 1.5 | 100 ± 5 | 13.32 ± 1.37 | 50 |
| TU369 | Schist | 18 | 0.84 | 41 | 0.78 | 313 | 76 | 0.804 | 3810 | 18.28 ± 3.3 | 10 ± 1 | 13.91 ± 1.34 | 11 |
| TU372 | Gneiss | 20 | 0.93 | 69 | 0.53 | 397 | 94.4 | 0.792 | 3769 | 22.52 ± 3.0 | 8 ± 1 | 13.86 ± 1.40 | 16 |
| **ALANYA** | | | | | | | | | | | | | |
| TU328 | Meta-sandstone | 20 | 2.70 | 91 | 1.56 | 548 | 96.66 | 1.14 | 9803 | 31.80 ± 3.7 | 15 ± 1 | - | - |
| TU333 | Sandstone | 20 | 3.35 | 114 | 2.12 | 729 | 40.13 | 1.02 | 4959 | 26.78 ± 2.7 | 24 ± 2 | - | - |
| TU335 | Schist | 20 | 3.69 | 97 | 2.69 | 716 | 69.46 | 1.27 | 6299 | 28.88 ± 3.2 | 23 ± 2 | - | - |

**AFT data age were calculated using a standard glass dosimeter CN5 and a ζ value of 334.04 ± 16.86 calculated with Durango and Fish Canyon apatite standards. $\rho_s$ – spontaneous track densities (× $10^5$ $cm^{-2}$) measured in internal mineral surfaces; $N_s$ – total number of spontaneous tracks; $\rho_i$ and $\rho_d$ – induced and dosimeter track densities (× $10^6$ $cm^{-2}$) on external mica detectors (g = 0.5); $N_i$ and $N_d$ – total numbers of tracks; $P(\chi^2)$ – probability of obtaining $\chi^2$-value for ν degrees of freedom (where ν = number of crystals – 1).**

## 5.2 THERMAL MODELING

Thermal modelling of fission-track data was performed on eight samples; the only ones where it was possible to identify a significant number of confined tracks. In this dissertation we choose as constraints for the begin of our time-temperature modelling the intrusion ages of the samples (550 My for TU299 TU315, TU364, TU368 and TU372; 416 My for TU311, TU362 and TU369). The intrusion ages were obtained by radiometric dating methods such Pb-Pb or U-Pb dating on zircon grains of the 'core' rocks of the Menderes Massif (e. g. Reischmann et al., 1991; Hetzel & Reischmann, 1996; Gessner et al., 2001c, 2004).

A significant number of confined tracks (>40) was obtained only from samples TU315 and TU368. Considering that acceptable T-t paths must have goodness of fit (G.O.F.) > 0.05, and correspond to cooling histories that are not ruled out by the data (Ketcham, 2005). In spite of the low number of confined tracks, the value of goodness of fit (G.O.F.) in all the sample is good. In just one case, TU315, one of the best in terms of number of track, this value is a bit low (0.34).

In general, the best-fit time-temperature paths given by the inverse model shows onset of rapid cooling at about 28 My. Below a summary of the main features of single T-t paths.

Sample TU299 (Fig. 5.3) was taken along the shore of Lake Bafa from granitoids of the Çine nappe. It has a magmatic age of 550 My and yielded an AFT age of 22.5 ± 1.7 My. Cooling occurred over a wide time span until the Early Miocene, in line with the AFT ages in this area.

TU311 (Fig. 5.4), again coming from Çine nappe, was taken next to the boundary, in the southern Çine submassif, between Çine and Selimiye nappes. AFT age is 26.3 ± 2.4 My. Cooling in this case indicates a rapid exhumation in the Late Oligocene - Early Miocene, again in agreement with the AFT ages for this area.

Sample TU315 (Fig. 5.5) was sampled just south of the town of Çine and belongs to the Çine nappe. AFT age is 20.9 ± 1.4 My and the cooling modeling indicates a rapid exhumation between Late Oligocene and Early Miocene, confirming the ages for this area.

Sample TU362 (Fig. 5.6) belongs to the Bayındır nappe and was sampled near the city of Buldan. AFT age is 18.5 ± 3.3 My. The modelled T-t path shows that such

relatively young central AFT age results from slow cooling over a wide time span from Early Oligocene to Early Pliocene.

Sample TU364 (Fig. 5.7) was sampled in the Bozdağ nappe, very close to the city of Buldan. AFT central age is 18.3 ± 1.9 My, coherent with the other available AFT ages from this area. The model indicates slow cooling and a prolonged residence of the sample in the apatite partial annealing zone, from the Late Eocene to the Middle Miocene.

Samples TU368 and TU369 yielded AFT central ages of 18.3 ± 1.5 My and 12.2 ± 3.3 My. They belong to the Bozdağ nappe and were sampled along the Alaşehir graben. These samples have virtually identical cooling histories (Figs. 5.8 and 5.9) and cooled below 120 and 60°C (i.e. the approximate lower and upper limits of the apatite partial annealing zone) at ca. 11 and 14 My, respectively.

Sample TU372 (Fig. 5.10) was collected north of Salihli city and belongs to the Bozdağ nappe. We obtained an AFT age of 22.5 ± 3.0 My and the modelling shows a long cooling history from the Early Oligocene to the Early Miocene.

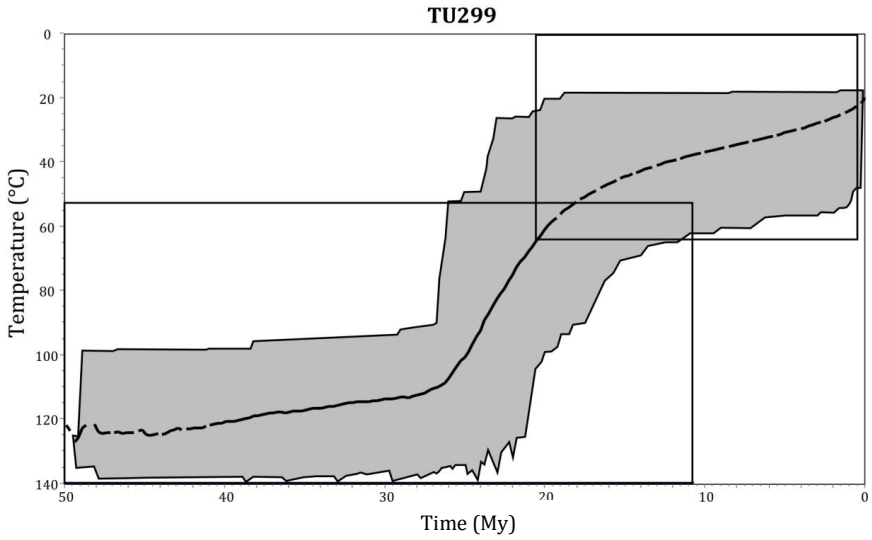


**Fig. 5.3 – Time-temperature paths for sample TU299 (Meta-granite, Neoproterozoic, Çine nappe) (cooling age 22.5 ± 1.7 My). Number of confined tracks: 10; model age 22.5 ± 1.7 My; measured age 22.4 ± 4.1 My; age GOF 0.96; length GOF 0.93. GOF= goodness-of-fit, values give an indication about the fit between observed and predicted data (value close to 1 showing a high degree of agreement).**

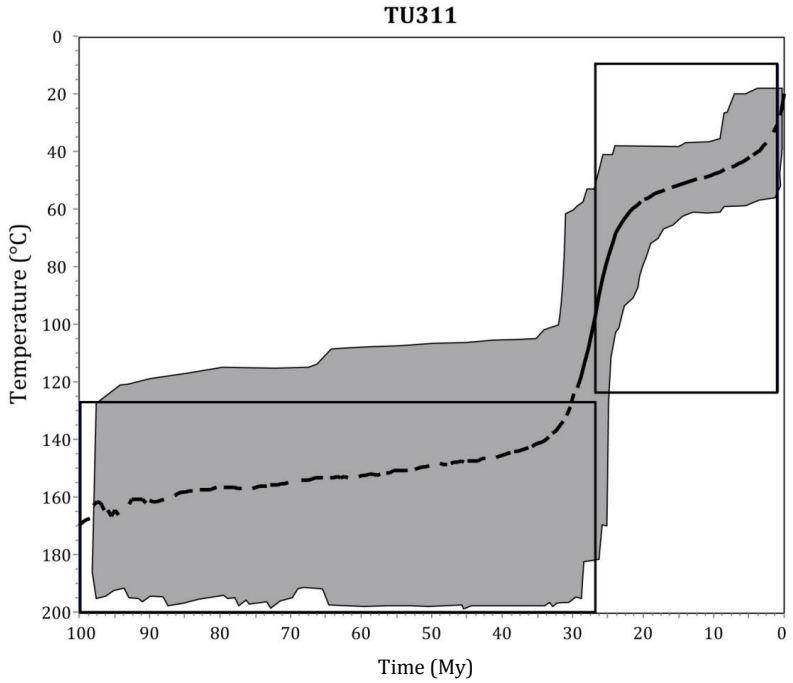


**Fig. 5.4 – Time-temperature paths for sample TU311 (Schist, Precambrian, Çine nappe) (cooling age 26.3 ± 2.4 My). Number of confined tracks: 24; model age 26.3 ± 2.4 My; measured age 26.2 ± 5.5 My; age GOF 0.95; length GOF 0.99. GOF= goodness-of-fit, values give an indication about the fit between observed and predicted data (value close to 1 showing a high degree of agreement).**

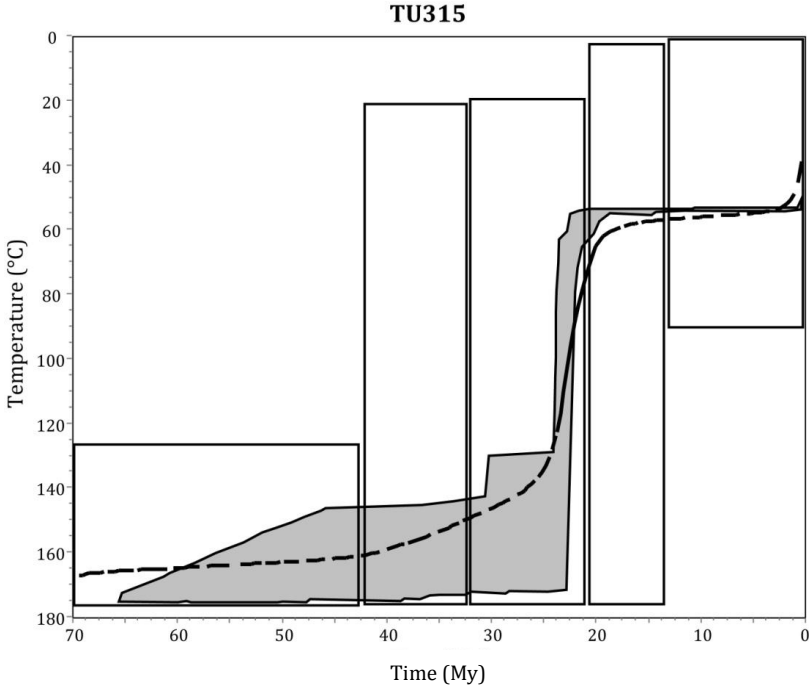


**Fig. 5.5 – Time-temperature paths for sample TU315 (Meta-granite, Neoproterozoic, Çine nappe) (cooling age 20.9 ± 1.4 My). Number of confined tracks: 45; model age 20.9 ± 1.4 My; measured age 20.9 ± 3.5 My; age GOF 0.99; length GOF 0.34. GOF= goodness-of-fit, values give an indication about the fit between observed and predicted data (value close to 1 showing a high degree of agreement).**

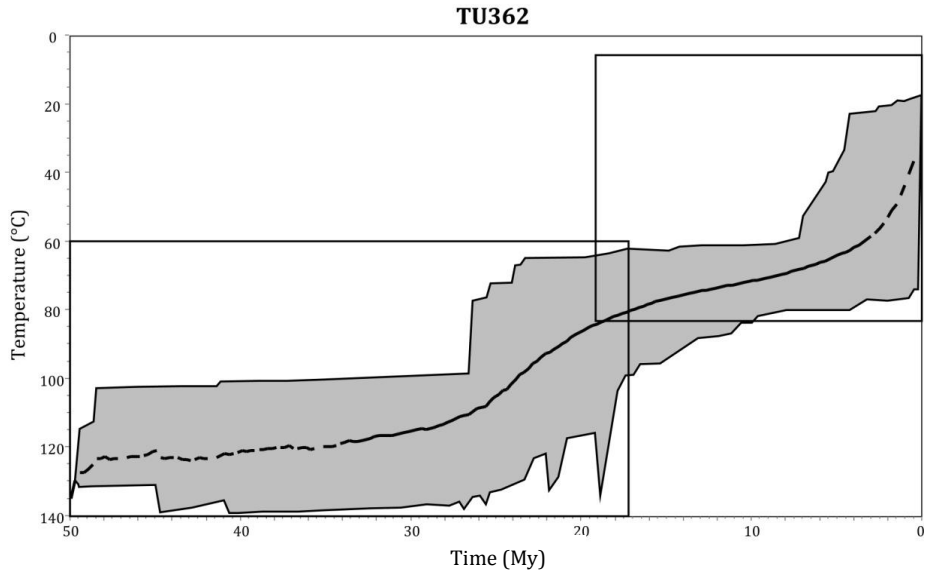


**Fig. 5.6– Time-temperature paths for sample TU362 (Quartzite, Permo-Carboniferous, Bayındır nappe) (cooling age 18.5 ± 3.3 My). Number of confined tracks: 8; model age 18.5 ± 3.3 My; measured age 18.5 ± 7.1 My; age GOF 0.99; length GOF 0.83. GOF= goodness-of-fit, values give an indication about the fit between observed and predicted data (value close to 1 showing an high degree of agreement).**

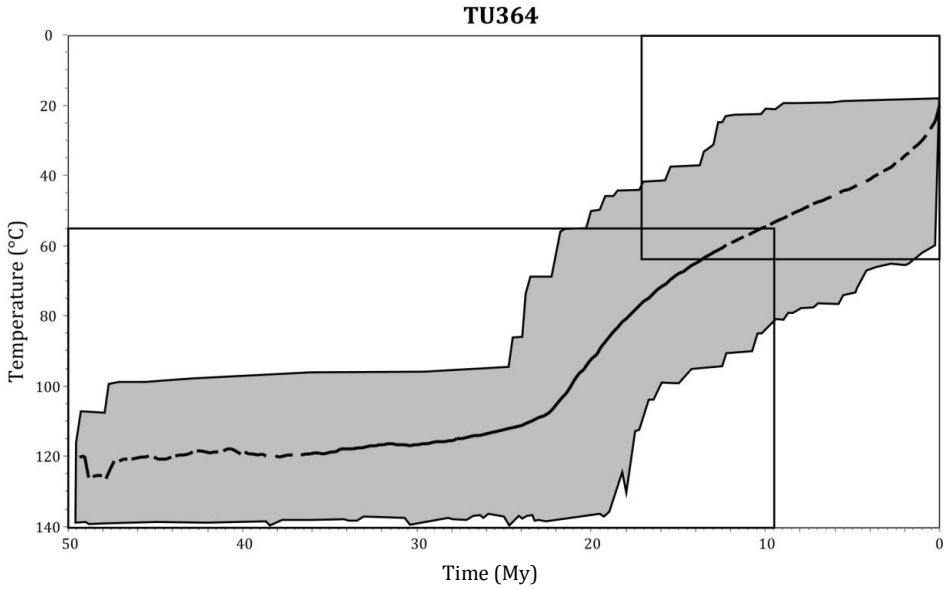


**Fig. 5.7 – Time-temperature paths for sample TU364 (Meta-granite, Precambrian, Bozdağ nappe) (cooling age 18.6 ± 1.9 My). Number confined tracks: 9; model age 18.4 ± 1.9 My; measured age 18.4 ± 3.8 My; age GOF 0.99; length GOF 0.98. GOF= goodness-of-fit, values give an indication about the fit between observed and predicted data (value close to 1 showing an high degree of agreement).**

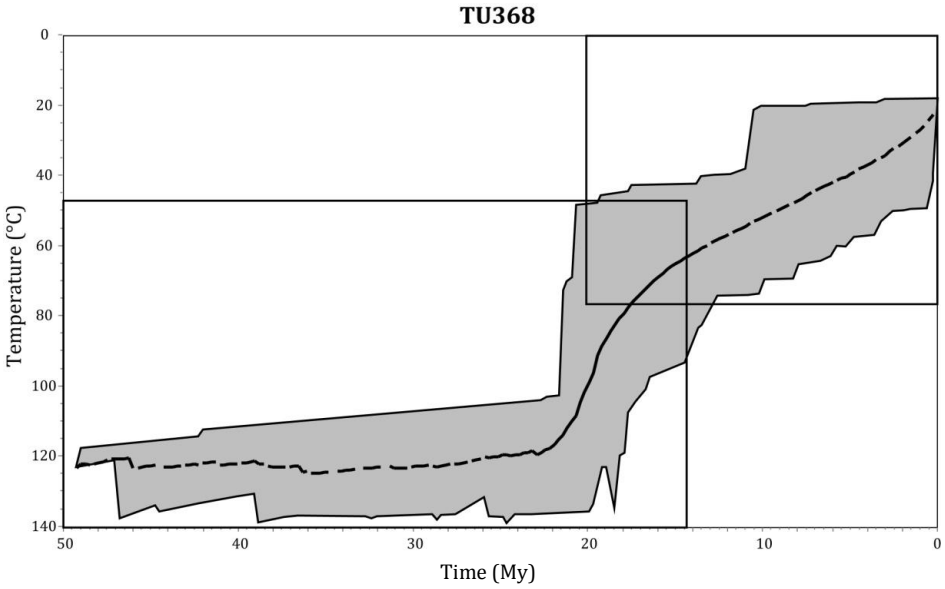


**Fig. 5.8 – Time-temperature paths for sample TU368 (Gneiss, Precambrian, Bozdağ nappe) (cooling age 18.3 ± 1.5 My). Number of confined tracks: 50; model age 18.3 ± 1.5 My; measured age 18.3 ± 3.8 My; age GOF 0.99; length GOF 0.94. GOF= goodness-of-fit, values give an indication about the fit between observed and predicted data (value close to 1 showing an high degree of agreement).**

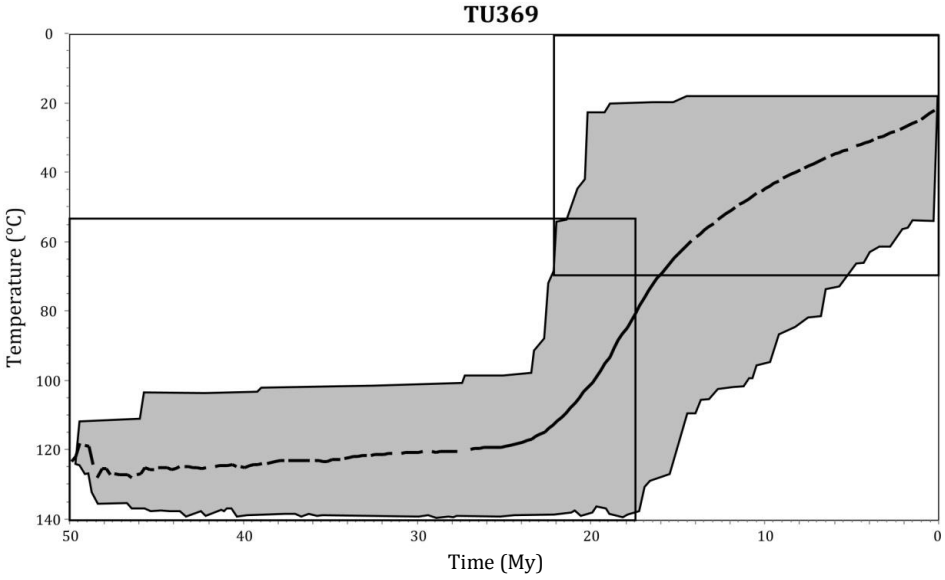


**Fig. 5.9 – Time-temperature paths for sample TU369 (Schist, Precambrian, Bozdağ nappe) (cooling age 18.2 ± 3.3 My). Number of confined tracks: 11; model age 17.6 ± 3.3 My; measured age 17.6 ± 6.0 My; age GOF 1.00; length GOF 1.00. GOF= goodness-of-fit, values give an indication about the fit between observed and predicted data (value close to 1 showing an high degree of agreement).**

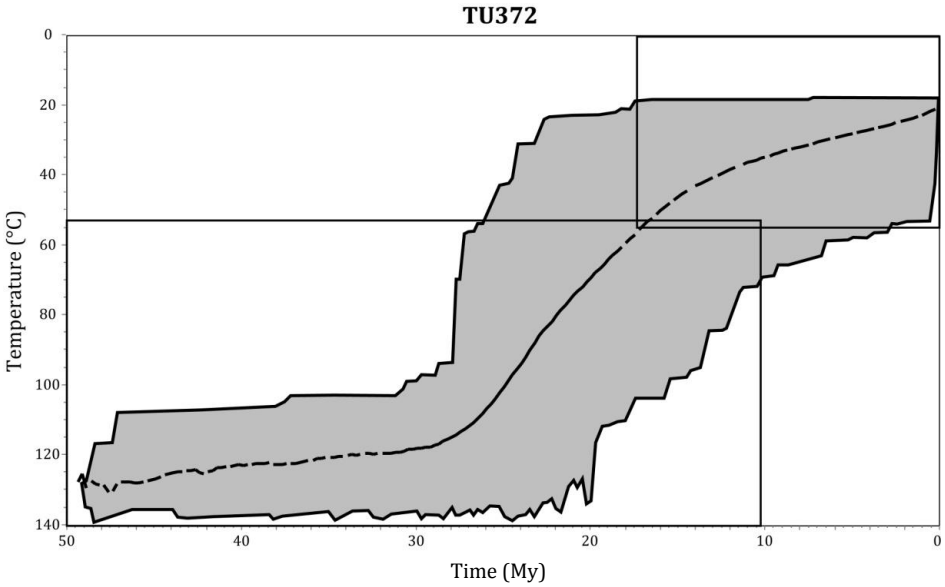


**Fig. 5.10 – Time-temperature paths for sample TU372 (Gneiss, Precambrian, Bozdağ nappe) (cooling age 22.5 ± 3.0 My). Number of confined tracks: 16; model age 22.5 ± 3.0 My; measured age 22.5 ± 6.3 My; age GOF 1.00; length GOF 0.99. GOF= goodness-of-fit, values give an indication about the fit between observed and predicted data (value close to 1 showing an high degree of agreement).**

## 5.3 AHe RESULTS

To have a better constrain on our AFT results, we tried to perform AHe dating for each sample. An intensive research of a reliable number of apatite crystals (3 minimum) was performed in the laboratory at the Institute of Geochemistry and Petrology at the ETH Zürich.

Due to the generally bad quality of the apatites, the standard requirements for AHe analysis (intact, clear, prismatic crystals; e.g. Ehlers & Farley, 2003) could be fulfilled only for the following samples: TU299, TU311, TU313, TU314, TU317, TU319, TU320, TU323 and TU359. Final results in table 3.2 show that only for two samples was possible to obtain a significative measure of He and Th; in figure 5.1 the AHe age for sample TU359 was obtained by the average of single grains ages.

Although bad data quality may influence not only reproducibility but also the age accuracy, the potential effect apparently does not invalidate the analyses, since AFT and AHe reset ages generally match well for sample TU314 whereas for the TU359 we were not able to obtain an AFT age (Fig. 5.1). In particular for the sample TU314 was obtained an age older than its AFT age: although there is a good

abundance of U and Th the causes for this aging can be many and often do not manage to identify.

**Table 5.2 – AHe results from western Anatolia**

| Sample | Replicate | Th/U (atomic) | Raw age (Ma) | Mass (µg) | Mwar (um) | U (ppm) | Th (ppm) | Sm (ppm) | $^4$He (nmol/g) | HAC | eU (ppm) | Corrected age (Ma) | ±σ (Ma) |
|---|---|---|---|---|---|---|---|---|---|---|---|---|---|
| TU314 | TU314a1 | 0.09623 | 23.15 | 5.32 | 67.81 | 21.68 | 2.02 | 0.38 | 0.33 | 0.79 | 22.15 | 29.35 | 0.40 |
| | TU314a2 | / | / | 1.99 | 41.12 | / | / | / | 0.18 | / | / | / | / |
| TU359 | TU359a2 | 12.8359 | 13.77 | 1.54 | 41.07 | 1.73 | 21.47 | 0.19 | 0.02 | 0.65 | 6.77 | 21.17 | 0.54 |
| | TU359a3 | 1.64787 | 20.15 | 2.58 | 47.69 | 2.81 | 4.49 | 0.20 | 0.02 | 0.71 | 3.86 | 28.21 | 0.54 |

**Raw age - grain age before applying the alpha ejection correction factor (FT); Mass and Mwar - mass and average radius of the single crystal; U - 4He concentration of U, Th, Sm and He; HAC – Homogeneous Alpha ejection Correction factor; eU- concentration of effective Uranium (eU=[U] + 0.235×[Th]); Corrected age – grain age corrected by the HAC factor; ±σ – analytical error on corrected age. 19 crystals were excluded from this compilation and not taken in account in the discussion. Criteria for discarding a crystal was too low concentration of U, Th and He.**

## 5.4 EROSIONAL RATE

***Age vs elevation analysis (AER)***

A widely used technique to derive exhumation rates utilizes the correlation of ages of a single isotopic system (e.g. AFT) with the elevation, the so-called age-elevation relationship (AER) or vertical transect approach (Wagner & Reimer, 1972; Schaer et al., 1975; Stüwe et al., 1994). The great advantage of this method is that no estimation of the geothermal gradient has to be made.

Fitzgerald et al. (1995) provide a good review of this method. The vertical transect approach is based on three important assumptions: (*a*) that the closure isotherm was flat at the time of closure; (*b*) at a given time, erosion rates were the same for samples composing the AER (spatially uniform erosion rate); and (*c*) the depth of the closure isotherm has remained constant, so that cooling of rocks can be accurately considered to represent their movement, relative to the surface, through a stationary isotherm.

An AER is expected to have a positive slope when erosion rates and rock uplift rates beneath it are uniform, and the horizontal distance between the samples is small or comparable to: (a) the vertical distance over which the samples were collected (as in high amplitude, low wavelength topography), and (b) the closure depth of the thermochronometer. In such cases, the closure isotherm at depth is sufficiently flat relative to the topography above it, so the slope of the AER is the erosion rate. Changes in the slope of the AER with elevation are typically interpreted to represent changes in erosion rate with time.

Fig. 5.11 shows our AER model. We used all the AFT ages available from the literature for the whole Menderes region. What emerges is that there is no relationship between AFT and elevation.

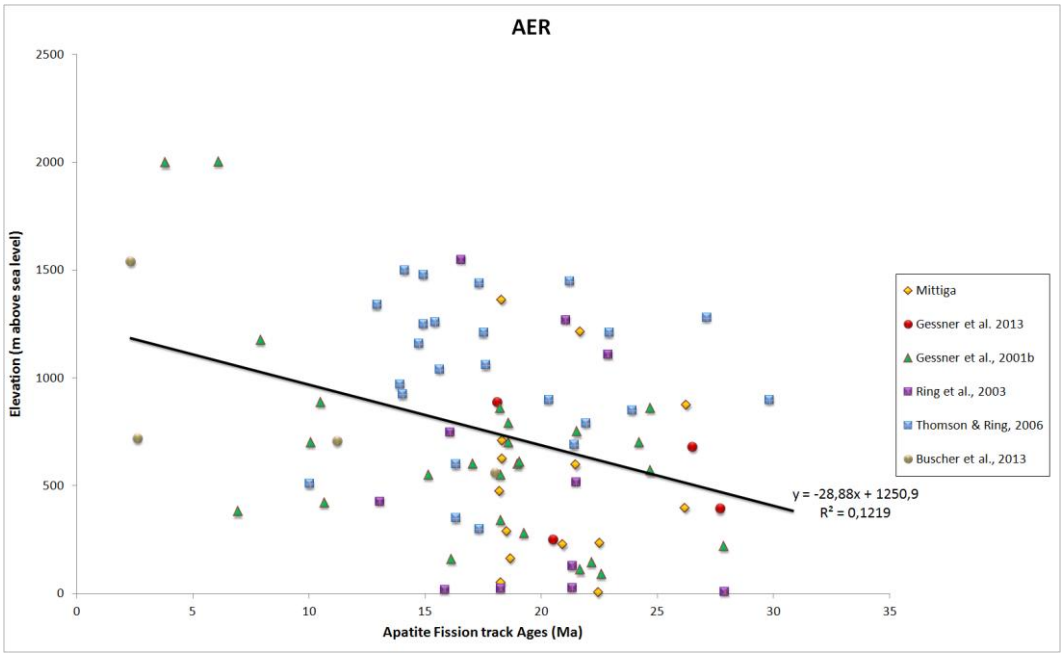


**Fig. 5.11 – Diagram of the relation between AFT ages and elevations; AFT ages source are shown in the legend.**

### *AFT and geothermal gradient*

As seen in Chapter IV erosional rates can be estimated by a modelling based on a simple mathematical relationship. After the calculation of the AFT ages, we estimated the erosion rate using the Willet & Brandon (2012) method starting from the following input data:

- duration of erosion before present = 35 My. This time span was chosen because we are interested in discovering the effects of erosion from the overall onset of extensional tectonism in the study area.
- geothermal gradient = 40C°/km. This datum comes from average surface heat flow of ca. 110 $mWm^{-2}$ in the Menderes Massif (Ilkışık, 1995) and heat flow models for the continental crust (Chapman & Furlong, 1992).
- elevation = depends on the sample;
- observed age = AFT age sample;
- surface temperature at mean elevation = an average temperature of 15°C was chosen for the Muğla region (Turkish State Meteorological Service, http://www.dmi.gov.tr). This choice is supported by the fact

that the no significant latitudinal change of the Menderes region has taken place from 35 My to the present (e.g. Stampfli & Hochard, 2009).

Based on our AFT data and the assumptions outlined above, the resulting erosion rates range between 0.1 and 0.2 km/My for the entire study area (Figs 5.12-5.16). It is very important to consider that these results are an average which assumes a uniform thermal history from AFT age to the surface, while the thermal modelings previously shown indicate a changing in the cooling rates.

These results can be set against the results of similar calculations in the northern Apennines of Italy (average 0.4 km/My; Thomson et al., 2010), the European Alps (between 0.4 and 0.7 km/My; Bernet et al., 2001), and in NE Sicily and the southernmost Italian peninsula (between ~0.7 to ~1.6 km/My; Cyr et al., 2010).

Erosion rates calculated using cosmogenic $^{10}$Be in a restricted area in the Bozdağ region (Central Menderes Metamorphic Core Complex) are somewhat higher (0.18-0.4 km/My; Buscher et al., 2013). However, the timescales for cosmogenically derived erosion rates cover a very recent time interval (von Blanckenburg, 2005), so the rates obtained from these authors are higher but range into a very different timescale. Cosmogenic $^{10}$Be rates determined by Buscher et al. (2013) were influenced by recent erosional processes and thus cannot indicate relationships with tectonic processes which affected the whole region over longer time spans.

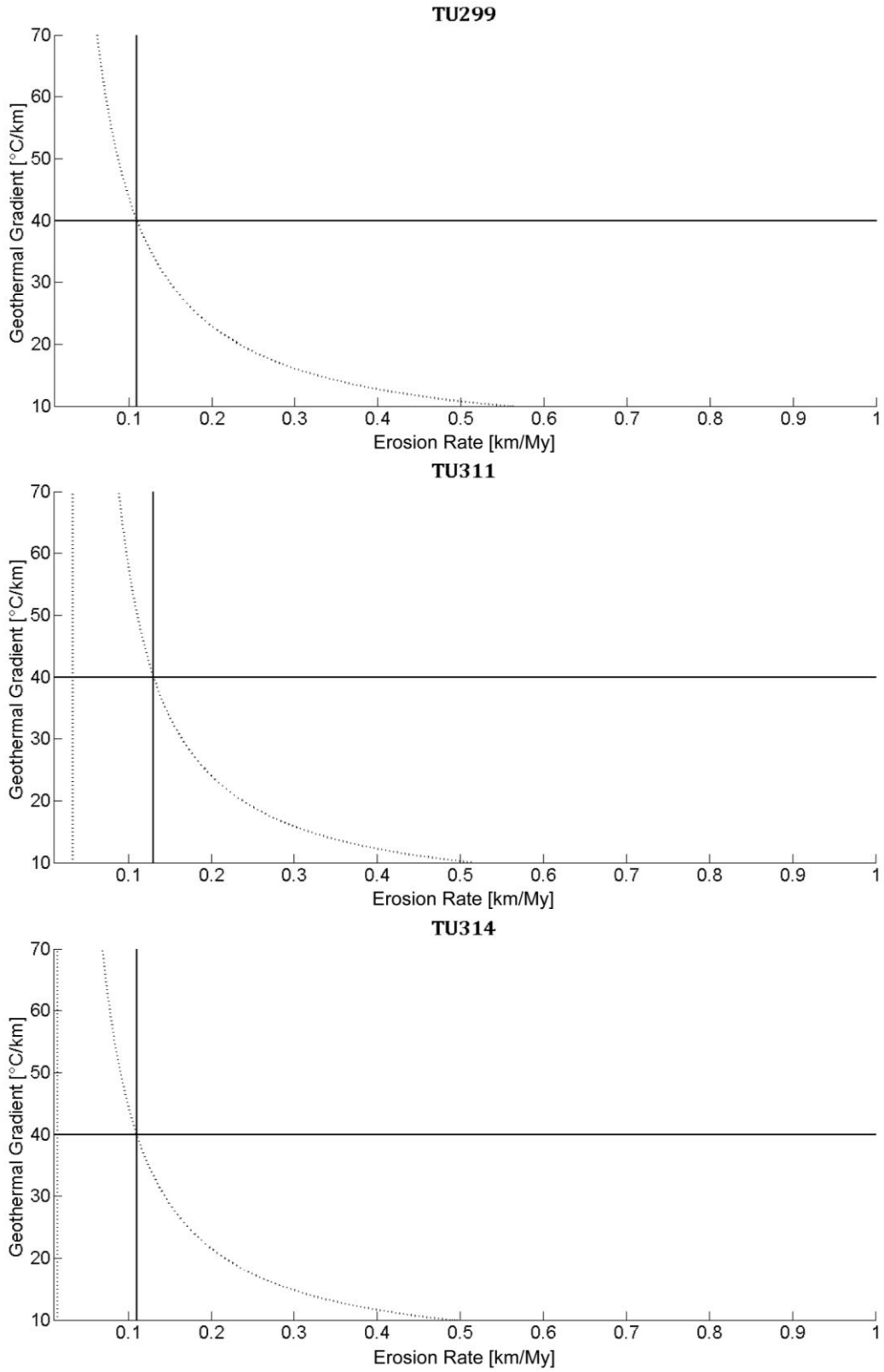


**Fig. 5.12 – Estimated erosional rate for AFT dated samples. Erosion rate is determined from the intersection of the assumed geothermal gradient and the dashed line representing the AFT age.**

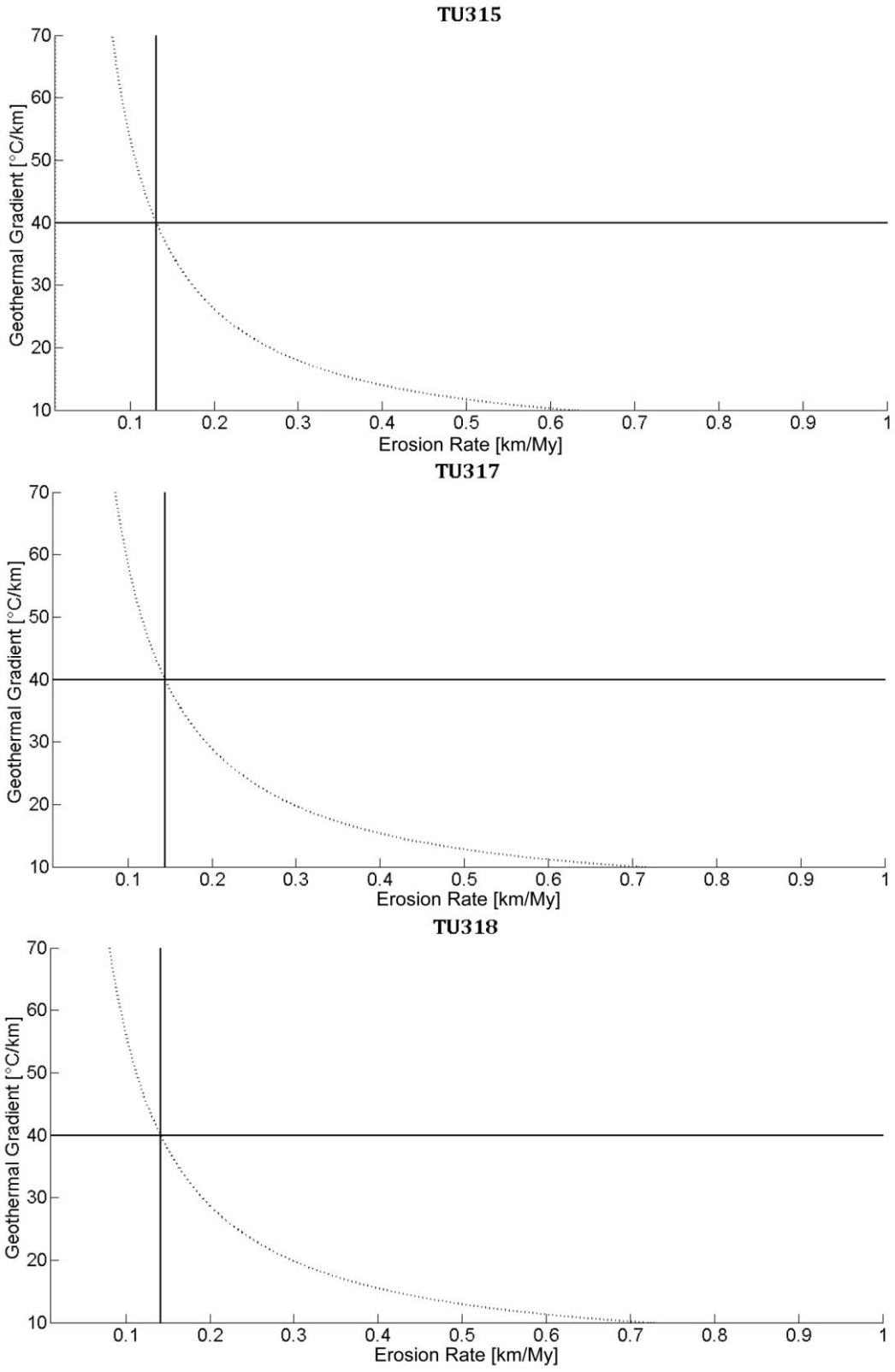


**Fig. 5.13 (continued)**

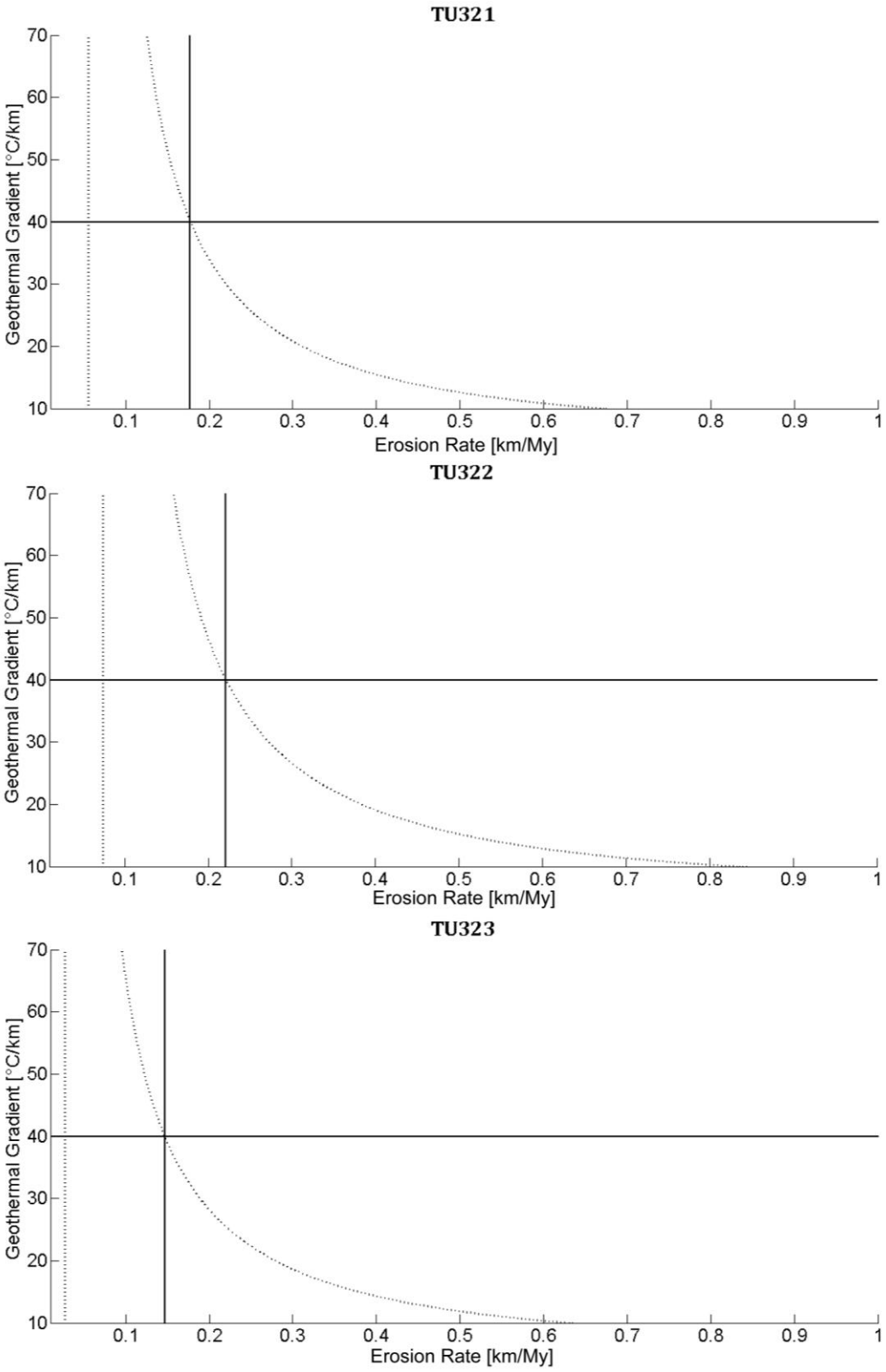


**Fig. 5.14 (continued)**

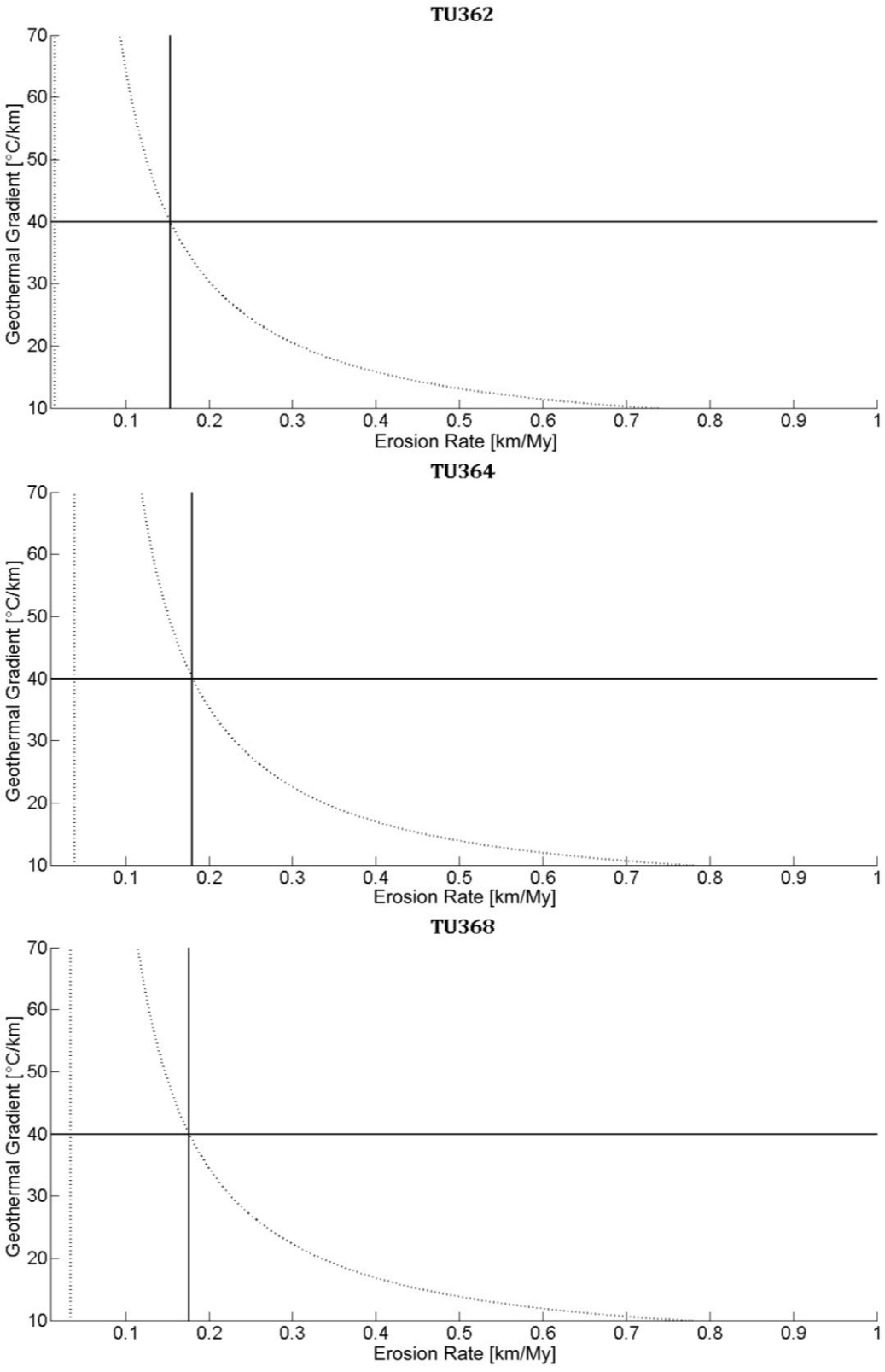


**Fig. 5.15 (continued)**

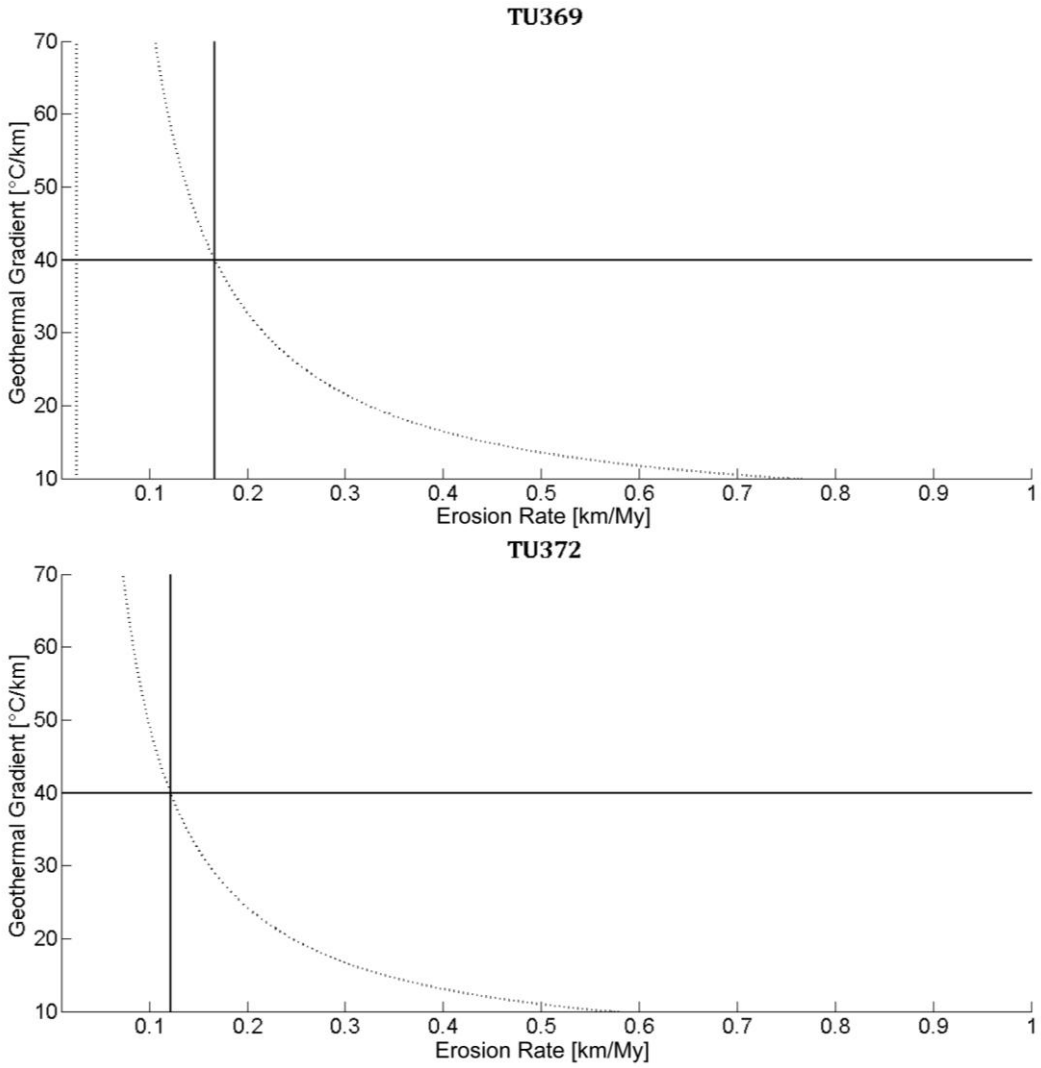


**Fig. 5.16 (continued)**

## 5.4 ZHe RESULTS

Parallel to the work in the Menderes and Alanya massifs, we tried to perform AFT analysis on a suite of samples collected in 2012 on the island of Cyprus. Despite an intensive laboratory work including more than forty mineral separations, apatite grains were absent. It was then decided to perform zircon (U-Th)/He analyses. The picking of the zircon was performed for samples CY5, CY6, CY7 and CY8; packets were sent to the *Radiogenic Helium Dating Laboratory* of the University of Arizona for He dating.

Three zircon crystals were chosen for each sample. Analytical results are shown in Table 5.3. In general, He, U, and Th contents, as well as Th/U ratios, are acceptable except for samples CY5_1, CY6_3 and CY7_2 whose results were discarded. Only one zircon crystal could be obtained from sample CY8; results from such grain had to be discarded because the obtained ZHe age was older than its magmatic age.

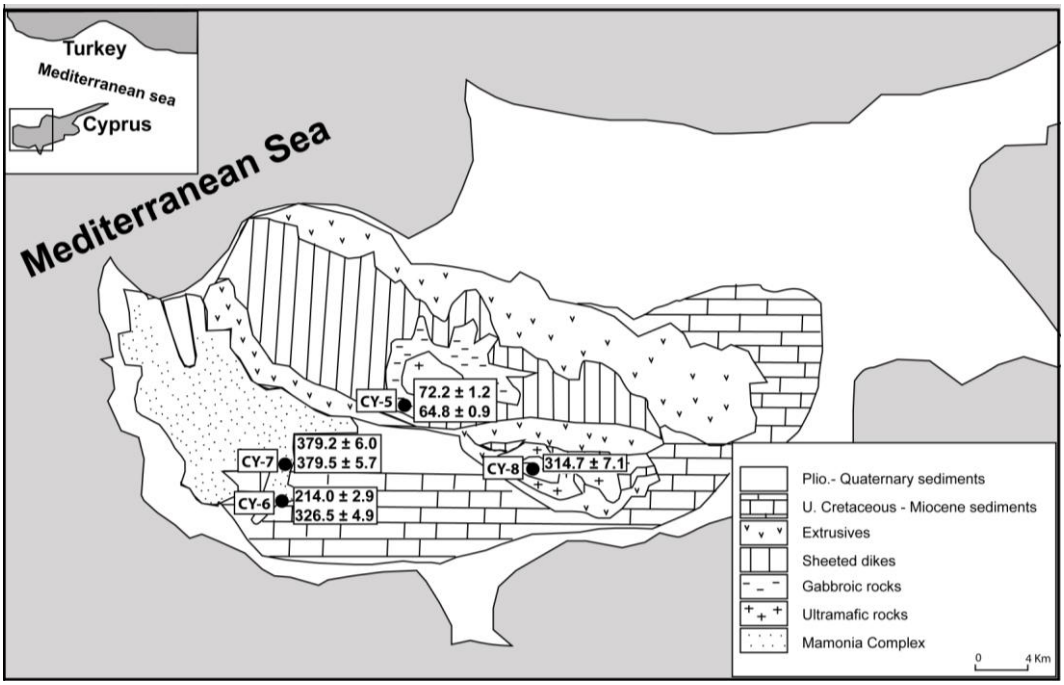


**Fig. 5.17 – Simplified geological sketch of the island of Cyprus, showing the ZHe ages obtained during this study (from Robertson & Xenophontos, 1997 mod.)**

The two ZHe ages calculated for the Troodos complex belongs to a little intrusive body of trondhjemite located at the top of the gabbro section. The magmatic age range between 92-90 My (Mukasa & Luden, 1987) while the ZHe ages calculated here are 72 My and 65 My. The ZHe ages obtained from the Troodos plagiogranites appears to be very different from the AHe ages obtained by Morag et al. (2013) from the Troodos sequence: these ages range between 22 My at the top of the Gabbro sequence to about 6 My at the bottom of the sequence. It will be discuss in the next chapter this difference.

As to the Mamonia Complex, four ages were obtained. : two, from the sample CY6, are 327 - 214 My and so point to a Middle Carboniferous age; two ages from the sample CY7 are 379 My and so point to a Late Devonian age.

**Table 5.3 – ZHe results from Cyprus**

| Sample | Replicate | Th/U (atomic) | Raw age (Ma) | Mwar (um) | U (ppm) | Th (ppm) | $^4$He (nmol/g) | eU (ppm) | Corrected age (Ma) | Mean age ± 1σ (Ma) | ± σ (Ma) |
|---|---|---|---|---|---|---|---|---|---|---|---|
| **CY5** | ~~CY5_1~~ | ~~2.7~~ | ~~47.71~~ | ~~48.68~~ | ~~1.84~~ | ~~4.95~~ | ~~0.78~~ | ~~3.00~~ | ~~64.53~~ | ~~15.61~~ | ~~24.19~~ |
| | CY5_2 | 0.8 | 51.26 | 41.91 | 207.72 | 174.62 | 69.07 | 248.76 | 72.19 | 1.15 | 1.59 |
| | CY5_3 | 0.9 | 42.55 | 34.87 | 181.68 | 175.01 | 51.33 | 222.81 | 64.78 | 0.85 | 1.30 |
| **CY6** | CY6_1 | 0.6 | 170.97 | 61.19 | 160.36 | 100.12 | 172.02 | 183.89 | 214.06 | 2.90 | 1.36 |
| | CY6_2 | 0.3 | 232.47 | 40.96 | 360.35 | 135.22 | 501.56 | 392.12 | 326.53 | 4.87 | 1.49 |
| | ~~CY6_3~~ | ~~4.8~~ | ~~11.15~~ | ~~37.00~~ | ~~1.01~~ | ~~4.74~~ | ~~0.13~~ | ~~2.13~~ | ~~16.91~~ | ~~0.83~~ | ~~4.91~~ |
| **CY7** | CY7_1 | 0.3 | 254.67 | 35.30 | 1207.39 | 416.33 | 1832.73 | 1305.23 | 379.15 | 5.99 | 1.58 |
| | ~~CY7_2~~ | ~~0.5~~ | ~~155.05~~ | ~~61.50~~ | ~~77.29~~ | ~~41.84~~ | ~~73.81~~ | ~~87.12~~ | ~~193.87~~ | ~~2.79~~ | ~~1.44~~ |
| | CY7_3 | 0.3 | 283.07 | 46.68 | 224.57 | 73.48 | 378.45 | 241.84 | 379.54 | 5.69 | 1.50 |
| **CY8** | CY8_1 | 0.2 | 234.64 | 46.73 | 137.87 | 34.63 | 188.57 | 146.01 | 314.72 | 7.11 | 2.26 |

**Raw age - grain age before applying the alpha ejection correction factor (FT); Mwar - average radius of the single crystal; U - 4He concentration of U, Th and He; eU- concentration of effective Uranium (eU= [U] + 0.235× [Th]); Corrected age – grain age corrected; ±σ – analytical error on corrected age. The data marked in red were discarded because of low isotopic content.** Rock types and UTM coordinates of samples are shown in Table 3.2.

Chapter VI

# DISCUSSION

## 6.1 GENERAL FEATURES OF METAMORPHIC CORE COMPLEXES

Until to 1970s various 'basement uplifts' associated with low-angle tectonic structures were generically described, particularly in the North America Cordillera, but their association with large detachment faults was not recognized (Anderson, 1942; Coney, 1974; Wright et al., 1974; Proffett, 1977). Based on the existing rheological models, the occurrence of large low-angle normal faults was deemed unrealistic. During the 1980's careful field mapping in the Basin and Range province of the southwestern United States (e.g. Wernicke, 1981; Wernicke & Axen, 1988) substantiated the existence of large-scale low-angle normal faults driving the exhumation of deep crustal levels.

A metamorphic core complex is *a domal or arched geologic structure composed of ductilely deformed rocks and associated intrusions underlying a ductile-to-brittle high-strain zone that experienced tens of kilometres of normal-sense displacement in response to lithospheric extension* (Whitney et al., 2013). The lithospheric extension that results in core-complex formation is commonly driven by plate divergence, such as mid-ocean ridges and along rifted continental margins. But extension can also occur in plate convergence settings by slab rollback (e.g., the backarc of an oceanic subduction zone) or by orogenic collapse under fixed boundary conditions or even during slow plate convergence (Rey et al., 2001). The resulting structure is a core complex, which so occurs in both continental and oceanic lithosphere.

In continental core complexes, the normal-sense high-strain zone corresponds to a profound metamorphic and/or stratigraphic discontinuity typically called a 'detachment fault', which is so named because rocks above and below the fault zone record different pressure-temperature-time-deformation histories (Whitney et al., 2013).

Many models for core-complex development have invoked isostatic rebound beneath the detachment fault to explain the arching of the fault and exhumation of the footwall (e.g., in the continents: Spencer, 1984; Wernicke & Axen, 1988; Brun & van den Driessche, 1994). Crustal flow beneath the extending upper crust has also been proposed to explain the domal structure of many continental core complexes, as well as the moderate topographic relief of the exhumed footwall despite tens of kilometres of offset and the existence of a flat Moho in many highly extended regions (e.g. Block & Royden, 1990; Buck, 1991; McKenzie et al., 2000).

Some of the most studied continental core-complex belts are in the North American Cordillera, the Aegean sea/western Turkey (e.g. Cycladic Blueschist and Menderes Massif) and Mongolia-China-Korea. Continental core complexes are typically elliptical, with a long axis averaging ca. 10-40 km. The footwall of core complexes is typically elevated above the surrounding rocks, in some cases by 1-2 km of relief (Whitney et al., 2013).

An important parameter controlling lower-crustal viscosity – and therefore coupling of deep and shallow crust – is the geotherm. This is of particular importance for thermochronometric studies such as the present work. An elevated geotherm appears to be necessary to the development of continental core complexes. Models of the influence of geotherm on core-complex generation can be divided into three categories (Fig. 6.1). In a warm crust, the deep crust is able to flow, but the strong coupling between deep and upper crust results in multiple upper-crust faults. In a hot crust, extension is localized in a single, large-offset detachment fault system that arches as the low-viscosity deep crust develops a core complex in the footwall. In a very hot crust, the combination of localized upper-crust extension and reduction of lower crust viscosity by partial melting results in exhumation of the deep crust; partially molten material is exhumed nearly isothermally and undergoes complex deformation during ascent, with contractional structures overprinted by extension (Whitney at al., 2013).

To better understand how these complexes form and evolve a knowledge of the main features of the hanging wall, the detachment fault(s), and the footwall is required. In most continental core complexes, hanging-wall rocks are present, although these typically have been at least partially removed by tectonic and/or erosional process. For example, in some of the Aegean core complexes, the hanging wall consists of ophiolitic rocks and unmetamorphosed sedimentary rocks, in places filling structural basin (Gautier et al., 1993). We have seen in Chapter II examples of such basins like the Kale-Tavas basin or the Denizli Molasse associated with the Menderes Massif.

In some continental core complexes, the detachment is not a single fault but is made up of multiple, closely spaced and anastomosing faults (Wernicke & Burchfiel, 1982). The uppermost detachment fault may have a particularly well-defined fault plane, typically dipping ≤30°. A region of brecciation and greenschist-facies alteration (recorded by secondary growth of chlorite ± epidote) may characterize

the structurally highest (brittle) regions of detachment zones if suitable lithologies are present (e.g., granitic gneiss) (Whitney et al., 2013).

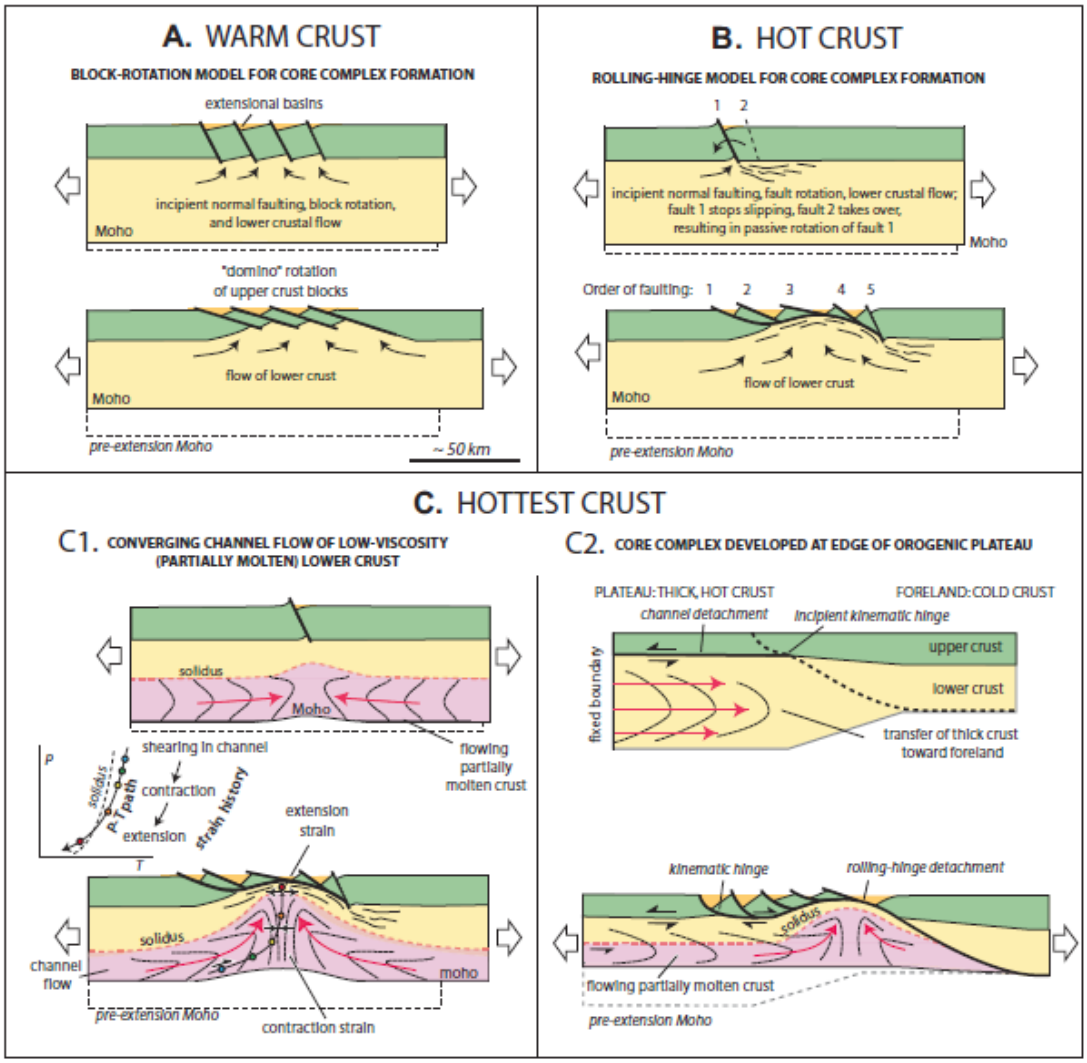


**Fig. 6.1 Modes of development of continental core complexes in warm, hot, and hottest crust. (A) Warm crust exhumes continental core complexes in footwall of normal faults that are distributed in the upper crust; for example, exhumation by domino-style rotation of upper-crust blocks. (B) Hot crust focuses faulting in the upper crust, leading to large-offset fault and exhumation of lower crust by development of rolling-hinge detachment (after Brun & van den Driessche, 1994). (C1) Hottest crust has significant partial melt; the low-viscosity lower crust flows in channels attracted by a focused zone of upper-crust extension; channels collide and move upward to fill the gap created by upper-crust extension; deep crustal rocks record significant decompression and deformation from contraction to extension as they are exhumed (after Rey et al., 2011). (C2) At the edge of an orogenic plateau, partially molten crust flows owing to lateral gradients in gravitational potential energy; note expected reversal of sense of shear (kinematic hinge) between "channel" and "rolling-hinge" detachments (after Teyssier et al., 2005).**

Thermochronometers with different closure temperatures can be used to evaluate the cooling rate of rocks in detachment zones and to determine the timing of displacement on the fault zone, displacement rate, and fault dip (Foster et al., 1990, 1993; John & Foster, 1993; Hetzel et al., 1995b; Foster & John, 1999; Wells et al., 2000; Ring et al., 2011). Typically, a suite of samples is collected along the slip direction of a detachment fault zone, and one or more thermochronometers (e.g. apatite ± zircon fission-track; and/or apatite ± zircon U-Th/He) are used to capture temperature-time information as a function of exhumation history on the detachment. Some detachment zones record a slow cooling stage (5–15 °C/m.y.) followed by more rapid cooling (70–100 °C/m.y.) (Scott et al., 1998; Wells et al., 2000). This trend has been interpreted to indicate a steepening of the fault through time or other changes in detachment zone geometry.

The footwall of most core complexes has a domal structure. Footwall rocks may record a wide range of ages—from pre- to syn-extension—of metamorphic, magmatic, and deformation events. Metamorphic grade may also vary within the footwall, not only as a function of structural level exposed, but also owing to the complex pressure-temperature (*P-T*) paths that rocks follow before and during extension (Whitney et al., 2013). Some core complexes contain one or more gneiss domes, typically beneath a carapace of high- to medium-grade metamorphic rocks (Brun & van den Driessche, 1994; Vanderhaeghe & Teyssier, 2001; Whitney et al., 2004). These have been called migmatite-cored metamorphic core complexes (Rey et al., 2009a, b), and their origin relates to regional extension and flow of deep crust beneath detachment faults. Studies have shown that the crystallization of the magmatic portions of migmatite domes in core complexes was followed by rapid cooling to T < 300 °C; cooling ages coincide with ages of synkinematic minerals (e.g., mica) in detachment fault zones (Malavieille et al., 1990; Maluski et al., 1991; Kruckenberg et al., 2008).

## 6.2 MENDERES MASSIF EVOLUTION

The AFT ages obtained from the samples collected in the Menderes Massif (Tab. 5.1) are concentrated between 26 and 18 My (Late Oligocene-Early Miocene). These ages are mostly from the Çine and Bozdağ nappe, while our attempt to date the

structurally lowest Bayındır nappe was less successful. According to the definition of the metamorphic core complexes, this means that most of our ages are concentrated in the domal migmatitic core.

Therefore in order to verify the robustness of our ages we created a summary map of all of the AFT ages from the Menderes region available in the literature (Buscher et al., 2013; Gessner et al., 2001a, 2013; Ring et al., 2003; Thomson & Ring, 2006). What emerges is that our ages fit well into the general framework (Fig. 6.2).

AFT ages are markedly different between the central part of the massif and the borders. Ages north of the Gediz detachment and south of the Büyük detachment range between the Late Oligocene and the Middle Miocene whereas in the region between these two detachments (Central Metamorphic Menderes Core Complex) the ages range between the Middle Miocene and the Early Pliocene (Fig. 6.3).

According to Gessner et al. (2001a, 2013) and Ring et al. (2003), this difference in the ages distribution can be interpreted as the evidence that the massif underwent two different stages of exhumation: a first phase, corresponding to the ages distribution in the northern and southern sub-massif, ranging between Late Oligocene and Middle Miocene; and a second phase, corresponding to the ages distribution in the central sub-massif, focused only in the central metamorphic core complex in the Late Miocene – Early Pliocene.

The hypothesis of a double stage evolution for the massif is well constrained by the recent data obtained from the Gediz detachment and the Simav detachment. The footwall of the Gediz and Simav detachment faults contain synextensional granitoid intrusions that were brought to the surface from mid-crustal levels.

Buscher et al. (2013), by AHe, ZHe and AFT analysis of these syntectonic granodiorites associated to the Gediz detachment, constrained the tectonic activity of these faults in a period between 15-16 My to Pliocene.

According to Işık et al. (2003), the well exposed Salihli granodiorite in the footwall of the Gediz shear zone exhibits an upward gradual change from undeformed isotropic granodiorite to granodioritic protomylonite, mylonite and ultramylonite.

$^{40}Ar/^{39}Ar$ (biotite and amphibole) ages of these granodiorite (Hetzel et al., 1995b) and of syntectonic mineral along the Gediz detachment fault (Lips et al., 2001) suggest that the granodiorite was emplaced in the Miocene (ca. 20 My) and was brittlely deformed along the detachment surface at around 12 My.

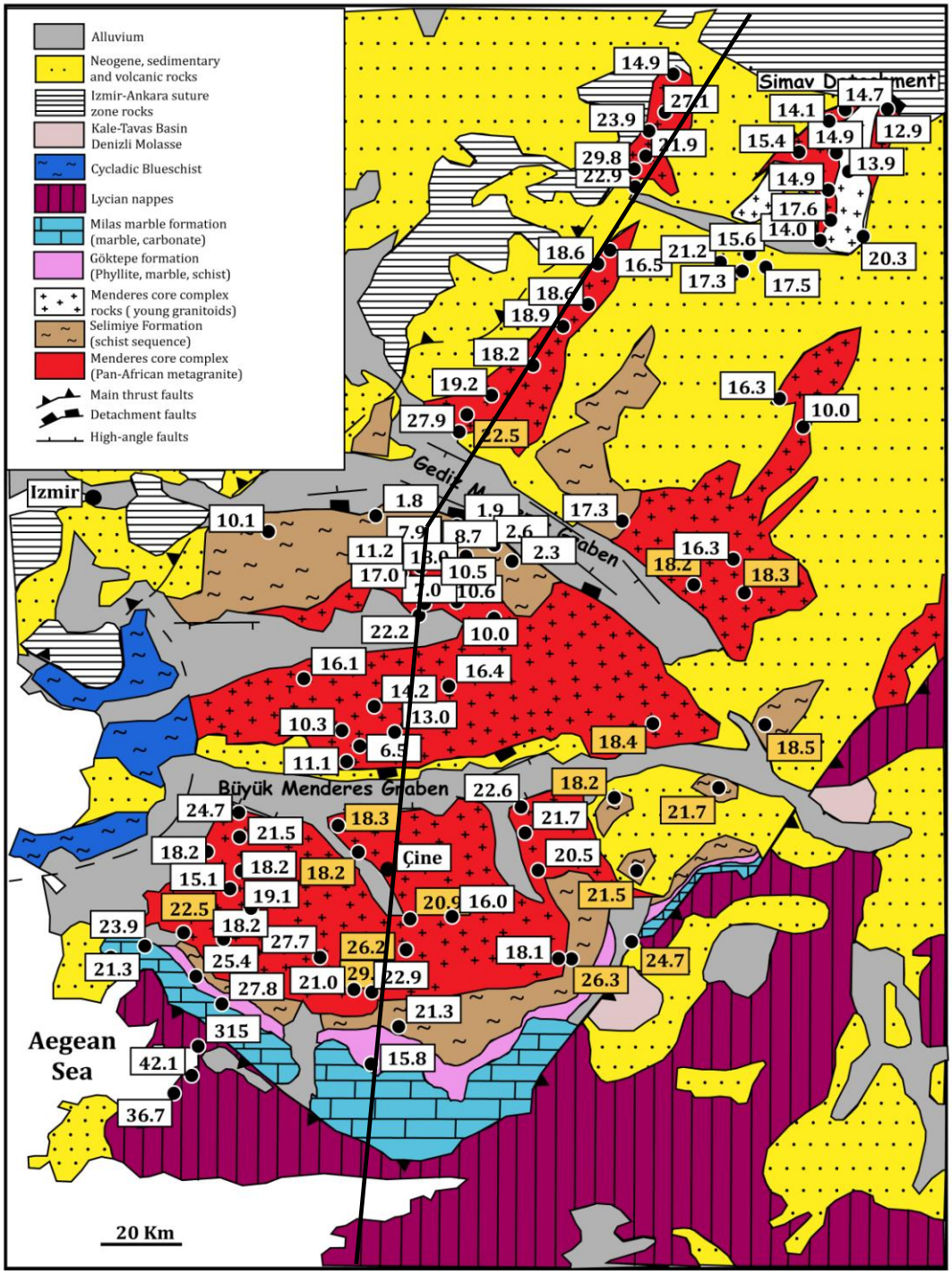


**Fig. 6.2 – Compilation of all AFT ages for the Menderes Massif (data from Buscher et al., 2013; Gessner et al., 2001a, 2013; Ring et al., 2003; Thomson & Ring, 2006). In orange the ages obtained during this dissertation (base map from Işık et al., 2003, mod.). Black line is the trace of the cross-section shown in Fig. 6.3.**

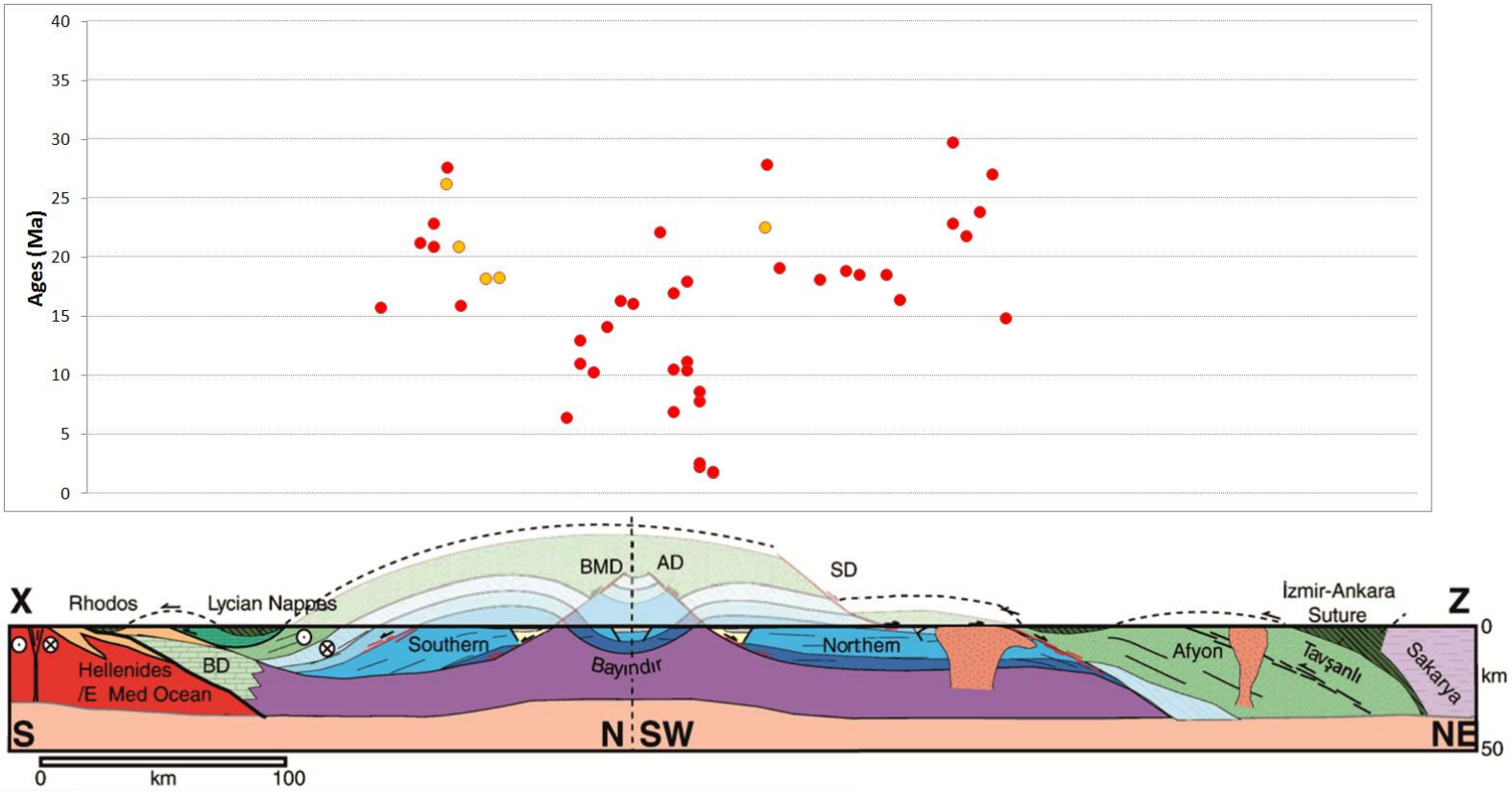


**Fig. 6.3 – Geological section of the Menderes Massif with AFT ages available within a distance of 20 km from the trace of the section of Figure 6.1. Red spots are ages from previous works, orange spots are ages from this dissertation (section from van Hinsbergen, 2010).**

The footwall of the Simav shear zone in the Eğrigöz sub-massif is intruded by two synextensional granitoids. Işık et al. (2003) recognized that kinematic indicators within the ductilely deformed high-grade metamorphic and granitoid rocks are similar to the ones along the Gediz shear zone and indicate a top to the NNE sense of shear, consistent with the Cenozoic regional extensional tectonics in western Turkey. The ductilely deformed part of the Eğrigöz granitoid is dated at 20–24 My (K–Ar on biotite; Bingöl et al., 1982) and at 20.19 ± 0.28 My ($^{40}Ar/^{39}Ar$ on biotite; Tekeli et al., 2001), suggesting that extension in western Turkey initiated in the Late Oligocene - Early Miocene. Işık et al. (2003) suggest that these two shear zones were produced by similar extensional processes, and that the available radiometric age determinations along the two shear zones and thermochronological data indicate that the Gediz detachment fault is younger than the Simav detachment fault.

Our thermal modelings in the samples along the Gediz detachment (TU362, TU364, TU368 and TU369, see Chapter V, Fig. 6.4) seem to be not related to the fault activity in the Late Miocene-Early Pliocene. Sample TU362 (Fig. 5.6) shows a cooling history which evidentiate the passage out the PAZ in the Early Pliocene; this could agree with the chronology of the tectonic activity along the Alaşehir/Gediz detachment, but this long permanence in the PAZ is also the effect of the very few measured confined tracks (see Tab. 5.1). Sample TU364 (Fig. 5.7) has a model which indicates slow cooling and a prolonged residence of the sample in the apatite PAZ: the suddenly increasing of the rate of passage through the PAZ corresponds to the Early Miocene and so hardly can indicate an effect of the tectonic activity of the Gediz detachment. Samples TU368 and TU369 shows the same cooling history as for TU364 (see Figs. 5.8 and 5.9) and so this can further indicate no relationship with the Gediz detachment. Although for the samples TU364 and TU369 it is to be taking in account the very few measured confined tracks which mean a huge error and so not very reliably (see Tab. 5.1), sample TU368 is highly reliably thanks to the elevate number of confined tracks (see Tab. 5.1).

Therefore the results of the thermal modeling of the samples studied during this dissertation (see Chapter V and Fig. 6.4) show a broad cooling/exhumation stage between the Late Oligocene and the Middle Miocene.

Furthermore the outer submassifs are characterized by a similar trend in the rate of cooling: slow cooling between the Late Eocene and the Oligocene and an acceleration of cooling between the Late Oligocene and the Middle Miocene.

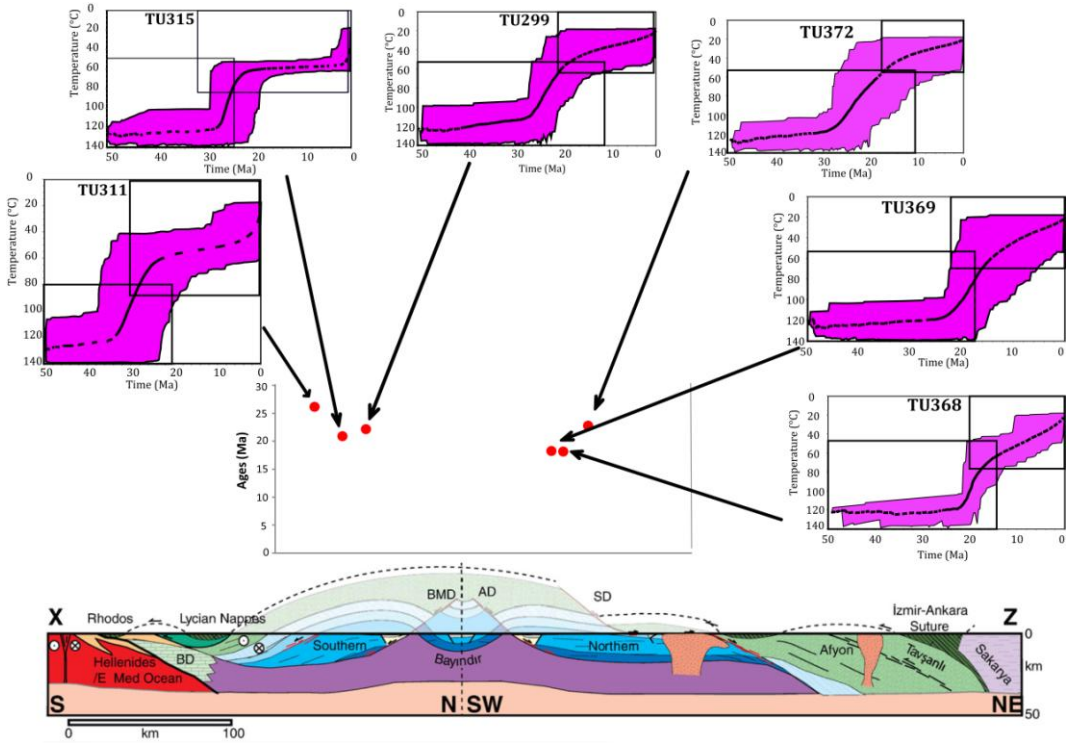


**Fig. 6.4 – Geological section of the Menderes Massif with the thermal models obtained in this dissertation and their geographic positions (section from van Hinsbergen, 2010).**

The thermochronological reconstruction shown in this dissertation can be also compared with those from Gessner et al. (2001a) and Ring et al. (2003). Gessner et al. (2001a) obtained from AFT analysis a two-stage cooling history: (1) an early phase of cooling commenced during the Late Oligocene and ended in the Early to Middle Miocene affecting the Gördes and Çine submassifs. During this period, temperatures within much of the Central Menderes Metamorphic Core Complex remained above ca. 110° C. (2) The second phase of cooling were obtained from the two detachments edging the Central Menderes Metamorphic Core Complex and indicated an age of Late Miocene – Pliocene with an accelerated cooling since ca. 5 My.

In both the Gördes and Çine Massifs, flat-lying Miocene sediments overlie the sub-horizontally foliated basement (Gessner et al., 2001a). Eocene foliation, bedding of the Miocene sediments and remnants of a Late Miocene erosion surface are parallel to each other and also parallel the fission-track cooling age pattern (Fig. 6.5). Across the Central Menderes Metamorphic Core Complex, however, Eocene

foliation and the boundaries of the tectonic units define an east-trending syncline with a wavelength of ca. 45 km and an amplitude of ca.10 km (Fig. 6.5). Across this syncline, fission-track cooling ages become younger in the hanging-wall displacement direction. Miocene sediments occur only in fault-bounded blocks in the hanging wall of the Gediz and Büyük detachments. As the earlier contractional history of the Central Menderes Metamorphic Core Complex is similar to that of the Gördes and Çine Massifs, syncline formation postdates earlier crustal shortening.

Ring et al. (2003) also recorded in the northern and the southern Menderes Massif the onset of cooling from 130° to around 60° C from Late Oligocene to Early Miocene. They also recorded from Late Miocene a second phase of cooling that affected much the Central Menderes Metamorphic Core Complex.

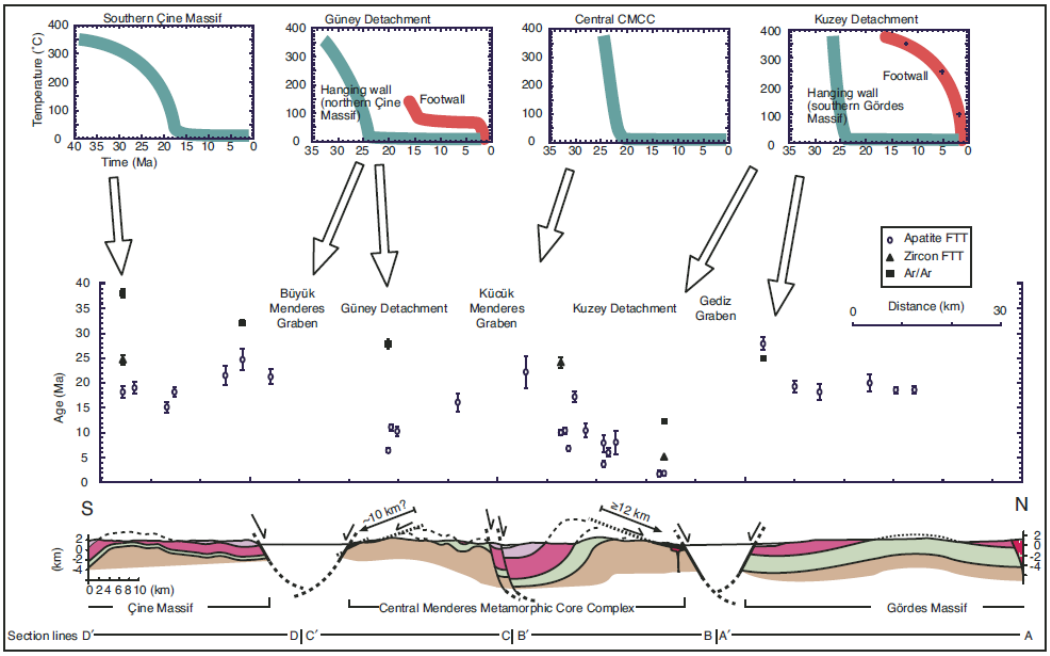


**Fig. 6.5 – Cross sections along the Menderes Massif and cooling ages within the Central Menderes Metamorphic Core Complex (CMCC). FTT—fission-track thermochronology. Notice that the cooling rate in the footwall of the Kuzey Detachment shows a pronounced increase at ca. 5 My. Dashed lines indicate inferred maximum depth of basement in grabens (Cohen et al., 1995). Modified from Gessner et al. (2001a).**

Ring et al. (2003) moreover proposed the results of the thermal history modeling of their AFT data as a series of contoured time-temperature slices, advancing in nine steps from Early Miocene times to the present (Fig. 6.6). They decided to take as starting point 30 My, assuming that earlier temperatures for all samples were hotter than ca. 130 °C. Below follows the description for each step:

- *28 My:* The first recorded cooling in the belt to temperatures within the apatite partial-annealing zone (PAZ) (see Chapter IV) occurred on the southern margin of the Gördes submassif.
- *25 My:* Cooling into the uppermost apatite PAZ occurred in the northern Çine submassif. At the same time cooling to temperatures in the lower apatite PAZ occurred in the southern Gördes submassif.
- *20 My:* In the Gördes submassif, cooling started to progress northward. Cooling in the Çine submassif continued and, in general, it seems that cooling progressed in a southerly direction.
- *18 My*: By this time much of the southern Gördes and the northern Çine submassifs are predicted to have been at temperatures in the lower apatite PAZ or below. With the exception of the basement block in the Küçük Menderes graben, the Central Menderes metamorphic core complex remains at temperatures >130 °C. The contoured temperature distribution in the northern Çine submassif is a little misleading because sample points are not evenly distributed but lie on two NNE–SSW transects. Therefore, the relatively warm area in the central part of the northern Çine submassif is an artifact of the contouring procedure.
- *14 My:* Cooling below temperatures of the apatite PAZ in northern part of the Gördes submassif and the southern part of the Çine submassif was completed. Temperatures throughout the Gördes and Çine submassifs were at surface values at this time, except a small warm spot in the southwestern Çine submassif. During the 18-14 Ma period, cooling took place in the southeastern part of the Central Menderes Metamorphic Core Complex. The contoured temperature distribution in the footwall of the Büyük is probably slightly misleading since the relatively cool samples in the Küçük Menderes graben in the centre of the Central Menderes Metamorphic Core Complex and those from the southeastern part of the Central Menderes Metamorphic Core Complex control the map pattern.
- *10 My*: Cooling to temperatures below the apatite PAZ at the margins of the Küçük Menderes graben occurred. Temperatures in the southern segment of the Central Menderes Metamorphic Core Complex remained at values of ca .80–90 °C. In the central part of the Central Menderes Metamorphic Core Complex cooling into the apatite partial-annealing zone has occurred.
- *5 My*: The northern flank of the Central Menderes Metamorphic Core Complex below the Gediz detachment remained at temperatures above 130 °C. The southern flank of the Central Menderes Metamorphic Core Complex below the

Büyük detachment is also thought to be at temperatures >80 °C, however, this inference is entirely based on one sample.

- *2 My*: The northern and southern flanks of the Central Menderes metamorphic core complex below the Büyük and Gediz detachments cool to similar temperatures of ca. 60–80 °C.
- *2-0 My*: The final cooling to surface temperatures occurred during the interval 2–0 My in the footwalls of the Büyük and Gediz detachments.

This model point out again a two-stage cooling history for the Menderes Massif. A first regionally significant phase of cooling in the Late Oligocene and Middle Miocene affected the outer two submassifs and the upper structural levels of the Central Menderes Metamorphic Core Complex (Fig. 6.6). In the northern part of the Gördes submassif, cooling was related to top-NNE movement on the Simav detachment, as the AFT ages show a northward-younging trend in the direction of movement on this detachment. In the Çine submassif, relatively rapid cooling in the Late Oligocene and Middle Miocene may have been related to top-S extensional reactivation of the basal thrust of the overlying Lycian nappes (Gessner et al., 2011).

The second phase of cooling is related to Middle Miocene - Pliocene extension, resulting in the formation of the Central Menderes Metamorphic Core Complex. Core-complex development caused the formation of supra-detachment basins, which document the ongoing separation of the Central Menderes Metamorphic Core Complex from the outer submassifs (Gessner et al., 2001a; Ring et al., 2003).

An extensive Middle Miocene - Pliocene erosion surface formed between these two phases of exhumation (Ring et al., 2003). This erosion surface, according to Yilmaz et al. (2000), can be recognizable in the Bozdağ Mountain in the Central Menderes Metamorphic Core Complex. Here it is possible to observe the relationship between this erosional surface and the exhumation that characterized the Central Menderes Metamorphic Core Complex. This erosion surface cuts all the Menderes metamorphic rocks and the cover sediments including Upper Miocene red clastics. The erosional surface has been fragmented by east-west trending steep faults, which also cut older structures, and produced the present Gediz Graben (Yilmaz et al., 2000).

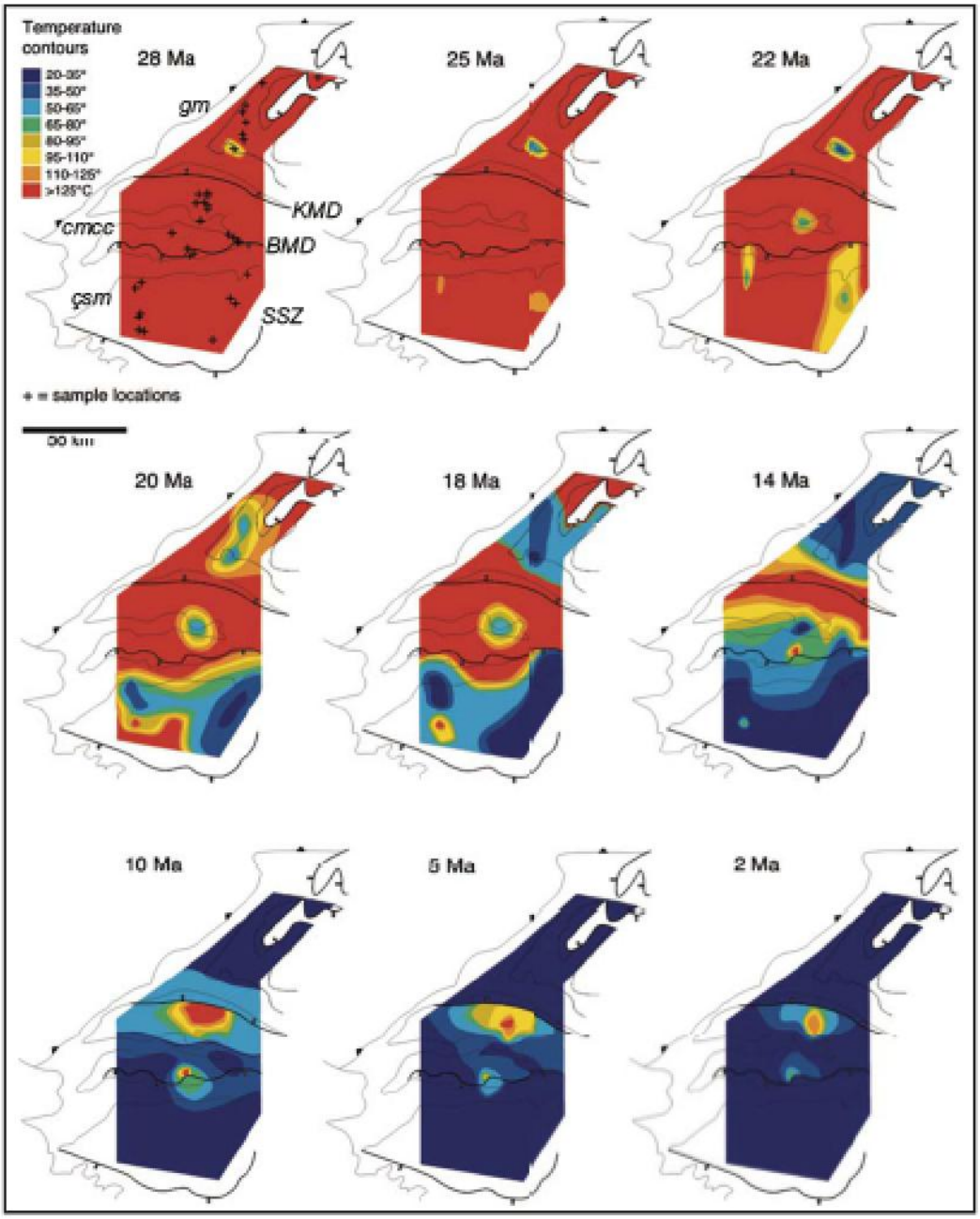


**Fig. 6.6 – Contoured time-temperature slices from 28 My to 2 My imposed on general outline of Menderes nappes with major detachments; map for 28 Ma shows locations of 34 samples used to construct maps. The contouring is strongly controlled by the distribution of the sample point. Contours were drawn by computer program but were subsequently manipulated to include geological information. Cooling below ca. 130 °C commenced in southern Gördes submassif at ca. 28 My but did not progress northward until 22–20 My. Cooling in northern Çine submassif started at 25 My and progressed southwards towards base of Lycian nappes. Down-faulted block in the central Central Menderes metamorphic core complex started to cool at 22 My. Footwall of Kuzey detachment remained at elevated temperatures above ca. 130 °C until 5 My; footwall of Guney detachment started to cool below ca. 130 °C at 14 My but final cooling only occurred after 2 My (from Ring et al., 2003).**

In this region Buscher et al. (2013) used AFT and $^{10}$Be cosmogenic to provide constraints on rock exhumation and landscape development. By $^{10}$Be method they were able to obtain an erosion rate value included between 0.18 and 0.4 Km/My.

This variation can be recognizable along the two flank of the Bozdağ Mountain (Fig. 6.7). The high rates of erosion in the southern part can be explained as the combined of different effects such the high susceptibly of the amphibolite-facies in the micaschists and paragneisses that make up the Çine and Bozdağ Nappe (see Chapter II) to weathering and erosion (Buscher et al., 2013). The northern flank was eroded at much lower rates and this can be explained by the presence of quartz-rich lithologies that are less susceptible to erosion (Buscher et al., 2013).

These results point out that in northern flank, where there were recent tectonic movement associated to the Gediz detachment, most exhumation occurred by tectonic denudation rather than erosion. For what concerns the southern flank, the elevate erosion rates means that erosion played a significant role in exhuming rocks.

The erosional rates obtained in this dissertation were evaluatated mainly on samples from Çine and Bozdağ nappes, but, due to their very low values, appears very difficult to relate them with any tectonic activity in the area. Moreover, due to the different timescale, appears very difficult to perform a comparison with the rates obtained by Buscher et al. (2013) from the southern flank of Bozdağ (Fig. 6.7).

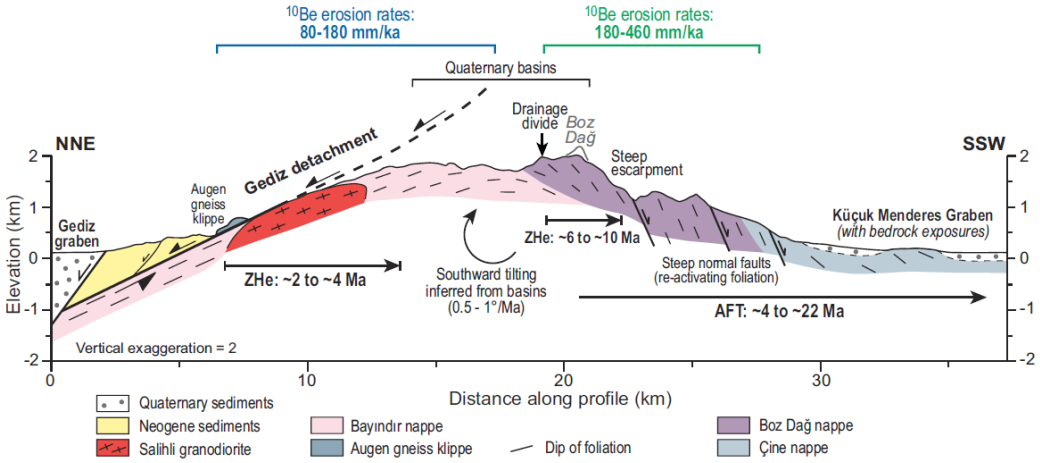


**Fig. 6.7 – Schematic profile across the Bozdağ block summarizing the prominent tectonic and geomorphological features and the results from thermochronological and cosmogenic $^{10}$Be data (Buscher et al., 2013; Gessner et al. 2001b; Ring et al. 2003).**

As a mean to summarize all of the data presented here we utilize the model by Gessner et al. (2013), where two stages of tectonic denudation of the Menderes Massif are shown. Extension first produced (Late Oligocene-Early Miocene) the exhumation of the southern and northern submassifs and then, starting from the Late Miocene, the exhumation of the central Menderes Massif (Fig. 6.8).

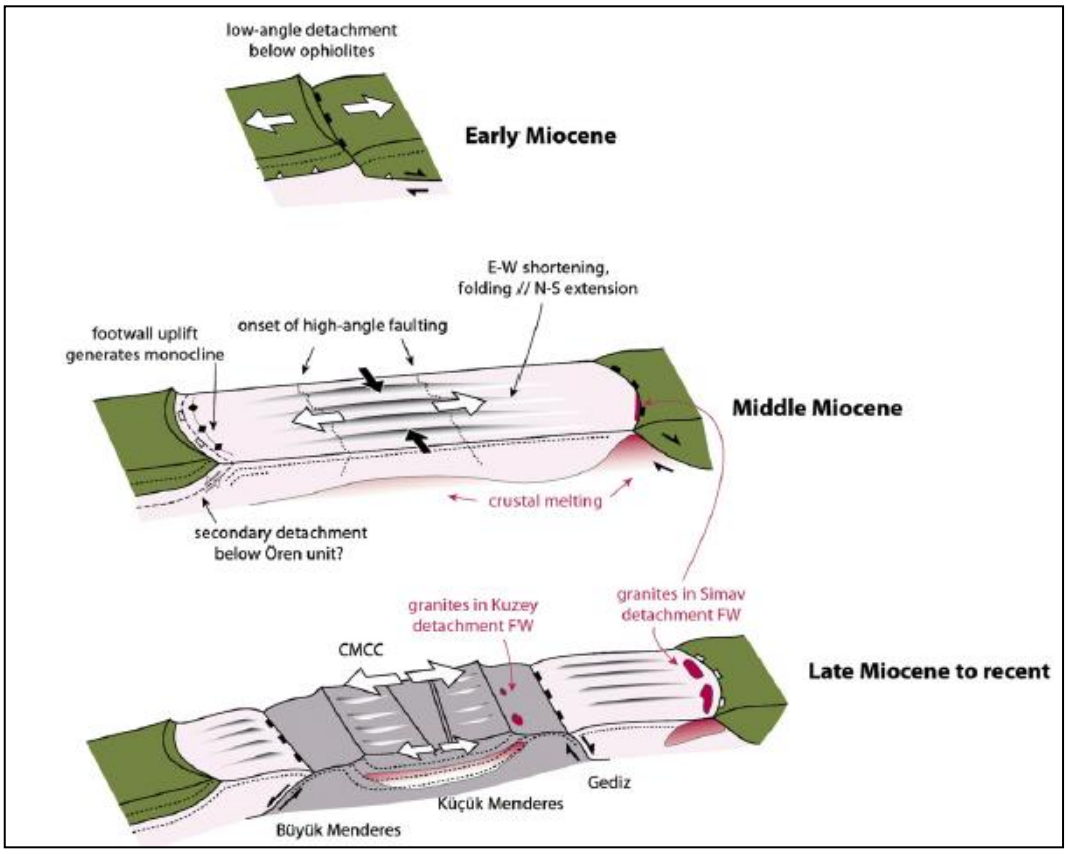


**Fig. 6.8 – Conceptual model of the two stage tectonic denudation of the Menderes Massif from the Early Miocene to the present. According to this model the monocline in the southern Menderes formed as footwall uplift after Miocene detachment faulting. Miocene crustal melts get exhumed either soon after intrusion in the north, or by the Gediz detachment in the Late Miocene. Corrugation occurring due to E-W shortening of the basement in the footwall of the Early Miocene detachments still shape the drainage of the Çine and Gördes submassifs; the CMCC footwall 'inherited' corrugations as topographic features that control the orientation of drainage in the Aydin and Bozdağ mountains (from Gessner et al., 2013).**

Based on the observation of a discontinuity in the lithospheric mantle between the Hellenide and the Anatolide domains, Gessner et al. (2013) proposed a model where this discontinuity determine a lithosphere-scale shear zone, the West Anatolia Transfer Zone (WATZ), which has accommodated the difference between fast

rollback of the slab in the Aegean and slow delamination of the Anatolian continental lithosphere since the Miocene, and that links the North Anatolian Fault zone to the Hellenic trench (Fig. 6.9).

The Late Oligocene-Early Miocene to recent crustal extension in the Anatolide belt in western Turkey is so linked to the sinistral transtension across the WATZ. However, according to this kinematic framework, the main driving force for the Menderes Massif exhumation is, as in the whole Aegean region, the slab roll-back. Due to this overall tectonic setting the massif has experienced NNE–SSW extension, including extensional detachment faulting, folding parallel to extension, doming and footwall uplift (Fig. 6.9).

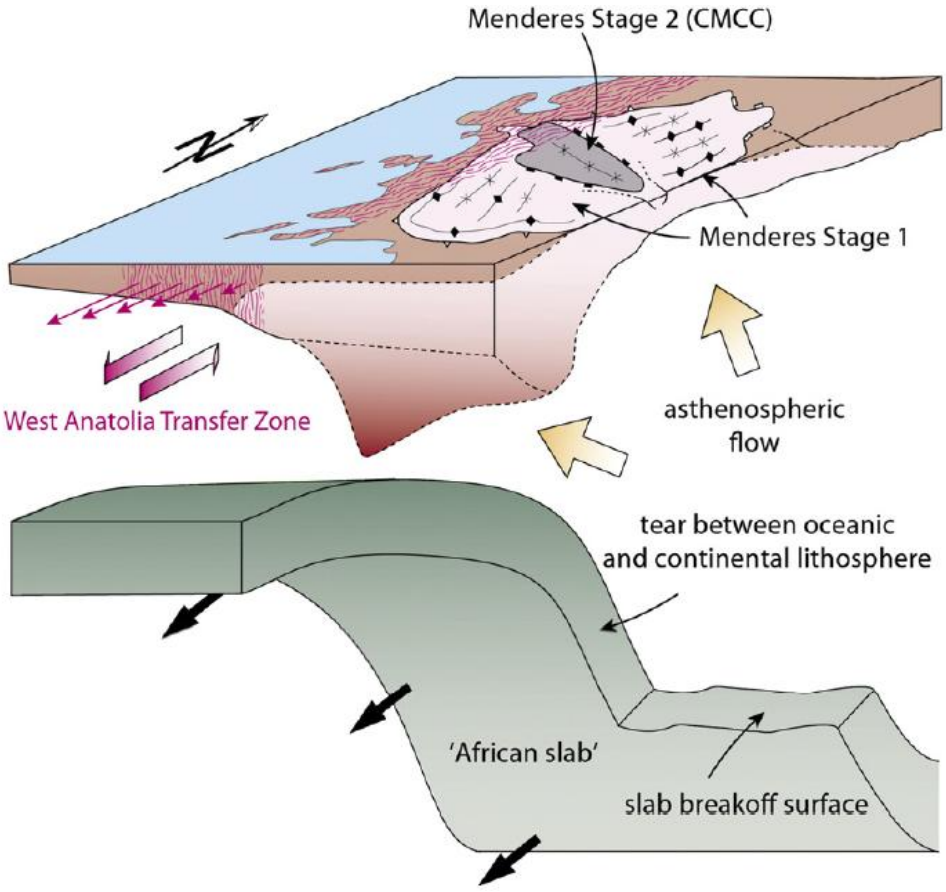


**Fig. 6.9 - Conceptual model of the present slab dynamics in southwest Turkey, where the southwest retreat of the Aegean slab with its vertical edge maintains a transtensional situation that controls the diffuse brittle deformation along the coast and inboard of the Aegean. The two stages of Menderes denudation exposed one of Earth's largest metamorphic core complexes displaying frozen in mid-crustal levels of transtensional deformation (from Gessner et al., 2013).**

## 6.3 ALANYA MASSIF EVOLUTION

The entire Tauride belt of central and western Anatolia experienced polyphase deformation during the Eocene (e.g. Gutnic et al., 1979; Eren, 2001; Robertson et al., 2012b). The present-day structural configuration around the Bay of Antalya features the unmetamorphosed, autochthonous Tauride carbonate succession overthrust by (i) unmetamorphosed Mesozoic continental margin-type sedimentary and volcanic rocks and also by (ii) ophiolitic rocks of the Antalya Complex (Antalya Nappes). The Eocene age of the youngest sedimentary rocks within the autochthonous carbonate platform, combined with structural evidence, indicates that the Antalya Complex was thrust northward over the Tauride autochthon during the Middle Eocene (Lutetian) (Robertson et al., 2013). To the south, the Antalya Complex is regionally overthrust northward by the metamorphic units of the Alanya Nappes.

This dissertation includes the first AFT ages for the Alanya Massif. All three FT ages cluster in the mid-Oligocene (32-27 My) and -despite the scarcity of data- we can recognize an overall younging of FT ages from north to south. The dataset presented here illuminates a previously unrecognized cooling event somewhat in contrast with existing tectonic interpretations for the Alanya Massif, emphasizing Eocene nappe stacking and exhumation (Okay & Özgül, 1984; Robertson et al., 2013; Çetinkaplan et al., 2014).

According to Robertson et al. (2013), after Eocene northward backthrusting, the Alanya Massif did not suffer any other significant tectonic event. The nappe structure of the region is covered by undeformed mid-Miocene shallow-marine carbonates (Fig. 6.13).

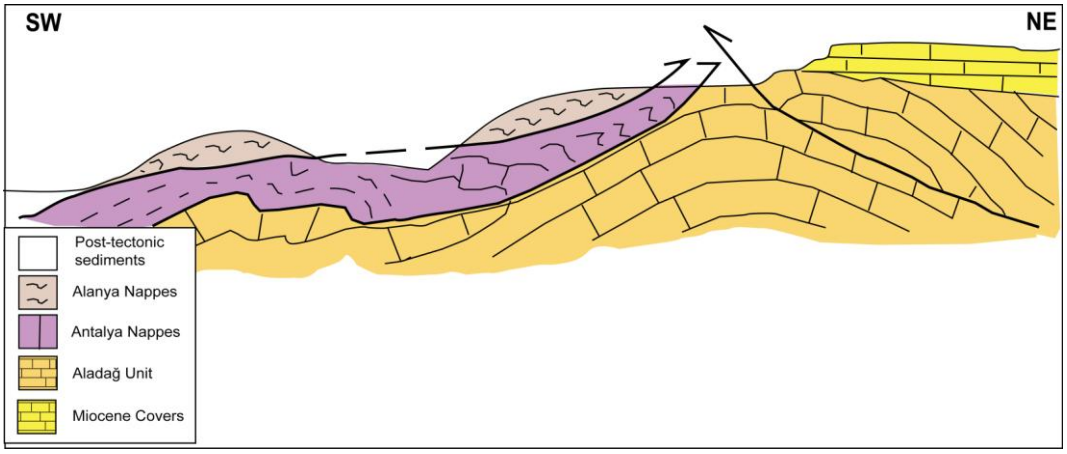


**Fig. 6.13 – Geological section of the Alanya Massif. The Alanya and Antalya nappes are piled on the relatively autochthon Tauride platform; note the position of the Alanya nappes thrusted over the Antalya nappes which crop out in the region in a tectonic window. To the NE an angular unconformity marks the transgression of mid-Miocene shallow-marine carbonates carbonate on the Aladağ unit.**

Recently Çetinkaplan et al. (2014) proposed the correlation of the Alanya nappes with the Bitlis terrain to the east. This is possible taking in account the same metamorphic grade of both the region. According to this interpretation, a ribbon-like microcontinent -the Bitlis-Alanya microcontinent- was located between the Anatolide-Tauride platform to the north and the Arabian plate to the south. Such microcontinent was involved into the northward subduction and deeply buried in the Late Cretaceous. Based on petrological evidence, Çetinkaplan et al. (2014) propose that the Alanya and Antalya units were originally a single unit belonging to the Bitlis-Alanya microcontinent. Part of this microcontinent was buried and metamorphosed during Late Cretaceous northward subduction under the Tauride platform, and then thrust to the north during Early-Middle Eocene time (Fig. 6.14).

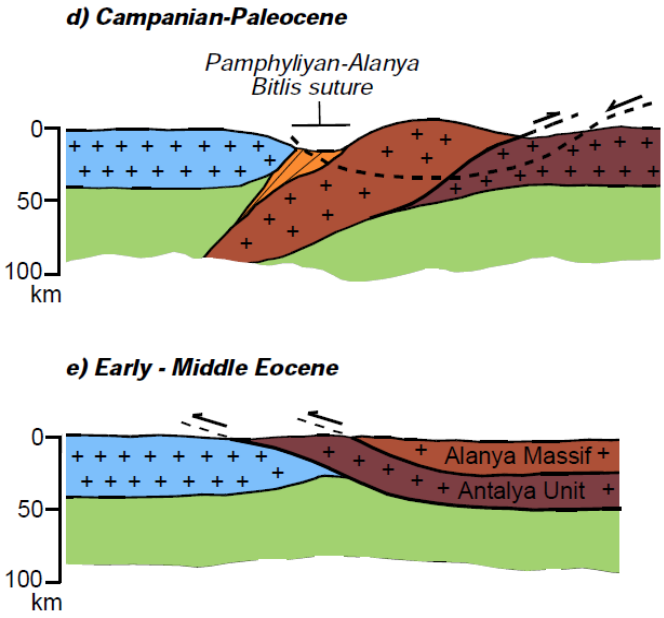


**Fig. 6.14 – Schematic Campanian-Paleocene and Early-Middle Eocene paleotectonic cross-sections for the Tauride region (Çetinkaplan et al., 2014). Sections are oriented north-south; north to the left.**

Previous paleotectonic models for the Tauride region agree on the fact that the present-day structural configuration of the Alanya Massif developed essentially in the Eocene (e.g. Robertson et al., 2013; Çetinkaplan et al., 2014). Albeit limited in number, the new apatite fission-track data presented in this dissertation point to a significant, previously unrecognized, phase of cooling/exhumation during the Oligocene. Such event modified significantly the thermal structure of the study area and therefore must be incorporated in any paleotectonic reconstruction of the area.

Clues on the overall stress regime responsible for the Oligocene cooling episode can be obtained considering the geology of the region surrounding the Alanya Massif. For example, we can consider the geological setting and the stratigraphy of the Adana-Cilicia basin. This basin separates the Misis-Kyrenia sector of northern Cyprus from the Taurus Mountains of Turkey and is assumed to be floored by continental crust. Offshore geophysical exploration and onshore stratigraphic analysis in the Adana region show that the lowermost unit of the sedimentary fill is Late Oligocene to Early Miocene (Aksu et al., 2005; Cosentino et al., 2012). As a result of the complex tectonic setting, the Adana-Cilicia Basin development has been alternatively associated with i) syn- or post-collisional tectonics related to slab dynamics (Williams, 1995; Robertson, 2004; Aksu et al., 2005); ii) the widespread transcurrent motion related to the development of the

East Anatolian Fault Zone (Kelling et al., 1987; Chorowicz et al., 1994); or iii) a combination of the two processes (Şengör et al., 1985; Dewey et al. 1986).

Despite the scarcity of structural and thermochronometric data from the Alanya Massif, we tentatively favour the interpretation of the mid-Oligocene cooling episode documented in this dissertation as the result of exhumation driven by extension. This is in view of the overall transition from a compressional (Eocene) to an extensional (?Oligocene-Miocene) regime recognizable over the entire Aegean and peri-Aegean regions. In these regions, the Late Cretaceous accretion of the Pelagonian, Sakarya and Anatolide-Tauride crustal fragments and the subsequent production of thickened crust, due to the closure of the Vardar ocean, was followed by a change of the tectonic regime. For example in the Rhodope region during the Late Eocene there were the first evidence for this change of tectonic regime as testified by the emplacement of different types of sedimentary basins associated with the major extensional faults and by abundant volcanic rocks. The latter also testify a change from a subduction enriched subcontinental lithospheric mantle source with fractional crystallization and crustal contamination to volcanic rocks that indicate an origin related to decompression melting of an enriched asthenospheric source (Burchfiel et al., 2008). Tectonic evolution of the Rhodope Mountains can be correlated with the northwestern Turkey, although the passages from a compressional to an extensional regime appear to be younger. The diachroneity of the change of regime between the southern Bulgaria and the northwest Turkey could be en effect of the not direct connection between the regions due to the presence of Thrace basin, which represent an area of high subsidence which evolved during the Eocene-Oligocene as a supradetachment basin (Kilias et al., 2013).

## 6.4 CYPRUS RESULTS

In the island of Cyprus it has been performed ZHe dating on samples taken both from the Troodos and the Mamonia complexes.

As for the plagiogranite CY5 sampled in the Troodos Massif, the ZHe ages were 72.2 ± 1.2 My and 64.8 ± 0.9 My. The magmatic ages for this plagiogranite is about 90 My and was calculated by the U-Pb method; we can conclude that our sample

cooled from 900° C (the closure temperature of the U-Pb geochronometer) to 180° C (the closure temperature of the ZHe geochronometer) in a time span ranging approximately between 20 and 27 My. Such cooling could be either (i) an effect of the normal magmatic cooling of the plagiogranites or (ii) a result of exhumation. AHe and AFT ages obtained by Morag et al. (2013) point to an exhumation of the Troodos Massif in the Plio-Pleistocene ages. According to these authors there was no evidence for significant uplift of the Troodos area prior to that time; therefore our ZHe ages cold be read as an substantial effect of the normal magmatic cooling.

The Troodos complex formed in a supra-subduction setting (e.g. Dilek et al., 2007; Metcalf & Shervais, 2008; Pearce & Robinson, 2010). In general, suprasubduction-zone ophiolites are intact structurally and stratigraphically and show evidence for nearly 100% extension. Such ophiolites are now inferred to have formed primarily by hinge retreat in the forearc of nascent or reconfigured island arcs, a model derived from studies of Cenozoic subduction systems in the western Pacific (Hawkins et al., 1984; Stern & Bloomer, 1992; Bloomer et al., 1995; Hawkins, 2003). Emplacement of these forearc assemblages onto the leading edge of partially subducted continental margins (Tethyan ophiolites) is a normal part of their evolution. In a paleogeographical reconstruction for the Late Cretaceous (70 My) the Troodos complex is shown as a forming ophiolitic complex on an independent plate (Fig. 6.15). This plate is comprised between the African plate and the Anatolide-Tauride domain; the latter was previously totally covered by the obduction of ophiolitic-type mélange originating from the southern Vardar ridge. During the Late Cretaceous the African plate limit in this region had become convergent, due to intra-oceanic subduction in the Neotethys and shortening affecting the Vardar region. The accelerated counter-clockwise rotation of the African plate during the Late Cretaceous will produce a continuous extrusion towards the southwest of the Troodos plate until the Eocene (Stampfli & Hochard, 2009). Considering this interpretation our hypothesis for a fast cooling of the plagiogranites finds a more consistent significance.

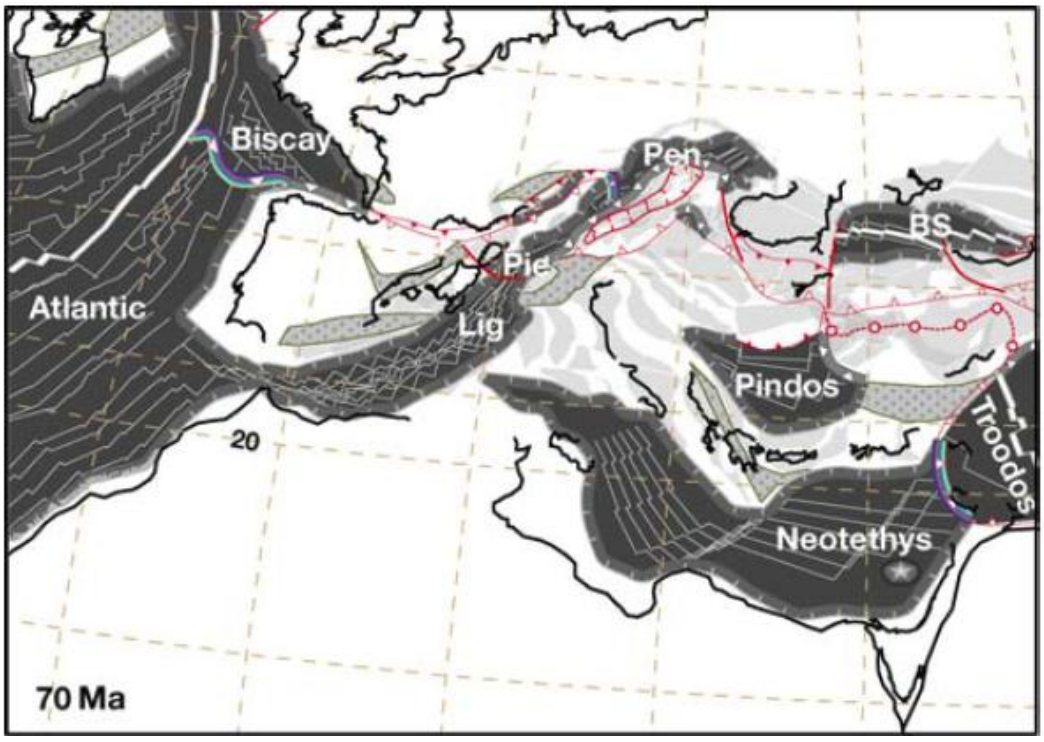


**Fig. 6.15 – Paleotectonic map of the Maastrichtian (70 My) of the Eurasia-Africa plates (from Stampfli & Hochard, 2009).**

As to the Mamonia Complex the results obtained are to refer to two samples: CY6 and CY7.

Sample CY6 is a quartzitic sandstone taken from the Vlambouros Formation in the Mamonia Complex and the depositional age for these sandstones is Late Triassic. For this sample were obtained two ZHe ages: 326.5 ± 4.9 My and 214.0 ± 2.9 My, these ages so point to a Middle Carboniferous time. Because of the ZHe ages are older than the depositional age of the sandstone these can evidentiate that the sandstone still show their pre-depositional age.

Sample CY7 is again quartzitic sandstone taken from the Vlambouros Formation in the Mamonia Complex, with a depositional age of the Late Triassic. The ZHe ages for this sample are 379.2 ± 6.0 My and 379.5 ± 5.7 My, these ages point to a Late Devonian age. Also in this sample the ZHe ages are older than the depositional age of the sandstone and so this mean that the sandstone still show their pre-depositional age.

The results for the Mamonia Complex are very significative because provide the evidence that the samples were never buried at temperature over 200° C that could have reset their age according to the ZHe method. The Mamonia Complex,

although testify an intense deformation in its fine-grained matrix, was so never buried over the 200° C.

The ZHe results on the Troodos and Mamonia complexes are coherent with the overall Late Cretaceous tectonic evolution (e.g. Robertson & Woodcock, 1979). According to this view the Troodos complex formed during this age and then was extruded because of the collision between Africa and Eurasia. The Mamonia complex formed as a mélange in the Late Triassic and was no longer involved in any tectonic evolution until the Miocene, when the Complex was involved into the final assembling of the island of Cyprus.

## 6.5 THERMOCHRONOLOGIC RESULTS AND OVERALL PALEOTECTONIC EVOLUTION OF THE STUDY AREA

In this section the main results of this dissertation will be discussed within the framework of a paleogeographic-paleotectonic reconstruction of the entire eastern Mediterranean region from the Late Cretaceous to the Late Miocene, in order to provide an integrated and unified view.

### 6.5.1 Late Cretaceous

Many studies of the Cretaceous evolution of Anatolia have called for a complex subduction zones configuration with multiple subduction fronts, micro-plates and triple junctions accommodating Africa–Europe convergence (e.g. Robertson & Ustaömer, 2011, Robertson et al., 2012a, 2013). Figure 6.17 shows a paleogeographic reconstruction of the Middle East highlighting the main geological environment (Barrier & Vrielynck, 2008). At that time there was northward subduction of the African plate under the Eurasian plate.

Starting from the Late Cretaceous there was the progressive closure of the Vardar ocean which induced the northward movement and accretion of the Pelagonian, Sakarya and Anatolide-Tauride crustal fragments (Burchfiel et al., 2008).

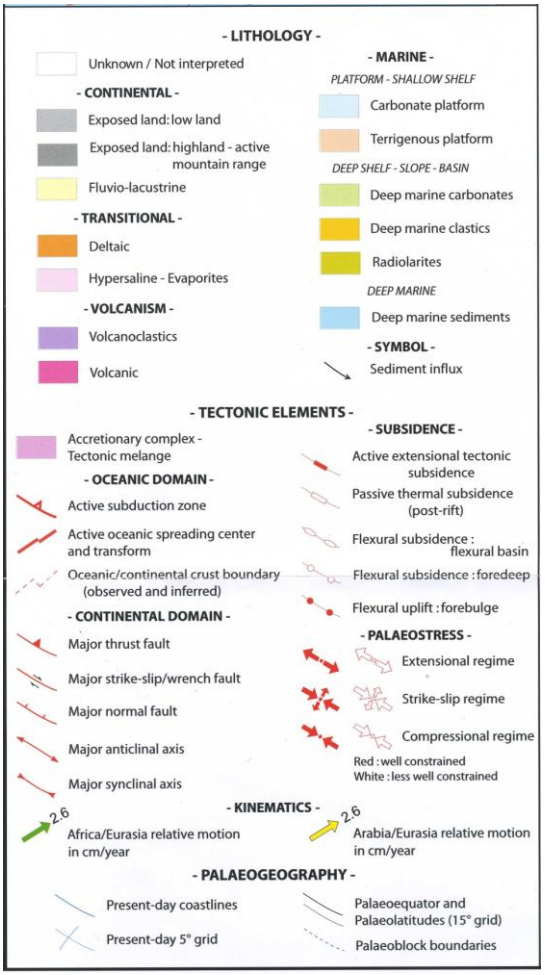


**Fig. 6.16 – Legend of the paleotectonic maps of Figs. 6.17-19-22-23-24.**

A further effect of this collisional phase was the production of thickened crust north of the suture in southern Bulgaria, eastern Macedonia, northern Greece and north westernmost Turkey. Crustal thickening was associated with regional metamorphism of Latest Cretaceous - Early Paleogene age, an example of this are the Rhodope-Strandja massifs.

To the south, large-scale obduction of Neotethyan ophiolites occurred along the northern margins of the Anatolide-Tauride terrane and the Arabian platform. South of the Pindos–Lycian basin the Menderes platform and the Antalya basin are not directly involved in tectonic activity.

In the Cyprus region the Mamonia Complex is represented as an active mélange in this time related to the intra-subduction zone associated to the genesis of the Troodos Complex, and this indicates that it will be reworked during the final emplacement of the island of Cyprus.

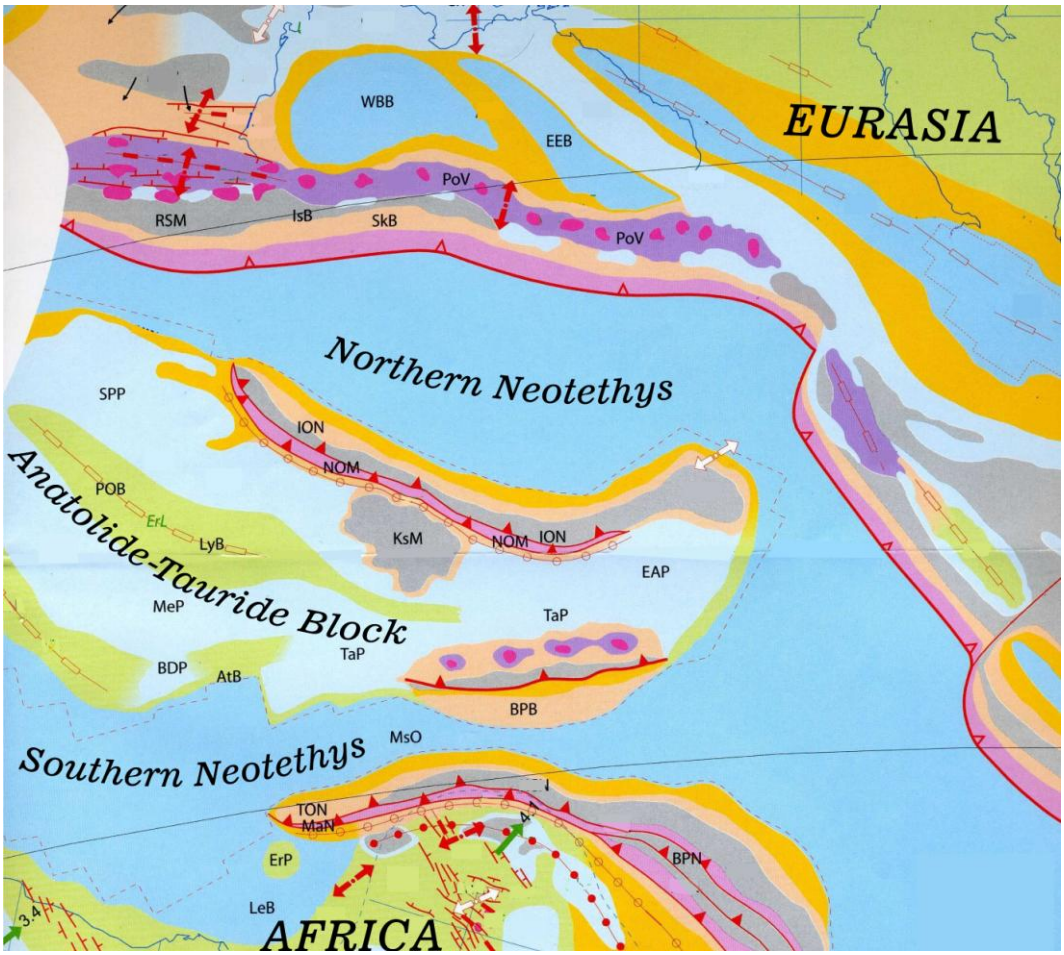


**Fig. 6.17 – Paleotectonic maps of the Middle East in the Early Campanian (80.6 – 83.5 My) (from Barrier & Vrielynck, 2008, mod.). AtB – Antalya Basin; BDP – Bey Dağlari Platform; BPB – Bitlis-Pütürge Block; BPN – Bisitoune Platform Nappe; EAP – East Anatolian platform; EEB – Eastern Black Sea Basin; ErP – Erathostenes Platform; ION – Izmir-Ankara-Erzincan Ophiolites Nappes; IsB – İstanbul Block; KsM – Kirşehir Massif; LeB – Levant Basin; LyB – Lycian Basin; MaN – Mamonia Nappe; MeP – Menderes Platform; MsO – Mesogea Ocean; NOM – North-Anatolian Ophiolitic Melange; POB – Pindos-Olonos Basin; PoV – Pontide Volcanic Arc; RSM – Rhodopes-Strandja Massif; SkB – Sakarya Basin; SPP – Serbo-Pelagonian Platform; TaP – Taurus Platform; TON – Troodos Ophiolite Nappe; WBB – Western Black Sea Basin.**

North of the Mamonia Complex the Troodos complex, as clearly shown by our (U-Th)/He results, begins to cool down in a very short time compared to its magmatic age. As to the Kyrenia Range, the regional unconformity between metamorphosed Triassic–Cretaceous platform carbonates and unmetamorphosed Upper Cretaceous–Paleogene pelagic carbonates and volcanic rocks (see Chapter II) indicates that by Late Maastrichtian time the carbonate platform rocks were exhumed and exposed on the seafloor in a submarine, pelagic-depositing setting by Late Maastrichtian time. What happened between the southern margin of the Tauride platform and the

northern region of the "proto-Cyprus" is unclear. The reconstruction shown in Fig. 6.17 does not show any tectonic activity in the region but, considering the Late Cretaceous HP-LT metamorphism of the Sugözü nappe, we can envision an subduction zone at this time. This implies an effective separation and a subsequent compressional phase between the "paleo-Cyprus" and the Tauride platform.

Robertson et al. (2012a) also proposed a paleogeographical reconstruction of the Middle East for the Late Cretaceous (fig. 6.18). In this map the Alanya nappes are interpreted as the southern margin of an 'Alanya ocean' that was located to the south of the Tauride carbonate platform. During the first phase of the Alpine orogeny, between the Late Cretaceous and the Paleocene, this ocean was subducted northward. This northward subduction led to Late Cretaceous thrusting and HP-LT metamorphism of the Sugözü nappe, the same metamorphism phase undergone by the Mesozoic carbonate platform of the Kyrenia Range in Cyprus (see Chapter II).

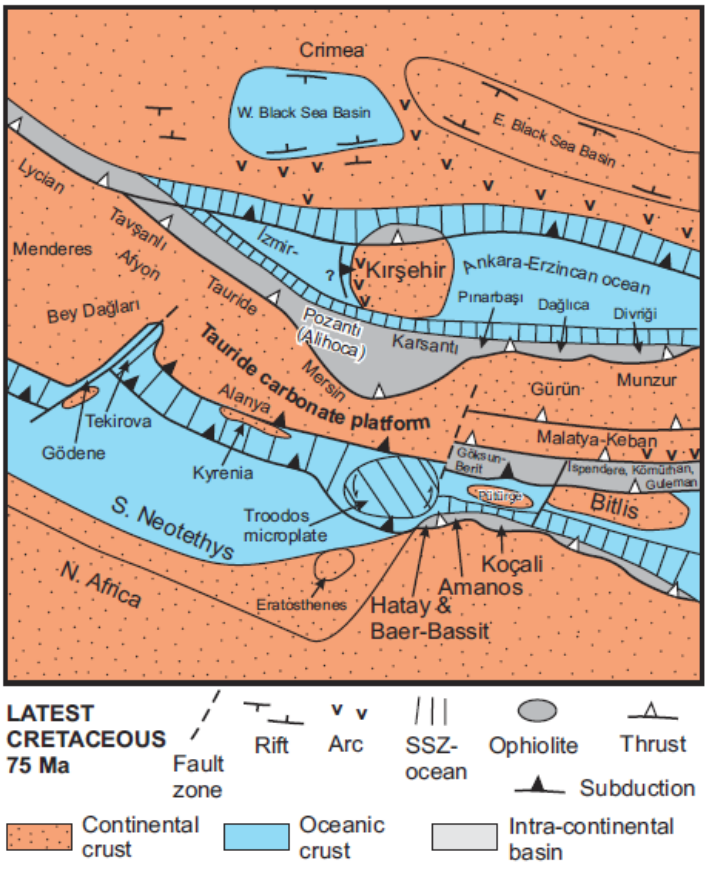


**Fig. 6.18 – Latest Cretaceous palaeogeography. This time span is characterized by southward obduction of supra-subduction zone ophiolites onto the Arabian continental margin and also onto several microcontinental units. South of the Tauride platform there is the narrow 'Alanya Ocean' (Robertson et al., 2012a).**

### 6.5.2 Eocene

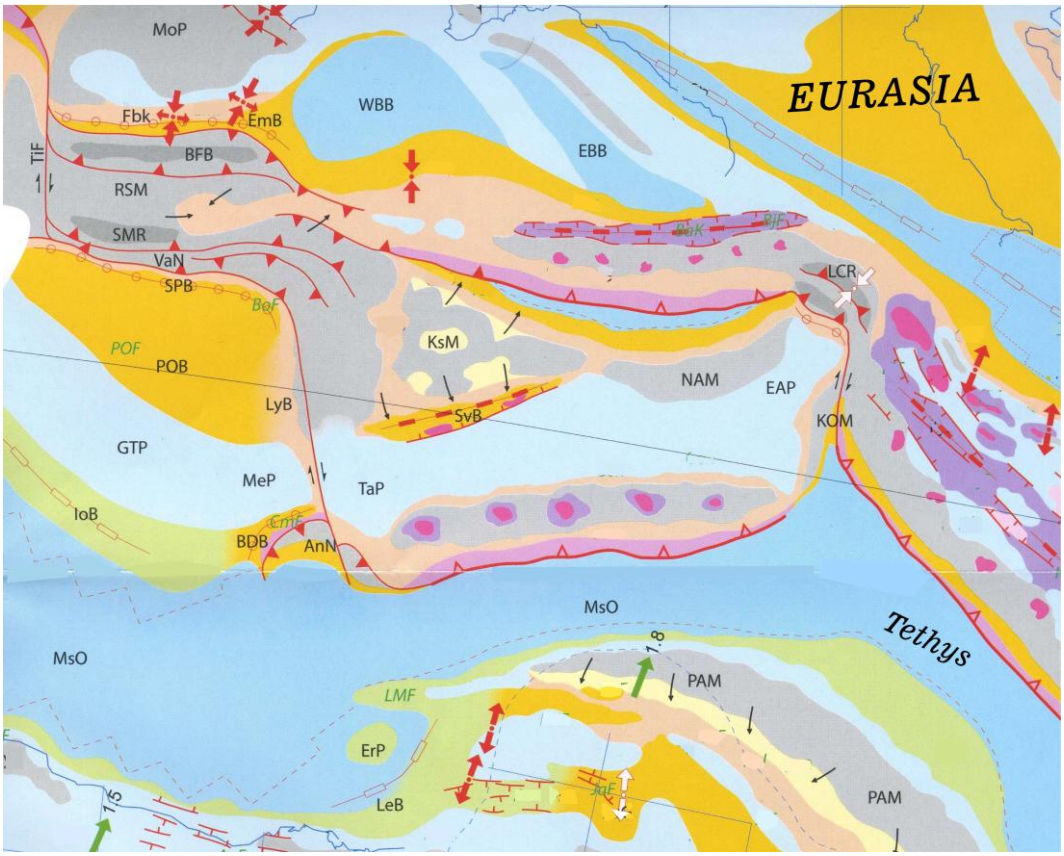


**Fig. 6.19 – Paleotectonic maps of the Middle East in the Ypresian (55.8 – 48.6 My) (from Barrier & Vrielynck, 2008, mod.). AnN – Antalya Nappes; BDB – Bey Dağlari Basin; BFB – Balkan Fold-Belt; EAP – East Anatolian Platform; EBB – Eastern Black Sea Basin; EmB – Emine Basin; ErP – Erathostenes Platform; Fbk – Forebalkan; GTP – Gavrovo-Tripolitza Platform; IoB – Ionian Basin; KOM – Köy Ophiolite Massif; KsM – Kirşehir Massif; LCR – Lesser Caucasus Range; LeB – Levant Basin; LMF – Middle-Lefkara Formation; LyB – Lycian Basin; MeP – Menderes Platform; MoP – Moesian Platform; MsO – Mesogea Ocean; NAM – North-Anatolian Massif; PAM – Peri-Arabian Massif; POB – Pindos-Olonos Basin; POF – Pindos-Olonos Flysch; RSM – Rhodopes-Strandja Massif; SMR – Serbo-Macedonian Range; SPB – Serbo-Pelagonian Basin; SvB – Sivas Basin; TaP – Taurus Platform; TiF – Timok Fault; WBB – Western Black Sea Basin.**

This time frame was characterized by the final collision between the Sakarya terrane to the north and the Anatolide domain to the south. The Tauride belt resulted directly from such collision. Moving away from the collision zone into the southern margin of the Tauride platform, there was the development of a long transform fault, related to the collision, which has an effect of amplify the structure of the Isparta region. Moreover along the southern margin of the Tauride platform, as a further effect of this collision, there was the development of a series of north-verging backthrusts. Within this context, the previously partially subducted Alanya nappes

were backthrust and began to be exhumed. Our Oligocene AFT ages from the Alanya Massif point to a later cooling/exhumation and, in reference to the Alanya-Bitlis microcontinent, might indicate that collisional deformation mirrored the counter clockwise rotation of the African-Arabia plate.

Moreover Robertson et al. (2012b) also proposed the genesis of the northward backthrusts related to closure of the Izmir-Ankara-Erzincan ocean which are the cause of the actual position of the Alanya nappes on the Antalya nappes (Fig. 6.20).

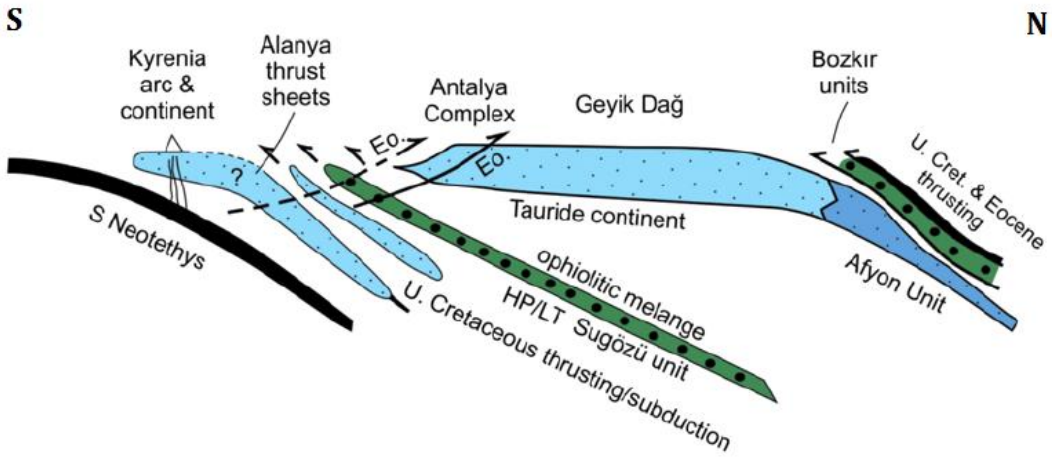


**Fig. 6.20 – The interpretation of the Alanya Massif by Robertson et al. (2013). This reconstruction, settled in the Eocene, show the northward backthrusting of the Alanya nappes on the Antalya nappes. Previous Late Cretaceous subduction determinate the northward carriage of the Alanya nappes, originated in a rift and small ocean basin in the south of the Tauride carbonate platform continent (from Robertson et al., 2013).**

Although the agreement on the cause for the exhumation of the Alanya Nappes, Robertson et al. (2013) proposed a paleogeographical reconstruction in the Eocene in which they substantially not provided the Alanya-Bitlis microcontinent (Fig. 6.21).

During the Eocene the Cyprus region was characterized by the clockwise rotation of the Troodos complex, as paleomagnetic reconstruction evidentiate (Morris et al., 1990), an effect of both the Arakapas transform fault and the extrusion due to the beginning of the collision between Arabia and Eurasia.

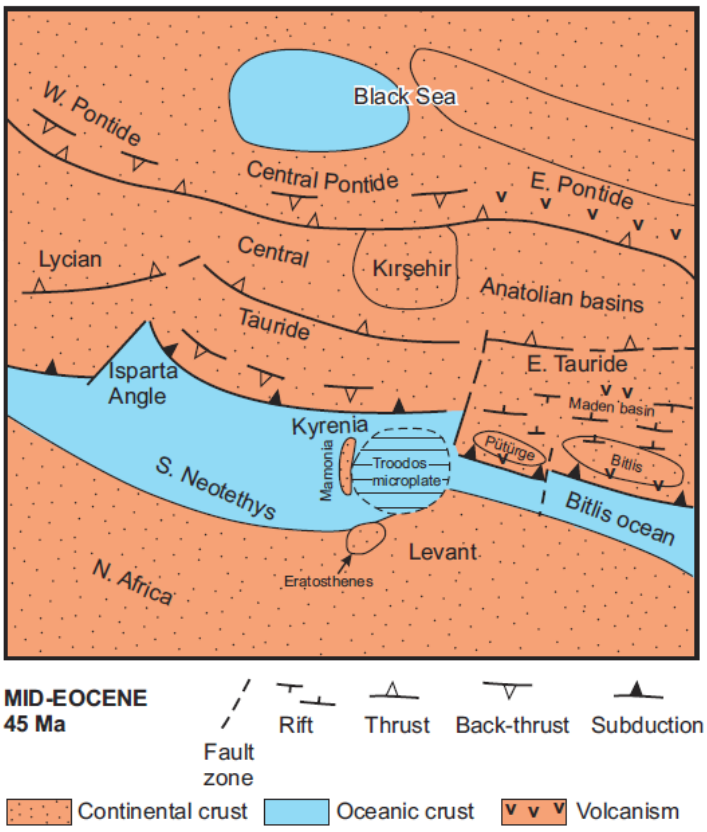


**Fig. 6.21 - Mid-Eocene palaeogeography. The İzmir–Ankara–Erzincan ocean is closed, northward subduction of the Southern Neotethys and related back-arc extension in SE Turkey (Maden basin) characterize this period. The paleo-rotation of the Troodos microplate was over by the Early Eocene. Some oceanic crust could remain north of the Pütürge and Bitlis massifs. Note the Alanya back-thrust in the southern part of the Central Tauride (from Robertson et al., 2012a).**

### 6.5.3 Early Oligocene

At this time the collision in the eastern part of the region, between Arabia and Eurasia, is about to be realized; at the same time in the Aegean region there was the began of an extensional regime as shown by marked subsidence in the Thrace basin and the extension within the Rhodopes-Strandja Massifs. Due to this complex evolution, it is better to approach first to the Alanya region - Cyprus and then the Menderes region.

As to the Alanya region, during the Oligocene, the previous Eocene backthrusts have exhumed the Alanya Nappes. This is constrained by our AFT ages which indicate a Rupelian age. Most likely this exhumation was due to the continuous roll-back of the African slab, the establishment of an extensional regime, and the opening of a “proto-Cilicia basin” (Fig. 6.22).

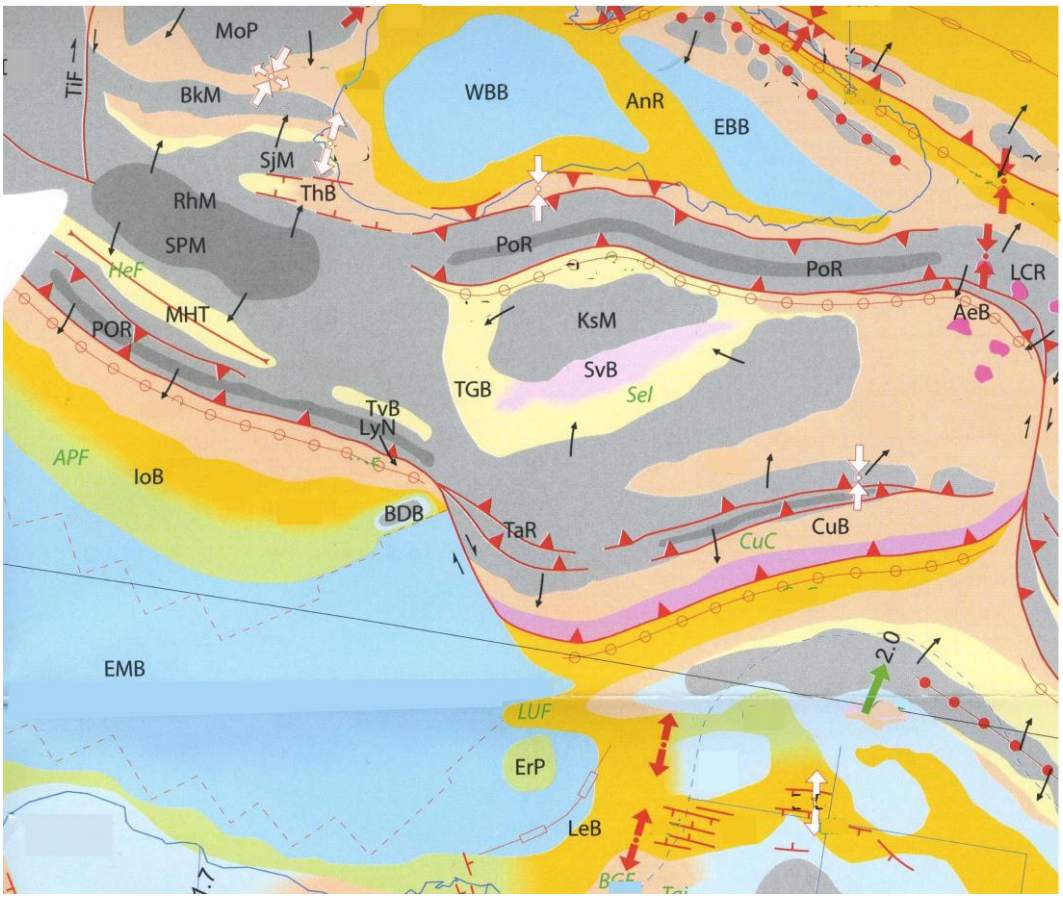


**Fig. 6.22 – Paleotectonic map of the Middle East in the Rupelian (33.9 – 28.4 My) (from Barrier & Vrielynck, 2008, mod.). AnR – Andrusov Ridge; APF – Agii-Pantes Formation; BDB – Bey Dağlari Basin; BkM – Balkan Massif; CuB – Güngüs Basin; CuC – Güngüs Complex; EBB – Eastern Black Sea Basin; EMB – East Mediterranean Basin; ErP – Erathostenes Platform; HeF – Heptakhorion Formation; IoB – Ionian Basin; KsM – Kirşehir Massif; LCR – Lesser Caucasus Range; LeB – Levant Basin; LyN – Lycian Nappes; LUF – Upper-Lefkara Formation; MHT – Meso-Hellenic Trough; MoP – Moesian Platform; POR – Pindos-Olonos Range; PoR – Pontides Range; RhM – Rhodopes Massif; SiB – Sirt Basin; SjM – Strandja Massif; SPM – Serbo-Pelagonian Massif; SvB – Sivas Basin; TaR – Taurus Range; TGB – Tuz-Gölü Basin; ThB – Thrace Basin; TiF – Timok Fault; TvB – Tavas Basin; WBB – Western Black Sea Basin.**

The latest Rupelian marks the beginning of the exhumation of the Menderes Massif. Progressive Aegean slab roll-back follows, also in this area, the switch from a compressional to an extensional regime (e.g. Jolivet & Faccenna, 2000; Brun & Faccenna, 2008; Burchfiel et al., 2008). The development of metamorphic core complexes, like the Rhodope or the opening of the Meso-Hellenic Trough, is clear examples of this tectonic change (Fig. 6.22). The AFT ages presented here indicate that cooling of the Menderes Massif began at the very end of the Rupelian, as a metamorphic core complex along an asymmetrical detachment. Exhumation of the

Menderes Massif was accompanied by the southern motion of the Lycian Nappes (Rimmelé et al., 2003).

Small sedimentary basins presently separate the Menderes Massif from the Lycian Nappes. In the Rupelian the Kale-Tavas basin is already active (Fig. 6.22). In this basin thick alluvial-fan conglomerates derived both from the Lycian Nappes and the Menderes Massif were deposited along a down-to-the-south normal fault system marking the northern basin margin (Akgün & Sözbilir, 2001). Other structural data indicate that the basins of the southern Menderes Massif (like the Kale-Tavas basin) formed by extension along similar normal faults systems (Çemen et al., 2006). Petrologic analysis of the basin-fill succession indicates invariably an unroofing sequence, i.e. the detrital provenance transition from the Lycian Nappes to the Menderes basement rock units (Bozkurt & Satir, 2000; Yilmaz et al., 2000; Sözbilir, 2002). This indicates that before the complete exhumation of the Menderes, there was an effective collapse of the previous Tauride orogen. The Lycian Nappes were originally covering the Menderes Massif and then, due to extension and uplift of the Menderes, collapsed generating a series of gravity thrusts which were the response to extensional rather than compressional movements.

### 6.4.4 Early Miocene

Two contrasting tectonic regimes characterize the geological evolution of the eastern Mediterranean region during the Miocene: (i) toward the west extension is predominant in the Aegean and peri-Aegean domains, including final exhumation of the Menderes Massif; (ii) toward the east compression is predominant along the Arabia-Eurasia collisional front. (e.g. Bozkurt, 2007; Brun & Faccenna, 2008; Burchfiel et al., 2008; Gessner et al., 2011)

Our thermochronologic data indicate that during Early Miocene time the Menderes Massif began its cooling. The paleogeographic reconstruction of Barrier & Vrielynck (2008) for the early Burdigalian (20-17 My) is in agreement with our results and represents the massif as an exposed highland (Fig. 6.23). Thanks to this uplift the southward transport of the Lycian Nappes continues, producing the partial covering of the Bey Dağlari Basin. The exhumation of the Menderes Massif is not an isolated event: Miocene extension is spread over a wide area (e.g. Bozkurt, 2007; Cavazza et al., 2009).

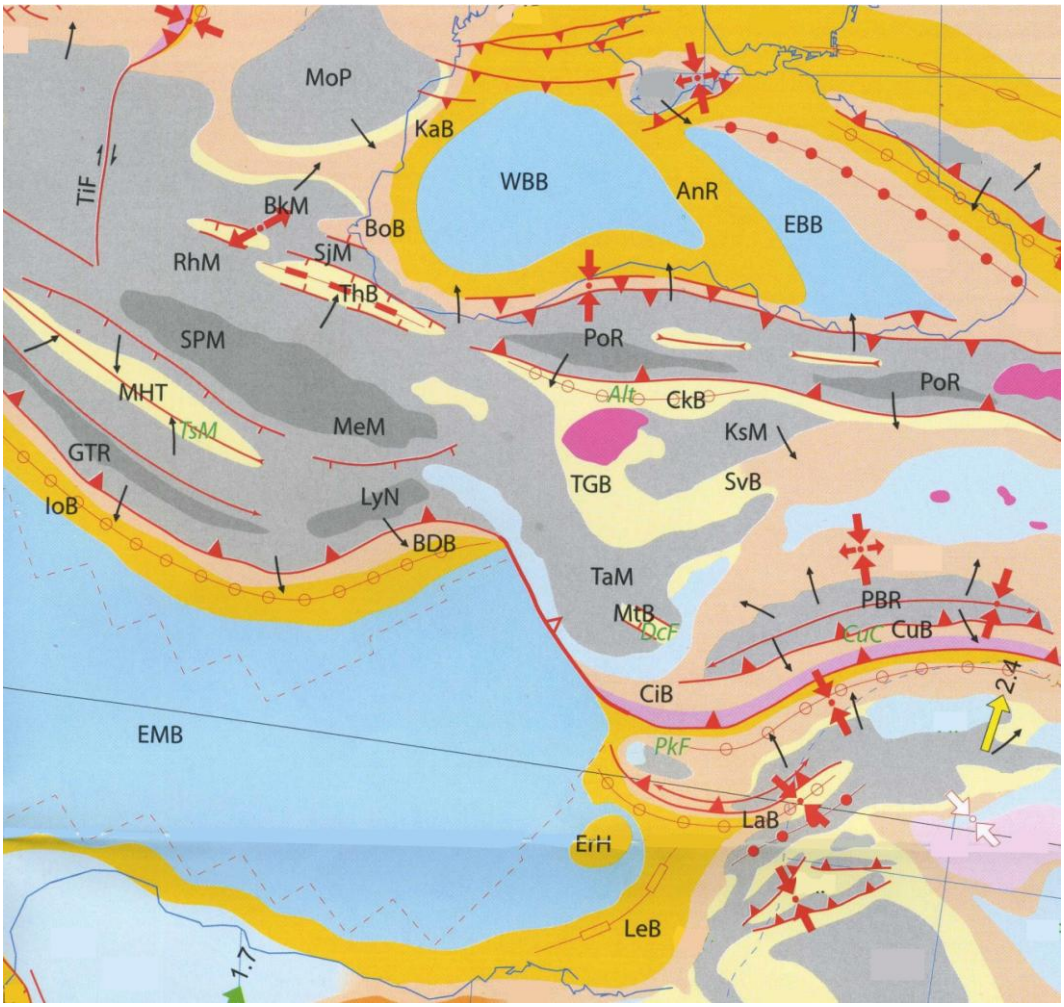


**Fig. 6.23 – Paleotectonic map of the Middle East in the early Burdigalian (20 - 17 My) (from Barrier & Vrielynck, 2008, mod.). Alt – Altintas Formation; AnR – Andrusov Ridge; BDB – Bey Dağlari Basin; BkM – Balkan Massif; BoB – Bourgas Basin; CkB – Çankiri Basin; CiB – Cilicia Basin; CuB – Cüngüs Basin; CuC – Cüngüs Complex; DcF – Derincay Formation; EBB – Eastern Black Sea Basin; EMB – East Mediterranean Ridge; ErH – Erathostenes High; GTR – Gavrovo-Tripolitza Ridge; IoB – Ionian Basin; KaB – Kamchia Basin; KsM – Kirşehir Massif; LeB – Levant Basin; LyN – Lycian Nappes; MeM – Menderes Massif; MHT – Meso-Hellenic Trough; MoP – Moesian Platform; MtB – Mut Basin; PBR – Pütürge-Bitlis Range; PkF – Pakhna Formation; PoR – Pontides Range; RhM – Rhodopes Massif; SjM – Strandja Massif; SPM – Serbo-Pelagonian Massif; SvB – Sivas Basin; TaM – Taurus Massif; TGB – Tuz-Gölü Basin; ThB – Thrace Basin; TiF – Timok Fault; TsM – Tsotyli Molasse; WBB – Western Black Sea Basin.**

As to the Alanya region, this period is characterized by subsidence in the Cilicia-Adana basin which separates the Alanya Massif –exhumed earlier- and the "proto-Cyprus" region (Aksu et al., 2005; Cosentino et al., 2012). Thanks to the continued convergence between Arabia and Eurasia, a new subduction zone began its activity offshore Cyprus to the south of the Mamonia mélange. Although this compressive regime in the northern portion of the "proto-island" the sedimentation

continues, as testified by the Pakhna Formation which overlies unconformably the Lefkara Formation. Furthermore during the early to mid-Miocene, the ophiolitic terrain of the Troodos was uplifted, as indicated in the map as exposed low land.

### 6.4.4 Late Miocene

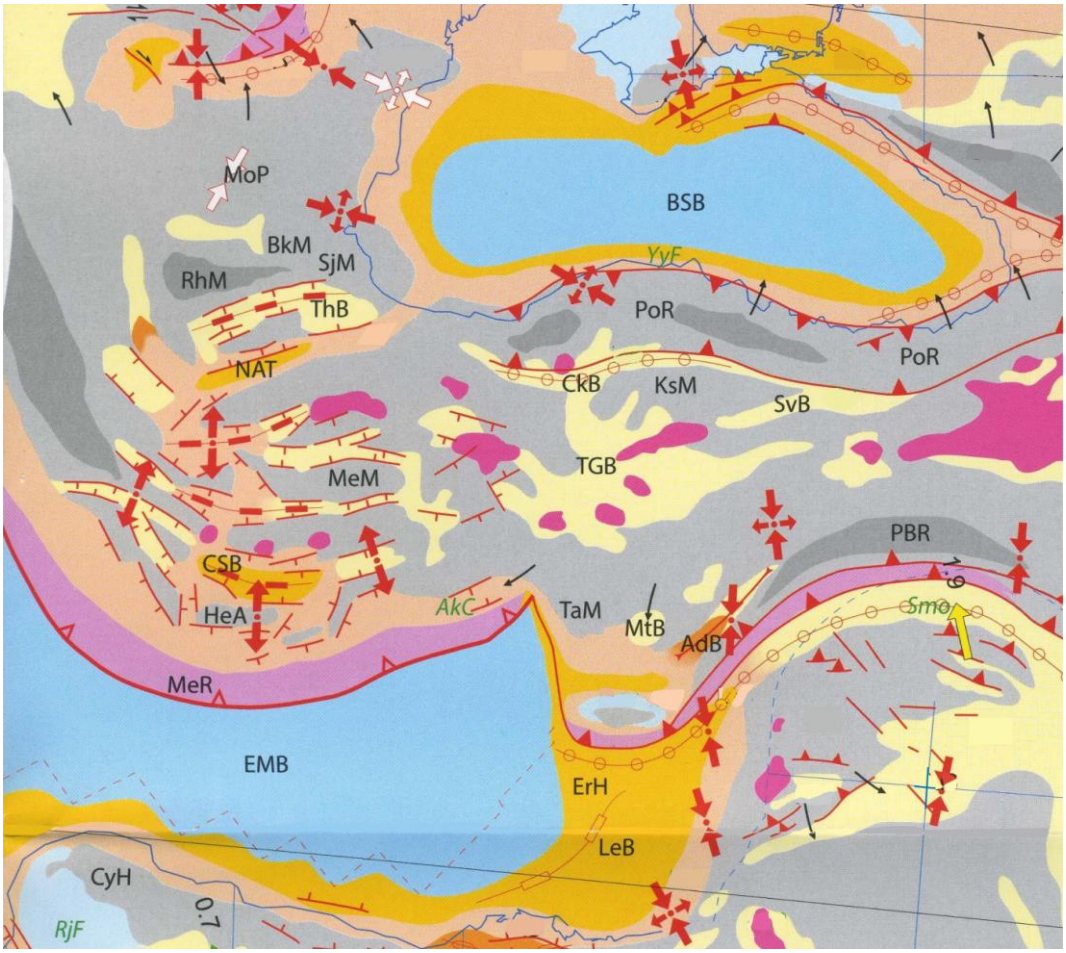


**Fig. 6.24 – Paleotectonic map of the Middle East in the Tortonian (11.6 – 7.2 My) (from Barrier & Vrielynck, 2008, mod.). AdB – Adana Basin; AkC – Aksu Conglomerate; BSB – Black Sea Basin; CkB – Çankiri Basin; CSB – Cretan Sea Basin; CyH – Cyrenaica High; EMB – East Mediterranean Ridge; ErH – Erathostenes High; HeA – Hellenic Arc; KsM – Kirşehir Massif; LeB – Levant Basin; MeM – Menderes Massif; MeR – Mediterranean Ridge; MoP – Moesian Platform; MtB – Mut Basin; NAT – North Aegean Trough; PBR – Pütürge-Bitlis Range; PoR – Pontides Range; RhM – Rhodopes Massif; SjM – Strandja Massif; SvB – Sivas Basin; TaM – Taurus Massif; TGB – Tuz-Gölü Basin; ThB – Thrace Basin.**

The Late Miocene represents the final stage of the tectonic evolution of the eastern Mediterranean region. What clearly characterizes this time is the final extensional regime which will culminate with the genesis of the Aegean sea. The Cretan Sea

basin and the Cordilleran-type metamorphic core complex of the Cyclades were added to the previous extensional structure like the Thrace basin. South to the Cretan sea basin the existence of the Mediterranean Ridge testifies that, despite the extension due to the slab roll-back, there is still subduction (e.g. Lister et al., 1984; Le Pichon et al., 2002; Jolivet & Brun, 2010)

According to all the low-temperature thermochronometric ages available in the literature, this extensional regime continues to involve the Menderes Massif. It is in fact during this time the exhumation of the Central Metamorphic Core Complex along the symmetrical detachments of Gediz and Büyük took place.

The intense mechanical coupling between Arabia and Eurasia characterizes the eastern Mediterranean region during this time (Okay et al., 2010). This compressional regime left the Alanya region *sensu stricto* largely unaffected whereas to the east the Adana basin was deformed by compressional structures (Aksu et al., 2005). The prolonged collision between Arabia and Africa will eventually produce the exhumation of the Pütürge-Bitlis Range (Okay et al., 2010) which is shown as an exposed highland in Fig. 6.24.

Chapter VII

# CONCLUSIONS

The eastern Mediterranean region is a complex area whose study is crucial for understanding the geological evolution of a large sector of the Alpine domain. In this dissertation, three key areas –the Menderes Massif, the Alanya Massif, and southern Cyprus– were chosen for thermochronological study in order to better constrain the main evolution phases of the region.

In the Menderes Massif, based on the determination of AFT ages in its southern and northeastern parts, it was possible to determine that the last significant episode of cooling/exhumation took place between the Late Oligocene and the mid-Miocene (Tab. 5.1; Fig. 5.1). These new results agree with those available in literature for these regions (Buscher et al., 2013; Gessner et al., 2001a, 2013; Ring et al., 2003; Thomson & Ring, 2006). By compiling a summary map showing AFT ages distribution over the entire massif, it was possible to subdivide the massif in two different regions. North and south of the two main detachments delimiting the central Menderes Massif, the age distribution range between the Late Oligocene and the Middle Miocene. In the central Menderes Massif the AFT ages are younger, ranging between the Late Miocene and the Pliocene. This difference is interpreted as the consequence of a two-step structural evolution: exhumation focused first along the border of the massif while its central portion was exhumed later. This model for the exhumation of the Menderes Massif can be constrained in several ways. For example, the T-t paths obtained from the inverse modeling of our AFT ages all points to a relatively fast cooling between the Late Oligocene and the Middle Miocene (Figs. 5.3 – 5.10). Cooling appears to be faster in the southern part of the massif rather than to the north, probably because of the asymmetrical geometry of the detachments controlling the exhumation of the lower plate. Thermal modelings for the central part of the massif from other works also recognized the second exhumation phase (Gessner et al., 2001a; Ring et al., 2003). The second phase of cooling/exhumation can be further constrained by the different ages of the detachments that mark the northern and the central part of the massif. The Simav (northern) detachment is radiometrically dated at ca. 20 My, and the detachment delimiting the northern part of the central Menderes Massif (Gediz) is dated at ca. 10 My (Işık et al. , 2003; Buscher et al., 2013). Therefore the radiometric age suggest that the Gediz detachment (central) is younger than the Simav (northern) and this could be the evidence of the response for the continuation of the extensional regime

in whole region. The results of this study are consistent with the interpretation of the Menderes Massif as a substantially symmetric tectonic exhumation.

This dissertation presents the first low-temperature thermochronometric determinations ever obtained from the Alanya Massif, consistently indicating a mid-Oligocene age of cooling/exhumation for the rocks of the Antalya and Alanya nappes. The origin of these nappes is still actively debated. Several authors (e.g. Robertson et al., 2012a) agree that the Alanya nappes were originally located along the southern margin of an 'Alanya ocean' to the south of the Tauride carbonate platform. Due to a first phase of northward subduction in the Late Cretaceous, the Alanya Nappes were subjected to HP/LT metamorphism. A subsequent collision-related, northward backthrusting during the Paleocene-Early Eocene –likely resulting from the final closure of the İzmir–Ankara–Erzincan ocean to the north– determined the present-day structural juxtaposition of these nappes over the Antalya complex. Based on metamorphic-grade correlations and structural-stratigraphic considerations, Çetinkaplan et al. (2014) proposed an alternative interpretation grouping the Alanya nappes with the Bitlis-Pütürge Massif to the east to form a coherent microcontinent. The northern margin of this microcontinent was partially subducted and then exhumed in the Late Paleocene thus forming Alanya nappes. According to this interpretation, compression-driven exhumation occurred between the Paleocene and the Eocene.

Despite their limited number, the apatite fission-track data from the Alanya Massif presented in this dissertation point to a significant, previously unrecognized, phase of cooling/exhumation during the Oligocene which must be incorporated in the paleotectonic reconstructions of the area and are relevant to larger scale paleogeographic reconstructions. At this early stage in the structural analysis of the Alanya Massif and the surrounding regions it is not possible to define whether the Oligocene cooling episode developed in an overall stress regime of syn-collisional compression or post-collisional extension. For the time being, we tentatively favour the interpretation of the mid-Oligocene cooling episode as the result of exhumation driven by extension. This is in view of the overall transition from a compressional (Eocene) to an extensional (?Oligocene-Miocene) regime recognizable over the entire Aegean and peri-Aegean region (see discussion in Chapter VI).

Due to the scarcity of apatite crystals, AFT analysis from the island of Cyprus gave no results and we performed instead (U-Th)/He analysis on more common

zircon crystals obtained from Late Cretaceous trondhjemite of the Troodos Massif igneous succession and from Triassic sandstones of the Mamonia Complex. Comparison of our ZHe results with preexisting U-Pb radiometric data points to a cooling of the Troodos plagiogranites from 900° C (the closure temperature of the U-Pb geochronometer) at 92-90 My (Mukasa & Luden, 1987) to 180° C (the closure temperature of the ZHe geochronometer) at 70-65 My (this dissertation) in a relatively short time span ranging approximately between 20 and 27 My. Such cooling could be either (i) an effect of the normal magmatic cooling of the plagiogranites or (ii) a result of exhumation (see Chapter VI for a discussion of these two hypotheses). ZHe results from the Triassic clastics enclosed within the mélange of Mamonia Complex indicate that such rock units never reached the closure temperature of the ZHe radiometric system, thus retaining the Paleozoic signature of a previous sedimentary cycle.

The results obtained in this dissertation from tectonically diverse areas such as the Menderes Massif, the Alanya Massif and southern Cyprus can be framed together by considering larger scale paleotectonic reconstructions such as those of Barrier & Vrielynck (2008). From this viewpoint, the overall progressive transition from Eocene compression to ?Oligocene-Miocene extension in the Aegean and peri-Aegean region is reflected in the low-temperature thermochronological record of the Menderes and Alanya massifs. The results from the Menderes Massif are in line with a substantial *corpus* of published data; those from the Alanya Massif point to a previously unrecognized episode of mid-Oligocene cooling/exhumation and deserve further investigation. Our efforts in Cyprus gave quantitatively modest results in the face of a considerable investment in terms of time and resources. In spite of this, the few analytical data obtained from the Troodos intrusives and the Mamonia mélange are worthy further attention.

# REFERENCES


Akbayram, K., Okay, A. I., Satir, M. & Topuz, G., 2009. *New U-Pb, Pb-Pb and Rb-Sr ages from northwest Turkey: Early Cretaceous continental collision in the Western Pontides*. In: 2nd International Symposium on the Geology of the Black Sea, Abstract Book, pp. 11–12.

Akkök, R., 1983. *Structural and metamorphic evolution of the northern part of the Menderes massif: new data from the Derbent area and their implication for the tectonics of the massif.* The Journal of Geology, Volume 91, pp. 342-350.

Akgün, F. & Sözbilir, H., 2001. *A palynostratigraphic approach to the SW Anatolian molasse basin: Kale-Tavas molasse and Denizli molasse*. Geodinamica Acta Volume 14, pp. 71-93.

Akıman, O., Erler, A., Göncüoğlu, M. C., Güleç, N., Geven, A., Türeli, T. K. & Kadıoğlu, Y. K., 1993. *Geochemical characteristics of granitoids along the western margin of the Central Anatolian Crystalline Complex and their tectonic implications*. Geological Journal, Volume 28, pp. 371-382.

Aksu, A. E., Calon, T. J., Hall, J., Mansfield, S. & Yaşar, D., 2005. *The Cilicia-Adana basin complex, Eastern Mediterranean: Neogene evolution of an active fore-arc basin in an obliquely convergent margin.* Marine Geology, Volume 221, pp. 121-159.

Altherr, R., Kreuzer, H., Wendt, I., Lenz, H., Wagner, G. A., Keller, J. et al., 1982. *A Late Oligocene/Early Miocene high temperature belt in the anti-cycladic crystalline complex (SE Pelagonian, Greece).* Geological Journal, Volume 23, pp. 97–164.

Altiner, D., Koçyiğit, A., Farinacci, A., Nicosia, U. & Conti, M. A., 1991. *Jurassic, Lower Cretaceous stratigraphy and paleogeographic evolution of the southern part of northwestern Anatolia*. Geologica Romana, Volume 28, pp. 13-80.

Altunkaynak, Ş., 2007. *Collision-driven slab break-off magmatism in northwestern Anatolia, Turkey*. Journal of Geology, Volume 115, pp. 63-82.

Anderson, E.M., 1942. *The Dynamics of Faulting and Dyke Formation with Application to Britain.* Edinburgh, Scotland, Oliver and Boyd, 191 p.

Andreucci, B., 2013. *Thermochronology of the Polish and Ukrainian Carpathians.* PhD thesis, University of Padua, Italy.

Andriessen, P. A. M., Boelrijk, N. A. I. M., Hebeda, E. H., Priem, H. N. A., Verdurmen, E. A. T. & Vershure, R. H., 1979. *Dating the events of metamorphism and granitic magmatism in the Alpine orogen of Naxos (Cyclades, Greece).* Contribution to Mineralogy and Petrology, Volume 69, pp. 215-225.

Armijio, R., Meyer, B., Hubert, A. & Barka, A., 1999. *Westward propagation of the North Anatolian Fault into the northern Aegean; timing and kinematics.* Geology, Volume 27, pp. 267-270.

Ashworth, J. R. & Evirgen, M. M., 1984. *Garnet and associated minerals in the southern margin of the Menderes Massif, southwest Turkey*. Geological Magazine, Volume 121, pp. 323-337.

Avigad, D., 1990. *The geodynamic evolution of the Cycladic massif (Aegean sea, Greece) – a contribution to the study of continental collision.* PhD Thesis, Hebrew University.

Avigad, D. & Garfunkel, Z., 1991. *Uplift and exhumation of high pressure metamorphic terrains: The example of the Cyclades blue-schist belt.* Tectonophysics, Volume 188, pp. 357–372.

Aydin, Y., 1974. *Etude pétrographique et géochimique de la partie centrale du Massif d'Istranca (Turquie)* [Ph.D. thesis]: Nancy, France, Université de Nancy, pp. 131.

Barbarand, J., Carter, A., Wood, I. & Hurford, T., 2003. *Compositional and structural control of fission-track annealing in apatite*. Chemical Geology, Volume 198, pp. 107–37.

Barka, A. A., 1992. *The North Anatolian fault zone.* Annual Tectonicae VI, Special Issue, pp. 164-195.

Baroz, F., 1979. *Etude géologique dans le Pentadaktylos et la Mesaoria (Chypre Septentrionale)*. Published Docteur D'Etat Thesis. Université de Nancy France, vols. 1 & 2.

Barrier, E. & Vrielynck, B., 2008. *Paleotectonic maps of the Middle East, atlas of 14 maps*. Commission de la carte géologique du Monde.

Bernet, M., Zattin, M., Garver, J. I., Brandon, M. T., & Vance, J. A., 2001. *Steady-state exhumation of the European Alps*. Geology, Volume 29, pp. 35-38.

Bernoulli, D., de Graciansky, P. C. & Monod, O., 1974. *The extension of the Lycian Nappes (SW Turkey) into the southeastern Aegean Islands.* Eclogae Geologicae Helvetiae, Volume 67, pp. 39-90.

Bingöl, E., Delaloye, M. & Ataman, G., 1982. *Granitic intrusions in western Anatolia: a contribution to the geodynamic study of this area.* Eclogae Geologicae Helvetiae, Volume 75, pp. 437–446.

Blake, M. C., Jr., Bonneau, M., Geyssant, J., Kienast, J.R., Lepvrier, C., Maluski, H. & Papanikolaou, D., 1981. *A geological reconnaissance of the Cycladic blueschist belt, Greece.* Geological Society of America Bulletin. Volume 92, No. 5, pp. 247-254.

Block, L. & Royden, L. H., 1990, *Core complex geometries and regional scale flow in the lower crust.* Tectonics, Volume 9, pp. 557–567.

Bloomer, S. H., Taylor, B., MacLeod, C. J., Stern, R. J., Fryer, P., Hawkins, J. W., & Johnson, L., 1995. *Early arc volcanism and the ophiolite problem: a perspective from drilling in the western Pacific*. Active margins and marginal basins of the western Pacific, 1-30.

Blumenthal, M. M., 1951. *Researches géologiques dans le Taurus occidental dans l'arrière-pays d'Alanya.* Public mineral research exploring institute Turkey, D5, pp. 134.

Bonev, N., Spikings, R., Moritz, R., & Marchev, P., 2010. *The effect of early Alpine thrusting in late-stage extensional tectonics: Evidence from the Kulidzhik nappe and the Pelevun extensional allochthon in the Rhodope Massif, Bulgaria.* Tectonophysics, Volume 488, pp. 256-281.

Bonneau, M., 1982. *Evolution géodynamique de l'arc égéen depuis le Jurassique Supérieur jusqu'au Miocéne.* Bulletin de la Société Géologique de France, Volume 7, pp. 229-242.

Bonneau, M. & Kienast, J. R., 1982. *Subduction, collision et schistes bleus: exemple de l'Egée, Gréce.* Bulletin de la Société Géologique de France, Volume 7, pp. 785-791.

Bonneau, M., Geyssant, J. & Lepvrier, C., 1978. *Tectonique alpine dans le massif d'Attique-Cyclade (Grèce): plis couches kilométriques dans l'ike de Naxos, consequences.* Revue de Geologie Dynamique et de Geographie Physique, Volume 20, pp. 109-122.

Bonneau, M., Kienast, J. R., Lepvrier, C., & Maluski, H., 1980. *Tectonique et metamorphisme haut pression d'age eocene dan les Hellenides: exemple de l'ile de Syros (Cyclades, Grece)*. Comptes Rendus de l'Académie des Sciences Paris, Volume 191, pp. 171-174.

Boztuğ, D., Tichomirowa, M. & Bombach, K., 2007. *207Pb - 206Pb single-zircon evaporation ages of some granitoid rocks reveal continent-oceanic island arc collision during the Cretaceous geodynamic evolution of the central Anatolian crust, Turkey*. Journal of Asian Earth Sciences, Volume 31, pp. 71–86.

Bozkurt, E., 2007. *Extensional v. contractional origin for the southern Menderes shear zone, SW Turkey: Tectonic and metamorphic implications.* Geological Magazine, Volume 144, pp. 191–210.

Bozkurt, E. & Oberhänsli, R., 2001. *Menderes Massif (Western Turkey): structural, metamorphic and magmatic evolution – a synthesis.* International Journal of the Earth Sciences, Volume 89, pp. 679-708.

Bozkurt, E., & Park, G. R., 1994. *Southern Menderes massif: An incipient metamorphic core complex in western Anatolia, Turkey.* Journal of the Geological Society of London, Volume 151, p. 213–216.

Bozkurt, E. & Satir, M., 2000. *The southern Menderes Massif (western Turkey): geochronology and exhumation history.* Geological Journal, Volume 35, pp. 285-296.

Bozkurt, E., Park, R. G. & Winchester, J. A., 1993. *Evidence against the core/cover interpretation of the southern sector of the Menderes Massif, west Turkey*. Terra Nova, Volume 5, pp. 445-451.

Bozkurt, E., Park, G., Loos, S. & Reischmann, T., 2001. *Discussion on the evolution of the Southern Menderes Massif in SW Turkey as revealed by zircon dating.* Journal of the Geological Society London, Volume 158, pp. 393–395.

Brandon, M. T., & Fellin, M. G., 2012. *Zetagev1.* Matlab script.

Braun, J., Van der Beek, P. & Batt, G., 2006. *Quantitative Thermochronology: Numerical Methods for the Interpretation of Thermochronological Data.* Cambridge University Press, Cambridge, New York.

Brown, S. A., & Robertson, A. H., 2003. *Sedimentary geology as a key to understanding the tectonic evolution of the Mesozoic–Early Tertiary Paikon Massif, Vardar suture zone, N Greece*. Sedimentary Geology, Volume 160, pp. 179-212.

Brown, S. A., & Robertson, A. H., 2004. *Evidence for Neotethys rooted within the Vardar suture zone from the Voras Massif, northernmost Greece*.Tectonophysics, Volume 381, pp. 143-173.

Brun, J. P. & Faccenna, C., 2008. *Exhumation of high-pressure rocks driven by slab rollback.* Earth and Planetary Science Letters, Volume 272, pp. 1-7.

Brun, J. P. & van den Driessche, J., 1994. *Extensional gneiss domes and detachment fault systems—Structure and kinematics.* Bulletin de la Société Géologique de France, Volume 165, pp. 519–530.

Brunn, J. H., de Graciansky, P. C., Gutnic, M., Juteau, T., Lefèvre, R., Marcoux, J., Monod, O. & Poisson, A., 1970. *Structures majeures et correlations stratigraphiques dans les Taurides occidentals.* Bulletin de la Société Géologique de France, Volume 12, pp. 515-556.

Buck, W. R., 1991. *Modes of continental lithospheric extension*. Journal of Geophysical Research, Volume 96, p. 20,161–20,178.

Buick, I. S., 1991. *Mylonitic fabric development on Naxos.* Journal of Structural Geology, Volume 13, pp. 643–655.

Burchfiel, B. C., Nakov, R., Dumurdzanov, N., Papanikolaou, D., Tzankov, T., Serafimovski, T., & Nurce, B., 2008. *Evolution and dynamics of the Cenozoic tectonics of the South Balkan extensional system*. Geosphere, Volume 4, pp. 919-938.

Buscher, J. T., Hampel, A., Hetzel, R., Dunkl I., Glotzbach, C., Struffert, A., Akal, C. & Rätz, M., 2013. *Quantifying rates of detachment faulting and erosion in the central Menderes Massif (western Turkey) by thermochronology and cosmogenic $^{10}$Be.* Journal of the Geological Society, London, Volume 170, no.4, pp. 669-683.

Buğfaycioğlu, Ç., 2004. *Tectono-metamorphic evolution of the northern Menderes massif: evidence from the horst between Gördes and Demirci basins (west Anatolia, Turkey).* PhD thesis, The graduate school of natural and applied sciences, middle east technical university, Ankara.

Calon, T. J., Aksu, A. E. & Hall, J., 2005a. *The Oligocene–Recent evolution of the Mesaoria Basin (Cyprus) and its western marine extension, Eastern Mediterranean*. Marine Geology, Volume 221, pp. 95–120.

Calon, T. J., Aksu, A. E. & Hall, J., 2005b. *The Neogene evolution of the Outer Latakia Basin and its extension into the Eastern Mesaoria Basin (Cyprus), Eastern Mediterranean*. Marine Geology, Volume 221, pp. 61–94.

Candan, O., 1995. *Menderes masifinde kalinti granulit fasiyesi metamorfizmasi* (in Turkish with English abstract). Turkish Journal of Earth Sciences, Volume 4, pp. 35-55.

Candan, O., Dora, O. Ö., Oberhänsli, R., Oelsner, F. C. & Dürr, S., 1997. *Blueschists relics in the Mesozoic series of the Menderes massif and correlation with Samos Island, Cyclades.* Schweizerische Mineralogische Und Petrographische Mitteilungen, Volume 77, pp.95-99.

Candan, O., Dora, O Ö, Oberhänsli, R., Çetinkaplan, M., Partzsch, J. H. & Dürr, S., 1998. *Pan-African high-pressure metamorphism in the Precambrian basement of the Menderes massif, Western Anatolia, Turkey.* Abstract 3th International Turkish Geological Symposium, p.275.

Candan, O., Dora, O. Ö., Oberhänsli, R., Çetinkaplan, M., Partzsch, J., Warkus, F. & Dürr, S., 2001. *Pan-African high-pressure metamorphism in the Precambrian basement of the Menderes massif, western Anatolia, Turkey.* International Journal of Earth Science, Volume 89, pp. 793-807.

Candan, O., Çetinkaplan, M., Oberhänsli, R., Rimmelé, G. & Akal, C., 2005. *Alpine high-P/low-T metamorphism of the Afyon Zone and implications for the metamorphic evolution of Western Anatolia, Turkey*. Lithos, Volume 84, pp. 102-124.

Candan, O., Koralay, O. E., Akal, C., Kaya, O., Oberhänsli, R., Dora, O. Ö., Konak, N. & Chen, F., 2011. *Supra-Pan-African unconformity between core and cover series of the Menderes Massif/Turkey and its geological implications.* Precambrian Research, Volume 184, pp. 1-23.

Carlson, W. D., Donelick, R. A. & Ketcham, R. A., 1999. *Variability of apatite fission-track annealing kinetics I: Experimental results*. Am. Mineral. 84, 1213–23.

Cavazza, W., Federici, I., Okay, A. I. & Zattin, M., 2012. *Apatite fission-track thermochronology of the Western Pontides (NW Turkey).* Geological Magazine, Volume 149, pp. 133-140.

Cavazza, W., Okay, A.I., & Zattin, M., 2009. *Rapid early-middle Miocene exhumation of the Kazdag metamophic core complex (Western Anatolia).* International Journal of Earth Sciences, Volume 98, pp. 1935–1947.

Cavazza, W., Roure, F., Spakman, Stampfli, G.M., & Ziegler, P.A., eds., 2004. *The TRANSMED Atlas: the Mediterranean Region from Crust to Mantle*. Heidelberg, Springer-Verlag, 141 pp. + CD-ROM.

Chapman, D. S., & Furlong, K. P., 1992. *Thermal state of the continental lower crust*. Continental lower crust, Volume 23, pp. 179-199.

Chatalov, G. A., 1988. *Recent developments in the geology of the Strandzha Zone in Bulgaria.* Bulletin of the Technical University of İstanbul, Volume 41, pp. 433-465.

Chen, F., Siebel, W., Satir, M., Terzioğlu, N. & Saka, K., 2002. *Geochronology of the Karadere basement (NW Turkey) and implications for the geological evolution of the İstanbul Zone.* International Journal Earth Sciences, Volume 91, pp. 469-481.

Chorowicz, J., P., Luxey, N., Lyberis, J., Carvalho, J. F., Parrot, T., Yürür, N., Gündoğdu, 1994. *The Mara Triple Junction (southern Turkey) based on digital elevation model and satellite imagery interpretation*. Journal of Geophysical Research, Volume 99, pp. 20, 225-20,242.

Collins, A. C., Gessner, K., Ring, U., & Güngör, T., 2002. *SHRIMP geochronology of granitoid rocks in the southern Anatolide Belt, western Turkey*. Geological Society of America Abstracts with Programs, Volume 34, p. 250.

Collins, A. S. & Robertson, A. H. F., 1997. *Lycian mélange, southwestern Turkey: An emplaced Late Cretaceous accretionary complex.* Geology, Volume 25, pp. 255-258.

Collins, A. S. & Robertson, A. H. F., 1998. *Processes of Late Cretaceous to Late Miocene episodic thrust-sheet translation in the Lycian Taurides, southwest Turkey.* Journal of the Geological Society, London, Volume 155, pp. 759-772.

Collins, A. S. & Robertson, A. H. F., 1999. *Evolution of the Lycian Allochthonous, western Turkey, as a north-facing Late Paleozoic to Mesozoic rift and passive continental margin.* Geological Journal, Volume 34, pp. 107-138.

Collins, A. S. & Robertson, A. H. F., 2003. *Kinematic evidence for Late Mesozoic–Miocene emplacement of the Lycian Allochthonous over the Western Anatolide Belt, SW Turkey.* Geological Journal, Volume 38, pp. 295–310.

Coney, P. J., 1974. *Structural analysis of the Snake Range "décollement," east-central Nevada.* Geological Society of America Bulletin, Volume 88, pp. 1237–1250.

Constantinou, G., 1980. *Metallogenesis associated with the Troodos ophiolite*. In Panayiotou, A. (ed.), *Ophiolites: Proceedings of the International Symposium, Cyprus,* 1979. Cyprus Geological Survey Department, pp. 663-674.

Cosentino, D., Schildgen, T. F., Cipollari, P., Faranda, C., Gliozzi, E., Hudàčkovà, N., Lucifora, S. & Strecker, M. R., 2012. *Late Miocene surface uplift of the southern margin of the Central Anatolian plateau, Central Taurides, Turkey.* Geological Society of America Bulletin, Volume 124, pp. 133-145.

Crowley, K. D., Cameron, M. & Schaefer, R. L., 1991. *Experimental studies of annealing etched fission tracks in fluorapatite*. Geochimica et Cosmochimica Acta, Volume 55, pp. 1449–1465.

Cyr, A. J., Granger, D. E., Olivetti, V., & Molin, P., 2010. *Quantifying rock uplift rates using channel steepness and cosmogenic nuclide–determined erosion rates: Examples from northern and southern Italy*. Lithosphere, Volume 2, pp. 188-198.

Çağlayan, M. A., Öztürk, Z., Sav, H., & Akat, U., 1980. *Menderes Masifi güneyine ait bulgular va yaptisal yorum.* Jeoloji Mühendisligi, Volume 10, pp. 9–19.

Çemen, I., Catlos, E. J., Göğüs, O. & Ozerdem, C., 2006. *Postcollisional extensional tectonics and exhumation of the Menderes Massif in the Western Anatolia extended terrane, Turkey.* Geological Society of America Special Paper, Volume 409, pp. 353-379.

Çetinkaplan, M., Pourteau, A., Candan, O., Koralay, E. O., Oberhänsli, R., Okay, A. I., Kozlu, H. & Chen, F., 2015. *P-T-t evolution of Eclogite/Blueschist Facies Metamorphism in Alanya Massif: Time and Space Relations with HP Event in Bitlis Massif, Turkey.* (2014).

Damon, P. E., Kulp, J. L., 1957. *Determination of radiogenic helium in zircon by stable isotope dilution technique.* American Geophysical Union Transactions, Volume 38, pp. 945-953.

Dannat, C., 1997. *Geochemie, Geochronologie und Nd- Sr-Isotopie der granitoiden Kerngneise des Menderes Massivs, SW-Türkei.* Ph.D. Thesis, Mainz, Germany, Johannes Gutenberg University, 120 p.

Dannat, C. & Reischmann, T, 1998. *Geochronological, geochemical and isotopic data on granitic gneisses from the Menderes Massif, SW Turkey*. 3rd International Turkish Geological Symposium, Middle East Technical University, Ankara, pp. 282.

Dannat, C. & Reischmann, T., 1999. *Single zircon ages of migmatites from the Menderes Massif, SW Turkey*. European Union of Geosciences Journal of Conference Abstracts, Volume 4, p. 805.

de Graciansky, P. C., 1966. *Le massif cristallin du Menderes (Taurus occidental Asie Mineure). Un exemple possible de vieux socle granitique remobilize.* Revue de Geologie Dynamique et de Geographie Physique, Volume 8, pp. 289-306.

de Graciansky, P. C., 1972. *Recherches géologiques dans le Taurus Lycien occidental*. D. S. Thesis, Universitè Paris Sud, Orsay, 571 pp.

Di Vincenzo, G., Carosi, R., & Palmeri, R., 2004. *The relationship between tectono-metamorphic evolution and argon isotope records in white mica: constraints from in situ 40Ar–39Ar laser analysis of the Variscan basement of Sardinia.* Journal of Petrology, Volume 45, pp. 1013-1043.

Dean,W. T., Martin, F., Monod, O., Demir, O., Rickards, R. B., Bultynck, P. & Bozdogan, N., 1997. *Lower Paleozoic stratigraphy, Karadere–Zirze area, Central Pontides.* In, Göncüoğlu, M. C. & Derman, A. S. (eds) *Early Palaeozoic Evolution in NW Gondwana*, pp. 32– 8. Turkish Association of Petroleum Geologists, Special Publication, Volume 3.

Dean, W. T., Monod, O., Rickards, R. B., Demir, O. & Bultynck, P., 2000. *Lower Paleozoic stratigraphy and paleontology, Karadere-Zirze area, Pontus Mountains, northern Turkey*. Geological Magazine, Volume 137, pp. 555-582.

Delaloye, M. & Bingöl, E., 2000. *Granitoids from western and northwestern Anatolia: Geochemistry and modeling of geodynamic evolution*. International Geology Review, Volume 42, pp. 241-268.

Dercourt, J., Zonenshain, L. P., Ricou, L. E., Kuzmin, V. G., Le Pichon, X., Knipper, A. L., Grandjacquet, C., Sbortshikov, I. M., Geyssant, J., Lepvrier, C., Pechersky, D. H., Boulin, J., Sibuet, J. C., Savostin, L. A., Sorokhtin, O., Westphal, M., Bazhenov, M. L., Laurer, J. P. & Biju-Duval, B., 1986. *Geological evolution of the Tethys belt from the Atlantic to the Pamir since the Lias*. Tectonophysics, Volume 123, pp.241-315.

Dercourt, J., Ricou, L. E. & Vrielynck, B., 1993. *Atlas Tethys Paleoenvironmental Maps.* Paris, Gauthier-Villars.

Demirtaşli, E., Turhan, N., Bilgin, A. Z. & Selim, M., 1984. *Geology of the Bolkar Mountains.* In Tekeli, O. & Göncüoğlu, M. C. (eds.) *Geology of the Taurus Belt. Proceedings International Symposium on the Geology of the Taurus Belt, Ankara, Turkey*. Mineral Resources and Exploration Institute of Turkey, pp. 12–141.

Dewey, J. F., Hempton, M. R., Kidd, W. S. F., Şaroğlu, F. T. & Şengör, A. M. C., 1986. *Shortening of continental lithosphere: the neotectonics of Eastern Anatolia—a young collision zone*. Geological Society, London, Special Publications, Volume 19, pp. 1-36.

Dilek, Y., Shallo, M. & Furnes, H., 2005. *Rift-drift, seafloor spreading, and subduction tectonics of Albanian ophiolites.* International Geology Review, Volume 47, pp. 147–176.

Dilek, Y., Furnes, H. & Shallo, M., 2007. *Suprasubduction zone ophiolite formation along the periphery of Mesozoic Gondwana*. Gondwana Research, Volume 11, pp. 453-475.

Donelick, R. A., Ketcham, R. A. & Carlson, W. D., 1999. *Variability of apatite fission-track annealing kinetics II: Crystallographic orientation effects.* The American Mineralogist, Volume 84, pp. 1224–1234.

Donelick, R. A., O'Sullivan, P. B. & Ketcham, R. A., 2005. *Apatite Fission-Track Analysis*. In Reiners, P. W. & Ehlers, T. A. (eds.), *Low Temperature Thermochronology: Techniques, Interpretations, and Applications*. Reviews in Mineralogy and Geochemistry, Volume 58, pp. 49-94.

Dora, O. Ö., Candan, O., Dürr, S. H. & Oberhänsli, R., 1995. *New evidence of the geotectonic evolution of the Menderes Massif, Proceedings of International Earth Sciences Colloquium on the Aegean Region: Güllük (Turkey)*. Volume 1, pp. 53–72.

Doutsos, T., Koukouvelas, L., Poulimenos, G., Kokkalas, S., Xypolias, P. & Skourlis, K., 2000. *An exhumation model for the south Peloponnesus, Greece.* International Journal of Earth Science, Volume 89, pp. 350-365.

Ducloz, C., 1972. *The Geology of the Bellapais-Kyrthrea Area of the Central Kyrenia Range*. Cyprus Geological Survey Bulletin, Volume 6, 75 pp.

Dumitru, T. A., 2000. *Fission-Track Geochronology*. In: Noller, J.S, Sowers, J.M. & Lettis, W.R. (eds.), *Quaternary Geochronology: Methods and Applications*. American Geophysical Union, Washington, DC, pp. 131-155.

Dürr, S., 1975. *Über Alter und geotektonische Stellung des Menderes Kristallins/SW Anatolien und seine Äquivalente in der Mittleren Aegean*. Habilitation thesis, University of Marburg.

Dürr, S., Altherr, R., Keller, J., Okrusch, M. & Seidel, E., 1978. *The median Aegean crystalline belt: stratigraphy, structure, metamorphism, magmatism.* In Closs, H., Roeder, D. & Schmidt, K. (eds.), *Alps, Apennine, Hellenides*, pp. 455-477, Stuttgart: Schweizerbartsche Verlagsbuchhandlung.

Ehlers, T. A., 2005. *Crustal thermal processes and the interpretation of thermochronometer data.* In Reiners, P. W. & Ehlers, T. A. (eds.) *Low-Temperature Thermochronology: Techniques, Interpretations, and Applications.* Reviews in Mineralogy and Geochemistry, Volume 58, pp. 315-350.

Ehlers, T. A. & Farley, K. A., 2003. *Apatite (U-Th)/He thermochronometry: methods and applications to problems in tectonic and surface processes.* Earth and Planetary Science Letters, Volume 206, pp. 1-14.

Elitok, Ö., 2012. *Geology, geochemistry and geodynamic implications of the mafic–ultramafic rocks from the northern part of the Antalya Complex, SW Turkey*. Tectonophysics, Volume 568, pp. 335-356.

Elmas, A. & Yiğitbaş, E. 2001. *Ophiolite emplacement by strike-slip tectonics between the Pontide Zone and the Sakarya Zone in northwestern Anatolia, Turkey.* International Journal of Earth Sciences Volume 90, pp. 257–69.

Elmas, A. & Yiğitbaş, E. 2005. *Comment on "Tectonic evolution of the Intra-Pontide suture zone in the Armutlu Peninsula, NW Turkey" by Robertson and Ustaömer.* Tectonophysics, Volume 405, pp. 213–21.

Engel, M. & Reischmann, T., 1997. *Geochronological data on granitoids gneiss from Paros, Greece, obtained by single zircon PB evaporation.* Terra Nova, Volume 9, p. 463.

England, P. & Molnar, P., 1990. *Surface uplift, uplift of rocks, and exhumation of rocks.* Geology. 18, 1173–77.

Erdoğan, B., 1990. *Tectonic relations between İzmir-Ankara Zone and Karaburun belt*. Bulletin of the Mineral Research and Exploration of Turkey, Volume 110, pp. 1-15.

Erdoğan, B. & Güngör, T., 1992. *Stratigraphy and tectonic evolution of the Northern Margin of the Menderes Massif.* Turkish Association of Petroleum Geologists Bulletin, Volume 4, pp. 9–34.

Erdoğan, B. & Güngör, T., 2004. *The problem of the core-cover boundary of the Menderes Massif and an emplacement mechanism for regionally extensive gneissic granites, western Anatolia (Turkey).* Turkish Journal of Earth Sciences, Volume 13, pp. 15–36.

Eren, Y., 2001. *Polyphase Alpine deformation at the northern edge of the Menderes–Taurus block, North Konya, Central Turkey*. Journal of Asian Earth Sciences, Volume 19, pp. 737–749.

Erler, A. & Göncüoğlu, M. C., 1996. *Geologic and tectonic setting of Yozgat batholith, northern central Anatolian crystalline complex, Turkey.* International Geology Review, Volume 38, pp. 714-726.

Ersoy, S., 1993. *The geological setting of the tectonic units situated on the SW Anatolia (Turkey) and their geodynamic development.* Bulletin of the Geological Society of Greece, Volume 28, pp. 617-628.

Farley, K. A., 2000. *Helium diffusion from apatite: General behavior as illustrated by Durango fluorapatite.* Journal of Geophysical Research, Volume 105, pp. 2903–2914.

Farley, K. A., 2002. (*U-Th)/He dating: techniques, calibrations, and applications.* In Noble Gases in Geochemistry and Cosmochemistry. Reviews in Mineralogy and Geochemistry, Volume 47, pp. 819–44.

Farley, K. A., Wolf, R. W., Silver, L. T., 1996. *The effects of long alpha-stopping distances on (U-Th)/He ages*. Geochimica et Cosmochimica Acta, Volume 60, pp. 4223-4229.

Fassoulas, C., Kilias, A. & Mountrakis, D., 1994. *Post-nappe stacking extension and exhumation of HP/LT rocks in the island of Crete, Greece.* Tectonics, Volume 13, pp. 127–138.

Faure, M., Bonneau, M. & Pons, J., 1991. *Ductile deformation and syntectonic granite emplacement during the late Miocene extension of the Aegean (Greece).* Bulletin de la Société de Géologique de France. Volume 162, pp. 3-12.

Fechtig, H. & Kalbitzer, S., 1966. *The diffusion of argon in potassium-bearing solids.* In Schaeffer, O. A. & Zahringer, J. (eds.), *Potassium-Argon Dating.* Springer, Berlin, pp. 68–106.

Federici, I., Cavazza, W., Okay, A. I., Beyssac, O., Zattin, M., Corrado, S. & Dellisanti, F., 2010. *Thermal Evolution of the Permo-Triassic Karakaya Subduction-accretion Complex Between the Biga Peninsula and the Tokat Massif (Anatolia).* Turkish Journal of Earth Sciences, Volume 19, pp. 409-429.

Feenstra, A., 1985. *Metamorphism of bauxites on Naxos, Greece.* Ph. D. Thesis, Rijksuniversiteit Utrecht, Geologica Ultraiectina, Volume 39, pp. 206.

Fitzgerald, P. G., Baldwin, S. L., Webb, L. E. & O'Sullivan, P. B., 2006. *Interpretation of (U-Th)/He single grain ages from slowly cooled crustal terranes: A case study from the Transantarctic Mountains of southern Victoria Land*. Chemical Geology, Volume 225, pp. 91–120.

Fitzgerald, P. G., Sorkhabi, R. B., Redfield, T. F., & Stump, E., 1995. *Uplift and denudation of the central Alaska Range: A case study in the use of apatite fission track thermochronology to determine absolute uplift parameters*. Journal of Geophysical Research: Solid Earth (1978–2012), Volume 100, pp. 20175-20191.

Fleischer, R. L. & Price, P. B., 1964. *Techniques for geological dating of minerals by chemical etching of fission fragment tracks*. Geochimica et Cosmochimica Acta, Volume 28, pp. 1705-1714.

Fleischer, R.L., Price, P.B. & Walker, R.M., 1965. *Effects of temperature, pressure, and ionization of the formation and stability of fission tracks in minerals and glasses.* Journal of Geophysical Research, Volume 70, pp. 1497–1502.

Fleischer, R.L., Price, P.B. & Walker, R.M., 1975. *Nuclear Tracks in Solids*. University of California Press, Berkely, pp. 605.

Flowers, R. M., Ketcham, R. A., Shuster, D. L. & Farley, K. A., 2009. *Apatite (U-Th)/He thermochronometry using a radiation damage accumulation and annealing model*. Geochimica et Cosmochimica Acta, Volume 73, pp. 2347–2365.

Foster, D. A., & John, B. E., 1999. *Quantifying tectonic exhumation in an extensional orogen with thermochronology: Examples from the southern Basin and Range Province*. In Ring, U., Brandon, M., Lister, G. S. & Willett, S. D., eds., *Exhumation Processes: Normal Faulting, Ductile Flow, and Erosion.* Geological Society of London Special Publication, Volume 154, pp. 356–378.

Foster, D. A., Harrison, T. M., Miller, C. F. & Howard, K. A., 1990. *The $^{40}Ar/^{39}Ar$ thermochronology of the eastern Mojave Desert, California, and adjacent western Arizona, with implications for the evolution of metamorphic core complexes.* Journal of Geophysical Research, Volume 95, pp. 20,005.

Foster, D. A., Gleadow, A. J. W., Reynolds, S. J. & Fitzgerald, P. G., 1993. *Denudation of metamorphic core complexes and the reconstruction of the transition zone, west-central Arizona: Constraints from apatite fission track thermochronology.* Journal of Geophysical Research, Volume 98, pp. 2167–2185.

Fytikas, M., Innocenti, F., Manetti, P., Mazzuoli, R., Peccerillo, A. & Villari, L., 1984. *Quaternary evolution of volcanism in the Aegean region.* Geological Society Special Publication, Volume 17, pp. 987-699.

Galbraith, R.F., 1981, *On statistical models for fission track counts: Math*. Geology, Volume 13, pp. 471–488.

Galbraith, R. F., 1990. *The radial plot; graphical assessment of spread in ages*. Nuclear Tracks and Radiation Measurement, Volume 17, pp. 207–214.

Gallagher, K., Brown, R. & Johnson, C., 1998. *Fission track analysis and its applications to geological problems*. Annual Review Earth Planet Science, Volume 26, pp. 519-572.

Gass, I. G., 1990. *Ophiolites and ocean lithosphere. Ophiolites Oceanic Crustal Analogues.* In: Malpas, J., Moores, E. M., Panayiotou, A. & Xenophontos, C. (eds.) *Proceedings of the Symposium, 'Troodos 1987'*. Geological Survey Department, Cyprus, 1–10.

Gautier, P., Brun, J. P., & Jolivet, L., 1993. *Structure and kinematics of Upper Cenozoic extensional detachment on Naxos and Paros (Cyclades Islands, Greece)*. Tectonics, Volume 12, pp. 1180–1194.

Gautier, P. & Brun, J. P., 1994. *Ductile crust exhumation and extensional detachments in the central Aegean (Cyclades and Evia islands)*. Geodinamica Acta, Volume 7, pp. 57-85.

Gautier, P., Brun, J. P., Moriceau, R., Sokoutis, D., Martinod, J. & Jolivet, L., 1999. *Timing, kinematics and cause of Aegean extension: a scenario based on a comparison with simple analogue experiments.* Tectonophysics, Volume 315, pp. 31-72.

Gemici, U., 2004. *Impact of acid mine drainage from the abandoned Halikoy mercury mine (Western Turkey) on surface and groundwaters.* Bulletin of Environmental Contamination and Toxicology, Volume 72, pp. 482–489.

Gessner, K., Collins, A. S., Ring, U., & Güngör, T., 2004. *Structural and thermal history of poly-orogenic basement: U-Pb geochronology of granitoids rocks in the southern Menderes Massif, Western Turkey.* Journal of the Geological Society London, Volume 161, pp. 93–101.

Gessner, K., Gallardo, L. A., Markwitz, V., Ring, U. & Thomson, S. N., 2013. *What caused the denudation of the Menderes Massif: Review of crustal evolution, lithosphere structure, and dynamic topography in southwest Turkey.* Gondwana Research, Volume 24, pp. 243-274.

Gessner, K., Piazolo, S., Güngör, T., Ring, U., Kroener, A., & Passchier, C. W., 2001a. *Tectonic significance of deformation patterns in granitoid rocks of the Menderes nappes, Anatolide Belt, Southwest Turkey*. International Journal of Earth Sciences, Volume 89, pp. 766–780.

Gessner, K., Ring, U. & Güngör, T., 2011. *Field Guide to Samos and the Menderes Massif: Along-Strike Variations in the Mediterranean Tethyan Orogen.* The Geological Society of America, Field Guide 23.

Gessner, K., Ring, U., Johnson, C., Hetzel, R., Passchier, C. W. & Güngör, T., 2001b. *An active bivergent rolling-hinge detachment system: Central Menderes metamorphic core complex in western Turkey.* Geology, Volume 29, pp. 611-614.

Gessner, K., Ring, U., Passchier, C. W. & Güngör, T., 2001c. *How to resist subduction: Evidence for large-scale out-of-sequence thrusting during Eocene collision in western Turkey.* Journal of the Geological Society of London, Volume 158, pp. 769–784.

Gessner, K., Ring, U., Passchier, C. W., Hetzel, R. & Okay, A. I., 2002. *Stratigraphic and metamorphic inversions in the central Menderes Massif; a new structural model; discussion and reply.* International Journal of Earth Sciences, Volume 91, pp. 168–172.

Gilbert, M. F. & Robertson, A. H. F. 2013. *Field relations, geochemistry and origin of the Upper Cretaceous volcaniclastic Kannaviou Formation in western Cyprus: evidence of a southerly Neotethyan volcanic arc*. In: Robertson, A. H. F., Parlak, O. & Ünlügenç, U. C. (eds) Geological Development of the Anatolian Continent and the Easternmost Mediterranean Region. Geological Society, London, Special Publications, Volume 372.

Gleadow, A. J. W., Duddy, I. R., Green, P. F. & Lovering, J. F., 1986. *Confined fission track lengths in apatite: a diagnostic tool for thermal history analysis.* Contribution to Mineralogy and Petrology, Volume 94, pp. 405-415.

Gleadow, A.J.W., Belton, D.X., Kohn, B.P. & Brown, R.W., 2002. *Fission track dating of phosphate minerals and the thermochronology of apatite*. Reviews in Mineralogy and Geochemistry, Volume 48, pp. 579-630.

Glodny, J. & Hetzel, R., 2007. *Precise U-Pb ages of syn-extensional Miocene intrusion in the central Menderes Massif, western Turkey.* Geological Magazine, Volume 144, pp. 235-246.

Green, P. F., Duddy, I. R., Gleadow, A. J. W. & Tingate, P. R., 1985. *Fission track annealing in apatite: track length measurements and the form of the Arrhenius plot.* Nuclear Tracks and Radiation Measurements, Volume 10, pp. 323–28.

Green, P. F., Duddy, I. R., Gleadow, A. J. W., Tingate, P. R., Laslett, G. M., 1986. *Thermal annealing of fission tracks in apatite: A qualitative description.* Chemical Geology, Volume 59, pp. 237-253.

Green, P. F., Duddy, I. R., Laslett, G. M., Hegarty, K. A., Gleadow, A. J. W. & Lovering, J.F., 1989. *Thermal annealing of fission tracks in apatite, 4. Quantitative modeling techniques and extension to geological timescales*. Chemical Geology (Isotope Geoscience Section), Volume 79, pp. 155–82.

Gutnic, M., Monod, O., Poisson, A. & Dumont, J. F., 1979. *Géologie des Taurides Occidentales (Turquie)*. Mémoires de la Société Géologique de France, Volume 137, pp. 1-112.

Görür, N. & Tüysüz, O., 2001. *Cretaceous to Miocene paleogeographic evolution of Turkey: implications for hydrocarbon potential*. Journal of Petroleum Geology, Volume 24, pp. 119-146.

Görür, N., Monod, O., Okay, A. I., Şengör, A. M. C., Tüysüz, O., Yiğitbaş, E., Sakinç, M. & Akkök, R., 1997. *Paleogeographic and tectonic position of the Carboniferous rocks of the western Pontides (Turkey) in the frame of the Variscan belt.* Bulletin Société Géologique de France, Volume 168, pp. 197-205.

Güngör, T. & Erdoğan, B., 2001. *Emplacement age and direction of the Lycian Nappes in the Söke-Selçuk region, western Turkey.* International Journal of Earth Sciences, Volume 89, pp. 874-882.

Gürer, F., Sanğu, E., Özburan, M., Gürbüz, A. & Sarica-Filoreau, N., 2013. *Complex basin evolution in the Gökova Gulf region: implications on the Late Cenozoic tectonics of southwest Turkey.* International Journal of Earth Science, Volume 102, pp. 2199-2221.

Gürer, F., and Yılmaz, Y., 2002. *Geology of the Ören and surrounding areas, SW Anatolia.* Turkish Journal of Earth Sciences, Volume 11, pp. 1–13.

Hagdorn, H., Göncüoğlu, M. C., 2007. *Early-Middle Triassic echinoderm remains from the Istranca Massif, Turkey*. Neues Jahrbuch für Geologie und Paläontologie, Volume 246, pp. 235-245.

Hakyemez, Y., Turhan, N., Sönmez, İ. & Sümengen, M., 2000. *Kuzey Kıbrıs Türk Cumhuriyeti'nin Jeolojisi (Geology of the Northern Cyprus Turkish Republic).* Ankara: Mineral Research and Exploration Institute of Turkey, Report, 44 pp.

Harris, N. B. W., Kelley, S. P. & Okay, A. I., 1994. *Post-collision magmatism and tectonics in northwest Turkey*. Contribution to Mineralogy and Petrology, Volume 117, pp. 241-252.

Harrison, R. W., Newell, W. L., Batihanli, H., Panayides, I., Mcgeehin, J. P., Mahan, S. A., Ozhur, A., Tsiolakis, E. & Necdet, M., 2004. *Tectonic framework and Late Cenozoic tectonic history of the northern part of Cyprus: implications for earthquake hazards and regional tectonics.* Journal of Asian Earth Sciences, Volume 23, pp. 191–210.

Hawkins, J. W., Bloomer, S. H., Evans, C. A., & Melchior, J. T., 1984. *Evolution of intra-oceanic arc-trench systems.* Tectonophysics, Volume 102, pp. 175-205.

Hawkins, J. W., 2003. *Geology of supra-subduction zones: Implications for the origin ofophiolites*. Ophiolite Concept and the Evolution of Geological Thought: Boulder, Colorado. Geological Society of America Special Paper, Volume 373, pp. 227-268.

Hayward, A. B., 1984. *Sedimentation and basin formation related to ophiolite nappe emplacement, Miocene, SW Turkey*. Sedimentary Geology, Volume 40, pp. 105-129.

Hetzel, R., Passchier, C. W., Ring, U. & Dora Ö. O., 1995a. *Bivergent extension in orogenic belts: The Menderes massif (southwestern Turkey).* Geology, Volume 23, pp. 455-458.

Hetzel, R., Ring, U., Akal, C. & Troesch, M., 1995b. *Miocene NNE-direct extensional unroofing in the Menderes Massif, southwestern Turkey.* Journal of the Geological Society of London, Volume 152, pp. 639–654.

Hetzel, R. & Reischmann, T., 1996. *Intrusion age of Pan-African augen gneisses in the southern Menderes massif and the age of cooling after Alpine ductile extensional deformation.* Geological Magazine, Volume 133, pp. 565-572.

Hetzel, R., Romer, R. L., Candan, O. & Passchier, C. W., 1998. *Geology of the Bozdağ area, central Menderes massif, SW Turkey: Pan-African basement and Alpine deformation.* Geologische Rundschau, Volume 87, pp. 394-406.

Hurford, A. J., 1990. *Standardization of fission track dating calibration: Recommendation by the Fission Track Working Group of the I.U.G.S.*

*Subcommission on Geochronology.* Chemical Geology (Isotope Geoscience Section), Volume 80, pp. 7-178.

Hurford, A. J. & Green, P. F., 1983. *The zeta age calibration of fission-track dating*. Chemical Geology (Isotope Geoscience Section), Volume 1, pp. 285-317.

İlbeyli, N., Pearce, J. A., Thirlwall, M. F. & Mitchell, J. G., 2004. *Petrogenesis of collision-related plutonis in Central Anatolia, Turkey*. Lithos, Volume 72, pp. 163-182.

İlkýşık, O. M., 1995. *Regional heat flow in western Anatolia using silica temperature estimates from thermal springs*. Tectonophysics, Volume 244, pp. 175–184.

Işık, V., & Tekeli, O., 2001. *Late orogenic crustal extension in the northern Menderes massif (western Turkey): evidences for metamorphic core complex formation*. International Journal of Earth Sciences, Volume 89, pp. 757–765.

Işık, V., Seyitoğlu, G. & Çemen, İ., 2003. *Ductile-brittle transition along the Alaşehir detachment fault and its structural relationship with the Simav detachment fault, Menderes massif, western Turkey.* Tectonophysics, Volume 374, pp. 1-18.

John, B. E. & Foster, D. A., 1993. *Structural and thermal constraints on the initiation angle of detachment faulting in the southern Basin and Range: The Chemehuevi Mountains case study.* Geological Society of America Bulletin, Volume 105, pp. 1091–1108.

Jolivet, L., 2001. *A comparison of geodetic and finite strain in the Aegean, geodynamic implications.* Earth and Planetary Science Letters, Volume 187, pp.95-104.

Jolivet, L. & Brun, J. P., 2010. *Cenozoic geodynamic evolution of the Aegean.* International Journal of Earth Sciences, Volume 99, pp. 109-138.

Jolivet, L. & Faccenna, C., 2000. *Mediterranean extension and the Africa-Eurasia collision.* Tectonics, Volume 6, pp. 1095-1106.

Jolivet, L. & Patriat, M., 1999. *Ductile extension and the formation of the Aegean sea.* In Durand, B., Jolivet, L., Horvath, F. & Séranne, M. (eds.), *The Mediterranean Basins; Tertiary Extension within the Alpine Orogen.* Special Publication Geological Society of London, pp. 427-456.

Jolivet, L., Daniel, J. M., Truffert, C. & Goffé, B., 1994a. *Exhumation of deep crustal metamorphic rocks and crustal extension in back-arc regions.* Lithos, Volume 33, pp. 3-30.

Jolivet, L., Brun, J. P., Gautier, P., Lallemant, S. & Patriat, M., 1994b. *3-D kinematics of extension in the Aegean from the Early Miocene to the Present, insight from the ductile crust.* Bulletin de la Société Géologique de France, Volume 165, pp. 195-209.

Jolivet, L., Faccenna, C., Goffé, B., Mattei, M., Rossetti, F., Brunet, C., Storti, F., Funiciello, R., Cadet, J. P., D'Agostino, N. & Parra T., 1998. *Midcrustal shear zones in postorogenic extension: Example from the northern Tyrrhenian Sea.* Journal of Geophysical Research, Volume 103, pp. 123-160.

Jolivet, L., Rimmelé, G., Oberhänsli, R., Goffé, B. & Candan, O., 2004. *Correlation of syn-orogenic tectonic and metamorphic events in the Cyclades, the Lycian nappes and the Menderes massif. Geodynamic implications.* Bulletin de la Société géologique de France, Volume 175, pp. 217-238.

Keay, S., Lister, G. & Buick, I., 2001. *The timing of partial melting, Barrovian metamorphism and granite intrusion in the Naxos metamorphic core complex, Cyclades, Aegean sea, Greece.* Tectonophysics, Volume 342, pp. 275-312.

Kelling, G., Gökçen, S. L., Floyd, P. A. & Gökçen, N., 1987. *Neogene tectonics and plate convergence in the eastern Mediterranean: new data from southern Turkey*. *Geology,* Volume 15, pp. 425–429.

Kempler, D., 1998. *Eratosthenes Seamount: The Possible Spearhead Of Incipient Continental Collision In The Eastern Mediterranean*. In, Robertson, A.H.F., Emeis, K.-C., Richter, C., and Camerlenghi, A. (eds), *Proceedings of the Ocean Drilling Program*, Scientific Results, Vol. 160

Kempler, D. & Garfunkel, Z., 1994. *Structures and kinematics in the northeastern Mediterranean: a study of an irregular plate boundary*. Tectonophysics, Volume 234, pp. 19–32.

Ketcham, R. A., 2005. *Forward and inverse modeling of low-temperature thermochronometry data.* In Reiners, P. W. & Ehlers, T. A. (eds.) *Low-Temperature Thermochronology: Techniques Interpretations, and Applications.* Reviews in Mineralogy and Geochemistry, Volume 58, pp. 275-314.

Ketcham, R. A., 2009. *HeFTy version 1.6.7*. Manual.

Ketcham, R. A., Donelick, R. A. & Carlson, W. D., 1999. *Variability of apatite fission-track annealing kinetics III: Extrapolation to geological time scales.* The American Mineralogist, Volume 84, pp. 1235-1255.

Ketcham, R. A., Carter, A. C., Donelick, R. A., Barbarand, J. & Hurford, A. J., 2007. *Improved modeling of fission-track annealing in apatite*. The American Mineralogist, Volume 92, pp. 799–810.

Kilias, A., Falalakis, G., & Mountrakis, D., 1999. *Cretaceous–Tertiary structures and kinematics of the Serbomacedonian metamorphic rocks and their relation to the exhumation of the Hellenic hinterland (Macedonia, Greece)*.International Journal of Earth Sciences, Volume 88, pp. 513-531.

Kilias, A., Fassoulas, C. & Mountrakis, D., 1994. *Tertiary extension of continental crust and uplift of Psiloritis metamorphic core complex in the central part of the Hellenic arc (Crete, Greece).* Geologische Rundschau, Volume 83, pp. 417–430.

Kilias, A., Falalakis, G., Sfeikos, A., Papadimitriou, E., Vamvaka, A. & Gkarlaouni, C., 2013. *The Thrace basin in the Rhodope province of NE Greece – A tertiary supradetachment basin and ts geodynamic implications.* Tectonophysics, Volume 595-596, pp. 90-105.

Koralay, O. E., Satir, M., & Dora, O. Ö, 1998. *Geochronologic evidence of Triassic graben for episodic two-stage extension in western Turkey.* Third International Turkish Geology Symposium, Middle East Technical University, Ankara, 31 August-4September 1998, Abstarcts, p. 285.

Koralay, O. E., Satir, M., & Dora, O. Ö., 2001. *Geochemical and geochronological evidence for Early Triassic calc-alkaline magmatism in the Menderes Massif, western Turkey.* International Journal of Earth Sciences, Volume 89, pp. 822–835.

Köksal, S., Romer, R. L., Göncüoğlu, M. & Toksoyköksal, F., 2004. *Timing of postcollisional H-type to A-type granitic magmatism: U-Pb titanite ages from the Alpine central Anatolian granitoids (Turkey)*. International Journal of Earth Sciences, Volume 93, pp. 974-989.

Krohe, A., & Mposkos, E., 2002. *Multiple generations of extensional detachments in the Rhodope Mountains (northern Greece): evidence of episodic exhumation of high-pressure rocks*. Special Publication-Geological Society of London, Volume 204, pp. 151-178.

Kruckenberg, S. C., Whitney, D. L., Teyssier, C., Fanning, M. & Dunlap, W. J., 2008. *Paleocene-Eocene migmatite crystallization, extension, and exhumation in the hinterland of the northern Cordillera: Okanogan dome, Washington, USA.* Geological Society of America Bulletin, Volume 120, pp. 912–929.

Kurt, H., Demirbag, E., & Kuscu, I., 1999. *Investigation of submarine active tectonism in the Gulf of Gökova, southwest Anatolia–southeast Aegean sea, by multi-channel seismic reflection data.* Tectonophysics, Volume 305, pp. 477–496.

Laslett, G. M., Green, P. F., Duddy, I. R., & Gleadow, A. J. W., 1987. *Thermal annealing of fission tracks in apatite 2. A quantitative analysis.* Chemical Geology (Isotope Geoscience Section), Volume 65, pp. 1– 13.

Le Pichon, X., Chamot-Rooke, N., Lallemant, S. L., Noomen, R. & Veis, G., 1995. *Geodetic determination of the kinematics of Central Greece with respect to Europe: implications for eastern Mediterranean tectonics.* Journal of Geophysical Research, Volume 100, pp. 12675-12690.

Le Pichon, X., Lallemant, S. J., Chamot-Rooke, N., Lemeur, D. & Pascal, G., 2002. *The Mediterranean Ridge backstop and the Hellenic nappes.* Marine Geology, Volume 186, pp. 111-125.

Lefèvre, R., 1967. Un nouvel element de la géologie du Taurus Lycien: les nappes d'Antalya (Turquie). Comptes rendus de l'Académie des *sciences* de Paris, Volume D265, pp. 1365-1368.

Lips, A. L. W., Cassard, D., Sözbilir, H., Yilmaz, H. & Wijbrans, J. R., 2001. *Multistage exhumation of the Menderes massif, western Anatolia (Turkey).* International Journal of Earth Science, Volume 89, pp. 781-792.

Lips, A. L. W., White, S. H. & Wijbrans, J. R., 1998. *$^{40}Ar/^{39}Ar$ laserprobe direct dating of discrete deformational events: a continuous record of early Alpine tectonics in the Pelagonian Zone, NW Aegean area, Greece.* Tectonophysics, Volume 298, pp. 133-153.

Lister, G. S. & Baldwin, S., 1993. *Plutonism and the origin of metamorphic core complexes.* Geology, Volume 21, pp. 607-610.

Lister, G. S., Banga, G. & Feenstra, A., 1984. *Metamorphic core complexes of cordilleran type in the Cyclades, Aegean sea, Greece.* Geology, Volume 12, pp. 221-225.

Loos, S. & Reischmann, T., 1999. *The evolution of the southern Menderes massif in SW Turkey as revealed by zircon datings.* Journal of Geological Society London, Volume 156, pp. 1021-1030.

Malavieille, J., Guihot, P., Costa, S., Lardeaux, J. M. & Gardien, V., 1990. *Collapse of thickened Variscan crust in the French Massif Central: Mont Pilat extensional shear zone and St. Etienne Late Carboniferous basin.* Tectonophysics, Volume 177, pp. 139–149.

Maluski, H., Costa, S. & Echtler, H., 1991. *Late Variscan tectonic evolution by thinning of earlier thickened crust. An $^{40}Ar$-$^{39}Ar$ study of the Montagne Noire, southern Massif Central, France.* Lithos, Volume 26, pp. 287– 304.

Makris, J., Ben-Avraham, Z., Behle, A., Ginzburg, A., Giese, P. & Steinmetz, L. 1983. *Seismic reflection profiles between Cyprus and Israel and their interpretation.* Geophysical Journal of the Royal Astronomical Society, Volume 75, pp. 575–591.

Malpas, J., Xenophontos, C. &Williams, D. 1992. *The Ayia Varvara Formation of S.W. Cyprus, a product of complex collisional tectonics.* Tectonophysics, Volume 212, pp. 193–211.

Malpas, J., Calon, T. & Squires, G. 1993. *The development of a Late Cretaceous microplate suture zone in SW Cyprus*. In: Prichard, H., Alabaster, T., Harris, N. B. & Neary, C. R. (eds) *Magmatic Processes and Plate Tectonics*. Geological Society, London, Special Publications, Volume 76, pp. 177–195.

McCay, G. A., Robertson, A. H., Kroon, D., Raffi, I., Ellam, R. M. & Necdet, M., 2013. *Stratigraphy of Cretaceous to Lower Pliocene sediments in the northern part of Cyprus based on comparative 87Sr/86Sr isotopic, nannofossil and planktonic foraminiferal dating.* Geological Magazine, Volume 150, pp. 333-359.

McClusky, S., Balassanian, S., Barka, A., Demir, C., Ergintav, S., Georgiev, I., Gurkan, O., Hamburger, M., Hurst, K., Kahle, H., Kastens, K., Kekelidze, G., King, R., Kotzev, V., Lenk, O., Mahmoud, S., Mishin, A., Nadariya, M., Ouzounis, A., Paradissis, D., Peter, Y., Prilepin, M., Reilinger, R., Sanli, I., Seeger, H. Tealeb, A., Toksöz, M. N. & Veis, G., 2000. *Global Positioning System constraints on plate kinematics and dynamics in the eastern Mediterranean and Caucasus.* Journal of Geophysical Research: Solid Earth (1978–2012), Volume 105, 5695-5719.

McKenzie, D., 1972. *Active tectonics in the Mediterranean region.* Geophysical Journal of the Royal Astronomical Society, Volume 30, pp. 109-185.

McKenzie, D., Nimmo, F., Jackson, J. A., Gans, P. B. & Miller, E. L., 2000. *Characteristics and consequences of flow in the lower crust.* Journal of Geophysical Research, Volume 105, pp. 11,029–11,046.

Metcalf, R. V. & Shervais, J. W., 2008. *Suprasubduction-zone ophiolites: Is there really an ophiolite conundrum?* Geological Society of America Special Papers, Volume 438, pp. 191-222.

Monod, O. 1977. *Récherches Géologique dans les Taurus occidental au sud de Beyşehir (Turquie)*. Thèse de Doctorat de Science, Université de Paris-Sud, Orsay, France.

Moore, W. J., McKee, E. H. & Akinci, Ö., 1980. *Chemistry and chronology of plutonic rocks in the Pontid Mountains, northern Turkey*. European Copper Deposits, pp. 209-216.

Moores, E. M. & Vine, F. J., 1971. *The Troodos Massif, Cyprus and other ophiolites as oceanic crust: evaluation and implication.* Philosophical Transactions Royal Society of London, Volume A268, pp. 433-466.

Morag, N., Haviv, I. & Katzir, Y., 2013. *From ocean depths to mountain tops: uplift of the Troodos Massif (Cyprus) constrained by (U-Th)/He thermochronology and geomorphic analysis.* Conference presentation abstract.

Morris, A., Creer, K. M. & Robertson, A. H. F., 1990. *Paleomagnetic evidence for clockwise rotations related to dextral shear along the Southern Troodos Transform Fault, Cyprus.* Earth and Planetary Science Letters, Volume 99, pp. 250-262.

Mountrakis, D., 1982. *Emplacement of the Kastoria ophiolite on the western edge of the Internal Hellenides.* Ofioliti, Volume 7, pp. 397–406.

Mountrakis, D., 1986. *The Pelagonian zone in Greece: A polyphase-deformed fragment of the Cimmerian Continent and its role in the geotectonic evolution of the Eastern Mediterranean.* Journal of Geology, Volume 94, pp. 335–347.

Mountrakis, D., Kilias, A., & Zouros, N., 1993. *Kinematic analysis and Tertiary evolution of the Pindos-Vourinos ophiolites (Epirus–Western Macedonia, Greece).* Bulletin of the Geological Society of Greece, Volume 28, pp. 111–124.

Mountrakis, D, 2006. *Tertiary and Quaternary tectonics of Greece.* Geological Society of America Special Papers, Volume 49, pp. 125-136.

Mukasa, S. B. & Ludden, J. N., 1987. *Uranium–lead ages of plagiogranites from the Troodos ophiolite, Cyprus, and their tectonic significance*. Geology, Volume 1, pp. 825–828.

Mussallam, K., & Jung, D., 1986. *Petrology and geotectonic significance of salic rocks preceding ophiolites in the Eastern Vardar Zone, Greece*. Tschermaks mineralogische und petrographische Mitteilungen, Volume 35, pp. 217-242.

Naeser, C. W., 1967. *The use of apatite and sphene for fission track age determinations.* Bulletin of Geological Society of America, Volume 78, pp. 1523-1526.

Naeser, N.D. & McCulloh, T.H., 1989. *Thermal History of Sedimentary Basins: Methods and Case Histories.* Springer-Verlag, Berlin.

Oberhänsli, R, Candan, O., Dora, O. Ö. & Dürr, S., 1997. *Eclogites within the Menderes Crystalline Complex, western Turkey, Anatolia.* Lithos, Volume 41, pp.135-150.

Oberhänsli, R., Monié, P., Candan, O., Warkus, F. C., Partzsch, J. & Dora, O. Ö., 1998a. *The age of blueschist metamorphism in the Mesozoic cover series of the Menderes Massif*. Schweizerische Mineralogische und Petrographische, Volume 78, pp. 309–316.

Oberhänsli, R., Partzsch, J., Çetinkaplan, M., & Candan, O., 1998b. *HP record in the Lycian Nappes (western Turkey).* Ankara, International Turkish Geology Symposium, 3rd, p. 274.

Oberhänsli, R., Partzsch, J. H., Candan, O. & Çetinkaplan, M., 2001. *First occurrence of Fe-Mg-carpholite documenting a high pressure metamorphism in metasediments of the Lycian Nappes, SW Turkey*. International Journal of Earth Sciences, Volume 89, pp. 867–873.

Oberhänsli, R., Romain, B., Candan, O., & Okay, A. I., 2012. *Dating subduction events in east Anatolia, Turkey*. Turkish Journal of Earth Sciences, Volume 21, pp. 1-17.

Okay, A. I., 1984. *Distribution and characteristics of the northwest Turkish blueschists*. In Dixon J. E. & Robertson A. H. F. (eds.), *The Geological Evolution of the Eastern Mediterranean*, Geological Society London Special Publication, Volume 17, pp. 455-466.

Okay, A. I., 1985. *Menderes Massif and the allochthonous in the region between the Bafa Lake, Muğla and Uşak (in Turkish).* Report of the Turkiye Petrolleri Anonim Ortaklığı (TPAO), no 2123.

Okay, A. I., 1989a. *Geology of the Menderes massif and the Lycian nappes south of Denizli, western Taurides.* Bulletin of the mineral research and exploration, Volume 109, pp. 37-51.

Okay, A. I., 1989b. *An exotic eclogite/blueschist slice in a Barrovian-Style metamorphic terrain, Alanya Nappes, Southern Turkey.* Journal of Petrology, Volume 30, pp. 107-132.

Okay, A. I., 1989c. *Alpine-Himalayan Blueschists.* Annual Review of Earth and Planetary Sciences, Volume 17, pp. 55-87.

Okay, A. I., 2001. *Stratigraphic and metamorphic inversions in the central Menderes massif: a new structural model.* International Journal of Earth Science, Volume 89, pp. 709-727.

Okay, A. I., 2008. *Geology of Turkey: a synopsis*. Anschnitt, Volume 21, pp. 19-42.

Okay, A. I. & Altıner, D., 2007. *A condensed Mesozoic section in the Bornova Flysch Zone: A fragment of the Anatolide-Tauride carbonate platform*. Turkish Journal of Earth Sciences, Volume 16, pp. 257-279.

Okay, A. I. & Göncüoğlu, M. C., 2004. *Karakaya Complex: a review of data and concepts.* Turkish Journal of Earth Sciences, Volume 13, pp. 77-95.

Okay, A. I. & Leven, E. J., 1996. *Stratigraphy and paleontology of the Upper Paleozoic sequence in the Pulur (Bayburt) region, Eastern Pontides.* Turkish Journal of Earth Sciences, Volume 5, pp. 145-155.

Okay, A. I. & Monié, P., 1997. *Early Mesozoic subduction in the Eastern Mediterranean: Evidence from Triassic eclogite in northwest Turkey*. Geology, Volume 25, pp. 595-598.

Okay, A. I. & Özgül, N., 1984. *HP/LT metamorphism and the structure of the Alanya Massif, Southern Turkey: an allochthonous composite tectonic sheet.* Geological Society, London, Special Publication, Volume 17, pp. 429-439.

Okay, A. I. & Şahintürk, Ö., 1997. *Geology of the Eastern Pontides.* In Robinson, A. G. (ed.), *Regional and Petroleum Geology of the Black Sea and Surrounding Region*, American Association of Petroleum Geologists (AAPG) Memoir No. 68, pp. 291-311.

Okay, A. I. & Satır, M., 2006. *Geochronology of Eocene plutonism and metamorphism in northwest Turkey: evidence for a possible magmatic arc*. Geodinamica Acta, Volume 19, pp. 251-266.

Okay, A. I. & Tüysüz, O., 1999. *Tethyan sutures of northern Turkey.* In: Durand, B., Jolivet, L., Horvath, F. & Séranne, M. (eds.), *The Mediterranean Basin: Tertiary Extension within the Alpine Orogen.* Geological Society, London, Special Publication, Volume 156, pp. 475-515.

Okay, A. I., Bozkurt, E., Satır, M., Yiğitbaş, E., Crowley, Q. G. & Shang, C. K., 2008a. *Defining the southern margin of Avalonia in the Pontides: geochronological data from the Late Proterozoic and Ordovician granitoids from NW Turkey.* Tectonophysics, Volume 461, pp. 252-264.

Okay, A. I., Monod, O. & Monié, P., 2002. *Triassic blueschists and eclogites from northwest Turkey: vestiges of the Paleo-Tethyan subduction*. Lithos, Volume 64, pp. 155-178.

Okay, A. I., Satır, M., Maluski, H., Siyako, M., Monie, P., Metzger, R. & Akyüz S., 1996. *Paleo- and Neo-Tethyan events in northwest Turkey: geological and geochronological constraints*. In Yin, A. & Harrison, M. (eds.), *Tectonics of Asia*, Cambridge University Press, pp. 420-441.

Okay, A. I., Satır, M. & Siebel, W., 2006a. *Pre-Alpide orogenic events in the Eastern Mediterranean region. European Lithosphere Dynamics.* Geological Society London Memories, Volume 32, pp. 389-405.

Okay, A. L., Satır, M., Tüysüz, O., Akyüz, S., & Chen, F., 2001. *The tectonics of the Strandja Massif: late-Variscan and mid-Mesozoic deformation and*

*metamorphism in the northern Aegean.* International Journal of Earth Sciences, Volume 90, pp. 217-233.

Okay, A.I., Satir, M., Zattin, M., Cavazza, W., & Topuz, G., 2008b. *An Oligocene ductile strike-slip zone: Uludag Massif, northwest Turkey – implications for escape tectonics.* Geological Society of America Bulletin, Volume 120, pp. 893-911.

Okay, A. I., Tüysüz, O., Satır, M., Özkan-Altiner, S., Altiner, D., Sherlock, S., & Eren, R. H., 2006b. *Cretaceous and Triassic subduction-accretion, high-pressure–low-temperature metamorphism, and continental growth in the Central Pontides, Turkey*. Geological Society of America Bulletin, Volume 118, pp. 1247-1269.

Okay, A. I., Şengör, A. M. C. & Görür, N., 1994. *Kinematic history of the opening of the Black Sea and its effect on the surrounding regions.* Geology, Volume 22, pp. 267–70.

Okay, A. I., Zattin, M., & Cavazza, W., 2010. *Apatite fission-track data for the Miocene Arabia-Eurasia collision.* Geology, Volume 38, pp. 35-38.

Ozerdem, C., Çemen, I., & Işik, V., 2002. *The Conglomerate member of the Gokceoren Formation, Ören Basin, western Turkey: Its age, sedimentology and tectonic significance*. Geological Society of America Abstracts with Programs, Volume 34, p. 250.

Özer, S., & Sözbilir, H., 2003. *Presence and tectonic significance of Cretaceous rudist species in the so-called Permo-Carboniferous Göktepe Formation, central Menderes metamorphic massif, western Turkey.* International Journal of Earth Sciences, Volume 92, pp. 397–404.

Özgül, N., 1976. *Toroslarin bazi temel jeoloji özellikleri.* Bulletin of the Geological Society of Turkey, Volume 19, pp. 65-78.

Özgül, N., 1984. *Stratigraphy and tectonic evolution of the Central Taurides*. In Tekeli, O. & Göncüoğlu, M. C. (eds.), *Geology of the Taurus Belt*, Mineral Research and Exploration Institute of Turkey, Ankara, 77-90.

Özgül, N., 1985. *The geology of the Alanya region (in Turkish with English Abstract).* In: Ketin Symposium. Geological Society of Turkey Publication, pp. 97-120.

Özkaya, I., 1990. *Origin of the allochthonous in the Lycian belt, Southwest Turkey.* Tectonophysics, Volume 177, pp. 367-379.

Parra, T., Vidal, O. & Jolivet, L., 2002. *Relation between deformation and retrogression in blueschist metapelites of Tinos Island (Greece) evidence by chlorite-mica local equilibria.* Lithos, Volume 63, pp. 41-66.

Paul, T. A. & Fitzgerald P. G.**,** 1992. *Transmission electron microscopy investigation of fission tracks in fluorapatite.* The American Mineralogist, Volume 77, pp. 336-344.

Pearce, J. A. & Robinson, P. T., 2010. *The Troodos ophiolitic complex probably formed in a subduction initiation, slab edge setting*. Gondwana Research, Volume 18, pp. 60-81.

Poisson, A., 1977. *Recherches géologiques dans les Taurides occidentals (Turquie).* Ph. D. Thesis, Universitè Paris Sud, Orsay, 795 pp.

Poisson, A., 1985. *The geological evolution of the eastern Mediterranean.* American Geological Society Special Publication, Volume 17, pp. 241-249.

Poisson, A., Guezou, J. C., Öztürk, A., İnan, S., Temiz, H., Gürsoy, H., Kavak, K. S. & Özden, S., 1996. *Tectonic setting and evolution of the Sivas basin, central Anatolia, Turkey.* International Geology Review, Volume 38, pp. 838-853.

Price, P. B. & Walker, R. M., 1963. *Fossil tracks of charged particles in mica and the age of minerals.* Journal of Geophysical Research, Volume 68, pp. 4847-4862.

Proffett, J. J., 1977. *Cenozoic geology of the Yerington District, Nevada, and implications for the nature and origin of Basin and Range faulting*. Geological Society of America Bulletin, Volume 88, pp. 247–266.

Régnier, J. L., Ring, U., Passchier, C. W., Gessner, K., & Güngör, T., 2003. *Contrasting metamorphic evolution of metasedimentary rocks from the Cine and Selimiye nappes in the Anatolide belt, western Turkey.* Journal of Metamorphic Geology, Volume 21, pp. 699–721.

Régnier, J. L., Metzger, J. E., & Passchier, C. W., 2006. *Metamorphism of Precambrian–Paleozoic schists of the Menderes core series and contact relationships with Proterozoic orthogneisses of the western Çine Massif, Anatolide belt, western Turkey.* Geological Magazine, Volume 144, pp. 67–104.

Reilinger, R. E., McClusky, S., Oral, M. B., King, R. W., Toksöz, M. N., Barka, A. A., Kinik, I., Lenk, O. & Sanli, I., 1997. *Global Positioning System measurements of present-day crustal movements in the Arabia-Africa-Eurasia plate collision zone.* Journal of Geophysical Research, Volume 102, pp. 9983-9999.

Reilinger, R., McClusky, S., Vernant, P., Lawrence, S., Ergintav, S., Cakmak, R., Ozener, H., Kadirov, F., Guliev, I., Stepanyan, R., Nadariya, M., Hahubia, G., Mahmoud, S., Sakr, K., ArRajehi, A., Paradissis, D., Al-Aydrus, A., Prilepin, M., Guseva, T., Evren, E., Dmitrotsa, A., Filikov, S. V., Gomez, F., Al-Ghazzi, R. & Karam, G., 2006. *GPS constraints on continental deformation in the Africa-Arabia-Eurasia continental collision zone and implications for the dynamics of plate interactions*. Journal of Geophysical Research, Volume 111.

Reiners, P. W., Spell, T. L., Nicolescu, S. & Zanetti, K. A., 2004. *Zircon (U-Th)/He thermochronometry: He diffusion and comparisons with 40Ar/39Ar dating.* Geochimica et Cosmochimica Acta, Volume 68, pp. 1857–1887.

Reiners, P. W. & Ehlers, T. A., 2005. *Low-Temperature Thermochronology: Techniques, Interpretations, Applications*. Reviews in Mineralogy and Geochemistry, Volume 58. Mineralogical Society of America, Geochemical Society, Chantilly, VA, pp 622.

Reiners, P. W. & Brandon, M. T., 2006, *Using Thermochronology to Understand Orogenic Erosion.* Annual Review of Earth and Planetary Sciences, Volume 34, pp. 419-466.

Reischmann, T., 1997. *Single zircon Pb/Pb dating of tectonic units from the metamorphic core complex of Naxos.* Terra Abstracts, Volume 9, p.496.

Reischmann, T., & Loos, S., 2001. *Discussion on the evolution of the Southern Menderes Massif in SW Turkey as revealed by zircon dating*. Journal of the Geological Society London, Volume 158, pp. 393–395.

Reischmann, T., Kröner, A., Todt, W., Dürr, S. & Şengör, A. M. C., 1991. *Episodes of crustal growth in the Menderes Massif, W Turkey, inferred from zircon dating.* Terra Abstracts, Volume 3, p. 34.

Rey, P. F., Vanderhaeghe, O., & Teyssier, C., 2001. *Gravitational collapse of the continental crust: Definition, regimes and modes*. Tectonophysics, Volume 342, pp. 435–449.

Rey, P. F., Teyssier, C. & Whitney, D. L., 2009a. *Crustal melting and core complex dynamics.* Geology, Volume 37, pp. 391–394.

Rey, P. F., Teyssier, C. & Whitney, D. L., 2009b. *The role of partial melting and extensional strain rates in the development of metamorphic core complexes (McMCC).* Tectonophysics, Volume 477, pp. 135–144.

Ricou, L. E., Burg, J. P., Godfriaux, I. & Ivanov Z., 1998. *Rhodope and Vardar: the metamorphic and olistostromic paired belts related to the Cretaceous subduction under Europe.* Geodinamica Acta, Volume 11, pp. 285-309.

Rimmelé, G., 2003. *Structural and metamorphic evolution of the Lycian Nappes and the Menderes massif (southwestern Turkey): geodynamics implications and correlations with the Aegean domain.* PhD thesis, Universität of Potsdam, Deutschland.

Rimmelé, G., Oberhänsli, R., Goffé, B., Jolivet, L., Candan, O. & Çetinkaplan, M., 2003. *Deformation history of the high-pressure Lycian Nappes and implications for tectonic evolution of SW Turkey*. Tectonics 22, 1007.

Rimmelé, G., Oberhänsli, R., Jolivet, L. & Goffé, B., 2001. *First structural data related to the low-grade high-pressure metamorphism in the metasediments of the Lycian nappes, SW Turkey.* European Union of Geosciences XI Journal of Conference Abstracts, p. 319.

Ring, U. & Layer, P. W., 2003. *High-pressure metamorphism in the Aegean, eastern Mediterranean: Underplating and exhumation from the Late Cretaceous until the Miocene to Recent above the retreating Hellenic subduction zone.* Tectonics, Volume 22, p. 1022.

Ring, U., Gessner, K., Güngör, T. & Passchier, C. W., 1999a. *The Menderes Massif of western Turkey and the Cycladic Massif in the Aegean – do they really correlate?* Journal of the Geological Society, London, Volume 156, pp. 3-6.

Ring, U., Laws, S. & Bernet, M., 1999b. *Structural analysis of a complex nappe sequence and late-orogenic basins from the Aegean Island of Samos, Greece.* Journal of Structural Geology, Volume 21, pp. 1575–1601.

Ring, U., Layer, P. W. & Reischmann, T., 2001a. *Miocene high-pressure metamorphism in the Cyclades and Crete, Aegean sea, Greece: evidence for large-magnitude displacement on the Cretan detachment.* Geology, Volume 29, pp. 395-398.

Ring, U., Willner, A. P., and Lackmann, W., 2001b. *Stacking of nappes with unrelated pressure-temperature paths: An example from the Menderes nappes of western Turkey.* American Journal of Science, Volume 301, pp. 912–944.

Ring, U., Thomson, S. N. & Bröcker, M., 2003. *Fast exhumation but little exhumation: The Vari detachment in the Cyclades, Greece.* Geological Magazine, Volume 159, pp. 225–228.

Ring, U., Glodny, J., Will, T. M. & Thomson, S., 2011. *Normal faulting on Sifnos and the South Cycladic detachment system, Aegean sea, Greece.* Journal of the Geological Society of London, Volume 168, pp. 751–768.

Robertson, A. H. F., 1998. *Mesozoic–Cenozoic tectonic evolution of the easternmost Mediterranean area: integration of marine and land evidence*. In Robertson, A. H. F., Emeis, K.-C., Richter K. C. & Camerlenghi A. (eds.), *Proceedings of the Ocean Drilling Program, Scientific Results,* Volume 160, pp. 723–82. College Station, Texas.

Robertson, A. H. F., 2000. *Mesozoic-Tertiary tectonic-sedimentary evolution of a south Tethyan oceanic basin and its margins in southern Turkey*. Geological Society of London Special Publication, Volume 173, pp. 97-138.

Robertson, A. H. F., 2007. *Overview of tectonic settings related to the rifting and opening of Mesozoic ocean basins in the Eastern Tethys: Oman, Himalayas and Eastern Mediterranean regions*. In: Karner, G., Manatschal, G. & Pinheiro, L. M. (eds.) *Imaging, Mapping and Modeling Continental Lithosphere Extension and Breakup*. Geological Society of London Special Publications, Volume 282, pp. 325–389.

Robertson, A. H. F. & Dixon, J. E., 1984. *Introduction: Aspects of the geological evolution of the Eastern Mediterranean.* In Dixon, J. E., and Robertson, A. H. F., eds., *The geological evolution of the Eastern Mediterranean*, Geological Society of London Special Publication, Volume 17, pp. 1–74.

Robertson, A. H. F. & Ustaömer, T. 2004. *Tectonic evolution of the Intra-Pontide suture zone in the Armutlu Peninsula, NW Turkey*. Tectonophysics, Volume 381, pp. 175–209.

Robertson, A. H. F. & Woodcock, N. H., 1979. *The Mamonia Complex, S. W. Cyprus: the evolution and emplacement of a Mesozoic continental margin.* Geological Society of America Bulletin, Volume 90, pp. 651–665.

Robertson, A. H. F. & Woodcock, N. H., 1986. *The role of the Kyrenia Range lineament, Cyprus, in the geological evolution of the Eastern Mediterranean area.* In Reading H. G., Watterson J. & White S. H. (eds.), *Major Crustal Lineaments and their Influence on the Geological History of the Continental Lithosphere*, pp. 141–71. Philosophical Transactions of the Royal Society of London, Series A, Volume 317.

Robertson, A. H. F. & Xenophontos, C., 1993. *Development of concepts concerning the Troodos ophiolite and adjacent units in Cyprus.* In Prichard, H. M., Alabaster, T., Harris, N. B. W. & Neary, C. R. (eds.), *Magmatic Processes and Plate Tectonics*. Geological Society Special Publication, Volume 76, pp. 85-119.

Robertson, A. H. F. & Xenophontos, C., 1997. *Cyprus.* Encyclopedia of European and Asian regional geology. Springer Netherlands, pp. 160-171.

Robertson, A. H. F., Clift, P. D., Degnan, P. J. & Jones, G., 1991. *Palaeogeographical and palaeotectonic evolution of the Eastern Mediterranean Neotethys*. Palaeoceanography, Palaeoclimatology, Palaeoecology, Volume 87, pp. 289–343.

Robertson, A. H. F., Dixon, J. E. & Brown, S., 1996. *Alternative tectonic models for the Late Paleozoic–Early Tertiary development of Tethys in the Eastern Mediterranean region*. Geological Society of London Special Publication, Volume 105, pp. 239–263.

Robertson, A. H. F., Parlak, O. & Ustaömer, T., 2012a. *Overview of the Palaeozoic–Neogene evolution of Neotethys in the Eastern Mediterranean region (southern Turkey, Cyprus, Syria)*. Petroleum Geoscience, Volume 18, pp. 381–404.

Robertson, A. H. F., Parlak, O. & Ustaömer, T., 2013. *Late Paleozoic-Early Cenozoic tectonic development of Southern Turkey and the easternmost Mediterranean region: evidence from the inter-relations of continental and oceanic units.* Geological Society of London Special Publications, Volume 372, pp. 9-48.

Robertson, A. H. F., Tasli, K. & Inan, N., 2012b. *Evidence from the Kyrenia Range, Cyprus, of the northerly active margin of the Southern Neotethys during Late Cretaceous-Early Cenozoic time.* Geological Magazine, Volume 149, pp. 264-290.

Robinson, P. T. & Malpas, J., 1990. *The Troodos ophiolite of Cyprus: new perspectives on its origin and emplacement.* In Malpas, J., Moores, E. M., Panayiotou, A. & Xenophontos, C. (eds.), *Ophiolites: Oceanic Crustal Analogues.* Cyprus Geological Survey Department, pp. 13-36.

Satir, M. & Friedrichsen, H., 1986. *The origin and evolution of the Menderes Massif, W-Turkey: A rubidium/strontium and oxygen isotope study.* Geologische Rundschau, Volume 75, pp. 703-714.

Schaer, J. P., Reimer, G. M., & Wagner, G. A., 1975. *Actual and ancient uplift rate in the Gotthard region, Swiss Alps: a comparison between precise levelling and fission-track apatite age*. Tectonophysics, Volume 29, pp. 293-300.

Schermer, E. R., 1993. *Geometry and kinematics of continental basement deformation during the Alpine orogeny, Mt. Olympus region, Greece.* Journal of Structural Geology, Volume 15, pp. 571-591.

Schuiling, R. D., 1962. *On petrology, age and structure of the Menderes migmatite complex (SW Turkey).* Bulletin of the Mineral Research and Exploration Institute of Turkey, Volume 58, pp. 71-84.

Seidel, E., Kreuzer, H. & Harre, W., 1982. *A Late Oligocene–Early Miocene high pressure belt in the External Hellenides.* Geologisches Jahrbuch, Volume E23, pp. 165–206.

Seyitoğlu, G. & Scott, B., 1996. *The cause of N-S extensional tectonics in Western Turkey: Tectonic escape vs Back-arc spreading vs orogenic collapse*. Journal of Geodynamics, Volume 22, pp. 145-153.

Seyitoğlu, G., Scott, B. C. & Rundle, C. C., 1992. *Timing of Cenozoic extensional tectonics in west Turkey.* Journal of the Geological Society, Volume 149, pp. 533-538.

Seyitoğlu, G., Tekeli, O., Çemen, I., Sen, S. & Işik, V., 2002. *The role of the flexural rotation/rolling hinge model in the tectonic evolution of the Alaşehir graben, western Turkey.* Geological Magazine, Volume 139, pp. 15-26.

Seyitoğlu, G., Işik, V. & Çemen, I., 2004. *Complete Tertiary exhumation history of the Menderes massif, western Turkey: An alternative working hypothesis*. Terra Nova, Volume 16, pp. 358–364.

Seymen, İ., 1983. *Tectonic features of the Kaman Group in comparison with those of its neighbouring formations around Tamadağ (Kaman-Central Anatolian Crystalline Complex).* Türkiye Jeoloji Kurumu Bülteni, Volume 26, pp. 89-98.

Sherlock, S., Kelley, S. P., Inger, S., Harris, N. & Okay, A. I., 1999. *40Ar/39Ar and Rb-Sr geochronology of high-pressure metamorphism and exhumation history of the Tavşanlı Zone, NW Turkey.* Contributions to Mineralogy and Petrology, Volume 137, pp. 46-58.

Shuster, D. L. & Farley, K. A., 2009. *The influence of artificial radiation damage and thermal annealing on helium diffusion kinetics in apatite*. Geochimica et Cosmochimica Acta, Volume 73, pp. 6183-196.

Shuster, D. L., Flowers, R. M. & Farley, K. A., 2006. *The influence of natural radiation damage on helium diffusion kinetics in apatite*. Earth and Planetary Science Letters, Volume 249, pp. 148–161.

Smith, A. G., Hynes, A. J., Menzies, M., Nisbet, E. G., Price, I., Welland, M. J. & Ferriére, J., 1975. *The stratigraphy of the Othris Mountains, Eastern Central Greece: A deformed Mesozoic continental margin sequence.* Eclogae Geologicae Helvetiae, Volume 68, pp. 463–481.

Sözbilir, H., 1997. *Stratigraphy and Sedimentology of the Tertiary Sequences in the Northeastern Denizli Province (Southwest Turkey).* PhD Thesis, Dokuz Eylül University Izmir-Turkey, 195 p.

Sözbilir, H, 2002. *Revised Stratigraphy and Facies Analysis of Paleocene-Eocene Supra-allochthonous Sediments (Denizli, SW Turkey) and Their Tectonic Significance.* Turkish Journal of Earth Sciences, Volume 11, pp. 87-112.

Sözbilir, H., Özer, S. & Sari, B. 2000. *Stratigraphy and tectonics of the Late Paleocene-Eocene supra allochthonous basin formed on the Lycian nappes, Denizli province-SW Turkey.* International Earth Sciences Colloquium on the Aegean Region, Abstracts, p. 32.

Spakman, W., 1990. *Tomographic images of the upper mantle below central Europe and the Mediterranean.* Terra Nova, Volume 2, pp. 542-553.

Spencer, J. E., 1984. *Role of tectonic denudation in warping an uplift of low-angle normal faults*. Geology, Volume 12, pp. 95–98.

Stampfli, G. M., & Borel, G. D., 2004. *The TRANSMED transects in space and time: constraints on the paleotectonic evolution of the Mediterranean domain*. In *The TRANSMED Atlas. The Mediterranean region from crust to mantle* (pp. 53-80). Springer Berlin Heidelberg.

Stampfli, G. & Hochard, C., 2009. *Plate tectonics of the Alpine realm*. In: Murphy, J. B., Keppie, J. D. & Hynes, A. J. (eds) *Ancient Orogens and Modern Analogues*, Geological Society of London, Special Publication no. 327, pp. 89–111.

Stern, R. J., & Bloomer, S. H., 1992. *Subduction zone infancy: examples from the Eocene Izu-Bonin-Mariana and Jurassic California arcs*. Geological Society of America Bulletin, Volume 104, pp. 1621-1636.

Stüwe, K., White, L. & Brown, R., 1994. *The influence of eroding topography on steady–state isotherms. Application to fission track analysis*. Earth Planetary Science Letters, Volume 124, pp. 63–74.

Sunal, G., Natal'in, B., Satir, M. & Toraman, E., 2006. *Paleozoic magmatic events in the Strandja Massif, NW Turkey*. Geodinamica Acta, Volume 19, pp. 283-300.

Şengör, A. M. C. & Yılmaz, Y., 1981. *Tethyan evolution of Turkey, a plate tectonic approach.* Tectonophysics, Volume 75, pp. 181-241.

Şengör, A. M. C., Altıner, D., Cin, A., Ustaömer, T. & Hsü, K. J., 1988. *Origin and assembly of the Tethyside orogenic collapse at the expense of Gondwana Land.* In Audley-Charles, M. G. & Hallam, A. (eds.), *Gondwana and Tethys.* Geological Society of London Special Publication, Volume 37, pp. 119–181.

Şengör, A. M. C., Görür, N. & Şaroğlu, F., 1985. *Strike-slip deformation, basin formation and sedimentation: strike-slip faulting and related basin formation in zones of tectonic escape: Turkey as a case study*. Strike-slip faulting and basin formation. Society of Economic Paleontologists and Mineralogist, Special Publication, Volume 37, pp. 227-264.

Şengör, A. M. C., Satir, M. & Akkök, R., 1984. *Timing of tectonic events in the Menderes Massif, western Turkey: implications for tectonic evolution and evidence for Pan-African basement in Turkey.* Tectonics, Volume 3, pp. 693-707.

Şengör, A. M. C., Yilmaz, Y. & Ketin, İ., 1982. *Remnants of a pre-Late Jurassic ocean in northern Turkey, Fragments of Permo-Triassic Paleo-Tethys: Reply.* Geological Society of America Bulletin, Volume 93, pp. 932-936.

Tagami, T. & O'Sullivan, P.B., 2005. *Fundamentals of fission-track thermochronology*. Reviews in Mineralogy and Geochemistry, Volume 58, pp. 19-47.

Tekeli, O., Işik, V., Seyitoğlu, G. & Çemen, I., 2001. *The 40Ar/Ar39 age of ductile extension and granitoid intrusions in the northern Menderes massif, western Turkey*. 4th Int. Turkish Geology Symposium Abstract, pp. 226.

Tekin, U. K., 1999. *Biostratigraphy and systematic of Late Middle to Late Triassic radiolarians from the Taurus mountains and Ankara region, Turkey.* Geologish Paläontologische Mitteilungen Innsbruck, Sonderband 5, pp. 1-296.

Teyssier, C., Ferré, E., Whitney, D. L., Norlander, B., Vanderhaeghe, O. & Parkinson, D., 2005. *Flow of partially molten crust and origin of detachments during collapse of the Cordilleran orogen.* In Bruhn, D. & Burlini, L. (eds.), *High-Strain Zones: Structure and Physical Properties.* Geological Society of London Special Publication, Volume 245, pp. 39–64.

Thomson, S. N. & Ring, U., 2006. *Thermochronologic evaluation of postcollision extension in the Anatolide orogen, western Turkey.* Tectonics, Volume 25, TC 3005.

Thomson, S. N., Brandon, M. T., Reiners, P. W., Zattin, M., Isaacson, P. J., & Balestrieri, M. L., 2010. *Thermochronologic evidence for orogen-parallel variability in wedge kinematics during extending convergent orogenesis of the northern Apennines, Italy*. Geological Society of America Bulletin, 122, pp. 1160-1179.

Topuz, G., Altherr, R., Satir, M. & Schwartz, W. H., 2004. *Low-grade metamorphic rocks from the Pulur Complex, NE Turkey: implications for the pre-Liassic evolution of the Eastern Pontides*. International Journal of Earth Sciences, Volume 93, pp. 72-91.

Topuz, G., Altherr, R., Schwartz, W. H., Dokuz, A. & Meyer, H. P., 2007. *Variscan amphibolites-facies rocks from the Kurtoğlu metamorphic complex (Gümüşhane area, Eastern Pontides, Turkey)*. International Journal of Earth Sciences, Volume 96, pp. 861-873.

Trotet, F., Jolivet, L. & Vidal, O., 2001a. *Tectono-metamorphic evolution of Syros and Sifnos Islands (Cyclades, Greece).* Tectonophysics, Volume 338, pp. 179-206.

Trotet, F., Vidal, O., & Jolivet, L., 2001b. *Exhumation of Syros and Sifnos metamorphic rocks (Cyclades, Greece). New constraints on the P-T paths.* European Journal of Mineralogy, Volume 13, pp. 901-920.

Tüysüz, O., 1999. *Geology of the Cretaceous sedimentary basins of the Western Pontides*. Geological Journal, Volume 34, pp. 75-93.

Ustaömer, P. A., Mundil, R. & Renne, P. R., 2005. *U/Pb and Pb/Pb zircon ages for arc-related intrusions of the Bolu Massif (W Pontides, NW Turkey): evidence for Late Precambrian (Cadomian) age.* Terra Nova, Volume 17, pp. 215-223.

Vandenberg, L. C. & Lister, G. S., 1996. *Structural analysis of basement tectonites from the Aegean metamorphic core complex of Ios, Cyclades, Greece.* Journal of Structural Geology, Volume 18, pp. 1437–1454.

Vanderhaeghe, O., 2004. *Structural development of the Naxos migmatite dome*. In Whitney, D .L., Teyssier, C., & Siddoway, C. S., eds., *Gneiss Domes in Orogeny,* Geological Society of America Special Paper 380, pp. 211–227.

Vanderhaeghe, O. & Teyssier, C., 2001. *Partial melting and flow of orogens.* Tectonophysics, Volume 342, pp. 451–472.

Van den haute, P. & De Corte, F., 1998. *Advances in Fission-Track Geochronology*. Kluwer Academic Publishers, Dordrecht, pp. 33-46.

van Hinsbergen, D. J. J., 2010. *A key extensional metamorphic complex reviewed and restored: The Menderes Massif of western Turkey.* Earth Science Reviews, Volume 102, pp. 60–76.

Von Blanckenburg, F., 2005. *The control mechanisms of erosion and weathering at basin scale from cosmogenic nuclides in river sediment*. Earth and Planetary Science Letters, Volume 237, pp. 462-479.

Varga, R. J. & Moores, E. M., 1985. *Spreading structure of the Troodos ophiolite, Cyprus*. Geology, Volume 13, pp. 846-850.

Vermeesch, P., 2008. *Three new ways to calculate average (U-Th)/He ages*. Chemical Geology, Volume 249, pp. 339–347.

Vernon, A. J., 2008. *Thermochronological approach to the late Neogene exhumation of the European Alps.* Ph.D. Thesis, University of Edinburgh, Scotland.

Wagner, G. A., 1968. *Fission track dating of apatites*. Earth and Planetary Science Letters, Volume 4, pp. 411-415.

Wagner, G. A., 1969. Spuren der spontanen Kernspaltung des $^{238}$Urans als Mittel zur Datierung von Apatiten und ein Beitrag zur Geochronologie des Odenwaldes. Neues Jahrbuch für Mineralogie Abhandlungen, Volume 110, pp. 252-286.

Wagner, G. A., & Reimer, G. M., 1972. *Fission track tectonics: the tectonic interpretation of fission track apatite ages*. Earth and Planetary Science Letters, Volume 14, pp. 263-268.

Wagner, G. A. & Van den Haute, P., 1992. *Fission-Track Dating*. Kluwer Academic Publishers, Dordrecht, 285pp.

Wells, M. L., Snee, L. W. & Blythe, A. E., 2000. *Dating of major normal fault systems using thermochronology: An example from the Raft River detachment, Basin and Range, western United States.* Journal of Geophysical Research, Volume 105, pp. 16,303–16,327.

Wernicke, B. 1981. *Low-angle normal faults in the Basin and Range Province—Nappe tectonics in an extending orogen.* Nature, Volume 291, pp. 645–648.

Wernicke, B. & Axen, G. J., 1988. *On the role of isostasy in the evolution of normal fault systems.* Geology, Volume 16, pp. 848–851.

Wernicke, B. & Burchfiel, B. C., 1982. *Modes of extensional tectonics.* Journal of Structural Geology, Volume 4, pp. 105–115.

Whitney, D. L. & Dilek, D., 2001. *Metamorphic and Tectonic Evolution of the Hırkadağ Block, Central Anatolian Crystalline Complex.* Turkish Journal of Earth Sciences, Volume 10, pp. 1-15.

Whitney, D. L. & Hamilton, M. A., 2004. *Timing of high-grade metamorphism in central Turkey and the assembly of Anatolia*. Journal of the Geological Society London, Volume 161, pp. 823-828.

Whitney, D. L., Teyssier, C. & Vanderhaeghe, O., 2004. *Gneiss domes and crustal flow*. In Whitney, D. L., Teyssier, C. & Siddoway, C. S., eds., *Gneiss Domes in Orogeny.* Geological Society of America Special Paper, Volume 380, pp. 15–33.

Whitney, D. L., Teyssier, C., Fayon, A. K., Hamilton, M. A. & Heizler, M. J., 2003. *Tectonic controls on metamorphism, partial melting, and intrusion: Timing of regional metamorphism and magmatism of the Niğde Massif, Turkey*. Tectonophysics, Volume 376, pp. 37-60.

Whitney, D. I., Teyssier, C., Rey, P. & Buck, R. W., 2013. *Continental and oceanic core complexes*. GSA Bulletin, Volume 125, pp. 273-298.

Wijbrans, J. & McDougall, I., 1988. *Metamorphic evolution of the Attic Cycladic metamorphic belt on Naxos (Cyclades, Greece) utilizing $^{40}Ar/^{39}Ar$ age spectrum measurements.* Journal of Metamorphic Geology, Volume 6, pp. 571-594.

Will, T., Okrusch, M., Schmädicke, E., & Chen, G., 1998. *Phase relations in the greenschist-blueschist-amphibolite-eclogite facies in the system Na2O-CaO-FeO-MgO-Al2O3-SiO2-H2O (NCFMASH), with application to metamorphic rocks from Samos, Greece.* Contributions to Mineralogy and Petrology, Volume 132, pp. 85–102.

Willett, S. D. & Brandon, M. T., 2012. *Some analytical methods for converting thermochronometric age to erosion rate.* Geochemistry Geophysics Geosystems, Volume 14, pp. 209-222.

Williams, G. D., Ünlügenç, U. C., Kelling, G. & Demirkol, C., 1995. *Tectonic controls on stratigraphic evolution of the Adana Basin, Turkey*. Journal of the Geological Society, Volume 152, pp. 873-882.

Wright, L. A., Otton, J. K. & Troxel, B. W., 1974. *Turtleback surfaces of Death Valley viewed as phenomena of extension*. Geology, Volume 2, pp. 53–54.

Yalınız, M. K., Göncüoğlu, M. C. & Özkan-Altiner, S., 2000. *Formation and emplacement ages of the SSZ-type Neotethyan ophiolites in Central Anatolia, Turkey: palaeotectonic implications*. Geological Journal, Volume 35, pp. 53-68.

Yiğitbaş, E., Elmas, A. & Yılmaz, Y. 1999. *Pre-Cenozoic tectono-stratigraphic components of the Western Pontides and their geological evolution.* Geological Journal, Volume 34, pp. 55–74.

Yiğitbaş, E., Kerrich, R., Yilmaz, Y., Elmas, A. & Xie, Q. L., 2004. *Characteristics and geochemistry of Precambrian ophiolites and related volcanics from the İstanbul-Zonguldak Unit, Northwestern Anatolia, Turkey: following the missing chain of the Precambrian South European suture zone to the east.* Precambrian Research, Volume 132, pp. 179-206.

Yılmaz, O. & Boztuğ, D., 1986. *Kastamonu granitoid belt of northern Turkey: First arc plutonism product related to the subduction of the paleo-Tethys*. Geology, Volume 14, pp. 179-183.

Yılmaz, O., Tüysüz, E., Yiğitbaş, Ş. C. Genç, A. M. C. Şengör, 1997. *Geology and tectonic evolution of the Pontides*, in: Robinson, A. G. (Ed.), *Regional and Petroleum geology of the Black Sea and surrounding region*, Memories of American Association of Petroleum Geologists, Volume 68, pp. 183–226.

Yılmaz Y., Genç, S. C., Yigitba¸ S. E., Bozcu, M. & Yilmaz, K., 1994. *Geological evolution of the late Mesozoic continental margin of northwestern Anatolia*. Tectonophysics, Volume 243, pp. 155–71.

Yılmaz, Y., Genç, Ş. C., Gürer, F., Bozcu, M., Yılmaz, K., Karacik, Z., Altunkaynak, Ş. & Elmas, A., 2000. *When did the western Anatolian grabens begin to develop?* Geological Society Special Publication, Volume 173, pp. 353–384.

Zeitler, P. K., Herczig, A. L., McDougall, I. & Honda, M., 1987. *U-Th-He dating of apatite: A potential thermochronometer*. Geochimica et Cosmochimica Acta, Volume 51, pp. 2865-2868.

Zitter, T. A. C., Woodside, J. M. & Mascle, J., 2003. *The Anaximander Mountains: a clue to the tectonics of southwest Anatolia*. Geological Journal**,** Volume 38, pp. 375–394.